NORTHROP TECHNICAL REPORT

THE EFFECTS OF DISCONTINUITIES ON COMPRESSION FATIGUE
PROPERTIES OF ADVANCED COMPOSITES

CONTRACT N00019-79-C-0275
CONTRACT N00019-79-C-0276

FINAL TECHNICAL REPORT

G. C. Grimes
D. F. Adams
E. G. Dusablon

October 1980

Prepared for:

DEPARTMENT OF THE NAVY
NAVAL AIR SYSTEMS COMMAND
WASHINGTON, D. C.   20361

by

Northrop Corporation
Aircraft Division
One Northrop Avenue
Hawthorne, California   90250

and

University of Wyoming
Composite Materials Research Group
Mechanical Engineering Department
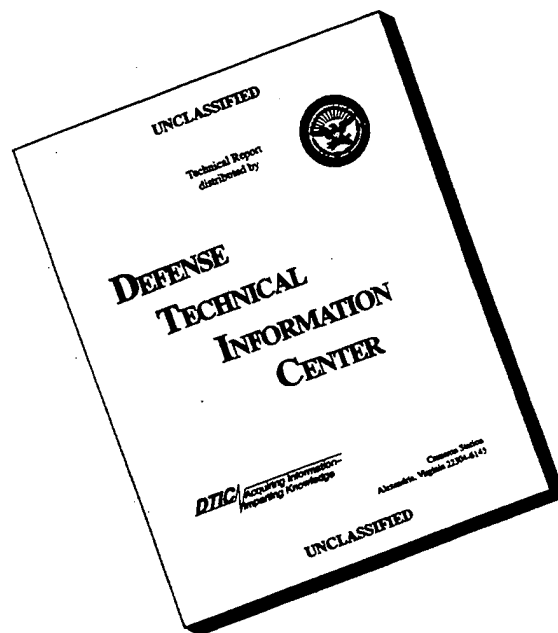Laramie, Wyoming   82071

NORTHROP TECHNICAL REPORT

Approved for Public Release; Distribution Unlimited

DISCLAIMER NOTICE

UNCLASSIFIED

Technical Report
distributed by

DEFENSE
TECHNICAL
INFORMATION
CENTER

DTIC Acquiring Information-
Imparting Knowledge

Cameron Station
Alexandria, Virginia 22304-6145

UNCLASSIFIED

THIS DOCUMENT IS BEST
QUALITY AVAILABLE. THE
COPY FURNISHED TO DTIC
CONTAINED A SIGNIFICANT
NUMBER OF PAGES WHICH DO
NOT REPRODUCE LEGIBLY.

REPORT DOCUMENTATION PAGE	READ INSTRUCTIONS BEFORE COMPLETING FORM

1. REPORT NUMBER	2. GOVT ACCESSION NO.	3. RECIPIENT'S CATALOG NUMBER

4. TITLE *(and Subtitle)*	5. TYPE OF REPORT & PERIOD COVERED
THE EFFECTS OF DISCONTINUITIES ON COMPRESSION FATIGUE PROPERTIES OF ADVANCED COMPOSITES	Final report for period covering 5-1-79 to 9-30-80
	6. PERFORMING ORG. REPORT NUMBER NOR 80-158

7. AUTHOR(s)	8. CONTRACT OR GRANT NUMBER(s)
G. C. Grimes, Northrop Corporation D. F. Adams, University of Wyoming E. G. Dusablon, Northrop Corporation	N00019-79-C-0275 (Northrop) N00019-79-C-0276 (University of Wyoming)

9. PERFORMING ORGANIZATION NAME AND ADDRESS	10. PROGRAM ELEMENT, PROJECT, TASK AREA & WORK UNIT NUMBERS
Northrop Corporation The University of Wyoming Aircraft Division College of Engineering One Northrop Avenue University Station Box 3295 Hawthorne, CA. 90250 Laramie, Wyoming 82071	

11. CONTROLLING OFFICE NAME AND ADDRESS	12. REPORT DATE
Department of the Navy Naval Air Systems Command Washington, D.C. 20361	October 1980
	13. NUMBER OF PAGES 343

14. MONITORING AGENCY NAME & ADDRESS(if different from Controlling Office)	15. SECURITY CLASS. (of this report)
	Unclassified
	15a. DECLASSIFICATION/DOWNGRADING SCHEDULE

16. DISTRIBUTION STATEMENT *(of this Report)*

Approved for public release, distribution unlimited

17. DISTRIBUTION STATEMENT *(of the abstract entered in Block 20, if different from Report)*

18. SUPPLEMENTARY NOTES

19. KEY WORDS *(Continue on reverse side if necessary and identify by block number)*

Graphite/Epoxy Composites	Compression	SEM
Analytical Predictions	Test Data	Residual Strength
Photomicrographic	Experimental Methods	Structural Design
Static and Fatigue	Moisture Absorption	Micromechanics
Mechanical Properties	Severe Environment	Macromechanics

20. ABSTRACT *(Continue on reverse side if necessary and identify by block number)*

This study is directed at assessing the static compression and $R = 10$ compression fatigue properties of graphite/epoxy composites with ply drop-off discontinuities under severe operating environments including room temperature dry and wet, $-65°F$ wet, and $218°F$ dry and wet. In 30-ply $[(\pm 45)_5/0_{16}/90_4]_c$ laminates, two $0°$ plies or four $45°$ plies are dropped off symmetrically in the middle of the specimen. Static strengths and moduli of elasticity are unaffected by these discontinuities, however, some proportional limit and Poisson's ratio values are changed significantly. At 1.25×10^6 cycles of

DD FORM 1473 EDITION OF 1 NOV 65 IS OBSOLETE
1 JAN 73

constant frequency fatigue the maximum endurance limit stress level is degraded significantly in all cases by the two 0° ply dropoffs, but for the four 45° ply dropoffs it is unaffected or increased significantly. Surviving specimens exhibit residual strength that varies directly with the maximum applied cyclic compressive stress up to a threshold level. Detail data tables and plots are included.

Scanning electron microscopy observations of the failed specimen fracture surfaces combined with micromechanics/point stress analysis and the analysis of ply dropoff effects are also included.

PREFACE

This report was prepared by the Northrop Corporation, Aircraft
Division, Hawthorne, California under Contract N00019-79-C-0275
and the University of Wyoming, Laramie, Wyoming under Contract
N00019-79-C-0276. The contracts were administered by the Naval Air
Systems Command with Mr. Maxwell W. Stander as the Navy Program Moni-
tor.

The processing, fabrication, and testing portions of the program
were conducted at Northrop under the direction of Mr. G. C. Grimes,
Program Manager, with the assistance of Edmond G. Dusablon. Mr. Grimes
reports to Dr. R. M. Verette, Manager of the Structural Mechanics
Research Department. Laminate processing was under the supervision
of W. Martin. Specimen fabrication was under the supervision of
R. Mihalco. Program testing was under the supervision of R. Mihalco
and A. McQuillian of MRL, and D. Atmur and T. Miller of ETL. Materials,
processing, fabrication, and testing were coordinated by J. Mays.
Data reduction was performed by Pat Griffith. Documentation was accom-
plished by B. Parish.

The analytical and failure analysis portions of this program were
performed by the Composite Materials Research Group at the University
of Wyoming under the direction of Dr. D. F. Adams, Program Manager,
Professor of Mechanical Engineering, assisted by Dr. M. M. Monib,
Assistant Professor. Contributions were also made by J. M. Mahishi,
Ph.D. student, and D. W. Peterson, D. S. Adams, C. J. Long, undergradu-
ate students, all of the Mechanical Engineering Department.

TABLE OF CONTENTS

TABLE OF CONTENTS (CONT'D)

TABLE OF CONTENTS (CONT'D)

TABLE OF CONTENTS (CONT'D)

LIST OF ILLUSTRATIONS

LIST OF ILLUSTRATIONS (CONT'D)

LIST OF ILLUSTRATIONS (CONT'D)

LIST OF ILLUSTRATIONS (CONCLUDED)

LIST OF TABLES

LIST OF TABLES (CONT'D)

SECTION 1

INTRODUCTION

1.1 GENERAL

This section details the purpose and scope of work at Northrop and the University of Wyoming. This is followed by a narrative, but brief, description of the balance of this report's contents.

1.2 PURPOSE AND SCOPE

The program was directed at assessing the compression fatigue properties of advanced composites with discontinuities which were exposed to simulated Naval Aircraft operating environments, dry and after moisture conditioning. The examination of compression fatigue of composites with discontinuities (particularly related to ply drop-off locations) in the presence of realistic environments was a pertinent topic since it has been observed that large strength reductions occurred under these circumstances as compared to room temperature dry (RTD) static compression strength.

To maximize the information obtained, the following ground rules were established.

- Fatigue loading was compression-compression (R=10) with initial applied compressive load resulting in a compressive strain of about −6000 μ in/in to simulate severe wing compression skin applications. Strain levels were increased or decreased after initial test results were observed in order to establish meaningful S-N data.

- Realistic design situations that were most vulnerable to compression fatigue and a severe environment were emphasized.

- Fatigue, static, and residual strength testing at −65F, RT and 218F was accomplished on specimens with and without discontinuities.

- Moisture conditioning of the specimens was to the 1% level and was accomplished such that moisture distribution through the thickness is held uniform.

Work at Northrop consisted of fabrication and testing of specimens. At the University of Wyoming, the work consisted of the analytical prediction of experimental behavior and the study of the failure surfaces of the failed specimens with the Scanning Electron Microscope (SEM).

1.3 REPORT

This report is made up of the summary of Section 2 followed by the fabrication and quality assurance of Section 3. Section 4 covers the experimental methods while Section 5 presents the detailed test results. Section 6 presents the analytical effort in detail and Section 7 gives the conclusions and recommendations. This is followed by the List of References and the Appendices A through G.

SECTION 2

SUMMARY

2.1 GENERAL

This section summarizes the results of the program to investigate the effects of ply drop-off discontinuities on the compressive fatigue properties of advanced composites. Section 2.2 summarizes the experimental data generated by Northrop in the program, whereas, Section 2.3 summarizes the analytical work done by the University of Wyoming.

2.2 EXPERIMENTAL DATA

2.2.1 Quality Assurance

The quality assurance program was established to insure that the quality level and consistency of the prepreg and cured laminates would be acceptable for use in manned aircraft primary structures. Materials and processes, traceability, performance, and destructive and nondestructive inspection requirements were established in the specification instruction sheets presented in Appendix A. These specification instruction sheets are based on industry and Northrop specifications covering the materials used in this study and on more general, but applicable, government specifications. The materials used in this investigation were purchased to the appropriate Northrop and industry specifications and then tested per those specifications. Also, the additional testing required in the quality control instruction sheets of Appendix A was conducted. In some cases, the test data generated and discussed below was used to establish the instruction sheet values.

The AS/3501 graphite/epoxy material acceptance testing was performed in accordance with Quality Control Instruction Sheet ID/CF No. 1* and pertinent Northrop and industry specifications. All test results met or exceeded the specification requirements.

---

*See Appendix A

Physical properties for laminate assemblies A and B are shown in Table 2.1. Generally, as the number of plies decreased, the fiber volume increased. For the 30, 28, and 26 ply thicknesses, laminate A had 54.5%, 57.5% and 58.3% fiber volume, respectively, while laminate B had 56.1%, 57.8%, and 58.5% fiber volume, respectively.

Specific gravity followed the same trend; whereas, the resin content by weight and thickness went down as the number of plies decreased. All these trends are compatible with each other. These variations are small with fiber volume ranging from 54.5% to 58.5 with a median value of 56.5%.

Transverse tension quality control tests for Laminate A are summarized in Table 2.2 for the three ply thicknesses: 30, 28 and 26. Mechanical properties are similar for all three thicknesses except for Poisson's ratio. From 30 to 28 plies (dropping two 0^0 plies) causes Poisson's ratio to increase 7% from 0.148 to 0.158 but reducing from 30 to 26 plies (dropping four 45^0 plies) causes Poisson's ratio to drop 33% from 0.158 to 0.102. The ultimate stresses range from 39.0 to 41.3 ksi, which is well above the 30 ksi minimum requirement of Q.C. Instruction Sheet ID/CF No. 3 (Appendix A). Dropping the two 0^0 plies reduces the transverse tension failure strain by 19% from 10.8 to 8.8×10^{-3} units, whereas, dropping four 45^0 plies reduced the strain to failure 10% to 9.7×10^{-3} units. Modulus of elasticity showed little change, ranging from 4.4 to 4.6×10^6 psi.

Quality control longitudinal and transverse compression test results are presented in Table 2.3 for Laminate A (longitudinal) and Laminate B (transverse) for each of the ply thicknesses. Dropping two 0^0 plies caused the longitudinal compression strength (-108.0 ksi) to increase by 11% to -119.4 ksi and the transverse compressive strength (-78.8 ksi) to increase 1% to -79.3 ksi. Dropping four 45^0 plies causes the longitudinal compressive strength (-108.0 ksi) to increase 13% to -122.0 ksi and the transverse compressive strength (-78.8 ksi) to decrease 7% to -73.6 ksi. However, all the longitudinal values exceed the -94 ksi requirement and all transverse values exceed the -50 ksi requirement of Q.C. Instruction Sheet No. 3 (Appendix A).

TABLE 2.1. SUMMARY OF PHYSICAL PROPERTIES FOR
LAMINATE ASSEMBLIES A & B.

Specimen No. & Statistical Value		Fiber Volume %*	No. of Plies	Resin Content % by Wt	Specific Gravity	Thickness In.
			- Laminate A (ACL-4210) -			
N = 8 FC-1	Mean	54.49	30	37.37	1.565	0.179
thru	S.D.	0.35		0.38	0.002	0.001
-8	C.V.	0.006		0.010	0.001	0.008
N = 4 FC'-9	Mean	57.46	28	34.58	1.581	0.158
thru	S.D.	0.32		0.30	0.002	0.001
-12	C.V.	0.006		0.009	0.001	0.008
n = 4 FC"-13A	Mean	58.34	26	33.76	1.585	0.146
thru	S.D.	0.54		0.48	0.003	0.001
-16A	C.V.	0.009		0.014	0.002	0.006
			- Laminate B (ACL-4211) -			
n = 4 FC-13B	Mean	56.11	30	36.14	1.579	0.180
thru	S.D.	3.58		2.74	0.033	0.001
-16B	C.V.	0.064		0.076	0.021	0.007
n = 4 FC'-17	Mean	57.82	28	34.29	1.583	0.162
thru	S.D.	0.46		0.44	0.002	0.001
-20	C.V.	0.008		0.013	0.001	0.004
n = 4 FC"-21	Mean	58.50	26	33.68	1.587	0.153
thru	S.D.	0.45		0.43	0.003	0.001
-25	C.V.	0.008		0.013	0.002	0.005

---

*Fiber Specific Gravity = 1.80
Resin Specific Gravity = 1.26

TABLE 2.2 SUMMARY QUALITY CONTROL TRANSVERSE TENSION DATA FROM
LAMINATE ASSEMBLY A (AVERAGE VALUES) - RTD.

Specimen ID	Primary Orientation* of Laminate Assy.	No. of Plies	Fiber Vol.%	Proportional Limit Stress ksi	Proportional Limit Strain 10^{-3} units	Failure Stress,*** ksi	Failure Strain 10^{-3} units	E_y 10^6 psi	ν_{yx} Poisson's Ratio	Failure Mode**
TTC-1-thru 4	$[(\pm 45)_5/0_{16}/90_4]_c$	30	54.5	21.2	4.8	41.3	10.8	4.4	0.148	EOT/GL-2,3A,1
TTC'-5-6	$[(\pm 45)_5/0_{14}/90_4]_c$	28	57.5	26.6	5.6	39.0	8.8	4.6	0.158	EOT-2, 3B, 1
TTC''-7,-8	$[(\pm 45)_3/0_{16}/90_4]_c$	26	58.3	22.4	4.8	39.6	9.7	4.6	0.102	EOT-2,3C, 1

*All specimens have loading direction 90^0 to primary axis of orientation

**

EOT - End of tab failure location
GL - Gage Length
 1 - Failure in 0^0 plies, net tension perpendicular to loading direction
 2 - Failure in 90^0 plies, net tension perpendicular to loading direction
3A - Failure in $\pm 45^0$ plies, large delamination and tension at $\pm 45^0$ to loading direction
3B - Failure in $\pm 45^0$ plies, medium delamination and tension at $\pm 45^0$ to loading direction
3C - Failure in $\pm 45^0$ plies, small delaminations and tension at $\pm 45^0$ to loading direction

Note: Bending, as recorded by back-to-back longitudinal strain gages, was within $\pm$ 5% of the mean strain level

***Minimum requirements per Q.C. Instruction Sheet ID/CF No. 3 (App. A) are: Transverse Tension (TT) = 30 ksi

TABLE 2.3 SUMMARY OF QUALITY CONTROL COMPRESSION DATA AVERAGES FROM LAMINATE ASSEMBLIES A&B – RTD.

Specimen ID	Laminate Assy.	Primary Orientation of Laminate Assy.	No. of Plies	Fiber Vol.%	Running Load at Fail., lbs/in	Failure Stress*, ksi	Failure Mode**
LC-1,-2	A	$[(\pm 45)_5/0_{16}/90_4]c$	30	54.5	-18.7	-108.0	DCS→N-EOS,DL→ E to M
LC'-3,4		$[(\pm 45)_5/0_{14}/90_4]c$	28	57.5	-18.0	-119.4	DL→E to M, DCS→N –EOS
LC"-3,4		$[(\pm 45)_3/0_{16}/90_4]c$	26	58.3	-17.4	-122.0	DCS,DL→N-EOS
TC-7,8	B	$[(\pm 45)_5/0_{16}/90_4]c$	30	56.1	-14.3	– 78.7	DCS,DL→MOS
TC'-9,-10		$[(\pm 45)_5/0_{14}/90_4]c$	28	57.8	-13.2	– 79.3	DCS, DL→M to E
TC"-11,-12		$[(\pm 45)_3/0_{16}/90_4]c$	26	58.5	-11.4	– 73.6	DCS,DL M to E

*Minimum requirements per Q.C. Instruction Sheet ID/CF No. 3 (Appendix A) are:
Longitudinal Compression (LC) = -94 ksi and transverse Compression (TC) = -50 ksi

**Failure modes and locations:
DCS – diagonal compression shear   M to E–middle to end
EOS – end of specimen   D –delamination
MOS – middle of specimen   N – near

Laminates A and B were cut up into thirteen subassemblies, fiberglass tabs were bonded onto the assemblies and they were sent through ultrasonic inspection with C-scan print-out and records. At the 0 dB sensitivity setting all thirteen subassemblies checked out to be excellent (95-100% signal transmission). At a more sensitive 6 dB setting the signal transmission ranged from 80 to 100%, apparently picking up the resin-rich pocket areas which were discussed in Reference (1) and have no detrimental effect on the mechanical properties being studied. Therefore all assemblies were judged as having excellent C-scans at the correct 0 dB reading. Only two of the five ply drop off No. 1 (two 0^0 plies) discontinuities were picked up by the C-scan but all the ply drop-off No. 2 (four 45^0 plies) discontinuities were picked up.

Based on the above nondestructive and destructive testing the laminate assemblies A and B and the thirteen subassemblies cut from them were of excellent quality and consistency. It is from these thirteen tabbed subassemblies that all program mechanical test specimens were cut.

2.2.2 Static, Fatigue and Residual Strength Properties

A summary of the static tension data obtained at RTD conditions is given in Table 2.4, below, for the plain laminate, ply drop-off No. 1, and ply drop-off No. 2 configurations. Ply drop-off No. 1 shows little change in tensile properties from that of the plain laminate, however, ply drop-off No. 2 shows a substantial difference from the plain laminate in strength

TABLE 2.4 SUMMARY OF AVERAGED STATIC TENSION DATA - RTD

Test Series	Discontinuity Configuration	Ultimate Stress, ksi	Failure Strain, 10^{-3} units	Modulus of Elasticity 10^6 psi	Poisson's Ratio
XX	Plain-30 plies	105.7	10.0	10.5	0.347
XXI	PDO #1, 28 plies	107.8	10.6	10.1	0.352
XXII	PDO #2, 26 plies	128.5	10.6	12.0	0.272

and modulus of elasticity, which are higher, and Poisson's ratio, which is lower. Strain to failure remains consistently the same for all configurations.

2.6

2.2.2.1 Ply Drop-Off Behavior at -65 FW

A summary of the compression static, fatigue and residual strength properties is given in Table 2.5 and Figures 2.1 and 2.2. The following paragraphs discuss these results.

At -65° FW PDO #1 discontinuity shows a static ultimate strength increase of 16% to -133.3 ksi from the plain laminate value of -113.6 ksi, whereas, the failure strain for PDO #1 goes up 26% to -17,100 μin/in from the plain laminate value of -13,533 μ-in/in. Modulus of elasticity for PDO #1 drops 9% to 9.4×10^6 psi from the plain laminate value of 10.4×10^6 psi. Proportional limit stress and strain values of PDO #1 configuration go up 20 and 22%, respectively. Poisson's ratio value for PDO #1 discontinuity drops 6% from the plain laminate value. In fatigue the endurance limit stress level for PDO #1 remains close to that of the plain laminate but as a percent of static strength it drops substantially. Residual strength stress level and precent of static strength value for PDO #1 both drop substantially compared to those of the plain laminate.

The PDO #2 discontinuity at -65° FW shows an increase in static ultimate strength of 15% to -131.0 ksi compared to the plain laminate value of -113.6 ksi, whereas, the failure strain level increases 1% from -13, 533 μ-in/in to -13,650 μin/in. Proportional limit stress for PDO#2 increased 59% to -53.4 ksi from the plain laminate value of - 33.6 ksi, while the proportional limit strain value increased 39% to -4900 μ-in/in from the plain laminate value of -3533 μ-in/in. Modulus of elasticity value of PDO#2 increases 7% to 11.11×10^6 psi from the plain laminate value of 10.37×10^6 psi. Poisson's ratio for PDO#2 drops 22% to 0.242 compared to the plain laminate value of 0.312. Endurance limit stress level in fatigue for PDO#2 increased 10% compared to the plain laminate, whereas, the endurance limit on a percent of the static strength remained about the same. The PDO#2 residual strength stress level and percent of static strength values are reasonably close to those of the plain laminate. The -65° FW moisture coupon (MC) level ranges from 1.10% to 1.14% at the end of testing.

TABLE 2.5 SUMMARY OF STATIC AND FATIGUE COMPRESSION PROPERTIES
(Thin section properties for PDO #1, #2)

| | | STATIC DATA | | | | | | | | FATIGUE DATA | | | | | | | | |
Discontinuity Configuration	Test Condition	Stress, Ksi Ultimate	Stress, Ksi Prop.Lim	Strain, μin/in Ultimate	Strain, μin/in Prop.Lim	Elastic Prop. E, 10⁶ psi	Prop. ν	Ref. Test Series	Avg. Moist. Content %	1.25x10⁶ Endurance Lim. or run-out Stress, ksi	Strain, μin/in	Endurance Lim or run-out as a % of Static Strength % of Static Stren.	% of Static Strain	Related R.S.* Stress, ksi	% of Static Stren	Ref. Test Ser.	Avg. Moist. Content %
Plain Laminate	-65°FW	-113.624	-33.654	-13533	-3533	10.37	0.312	I	1.108	-82.961	-11089	73.01	81.94	-144.13	126.85	II	1.119
PDO #1	-65°FW	-132.287	-40.413	-17100	-4300	9.41	0.292	IV	1.139	-78.702	-9132	59.49	53.40	-99.13	74.94	VIII	1.117
PDO #2	-65°FW	-131.028	-53.413	-13650	-4900	11.11	0.242	XII	1.119	-96.342	-9441	73.53	69.16	-154.64	118.02	XVI	1.095
Plain Laminate	RTD	-105.031	-48.572	-11816	-4666	10.40	0.325	**	—	-79.392	-9000	75.59	76.17	-85.08	95.40	**	—
PDO #1	RTD	-107.415	-36.830	-13217	-4100	9.10	0.260	V	0.125	-54.945	-6493	51.15	49.13	-112.94	105.14	IX	0%
PDO #2	RTD	-107.159	-39.830	-12183	-4267	9.88	0.193	XIII	0%	-73.309	-7585	68.41	62.26	-119.96	111.95	XVII	0.027
Plain Laminate	RTW	-95.945	-43.093	-10478	-4131	10.03	0.316	**	1.425	-66.790	-7500	69.61	71.58	-60.98	80.47	**	1.259
PDO #1	RTW	-106.042	-35.856	-13250	-3825	9.76	0.199	VI	0.920	-58.651	-7074	55.31	53.39	-104.69	98.72	X	1.072
PDO #2	RTW	-107.379	-52.872	-10675	-4200	11.49	0.152	XIV	0.979	-78.564	-8005	73.17	74.99	-113.80	105.96	XVIII	1.079
Plain Laminate	218°FW	-75.872	-33.740	-8381	-3959	10.37	0.244	**	1.272	-63.343	-7069	83.48	84.35	-102.53	135.14	III	1.021
PDO #1	218°FW	-75.171	-35.026	-8300	-3475	10.13	0.310	VII	1.059	-51.760	-6161	68.85	74.23	-70.94	94.42	XI	1.089
PDO #2	218°FW	-89.353	-38.409	-9117	-3700	10.53	0.243	XV	1.131	-61.431	-6438	68.75	70.61	-95.95	107.38	XIX	1.145
Plain Laminate	218°FD	-89.178	-40.431	-9637	-3798	10.53	0.234	**	—	—	—	—	—	—	—	—	—

*Residual strength shown is that related to fatigue endurance limit specimen
**These data taken from Reference (1): RTD and 218° FD Static – Table 5.16, RTW and 218° FW Static – Table 5.17,
RTD Fatigue – Table 5.18, RTW Fatigue – Table 5.19, RTD/218° F, and RTW/218° F
Residual Strength – Table 5.24

⊙ Residual strength values obtained at 218° F, i.e., percentage values are based on related static values, e.g.,
218° FD or 218° FW values

⊛ Moisture coupons dried for 48 hours @ 170° F in air prior to conditioning; measurements taken after completion
of test series testing

Figure 2.1. Summary of Static Compression Properties.

A- Plain Laminate,-65°FW

B- PDO# 1,-65°FW

C- PDO# 2,-65°FW

D- Plain Laminate,RTD

E- PDO# 1,RTD

F- PDO# 2,RTD

G- Plain Laminate,RTW

H- PDO# 1,RTW

I- PDO# 2,RTW

J- Plain Laminate,218°FW

K- PDO# 1,218°FW

L- PDO# 2,218°FW

M- Plain Laminate,218°FD
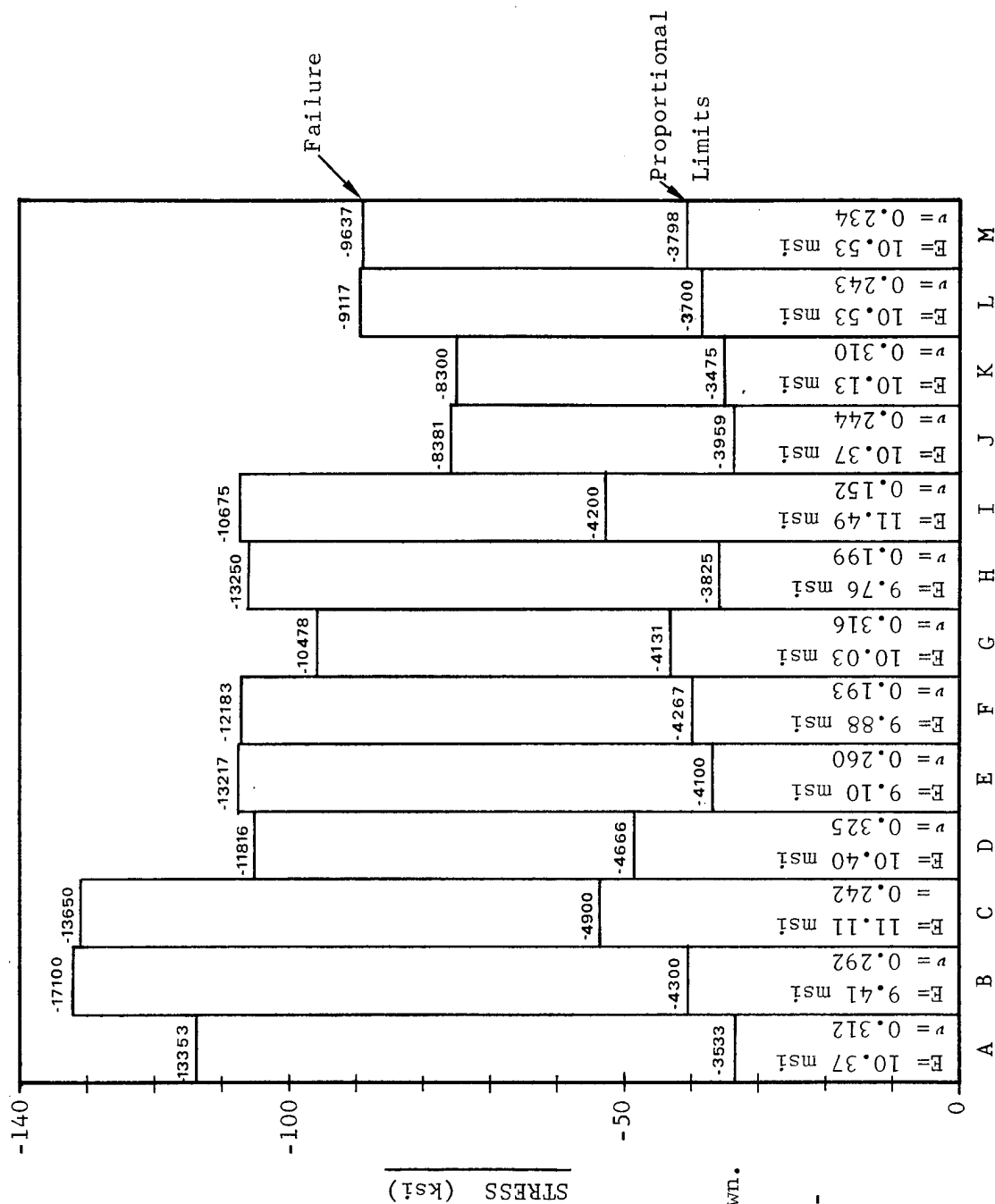
Note: a) Ultimate strengths
plotted, failure
strain numbers shown.
b) Proportional limit
stresses plotted,
related strain num-
bers shown.

2.9

A- Plain Laminate, -65°FW
B- PDO #1, -65°FW
C- PDO #2, -65°FW
D- Plain Laminate, RTD
E- PDO #1, RTD
F- PDO #2, RTD
G- Plain Laminate, RTW
H- PDO #1, RTW
I- PDO #2, RTW
J- Plain Laminate, 218°FW
K- PDO #1, 218°FW
L- PDO #2, 218°FW
M- Plain Laminate, 218°FD

Note: a) Residual strength
stresses plotted,
related strain
numbers shown.

b) Endurance limit
(1.25 x 10^6
cycles) stresses
plotted, related
strains numbers
shown.
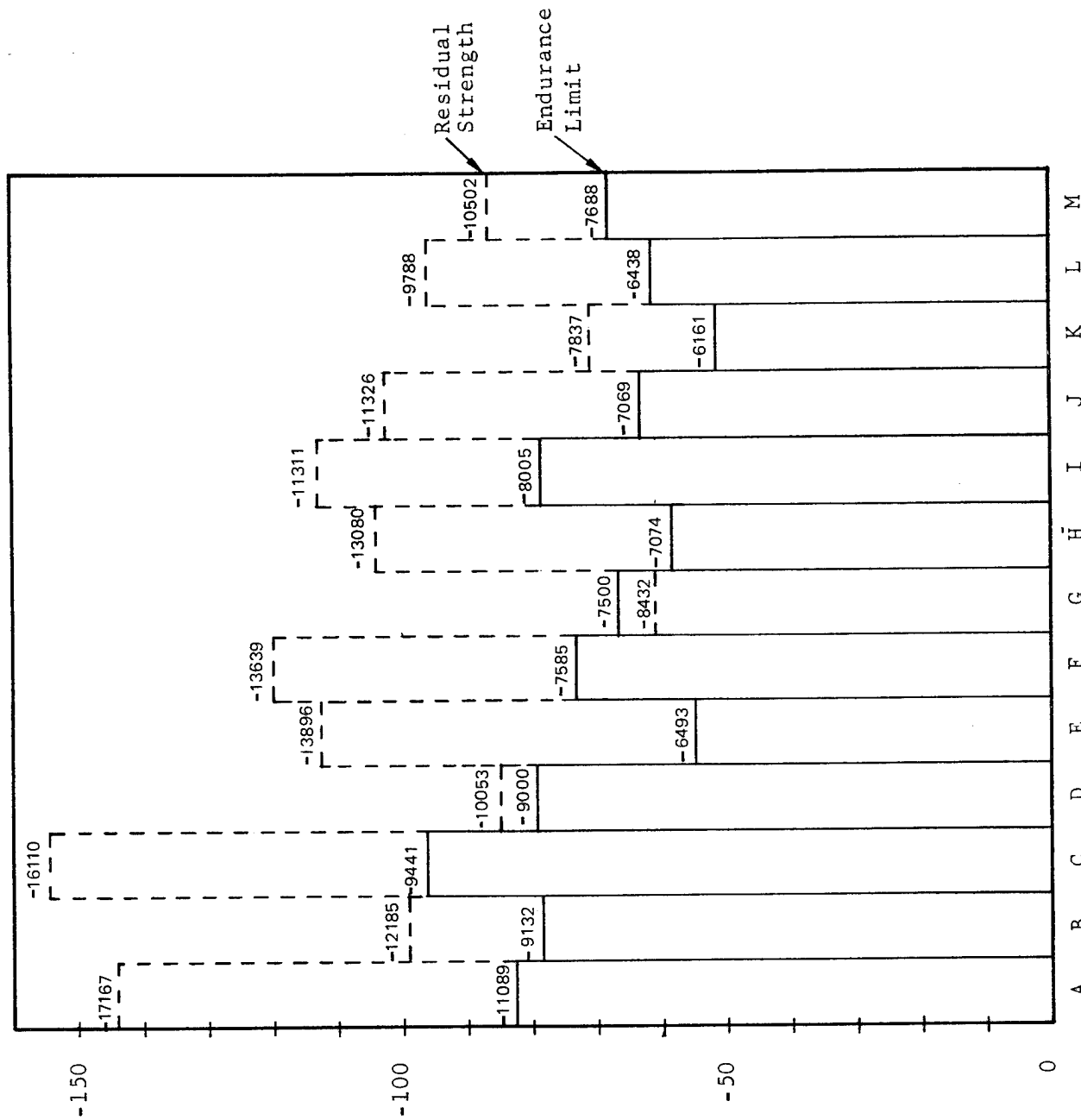
FIGURE 2.2. Summary of Compression Fatigue and Residual Strength Properties

2.10

In summary, the thin section $[(\pm 45)_5/0_{14}/90_4]_c$ PDO #1 static behavior at -65°FW exhibits substantial increases in ultimate and proportional limit stress and strain levels, whereas, modulus of elasticity and Poisson's ratio show small decreases compared to the $[(\pm 45)_5/0_{16}/90_4]_c$ plain laminate. In fatigue the -65°FW thin section PDO #1 1.25×10^6 cycle endurance limit is about the same as that of the plain laminate, but as a percent of static strength it drops substantially. The -65°FW residual strength for the thin section PDO #1 drops significantly in stress level and in percent of static strength compared to that of the plain laminate.

For thin section $[(\pm 45)_3/0_{16}/90_4]_c$ PDO #2 the static behavior at -65°FW shows large increases in ultimate and proportional limit stress levels and proportional limit strain levels compared with the $[(\pm 45)_5/0_{16}/90_4]_c$ plain laminate. Ultimate strain level for thin section PDO #2 remains approximately the same as that of the plain laminate, whereas, PDO #2 modulus of elasticity shows a slight increase and the Poisson's Ratio exhibits a significant drop compared to that of the plain laminate. The 1.25×10^6 cycle fatigue endurance limit stress level for thin section PDO #2 increases significantly, but as a percent of static strength, it remains the same when compared to plain laminate values. Residual strength stress level and percent of static strength values for thin section PDO #2 remain about the same as those for the plain laminate.

2.2.2.2 <u>Ply Drop-Off Behavior at RTD</u>

For thin section $[(\pm 45)_5/0_{14}/90_4]_c$ PDO #1 static properties at RTD conditions, the ultimate stress and strain levels of -107.4 ksi and $-13,217$ μ-in/in are slightly higher than the $[(\pm 45)_5/0_{16}/90_4]_c$ plain laminate values of -105.0 ksi and $-11,816$ μ-in/in, respectively. Proportional limit stress level (-36.8 ksi) for thin section PDO #1 shows a significant drop while the related strain level (-4100 μ-in/in) shows a small decrease compared with the plain laminate values of -48.6 ksi and -4666 μ-in/in, respectively. The thin section PDO #1 modulus of elasticity of 9.10×10^6 psi and Poisson's ratio of 0.260 show significant drops from the plain laminate values of 10.4×10^6 psi and 0.325, respectively. Fatigue endurance limit stress level and percent of static strength at 1.25×10^6 cycles for PDO #1 show a substantial drop, whereas, the residual strength stress level and

percent of static strength values exhibit large increases compared to the related plain laminate values.

The PDO #2 thin section $[(\underline{+}45)_3/0_{16}/90_4]_c$ static ultimate values of -107.2 ksi stress and -12,183 μ-in/in strain, and static proportional limit values of -39.8 ksi stress and -4267 μ-in/in strain exhibit about the same behavior as PDO #1. Modulus of elasticty (9.88×10^6 psi) shows a small drop, while Poisson's ratio (0.193) exhibits a large drop compared to the plain laminate values of 10.40×10^6 psi and 0.325, respectively. Endurance limit (1.25×10^6 cycles) stress level and percent of static strength values show small drops compared to the related plain laminate values. Residual strength stress level and percent of static strength values increase significantly compared to the related plain laminate values. Moisture coupon pickup ranged from 0% to 0.125%.

In summary, for PDO #1 and PDO #2 at RTD conditions, the thin section static ultimate stress and strain levels and modulus of elasticity values remain about the same as those of the plain laminate. However, the thin section proportional limit stress and strain values and Poisson's ratio exhibit significant drops for both PDO #1 and PDO #2 at RTD conditions. But, in fatigue the PDO #1 endurance limit exhibits a small drop compared to the plain laminate values. Residual strength of both PDO #1 and PDO #2 show significant increases compared to the related plain laminate values.

2.2.2.3 Ply Drop-Off Properties at RTW

The RTW thin section $[(\underline{+}45)_5/0_{14}/90_4]_c$ PDO #1 static ultimate stress (-106.0 ksi) and strain (-13,250 μ-in/in) levels show small increases compared with the $[(\underline{+}45)_5/0_{16}/90_4]_c$ plain laminate properties of -95.9 ksi and -10,478 μ-in/in., respectively. Thin section RTW proportional limit stress (-35.9 ksi) and strain (-3825 μ-in/in) values for PDO #1 show small and significant drops, respectively, compared with the related plain lamin- ate values of -43.1 ksi and -4131 μ-in/in, while the RTW PDO #1 modulus of elasticity of 9.76×10^6 psi drops slightly, and the Poisson's ratio of 0.119 shows a substantial drop compared with the related plain laminate values of 10.03×10^6 psi and 0.316. Fatigue endurance limit at 1.25×10^6 cycles for PDO #1 at RTW conditions shows significant drops in both stress level and percent of static strength compared with the related plain

laminate values. Residual strength stress level and percent of static strength values exhibit substantially higher values than the same values for plain laminates.

The PDO #2 RTW static values of -107.4 ksi ultimate stress, -10,675 μ-in/in strain to failure, -52.9 ksi proportional limit stress, -4200 μ-in/in proportional limit strain, and the 0.152 Poisson's ratio exhibit the same trends as PDO #1 values, relative to the plain laminate values. Modulus of elasticity of 11.49×10^6 psi for RTW PDO #2 shows a small increase compared with the plain laminate value. Endurance limit fatigue values for RTW PDO #2 exhibit small to medium increases in stress level and percent of static strength values, whereas, residual strength values show a substantial increase compared with plain laminate properties. Moisture coupons showed absorption levels of 0.929 to 1.42% by weight for plain laminate, PO #1 and PDO #2 configurations.

In summary the RTW PDO #1 and #2 configurations show small increases in ultimate stress and strain levels and substantial decreases in proportional limit stress levels and Poisson's ratio values compared with the related plain laminate values. Proportional limit strain levels at RTW for both PDO #1 and #2 did not change much from the plain laminate values. At RTW conditions, the modulus of elasticity values for PDO #1 showed a small drop and for PDO #2 a medium increase compared with the related plain laminate values. For RTW fatigue endurance limits the PDO #1 values were significantly lower, while PDO #2 values were significantly higher than those of the plain laminate. Residual strength values at RTW conditions for PDO #1 and #2 were substantially higher than the related plain laminate value.

2.2.2.4 Ply Drop-Off Properties at 218^0 FW

At 218^0 FW static properties of thin section $[(\pm45)_5/0_{14}/90_4]$ PDO #1 were -75.2 ksi ultimate stress, -8300 μ-in/in strain to failure, - 35.0 ksi proportional limit stress, -3475 μ-in/in proportional limit strain, and a modulus of elasticity value of 10.13×10^6 psi which were close to the values measured on the $[(\pm45)_5/0_{16}/90_4]_c$ plain laminate. Poisson's ratio of 0.310 was up substantially over the 0.244 value for the plain laminate.

Fatigue endurance limit at 1.25×10^6 cycles for 218^0 FW PDO #1 showed a significant drop over that exhibited by the plain laminate as did the residual strength values.

For PDO #2 at 218^0 FW the static ultimate stress level of -89.4 ksi and strain level of -9117 μ-in/in showed a significant increase, whereas, the proportional limit stress (-38.4 ksi) and strain (-3700 μ-in/in), the modulus of elasticity (10.53×10^6 psi), and the Poisson's Ratio (0.243) were in the same range as the plain laminate properties. For the 218^0 FW PDO #2 1.25×10^6 cycles fatigue endurance limit, the stress level is about the same but the percent of static strength value is substantially less then the related properties from the plain laminate. Residual strength is somewhat less than that of the plain laminate. Moisture coupon absorption data for plain, PDO #1 and PDO #2 laminates ranged from 1.02% to 1.27%.

In summary, the main differences of the two ply drop-off properties at 218^0 FW from those of the plain laminate were: PDO #2 had a significantly higher ultimate strength, PDO #1 had a significantly higher Poisson's Ratio, and both PDO #1 and #2 had significantly lower percent of static strength endurance limit value, while PDO #1 had a somewhat lower endurance limit stress level.

2.2.3 Moisture Data

A summary of all moisture coupon data is presented in Table 2.6 below.

TABLE 2.6. SUMMARY OF MOISTURE ABSORPTION.

Static Value	Mean % Wt Loss in Drying	After Moisture Conditioning		After Completion of Test Series Testing	
		Mean % Wt Gain For Dried Coupons	Mean % Wt Gain For Undried Coupons	Mean % Wt Gain For Dried Coupons	Mean % Wt Gain For Undried Coupons
Mean	-0.159	1.106	0.950	1.092	1.106
S.D.	--	0.055	0.066	0.052	0.055
C. V.	--	0.049	0.069	0.048	0.049

Note that there is little difference in the moisture content immediately after moisture conditioning compared with after testing. Also observe that the dried specimens picked up an additional amount of moisture over the undried ones equal to the amount lost in drying.

2.3 ANALYTICAL WORK AT THE UNIVERSITY OF WYOMING

Analytical work performed by the Composite Materials Research Group at the University of Wyoming was focused in three primary areas, viz, scanning electron microscopy (SEM) of failed specimen fracture surfaces, combined micromechanics/point stress analysis of laminate response, and analysis of ply drop-off effects.

2.3.1 Scanning Electron Microscopy

A significant amount of scanning electron microscopy (SEM) work had been performed as part of the first-year program [1]. Additional studies were made, to determine the influence of the -65°F test temperature, not considered previously, and the ply drop-offs, also a new aspect. The extensive SEM examinations confirmed observations reported in the prior study [1]. In addition, the more brittle fracture response of the -65°F tests, for both static and fatigue loadings, as observed on the gross failure level, was also evident in the micro level fracture response. There was an increase in delamination of plies near the gross fracture surface with decreasing temperature, the differences between room temperature and -65°F failures being readily observed.

The general failure mode in graphite/epoxy composites containing 0° plies and subjected to axial compression appears to be debonding at the fiber-matrix interface in these primary load-carrying plies, followed by fiber micro-buckling. The local collapse of these 0° plies then propagates to cause a total fracture, with a number of secondary modes being initiated. This is consistent with the micromechanics predictions of high stresses at the fiber-matrix interface.

The SEM observations failed to document the presence of the ply drop-offs. In all cases, the primary fracture surface, or secondary fracture surfaces, appeared to occur at these sites, thus obscuring the presence of the ply discontinuities. This is significant, of course, since it verified the presence of stress concentrations caused by the ply drop-offs. It is recommended that in future work, some static specimens be subjected to only partial loadings, and fatigue specimens which exhibit runout, be sectioned and examined in the SEM, to identify failure initiation sites, and the influence of the ply drop-offs.

2.3.2 Combined Micromechanics/Point Stress Analysis

In the first-year study [1], the University of Wyoming's elastoplastic, finite element micromechanics analysis was used to analyze unidirectional composite experimental data, with excellent results. This analysis was extended during the second-year effort, to permit the study of the first-year $[\pm 45]_{ns}$ laminate and the second-year F-18 laminate compression data. This required the addition of a longitudinal shear loading capability to the existing micromechanics analysis, and the development of a method of coupling the micromechanics analysis with a laminate analysis. The classical laminate point stress analysis was used for demonstration purposes. In future work, a newly developed three-dimensional finite element laminate analysis will be used, being more accurate.

Nevertheless, the results obtained in the present effort, as presented in Section 6.3, were excellent, good correlations between theory and experiment for both laminate types, at all of the various temperature/moisture content combinations, being obtained. This was demonstrated by comparing predicted and measured stress-strain response of the laminate. The primary remaining task appears to be the addition of a crack propagation capability to the analysis. At present, the analysis terminates at predicted first failure. Thus, it does not model the full stress-strain response to gross fracture that is obtained experimentally. A crack propagation capability has now been developed as part of another study, and needs only to be combined with the present longitudinal shear micromechanics analysis.

As demonstrated in Section 6.3, the complete internal stress distribution in the individual plies of the laminate is available. This information is used to explain the occurrance of specific failure modes for given laminate orientation, environmental preconditioning, and loading conditions. These are then correlated with SEM observations of actual composite failures. The true goal of the analytical work is to provide guidelines for the design of laminates for specific applications, thus avoiding extensive screening tests at the experimental level, which is much more costly and time consuming.

The good correlations between theoretical predictions and experimental data presented here demonstrate the feasability of this approach.

2.3.3 Analysis of Ply Drop-off Effects

Because of the complex geometry which exists in the vicinity of a ply drop-off, as evidenced by the photomicrographs presented in Section 6.4, and the importance of interlaminar stresses near free edges, a three-dimensional analysis is almost mandatory. Such analyses, which include elastoplastic response of the individual orthotropic plies, have not previously existed. With the completion of such an analysis toward the end of the present program, the necessary analytical tool is now available.

Although not completed in time to permit the presentation of detailed results in this report, this new analysis and related computer program have been thoroughly checked out, and a number of sample cases run. Thus, it is expected that detailed results will be included in a subsequent NASC report.

Work has proceeded on the definition of the ply geometries involved, examples being included in the present report. It is anticipated that the detailed analysis of these ply drop-offs will result in a major contribution to the understanding of the stress concentrations induced. This will lead to the establishment of specific guidelines for designing composite structures in applications where it is necessary to vary the laminate configuration from region to region, the F-18 aircraft being one example.

SECTION 3

FABRICATION AND QUALITY ASSURANCE

3.1   GENERAL

The purpose of this section is to define the fabrication processes
and quality assurance used in the program. Section 3.2 covers the fabrica-
tion details and Section 3.3 details the quality assurance effort used to
maintain and verify the quality level.

3.2   FABRICATION, MATERIALS, AND PROCESSES

The three laminate orientations used in the study of ply drop-offs
were: the basic 30-ply Ⓒ type, the 2-ply drop-off 28-ply Ⓒ' type, and
the 4-ply drop-off Ⓒ'' type. Condensed and full lamination codes for these
laminates are given in Table 3.1. Figures 3.1 and 3.2 present the ply drop-
offs in detail.

3.2.1 Scope

Program laminates were fabricated per Figures 3.3, 3.4, and 3.5 with
subassemblies subsequently cut from them for tabbing and inspection with
specimens cut as follows:

1. 24 static and fatigue compression specimens without discontinuities
    (obtained from subassemblies A-1 & A-2).

2. 3 static tension specimens without discontinuities (Subassembly
    A-3).

3. 48 static and fatigue compression specimens with ply drop-off
    (PDO) #1 discontinuities (Subassemblies A-4, A-5, B-10, &
    B-11).

4. 3 static tension specimens with PDO #1 discontinuities (Subassem-
    bly A-6).

5. 48 static and fatigue compression specimens with PDO #2 discon-
    tinuities (Subassemblies A-7, A-8, B-12, & B-13).

TABLE 3.1 CONDENSED AND FULL LAMINATION CODES (AS/3501-6 GRAPHITE/EPOXY)*

Condensed Code	Section ID	Full Lamination Sequence Code	No. of Plies
$[(\underline{\pm45})_5/0_{16}/90_4]_c$	C	$[\overline{\pm45}/0/90/0_3/90/0_3/\overline{\pm45}/0/\underline{\pm45}]_S$	30
$[(\underline{\pm45})_5/0_{14}/90_4]_c$	C'	$[\overline{\pm45}/0/90/0_3/90/0_2/\overline{\pm45}/0/\underline{\pm45}]_S$	28
$[(\underline{\pm45})_3/0_{16}/90_4]_c$	C"	$[\overline{\pm45}/0/90/0_3/90/0_4/\underline{\pm45}]_S$	26

*Type prepreg by Hercules, Inc.

Notes: 1. Ply drop-off (PDO) #1 is the symmetrical transition from Section C to Section C'.

2. Ply drop-off (PDO) #2 is the symmetrical transition from Section C to Section C".

3. In making the laminates, all the thickness change is taken on one side only (see Figure 3.5).

Ⓒ   Ⓒ'

1	-45		-45	1
2	+45		+45	2
3	0		O	3
4	90		90	4
5	0		O	5
6	0		O	6
7	0		O	7
8	90		90	8
9	0	End Of Ply ⟶|		
10	0		O	9
11	0		O	10
12	-45		-45	11
13	+45		+45	12
14	0		O	13
15	+45		+45	14
16	-45		-45	15
17	0		O	16
18	+45		+45	17
19	-45		-45	18
20	0		O	19
21	0		O	20
22	0	End Of Ply ⟶|		
23	90		90	21
24	0		O	22
25	0		O	23
26	0		O	24
27	90		90	25
28	0		O	26
29	+45		+45	27
30	-45		-45	28

℄⟶ (at row 15/16, left)   ⟵℄ (at row 14/15, right)

╲— Tool Surface (Ref)
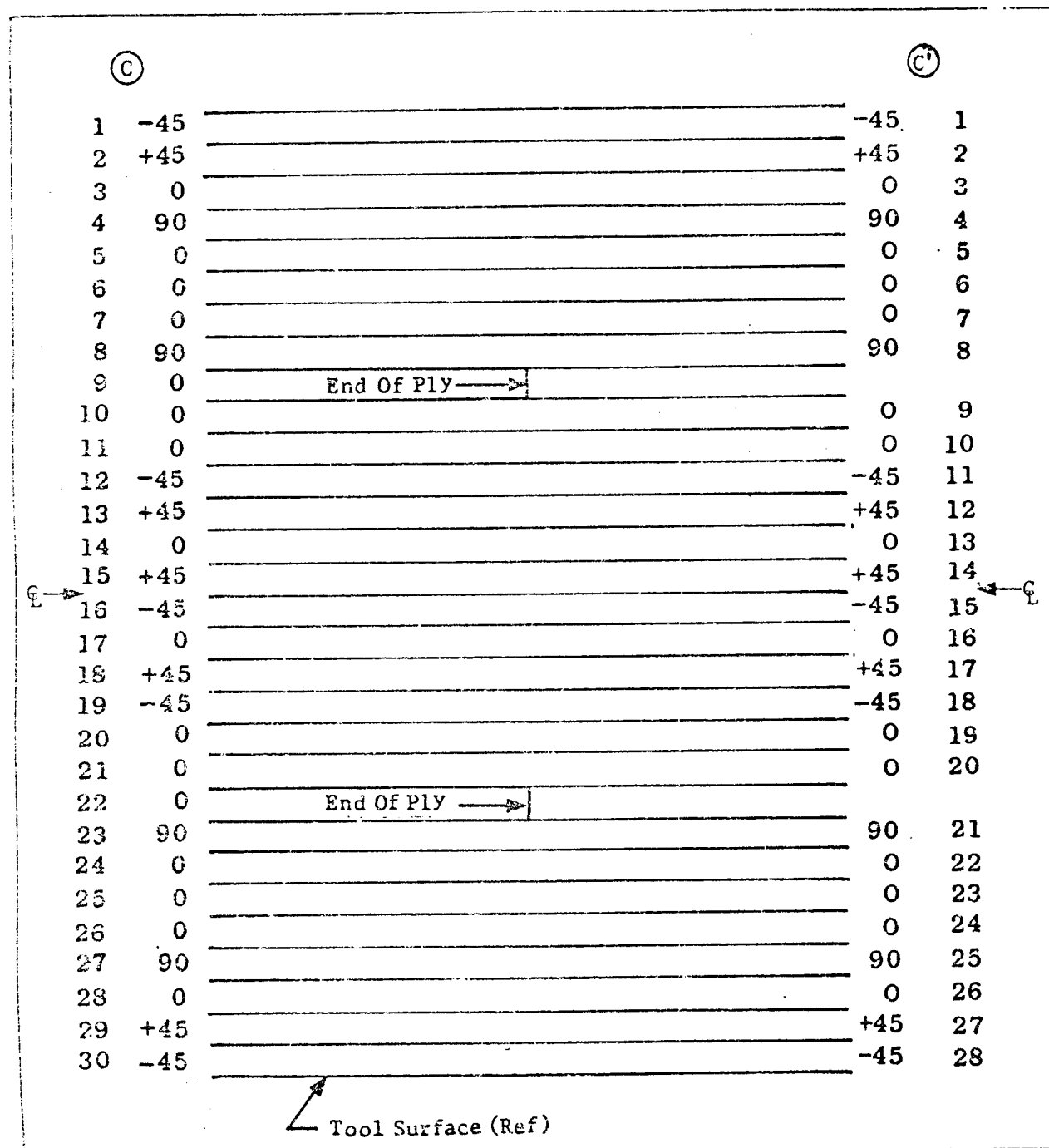
Figure 3.1. Details of Ply Drop-Off No. 1.

(C')

#	angle		angle	#
1	-45		-45	1
2	+45		+45	2
3	0		0	3
4	90		90	4
5	0		0	5
6	0		0	6
7	0		0	7
8	90		90	8
9	0		0	9
10	0		0	10
11	0		0	11
		←→ 1/2" ←→	-45 → End Of Ply	12
			+45 → End Of Ply	13
12	0		0	14
13	+45		+45	15
14	-45		-45	16
15	0		0	17
			+45 → End Of Ply	18
			-45 → End Of Ply	19
16	0	←→ 1/2" ←→	0	20
17	0		0	21
18	0		0	22
19	90		90	23
20	0		0	24
21	0		0	25
22	0		0	26
23	90		90	27
24	0		0	28
25	+45		+45	29
26	-45		-45	30

(C)

Tool Surface (Ref)
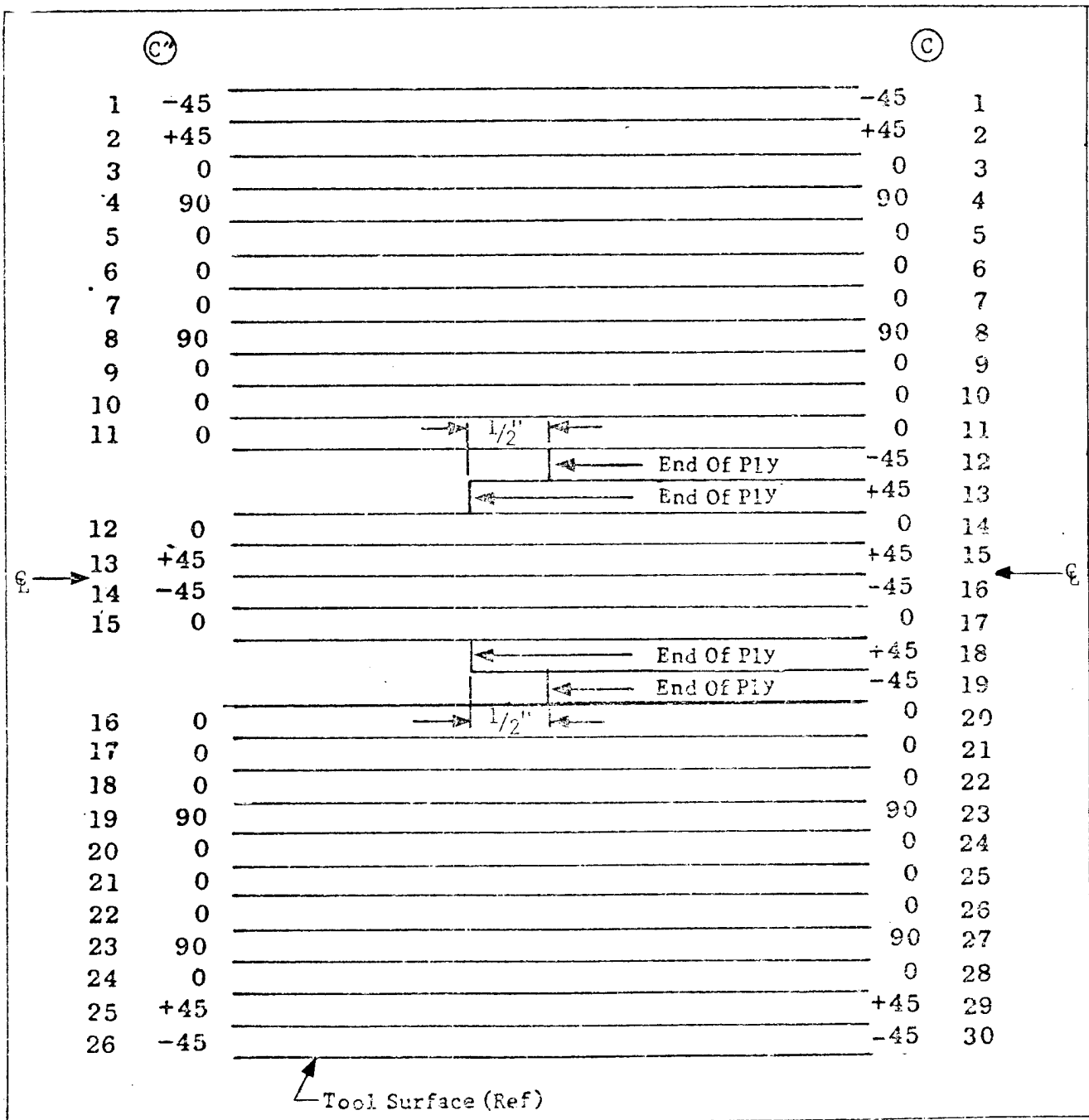
Figure 3.2 Details of Ply Drop-Off No. 2
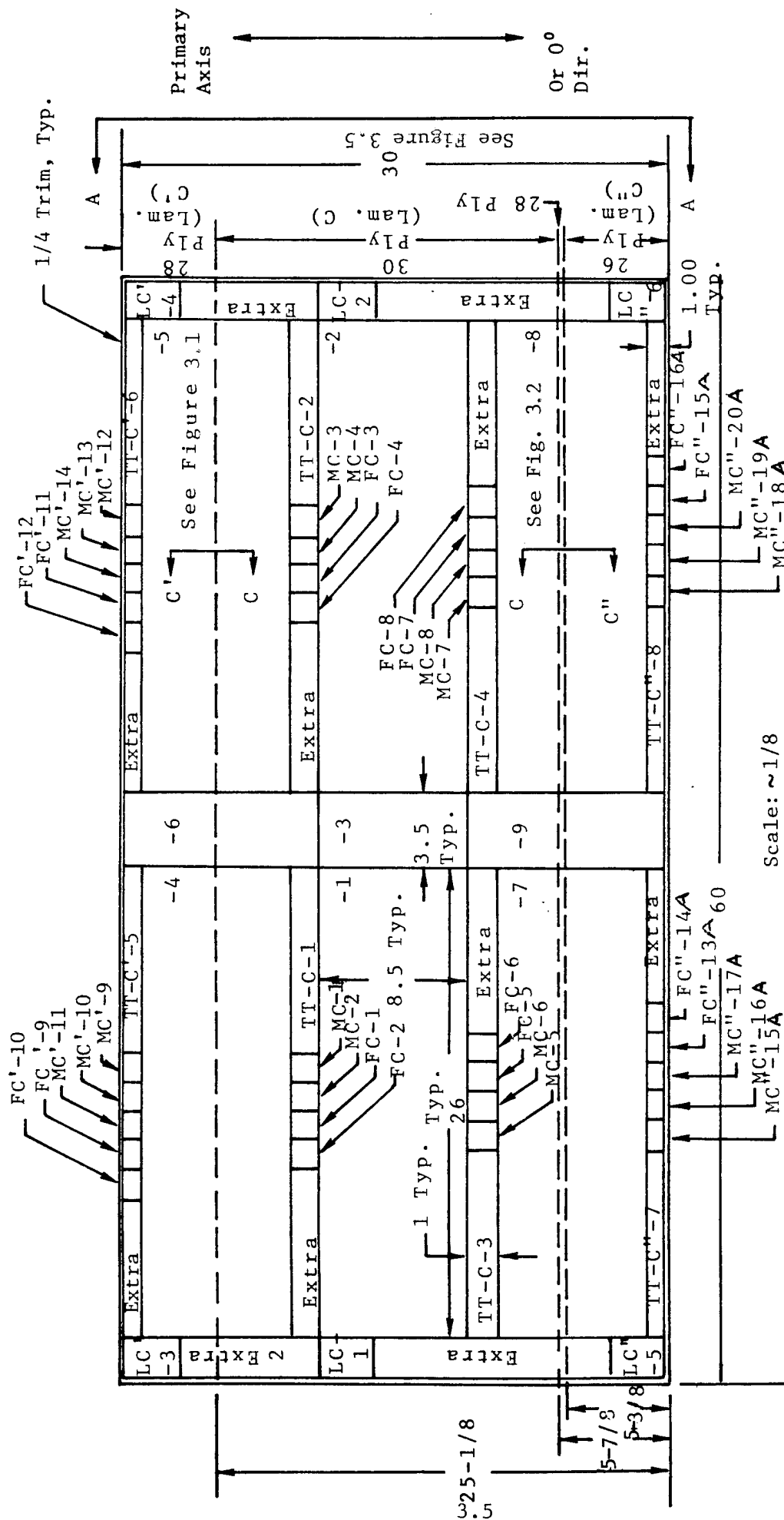
NOTES:

1. Make laminate assembly per Process Instruction Sheet ID/CF No. 1 Gr/Ep and glass/epoxy prepreg are to be per Q.C. Instruction Sheet ID/CF No. 1. Adhesive materials are to be per Q.C. Instruction sheet No. 2.

2. 1/8 inch allowed for each undimensioned internal boundary line on this assy.

3. -1, -2, etc denote subassembly locations.

4. The MC, FC, and TT-C specimens are 30 plies thick, MC', FC', and TT-C' specimens are 28 plies thick and MC", FC", and TT-C" specimens are 26 plies thick.

Figure 3.3   Laminate Assembly - A

Scale: ~1/8

Primary Axis

Or 0° Dir.

1/4 Trim, Typ.

See Figure 3.5

30

28 Ply (Lam. C')

30 Ply (Lam. C)

28 Ply

26 Ply (Lam. C")

See Figure 3.1

See Fig. 3.2

C'   C   C"

LC'-4   LC-2   LC"-6
LC"-3   Extra 2   LC"-1   Extra   LC"-5

-5   -8   -164   1.00 Typ.

TT-C'-6   TT-C-2   Extra   TT-C"-8

FC'-12   FC'-11   MC'-14   MC'-13   MC'-12
MC-3   MC-4   FC-3   FC-4
FC-8   FC-7   MC-8   MC-7
FC"-15A   MC"-20A   MC"-19A   MC"-18A

Extra   Extra   Extra

-4   -1   -9

TT-C'-5   TT-C-1   Extra   TT-C"-7

-6   -3   -9

FC-2 8.5 Typ.
3.5 Typ.

FC'-10   FC'-9   MC'-11   MC'-10   MC'-9
MC-1   MC-2   FC-1
FC-5   FC-6   MC-5   MC-6
FC"-14A   FC"-13A 60   MC"-17A   MC"-16A   MC"-15A

1 Typ. Typ.   26

TT-C-3   TT-C"-7

25-1/8

5-7/8   5-3/8

3.5

Figure 3.4. Laminate Assembly – B

NOTES:

1. Same as on Figure 3.3
2. 1/8 inch allowed for each undimensioned internal boundary line on this assembly.
3. Same as on Figure 3.3
4. Same as on Figure 3.3

Scale: ~ 1/8

Lam−A:30"
Lam−B:20"

©

1	−45
2	+45
3	0
4	90
5	0
6	0
7	0
8	90
9	0
10	0
11	0

← End Of Ply
← End Of Ply

12	0
13	+45
14	−45
15	0

ℓ

← End Of Ply
← End Of Ply

16	0
17	0
18	0
19	90
20	0
21	0
22	0
23	90
24	0
25	+45
26	−45

Tool Surface (Ref)

Lam−A:5$\frac{3}{8}$
Lam−B:5$\frac{3}{8}$
Lam−A:5$\frac{7}{8}$
Lam−B:5$\frac{7}{8}$
Lam−A:25$\frac{1}{8}$
Lam−B:15$\frac{3}{8}$

Figure 3.5 Section A-A

3.7

Figure showing a composite laminate ply stack-up (Section A-A). The center column labeled C lists ply numbers 1 through 30 with their orientations:

Ply	Orientation
1	−45
2	+45
3	0
4	90
5	0
6	0
7	0
8	90
9	0
10	0
11	0
12	−45
13	+45
14	0
15	+45
16	−45
17	0
18	+45
19	−45
20	0
21	0
22	0
23	90
24	0
25	0
26	0
27	90
28	0
29	+45
30	−45

End Of Ply (at plies 12, 13, 18, 19 left side; 9 and 22 right side)

¢

Tool Surface (Ref)

Tool Surface

5 Section A-A

3.7

(C)				(C')	
−45			−45	1	
+45			+45	2	
0			0	3	
90			90	4	
0			0	5	
0			0	6	
0			0	7	
90			90	8	
0	End Of Ply →				
0			0	9	
0			0	10	
−45			−45	11	
+45			+45	12	
0			0	13	
+45			+45	14	
−45			−45	15	
0			0	16	
+45			+45	17	
−45			−45	18	
0			0	19	
0			0	20	
0	End Of Ply →				
90			90	21	
0			0	22	
0			0	23	
0			0	24	
90			90	25	
0			0	26	
+45			+45	27	
−45			−45	28	

Tool Surface (Ref)

6. 3 static tension specimens with PDO #2 discontinuities (Subassembly A-9).

7. Appropriate moisture control travelers (MC's), fiber volume specimens (FC's), transverse tension (TT's), longitudinal compression (LC's), and transverse compression (TC's) coupons were cut and tested as detailed for monitoring the moisture content and quality of the laminates and subassemblies.

8. Figures 3.6 and 3.7 show the configuration of the program static compression and R=10 compression-compression fatigue specimens without ply drop-offs and with ply drop-offs, respectively. Figure 3.8 shows the longitudinal static tension specimen configuration without and with ply drop-offs. Figure 3.9 shows the plain laminate transverse tensile specimen configuration.

3.2.2 Laminate Assembly A: Description

The following notes detail the laminate and specimen fabrication and related quality assurance:

1. After postcure, Laminate Assy.-A (Figure 3.3) was cut into subassemblies and Q.C. specimens as shown and one or more of the adjacent moisture control travelers (MC's) as required were attached to each subassembly with a wire. "Extra" material was stored in foil-plastic bags.

2. Subassemblies-1, -2, -4, -5, -7, & -8 had fiberglass tabs bonded onto them, back-to-back, along the 26 inch dimension on opposite edges in conformance with the tabs shown in Figures 3.6 and 3.7.

3. Subassemblies -3, -6, & -9 had fiberglass tabs bonded onto them, back-to-back, along the 3.5 inch dimension on opposite edges in conformance with the tabs shown in Figure 3.8.

4A. Quality control transverse tensile specimens were cut, tabbed, and tested per Figure 3.9 at RTD conditions and in accordance with Q.C. Instruction Sheet ID/CF No. 3*.

4B. Q.C. longitudinal compression specimens LC-1, -2, and LC'-3, -4, and LC"-5, -6 were cut and tested per Q.C. Instruction Sheet ID/CF NO.3* by ETL.

5. Balance of moisture control travelers (MC's) not used with subassemblies above were stored in plastic-foil bags for use with test series.

---

*See Appendix A
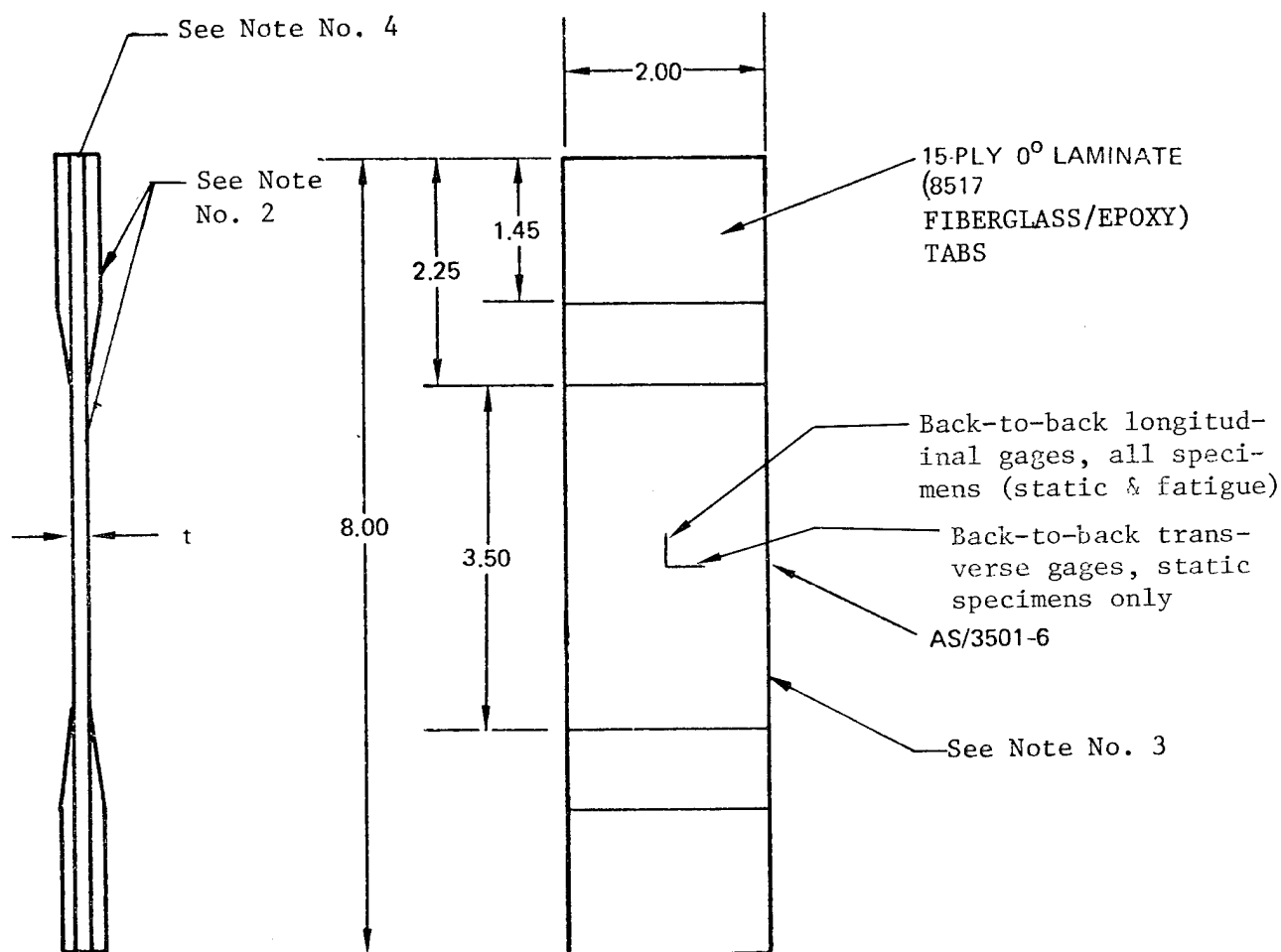
3.9

See Note No. 4

See Note No. 2

2.00

15-PLY 0° LAMINATE (8517 FIBERGLASS/EPOXY) TABS

1.45

2.25

8.00

t

3.50

Back-to-back longitudinal gages, all specimens (static & fatigue)

Back-to-back transverse gages, static specimens only

AS/3501-6

See Note No. 3

1. BOND 8517 TABS WITH AF-143 ADHESIVE.

2. SPECIMEN THICKNESS SHALL NOT VARY MORE THAN ±0.005 INCH FROM NOMINAL.

3. SPECIMEN LONGITUDINAL EDGES SHALL BE PARALLEL TO 0.005 INCH.

4. TOP END AND BOTTOM END SURFACES SHALL BE FLAT AND PARALLEL TO 0.001.

5. USE "ATMUR" FATIGUE AND STATIC TEST FIXTURES AS REQUIRED.

Figure 3.6   Test Specimen, Plain Laminate-Static And Fatigue
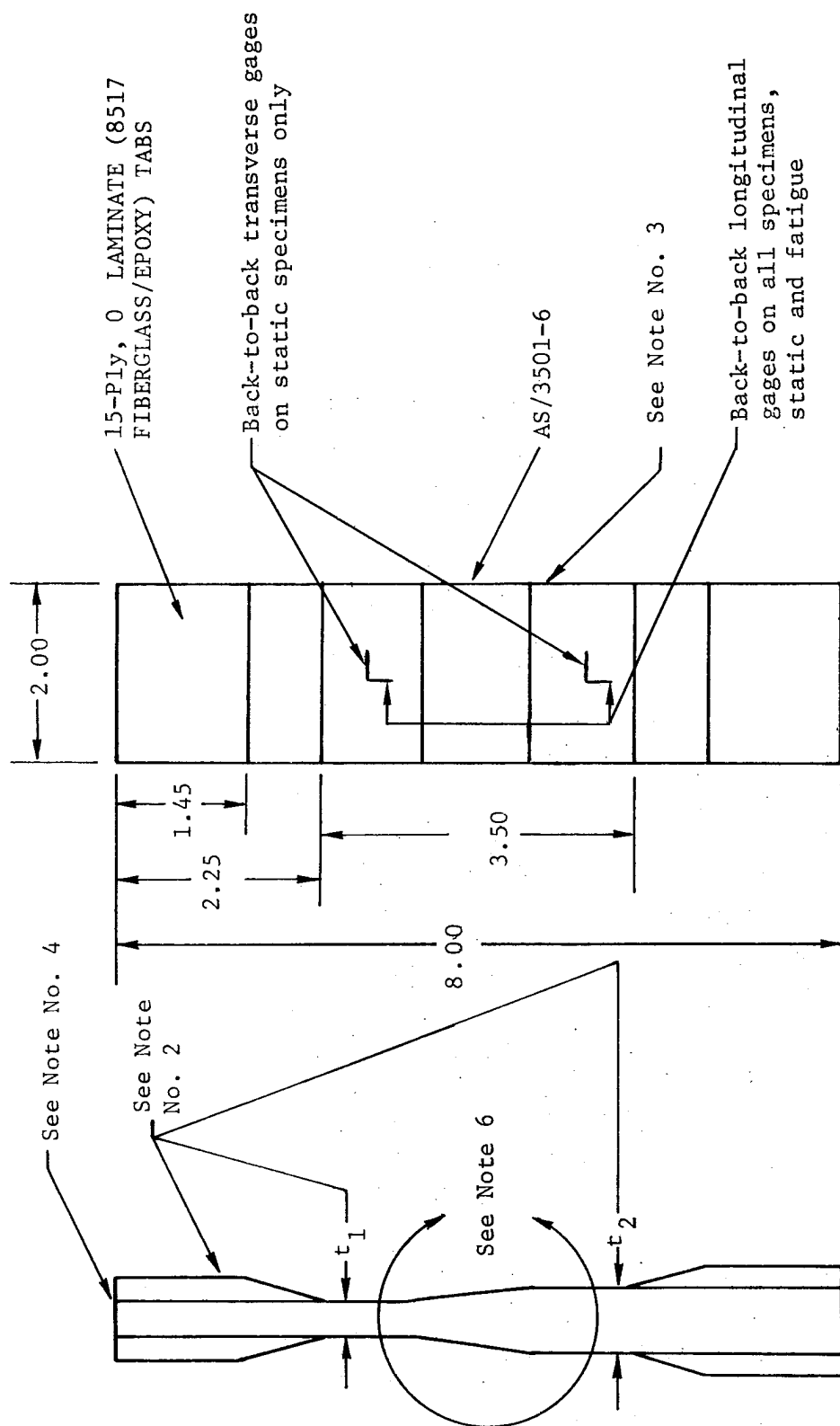
15-Ply, 0 LAMINATE (8517 FIBERGLASS/EPOXY) TABS

Back-to-back transverse gages on static specimens only

AS/3501-6

See Note No. 3

Back-to-back longitudinal gages on all specimens, static and fatigue

2.00

1.45

2.25

3.50

8.00

See Note No. 4

See Note No. 2

See Note 6

t_1

t_2

1. BOND 8517 TABS WITH AF-143 ADHESIVE.
2. SPECIMEN THICKNESS SHALL NOT VARY MORE THAN ± 0.005 INCH FROM NOMINAL.
3. SPECIMEN LONGITUDINAL EDGES SHALL BE PARALLEL TO 0.005 INCH.
4. TOP END AND BOTTOM END SURFACES SHALL BE FLAT AND PARALLEL TO 0.001 INCH.
5. USE "ATMUR" STATIC AND FATIGUE TEST FIXTURES AS REQUIRED.
6. SEE FIGURES 3.1 AND 3.2 FOR DETAILS.

Figure 3.7 Test Specimen, Ply Drop-Off – Static and Fatigue

3.11

Figure 3.8 Longitudinal Tensile Specimens – Laminate A

NOTES: (for A and B)

1. Bond 8517 tabs with AF-143 adhesive.

2. Specimen thickness shall not vary more than ± 0.005 inch from nominal.

3. Specimen longitudinal edges shall be parallel to 0.005 inch.

4. Top end and bottom end surfaces shall be flat and parallel to 0.010 inch.

5. Strain gages shall be Micromeasurements EA 03-250BF-350 or equivalent, located as shown.

6. Testing shall be in accordance with ASTM D-3039.

7. See Figures 3.1 and 3.2 for details.

A. Specimens from Subassemblies A-6 and A-9 (See Note No. 6 for testing instructions).

B. Specimens from Subassembly A-3 (See Note 6 for testing instructions).

3.12

15 Ply 0° Laminate
(8517 Fiberglass/Epoxy)
Tabs

See Note No. 4

Typ. 45°

See Note No. 1

See Note No. 2 (Typ)

2

5.0

Gr./Ep

0.5

See Note No. 5

10.0

$t_1, t_2,$ or t_3 (Lam. orientations c, c', or c")

See Note No. 3

1.00

NOTES:

1. Bond 8517 tabs with AF-143 adhesive.

2. Specimen thickness shall not vary more than ±0.005 inch from nominal.

3. Specimen longitudinal edges shall be parallel to 0.005 inch.

4. Top end and bottom end surfaces shall be flat and parallel to 0.010

5. Strain gages shall be Micro-Measurements EA 03-250BF-350 or equivalent, located as shown.

6. Testing shall be in accordance with ASTM D-3039.

Figure 3.9.   Transverse Tensile Specimens

6. Fiber volume, void volume, etc. tests were performed on all
    FC-, FC', and FC"-specimens per Q.C. Instruction Sheet ID/CF
    No. 3*.

7. Tabbed subassemblies - 1 thru -9 were ultrasonically inspected
    (nondestructively) with a C-scan readout per Q.C. Instruction Sheet
    ID/CF No. 4*.

8. After acceptance of the Q.C. physical and mechanical property
    tests and the NDI C-scan data by the program office, program
    specimen cutting was accomplished.

9. Tabbed subassemblies -1 and -2 were cut into 12 program compres-
    sion specimens each, per Figure 3.6. Specimens were numbered as
    follows: Laminate Assembly No. - Subassembly No. - Specimen No.(1-12).

10. Tabbed subassemblies -4, -5, -7 and -8 were cut into 12 compres-
    sion specimens each, per Figure 3.7. Specimens were numbered
    as follows: Laminate Assembly No. -Subassembly No. -Specimen
    No. (1-12).

11. Tabbed subassemblies -3, -6, and -9 were cut into 3 program
    tensile specimens, each per Figure 3.8, in accordance with the
    appropriate configuration. Specimens were numbered as follows:
    Laminate Assembly No. -Subassembly No. -Specimen No. (1-3).

12. Once cut, all program specimens were stored in foil-plastic
    bags until tested.

13. Program compression specimens from subassemblies -1, -2, -4, -5,
    -7, and -8 were delivered to the Engineering Test Laboratory
    (ETL) (3183/62) for testing.

14. Program tension specimens from subassemblies -3, -6, and -9
    were delivered to the Support Services Laboratory for testing.

3.2.3. Laminate Assembly B: Description

The following notes detail the laminate and specimen fabrication and
related quality assurance:

1. After postcure, Laminate Assy.-B (Figure 3.4) was cut into sub-
    assemblies and Q.C. specimens as shown and one or more of the
    adjacent moisture control travelers (MC's) as required were
    attached to each subassembly with a wire. "Extra" material
    was stored in foil-plastic bags.

2. Subassemblies -10, -11, -12, and -13 had fiberglass tabs bonded
    onto them, back-to-back, along the 26 inch dimension on
    opposite edges in conformance with the tab shown in Figure 3.2.

---

* Ibid

3. Q.C. transverse compression specimens TC-7, -8, and TC'-9, -10, and TC" -11, 12 were cut and tested per Q.C. Instruction Sheet ID/CF No. 3* by ETL.

4. Balance of moisture control traveler's (MC's) not used with assemblies above were stored in plastic foil bag for use with the test series.

5. Fiber volume, void volume, etc., tests were performed on all FC,- FC'-, and FC" -specimens per Q.C. Instruction Sheet ID/CF NO. 3.*

6. Tabbed subassemblies -10 thru -13 were nondestructively inspected (ultrasonically) with a C-scan readout per Q.C. Instruction Sheet ID/CF No. 4*.

7. After acceptance by the program office of the Q.C. physical and mechanical property tests and the NDI C-scan data, program specimen cutting was accomplished.

8. Tabbed subassemblies -10, -11, -12, and -13 were cut into 12 program compression specimens, each, per Figure 3.7. Specimens were numbered as follows: Laminate Assembly No. -Subassembly No. -Specimen No. (1-12).

9. Once cut, all program specimens were stored in foil-plastic bags until tested.

10. Program compression specimens from subassemblies -10, -11, -12, and -13 were delivered to the Engineering Test Laboratory for testing.

3.2.4 Material Acceptance Testing

The Hercules material certification**test results on their AS/3501-6 graphite/epoxy are summarized in Tables 3.2 and 3.3 and are found to conform to the requirements of Q.C. Instruction Sheet ID/CF No. 1 (Appendix A). Northrop prepreg acceptance test data performed in accordance with Northrop Specification NAS-1371, are presented in Table 3.4 and are found to conform to the requirements of Q.C. Instruction Sheet ID/CF No. 1 (Appendix A). Gel time tests at 350°F as described in Northrop Specification NAI-1371 are also presented for information purposes.

The cured laminate acceptance test data performed at Northrop is presented in Table 3.5. Note that the specific gravity, fiber volume %, and transverse tension strain exceed the requirements set forth in Q.C.

---

*Ibid
**See Appendix B

TABLE 3.2 HERCULES CERTIFICATION* TEST DATA ON FIBERS AND LAMINATE
(AS1 Fibers and AS/3501-6 Graphite/Epoxy Laminate)[a]

PROPERTY	GRAPHITE FIBERS [c,d,e]	AVERAGE/MINIMUM VALUE 0° DIRECTION $(0)_c$ LAMINATE [f]	TEST ENVIRONMENT
Tensile Strength, ksi	466.0	253/222	RTD
Tensile Modulus, 10^6 psi	33.9	20.7/20.5	RTD
Elongation, 10^3 μ-in/in	—	12.4/10.6	RTD
Short Beam Shear, ksi	—	20.1/20.0	RTD
Short Beam Shear, ksi	—	13.3/13.0	250^oF-D
Short Beam Shear, ksi	—	9.8/9.6	250^oF-W[b]

a. Prepreg Lot 1261/7-A
b. After 24 hr water boil
c. Fiber Lot 136-1

d. Fiber Density = 0.0648 lbs/in^3 (S.G. = 1.7945)
e. Fiber Weight/Unit Length = 45.09 lbs/in X 10^{-6}
f. Cured laminate ply thickness = 0.0053 in.

*See Appendix B

3.16

TABLE 3.3 HERCULES CERTIFICATION* TEST DATA ON PREPREG LOT 1261/7A*
(AS/3501-6 Graphite/Epoxy)

LOT NO.	AVERAGE/MINIMUM		RESIN FLOW, %	VOLATILES %	TACK
	RESIN CONTENT BY WEIGHT, %	FIBER AREAL WEIGHT, gm/m^2			
1261/7-A	43.3/43.2	147/146	17.5	0.96	Conforms

*See Appendix B
**Fiber Lot: 136-1

TABLE 3.4 PREPREG ACCEPTANCE TESTING AT NORTHROP
(Hercules AS/3501-6)

Test Procedure: Northrop Specification NAI-1371

STATIS-TICAL VALUE	RESIN CONTENT %	VOLATILE % @ $350^{O}F$	FLOW %	$350^{O}F$ GEL TIME, MIN	TACK	FIBER WT/ AREA
Mean	43.82	0.70	26.86	14.83	Pass	150.94
S.D.	3.17	0.09	1.74	0.29	—	10.60
C.V.	0.072	0.130	0.065	0.020	—	0.070

_____

Notes:

a. Prepreg Lot No. 1261/7-A

b. Resin Lot: 064K and 064L

c. Fiber Lot: 136-1

d. Mfg. Date 7/12/79

e. Test Data 8/8/79

f. No. of Determinations, N = 3

g. Acceptance Requirements: Q.C. Instruction Sheet ID/CF No. 1 (Appendix A)
    & MCAIR P.S. 21332

h. Ref: Laminate Acceptance Test Panel ACL-4177
          Laminate F.V. = 64.49% by Volume
          Laminate Resin Content = 28.52% by Wt.

TABLE 3.5 LAMINATE ACCEPTANCE TESTING AT NORTHROP -RTD (Hercules AS/3501-6 $[0]_{16T}$ Laminate ACL-4177)

Test Procedure: Northrop Specification IT-58 and Q.C. Instruction Sheet ID/CF No. 1 (App. A).

STATISTICAL VALUE	RESIN CONTENT % BY WT	SPECIFIC GRAVITY	FIBER VOL. %	VOID VOL. %	TRANSVERSE TENSION			LONGITUDINAL/FLEXURE		SHORT BEAM SHEAR, ksi	PREPREG MAT'L LOT/ROLL
					STR ksi	STRAIN μ-in/in	MOD 10^6 psi	STR ksi	MOD 10^6 psi		
Mean	28.52	1.624	64.49	0	7970	6287	1.28	235.1	17.2	18.930	1261/7A
S.D.	0.43	0.002	0.46	0	1635	1356	0.01	12.6	0.4	0.187	—
C.V.	0.015	0.001	0.007	0	0.205	0.216	0.008	0.054	0.021	0.010	—
N	2	2	2	2	3	3	3	3	3	5	—

Notes: Testing Date: 8/24/79 - 8/28/79

Acceptance Requirements: Q.C. Instruction Sheet No. 1 (Appendix A) and MCAIR MMS-549

Averaged Laminate Thickness = 0.083 in.

Instruction Sheet ID/CF No. 1 (Appendix A). Also, note that short beam shear test data exceed the requirements set forth in McAir MMS-549.

3.3 QUALITY ASSURANCE

Results of the physical property measurements on Laminate A are presented in Table 3.6, whereas, those on Laminate B are given in Table 3.7. Laminate A fiber volumes are: 54.49% for the 30-ply section, 57.46% for the 28-ply section, and 58.34% for the 26-ply section with related thicknesses of 0.179 in., 0.158 in., and 0.146 in. Samples from each of the different areas of the same thickness show consistent fiber volume properties with little scatter. Void volumes are 0%. For Laminate B the fiber volumes are: 56.11% for the 30-ply section, 57.82% for the 28-ply section, and 58.50% for the 26-ply section with the related thicknesses being 0.180 in., 0.162 in., and 0.153 in. Void volumes are 0%.

The Q.C. destructive test mechanical properties of the two laminate assemblies were determined using two longitudinal compression (Laminate A) and two transverse compression (Laminate B) specimens, both at each of three thicknesses, with results shown in Table 3.8. Note that all compression specimens exceed the specification requirement of -94 ksi longitudinal and -50 ksi transverse established in Q.C. Instruction Sheet ID/CF No. 3 (see Appendix A). Transverse mechanical property tension tests were performed on Laminate A for a quality assurance check on mechanical properties with results shown in Table 3.9. Also, note that all transverse tension test specimens exceed the specification minimum requirement of 30 ksi established in Q.C. Instruction Sheet ID/CF No. 3 (See Appendix A).

After the two laminates (A and B) were fabricated (per Process Instruction Sheet ID/CF No. 1, Appendix A) and cut into subassemblies in accordance with Figures 3.3 and 3.4, they were nondestructively inspected (per Q.C. Instruction Sheet ID/CF No. 4). This nondestructive inspection utilized the ultrasonic reflector plate technique* with a C-scan printout**. The C-scan was used to provide a record of laminate subassembly quality and was not a vehicle for "rejecting" parts. The sensitivity of the C-scan

---

*See Appendix F
**See Appendixes A and F

TABLE 3.6 LAMINATE A (ACL-4210) PHYSICAL PROPERTIES* (Void Volume = 0%)
AS/3501-6 Graphite/Epoxy Prepreg Lot 1261/7-A

SPECIMEN NO.	FIBER VOLUME %	NO. OF PLIES	RESIN CONTENT % BY WT.	SPECIFIC GRAVITY	THICKNESS, IN.
FC-1	54.86	30	36.97	1.5668	0.178
-2	54.94		36.91	1.5676	0.176
-3	53.98		37.79	1.5618	0.180
-4	54.14		37.76	1.5655	0.179
-5	54.42		37.35	1.5635	0.180
-6	54.22		37.55	1.5628	0.180
-7	54.61		37.18	1.5648	0.179
-8	54.74		37.05	1.5653	0.179
M	54.49	30	37.37	1.5648	0.179
S.D.	0.35		0.38	0.0020	0.001
C.V.	0.006		0.010	0.001	0.008
FC-9	57.01	28	34.99	1.5785	0.157
-10	57.44		34.62	1.5814	0.158
-11	57.74		34.31	1.5821	0.159
-12	57.64		34.41	1.5818	0.156
M	57.46	28	34.58	1.5810	0.158
S.D.	0.32		0.30	0.0017	0.001
C.V.	0.006		0.009	0.001	0.008
FC-13 A	58.28	26	33.84	1.5856	0.145
-14 A	58.77		33.37	1.5876	0.147
-15 A	57.59		34.42	1.5807	0.146
-16 A	58.70		33.43	1.5812	0.146
M	58.34	26	33.76	1.5853	0.146
S.D.	0.54		0.48	0.0032	0.001
C.V.	0.009		0.014	0.002	0.006

* Fiber Specific Gravity = 1.80

  Resin Matrix Specific Gravity = 1.26

TABLE 3.7 LAMINATE B (ACL-4211) PHYSICAL PROPERTIES[*] (Void Volume = 0%)
AS/3501-6 Graphite/Epoxy Prepreg Lot 1261/7A

SPECIMEN NO.	FIBER VOLUME %	NO. OF PLIES	RESIN CONTENT % BY WT.	SPECIFIC GRAVITY	THICKNESS, IN.
FC-13B	61.39	30	32.13	1.6282	0.180
-14B	55.15		36.66	1.5674	0.179
-15B	54.42		37.60	1.5646	0.181
-16B	53.49		38.17	1.5573	0.182
M	56.11	30	36.14	1.5794	0.180
S.D.	3.58		2.74	0.0328	0.001
C.V.	0.064		0.076	0.021	0.007
FC-17	58.34	28	33.76	1.5855	0.162
-18	57.79		34.42	1.5836	0.162
-19	57.92		34.18	1.5838	0.163
-20	57.23		34.81	1.5801	0.163
M	57.82	28	34.29	1.5832	0.162
S.D.	0.46		0.44	0.0023	0.001
C.V.	0.008		0.013	0.001	0.004
FC-21	58.30	26	33.80	1.5859	0.153
-22	57.96		34.22	1.5831	0.153
-23	58.95		33.27	1.5903	0.154
-24	58.79		33.41	1.5891	0.152
M	58.50	26	33.68	1.5871	0.153
S.D.	0.45		0.43	0.0032	0.001
C.V.	0.008		0.013	0.002	0.005

[*]Fiber Specific Gravity = 1.80

Resin Specific Gravity = 1.26

TABLE 3.8 QUALITY CONTROL COMPRESSION DATA FROM LAMINATE ASSEMBLIES A AND B – RTD.

Lam. Assy	Specimen Number ***	Primary Orientation of Laminate Assembly	No. of Plies	Fbr Vol %	Width, in.	Thickness, in.	Area, in²	Failure Load, kips	Failure Stress* ksi	Running Load, kips/in	Failure Mode**
A	LC-1	$[(\pm45)_5/0_{16}/90_4]_c$	30		1.9911	0.1727	0.3439	-37.900	-110.199	-19.035	DCS, DL→N-EOS
	LC-2				1.9909	0.1742	0.3468	-36.700	-105.822	-18.434	DL→E to M, DCS→N-EOS
	Avg.			54.49		0.1734			-108.010	-18.734	DCS→N-EOS, DL→E to M
	LC'-3	$[(\pm45)_5/0_{14}/90_4]_c$	28		1.9905	0.1453	0.2892	-35.200	-121.737	-17.684	DL, DCS→N-EOS
	LC'-4				1.9904	0.1564	0.3112	-36.400	-116.954	-18.288	DL→E to M, DCS→N-EOS
	Avg.			57.46		0.1508			-119.346	-17.986	DL→E to M, DCS→N-EOS
	LC"-5	$[(\pm45)_3/0_{16}/90_4]_c$	26		1.9903	0.1428	0.2843	-37.000	-130.151	-18.590	DCS, DL→N-EOS
	LC"-6				1.9906	0.1430	0.2847	-32.400	-113.795	-16.276	DCS, DL→N-EOS
	Avg.			58.34		0.1429			-121.973	-17.433	DCS, DL→N-EOS
B	TC-7	$[(\pm45)_5/0_{16}/90_4]_c$	30		1.9902	0.1818	0.3618	-27.400	-75.741	-13.767	DCS, DL→MOS
	TC-8				1.9902	0.1812	0.3606	-29.500	-81.801	-14.822	DCS, DL→MOS
	Avg.			56.11		0.1815			-78.771	-14.294	DCS, DL→MOS
	TC'-9	$[(\pm45)_5/0_{14}/90_4]_c$	28		1.9907	0.1670	0.3324	-26.100	-78.510	-13.111	DCS, DL→N-EOS
	TC'-10				1.9906	0.1670	0.3324	-26.600	-80.031	-13.363	DCS, DL→MOS
	Avg.			57.82		0.1670			-79.270	-13.237	DCS, DL→M to E
	TC"-11	$[(\pm45)_3/0_{16}/90_4]_c$	26		1.9907	0.1551	0.3088	-21.900	-70.913	-11.001	DCS, DL→MOS
	TC"-12				1.9909	0.1532	0.3050	-23.300	-76.391	-11.703	DL, DCS→M to E
	Avg.			58.50		0.1542			-73.652	-11.352	DCS, DL→M to E

*Minimum requirements per QC Instruction Sheet ID/CF No. 3 (Appendix A) are:
  Longitudinal Compression (LC) = -94 ksi and Transverse Compression (TC) = -50 ksi

**Failure modes and locations: DCS – diagonal compression shear   M to E – middle to end
       EOS – end of specimen   DL – delamination
       MOS – middle of specimen   N – near

***For locations on laminate assemblies, see Figures 3.3 and 3.4.

TABLE 3.9 QUALITY CONTROL TRANSVERSE* TENSION DATA FROM LAMINATE A – RTD.

Specimen No.	Primary** Orientation of Laminate Assembly	# of Plies	V_f %	Width, in.	Thickness, in.	Area in²	Proportional Limit Stress, ksi	Proportional Limit Strain, 10⁻³ units	Failure*** Stress ksi	Failure*** Strain, 10⁻³ units	E_y, 10⁶ psi	ν_{yx} Poisson's Ratio	Failure Mode**
TTC-1	$[(\pm45)_5/0_{16}/90_4]_c$	30		1.072	0.175	0.1876	21.322	4.915	35.821	9.550	4.35	0.145	EOT-2, 3A, 1 order
-2				1.068	0.176	0.1880	20.479	4.600	44.043	11.780	4.38	0.155	" " " "
-3				1.062	0.176	0.1869	22.124	4.910	45.158	11.830	4.40	0.146	" " " "
-4				1.068	0.176	0.1880	20.824	4.600	40.106	9.930	4.44	0.144	GL -2
Mean			54.49		0.176		21.187	4.756	41.282	10.772	4.39	0.148	EOT/GL-2, 3A, 1 order
S.D.					–		0.714	0.180	4.237	1.202	0.038	0.005	
C.V.					–		3.4 %	3.8 %	10.3 %	11.2 %	0.9 %	3.4 %	
TTC'-5	$[(\pm45)_5/0_{14}/90_4]_c$	28		1.059	0.156	0.1652	25.424	5.500	38.317	8.680	4.54	0.152	EOT-2, 3B, 1 order
-6				1.065	0.152	0.1619	27.795	5.780	39.716	8.840	4.76	0.164	" " " "
Mean			57.46		0.154		26.610	5.640	39.016	8.760	4.65	0.158	EOT-2, 3B, 1 order
TTC"-7	$[(\pm45)_3/0_{16}/90_4]_c$	26		1.061	0.143	0.1517	21.424	4.510	42.716	10.880	4.68	0.105	EOT-2, 3C, 1 order
-8				1.074	0.142	0.1525	23.279	5.070	36.525	8.450	4.55	0.100	" " " "
Mean			58.34		0.142		22.352	4.790	39.620	9.665	4.62	0.102	EOT-2, 3C, 1 order

*All specimens have loading direction 90° to primary axis of orientation

** EOT – End of tab failure location
    GL – Gage Length
    1 – Failure in 0° plies, net tension perpendicular to loading direction
    2 – Failure in 90° plies, net tension perpendicular to loading direction
    3A – Failure in ±45° plies, large delamination and tension at ±45° to loading direction
    3B – Failure in ±45° plies, medium delamination and tension at ±45° to loading direction
    3C – Failure in ±45° plies, small delaminations and tension at ±45° to loading direction.

Note: Bending, as recorded by back-to-back longitudinal strain gages, was within ± 5% of the mean strain level.

***Minimum requirements per Q.C. Instruction Sheet 1D/CF No. 3 (App. A) are: Transverse Tension (TT) = 30 ksi

is important in detecting possible defects in the laminate such as porosity, voids, delaminations and foreign inclusions. To set the proper sensitivity on the instrumentation, a small piece of lead tape on the back side of a subassembly was used as the defect standard. The thirteen subassemblies cut from the two laminates were ultrasonically inspected with a C-scan readout. Table 3.10 presents the results of the ultrasonic inspection along with the Q.C. physical and mechanical property results for each subassembly. Note that there are two C-scans of each subassembly, one being at a more sensitive setting (6 dB) than the other (0 dB). All of the C-scans at the less sensitive setting (0 dB) showed the subassemblies to be of high quality with no defect areas. Inspection of these C-scans reveals several characteristics typical of the subassemblies. The light areas on the scans which show reduced signal transmission are assumed to be resin-rich pockets, because of the similarity with C-scans that were correlated with photomicrographs in Section 3 of Ref. (1).

For some reason the 2 ply-drop off discontinuity (PDO #1), $\copyright$ - $\copyright'$, was not picked up in Laminate A by the ultrasonic C-scan but was picked up in Laminate B. The 4 ply drop-off discontinuity (PDO #2), $\copyright$ - $\copyright''$, was picked up by the C-scan in both Laminates A and B. There appears to be a weak, direct, correlation between the fiber volume percent and the Q.C. longitudinal compression results. Both these properties appear to have a weak correlation to the 6 dB C-scan results. Both of these weak correlations are an indication of some degree of resin rich areas and not defects. From this it can be concluded that the 0 dB (less sensitive) setting was sufficient to determine that these subassemblies were defect free, while the more sensitive setting of 6 dB appears to hold promise for finding resin rich areas that cause small to medium decreases in fiber volume percent and longitudinal compression strength on multi-directional laminates such as those used herein.

TABLE 3.10 - SUMMARY OF ULTRASONIC INSPECTION RESULTS AND Q.C. DESTRUCTIVE TESTS FOR EACH SUBASSEMBLY

Item No.	Sub-Assembly Identification	Laminate Assembly Identification	Discontinuity Configuration	Sensitivity Setting (dB)	Sensitivity Signal Transmission Through the Thickness 80-84% (Poor)	85-89% (Fair)	90-94% (Good)	95-100% (Excellent)	Ply Drop-off Visible?	Fiber Volume Percent Mean	S.D.	C.V.	n	Q.C. Compression RTD-Longitudinal (KSI)	RTD-Transverse (KSI)	RTD Q.C. Transverse Tension (KSI)
1	4210-1	A	© Plain Laminate	0				X	--	54.64	0.33	0.006	4	-108.01	--	40.49
				6	X				--							
2	4210-2	A	© Plain Laminate	0				X	--	54.36	0.36	0.007	4	-108.01	--	42.07
				6				X	--							
3	4210-3	A	© Plain Laminate	0				X	--	54.49	0.35	0.006	8	-108.01	--	41.28
				6	X				--							
4	4210-4	A	© - ©', PDO No. 1	0				X	No	56.06	1.35	0.024	4	-119.35	--	37.07
				6				X	No							
5	4210-5	A	© - ©', PDO No. 1	0				X	No	55.88	2.10	0.038	4	-119.35	--	41.88
				6		X			No							
6	4210-6	A	© - ©', PDO No. 1	0				X	No	55.97	1.64	0.029	8	-119.35	--	39.47
				6	X				No							
7	4210-7	A	© - ©", PDO No. 2	0				X	Yes	56.45	2.41	0.043	4	-121.97	--	43.94
				6				X	Yes							
8	4210-8	A	© - ©", PDO No. 2	0				X	Yes	56.41	2.06	0.036	4	-121.97	--	38.32
				6			X		Yes							
9	4210-9	A	© - ©", PDO No. 2	0				X	No	56.41	2.08	0.037	8	-121.97	--	41.13
				6			X		Yes							
10	4211-10	B	© - ©', PDO No. 1	0				X	Yes	58.17	2.56	0.044	4	--	-78.09	--
				6		X			Yes							
11	4211-11	B	© - ©', PDO No. 1	0				X	Yes	55.76	2.14	0.038	4	--	-78.09	--
				6		X			Yes							
12	4211-12	B	© - ©", PDO No. 2	0				X	Yes	58.20	2.55	0.044	4	--	-76.37	--
				6		X			Yes							
13	4211-13	B	© - ©", PDO No. 2	0				X	Yes	56.44	2.84	0.050	4	--	-76.37	--
				6				X	Yes							

SECTION 4

EXPERIMENTAL METHODS

4.1 GENERAL

The purpose of this section is to describe in detail the specimens, fixtures, instrumentation and testing procedures used in the experimental program. Section 4.2 covers specimens and fixtures, and instrumentation is presented in Section 4.3. Testing procedures are detailed in Section 4.4, and moisture conditioning is discussed in Section 4.5.

4.2 SPECIMENS AND FIXTURES

Specimens tested in this program had a plain laminate ply orientation code of $[(\pm45)_5/0_{16}/90_4]_c$ with ply drop-off discontinuity orientation codes of $[(\pm45)_5/0_{14}/90_4]_c$ and $[(\pm45)_3/0_{16}/90_4]_c$. The discontinuities in the specimens were introduced by decreasing the number of plies in a specimen from 30 (plain laminate) to 28 (ply drop-off No. 1) or to 26 (ply drop-off No. 2). Figures 3.1 and 3.2 present the physical details of ply drop-off numbers 1 and 2.

For quality control testing in static compression, the ETL specimen and fixture shown in Figure 4.1 was used. For program static, fatigue, and residual strength testing in compression, the specimens detailed in Figures 3.6 and 3.7 were used. For program tensile testing the specimen used is· shown in Figure 3.8. Figure 4.2 presents the test fixture used for fatigue testing. The specimen and an exploded view of the jig are shown in Figure 4.3. This fixture was used for R=10 compression-compression fatigue testing of the laminate specimens. An overall view is shown in Figure 4.4. All program static and residual strength tests were performed in the same fixture used in fatigue testing.

4.3 INSTRUMENTATION

Strain gages were used on all specimens requiring instrumentation. The gages were 350 ohm with a Type 03 (micromeasurements designation) compat-

UNLESS OTHERWISE SPECIFIED, 0.XX DIMENSION SHALL
            BE ± 0.30 INCH
            0.XXX DIMENSION SHALL
            BE ± 0.010 INCH

1. TOP AND BOTTOM SURFACES SHALL BE FLAT AND
   PARALLEL TO 0.005 INCH.

2. SPECIMEN THICKNESS SHALL NOT VARY MORE THAN
   0.005 INCH FROM NOMINAL.

3. SPECIMEN LONGITUDINAL EDGES SHALL BE PARALLEL
   TO ± 0.003 INCH.

4. FOR LONGITUDINAL TEST SPECIMENS, 0° FIBERS
   PARALLEL TO 3.000 INCH SIDES.

5. FOR TRANSVERSE TEST SPECIMENS/0° FIBERS PERPEN-
   DICULAR TO 3.000 INCH SIDES.

STRAIN GAGES, IF SPECIFIED
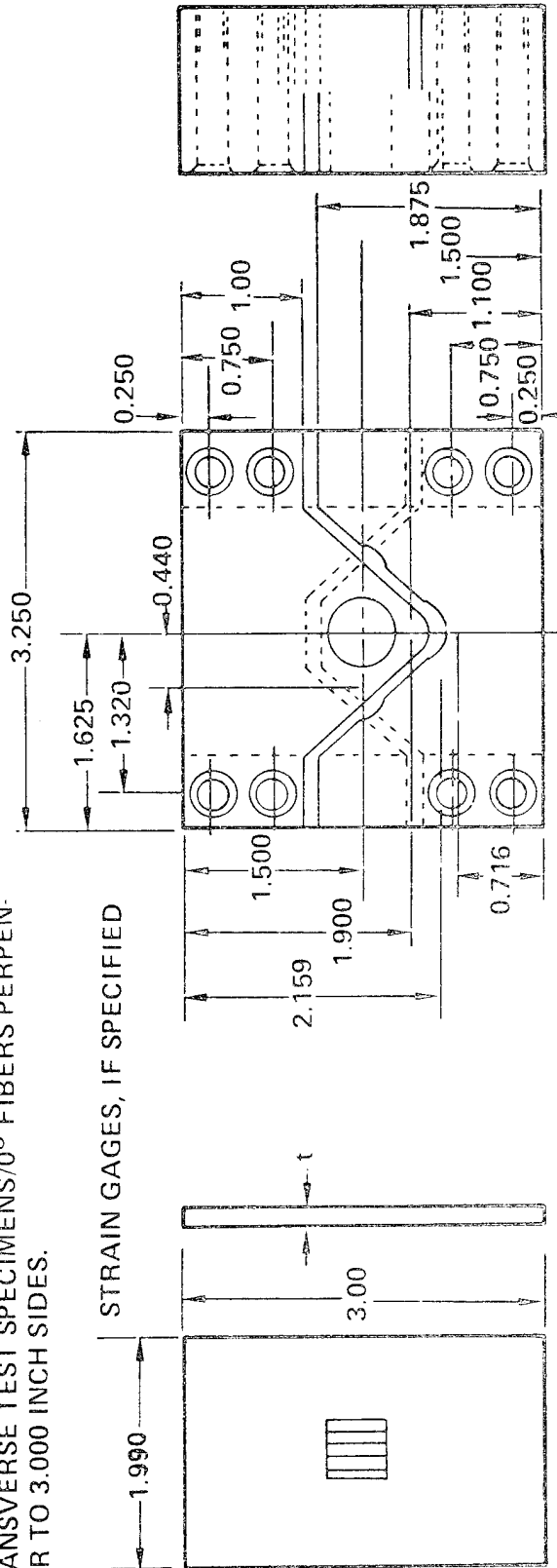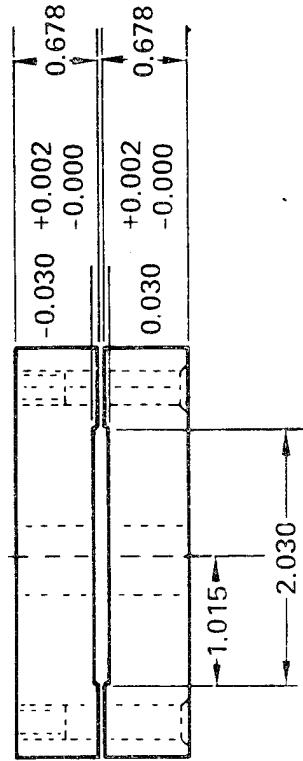
Figure 4.1 Static Test Specimen and Fixture.

4.2
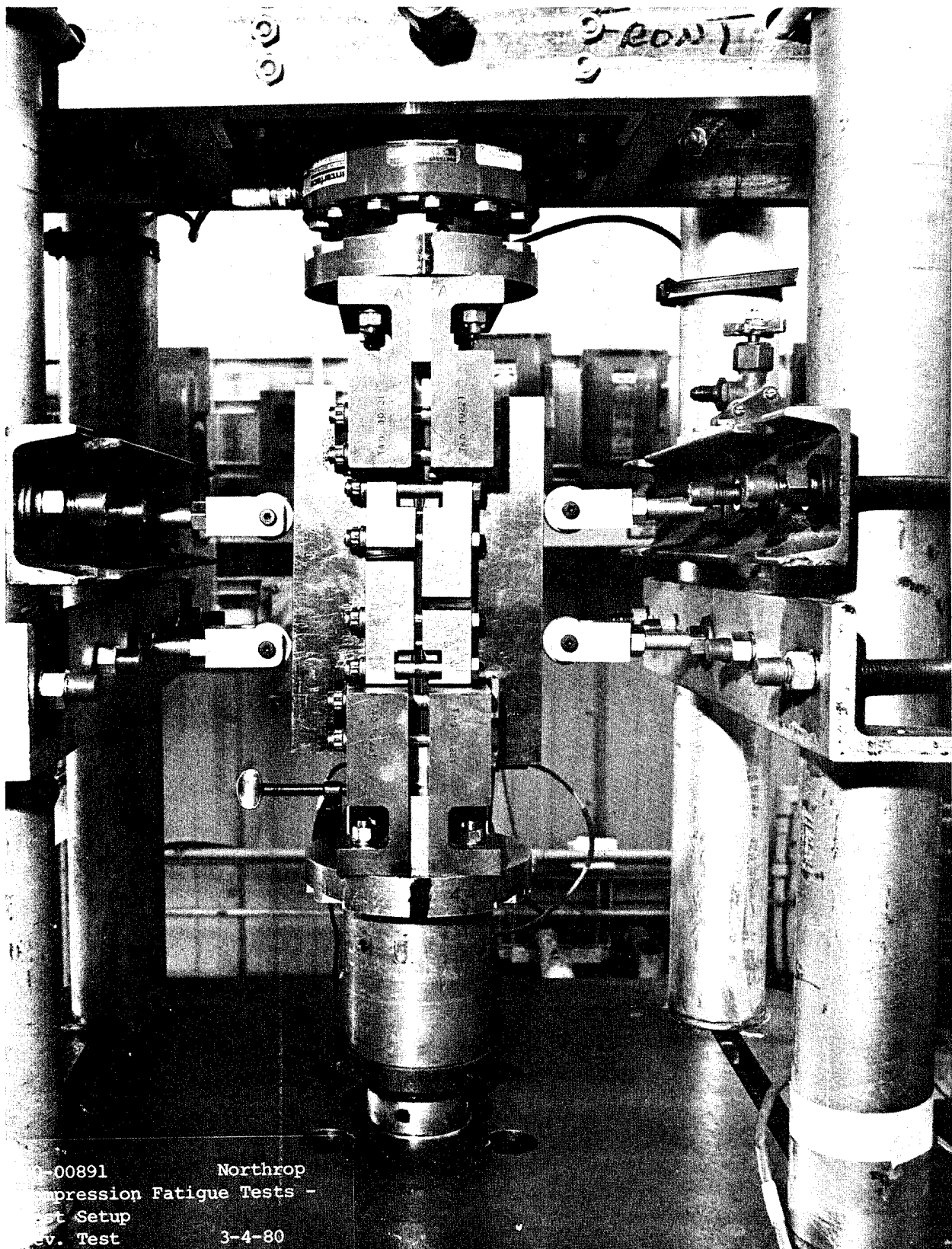
Figure 4.2 Test Fixture For Fatigue Testing
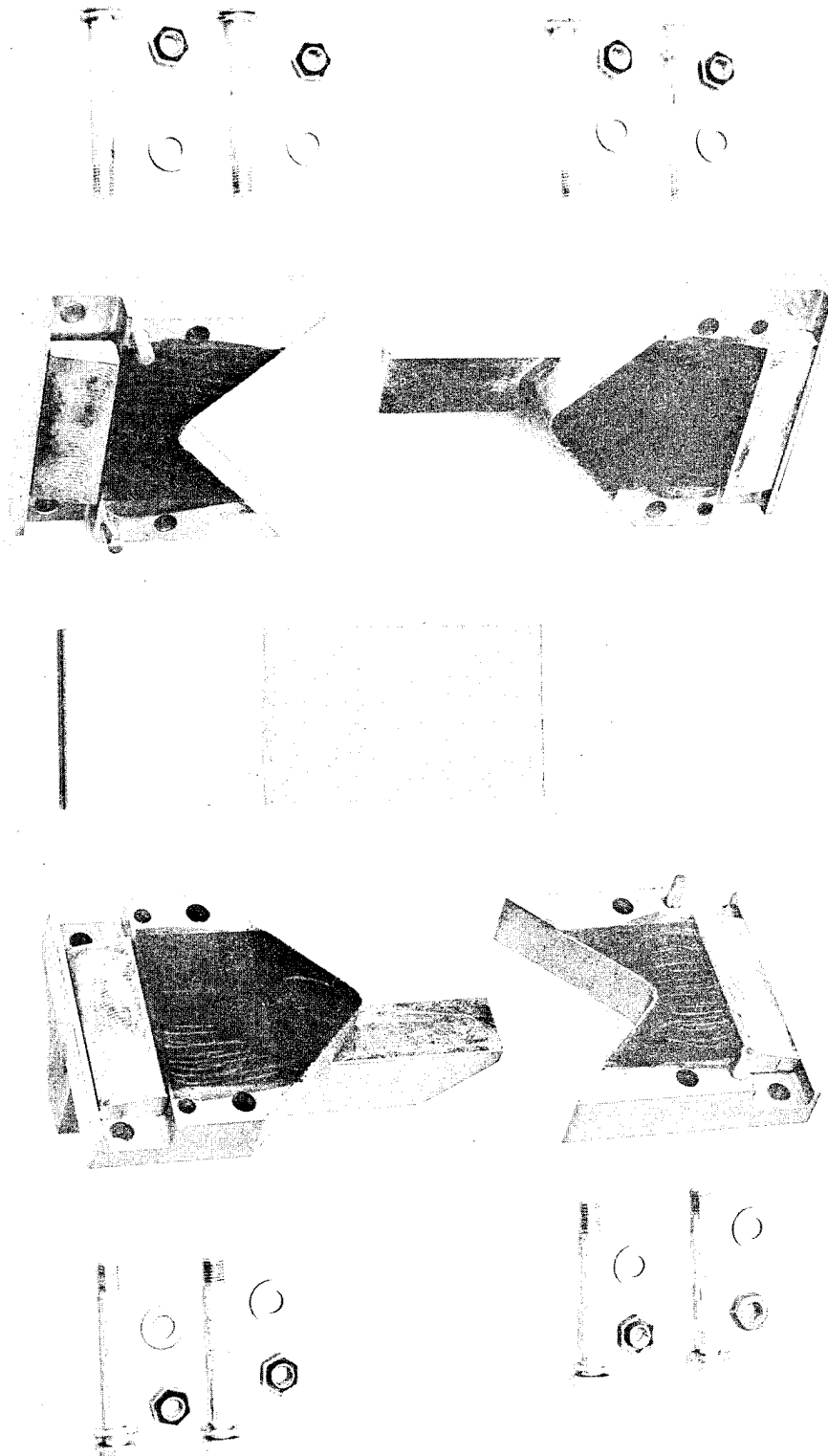
Figure 4.3   Compression Fatigue Support Fixture
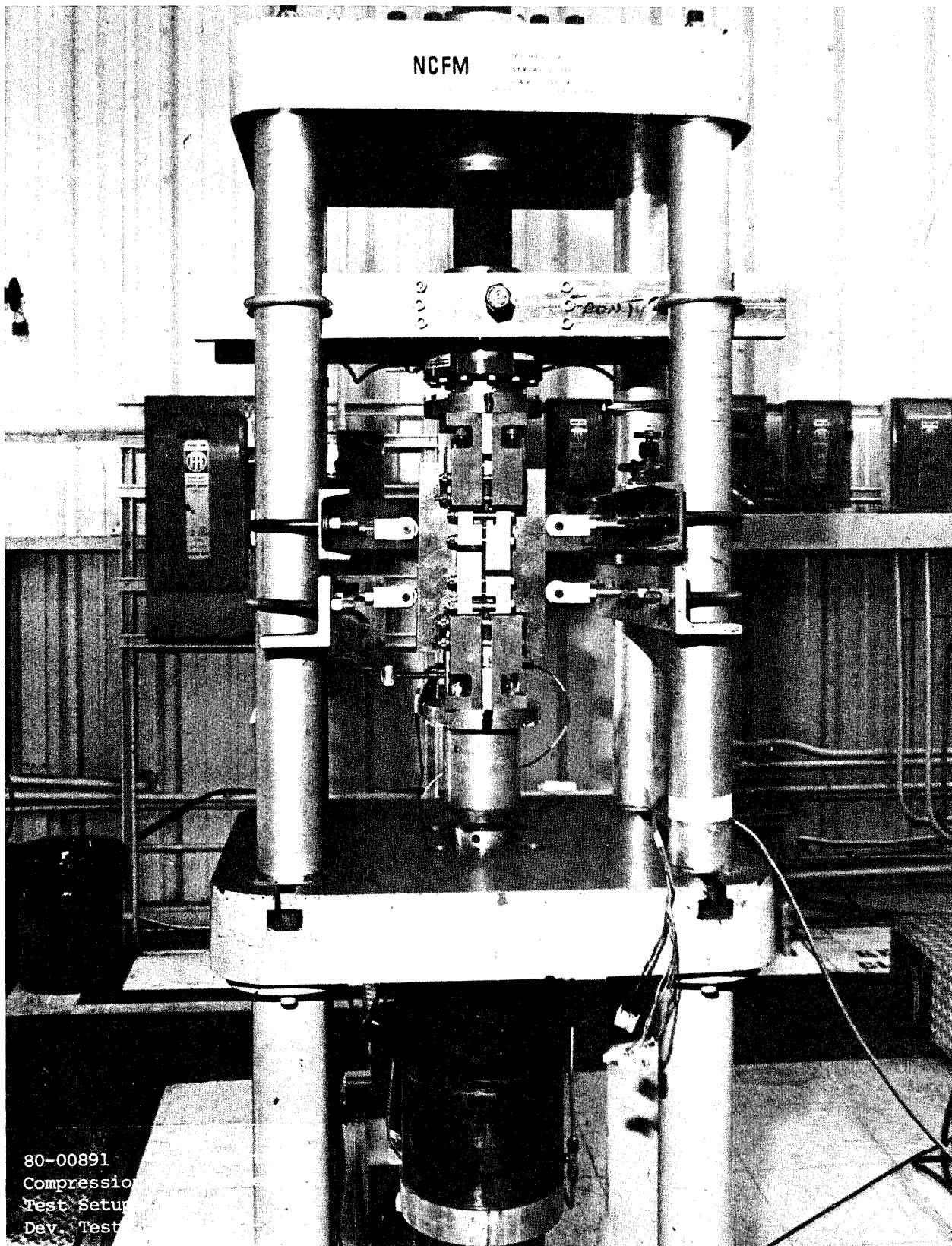
Figure 4.4 Overall View of Fatigue Set Up

4.5

ible backing. On the wet specimens, the gages were installed after moisture conditioning. Loads and strains were recorded using a "stop and read" digital strain indicator or an SR-4 visual strain indicator.

4.4 TESTING

All compression (static and fatigue) testing was performed by the Northrop Engineering Test Laboratory and all tension testing was performed by the Northrop Materials Research Laboratory.* For the static and residual strength tests, the specimens were loaded in constant magnitude increments. The magnitude of the increments varied depending upon the specimen being tested. Load verses strain data was recorded to failure. The program test matrix, showing the test series matchup with the specimen type, is given in Table 4.1. Table 4.2 presents the Test Series/Fixture matchup.

Fatigue loading was as follows:

a. Constant amplitude, constant frequency sine wave form fatigue loading was used.

b. The tests were conducted with air blowing over the specimens in order to keep the temperature rise below 5^{0}F. Frequency was 10 Hz.

c. Strain (stress) ratio R=10 was used on all tests. Minimum strain (maximum compression strain) was -6000 μin/in or (-5000 μin/in for 218^{0}FW, see Table 4.3) on the first specimen of each group of 10 tested. Subsequent testing was at higher or lower strain levels depending on whether the specimen failed before reaching 1.25×10^{6} cycles or runout at that level. This was done to provide an adequate distribution of data points on the S-N curves.

d. Specimens were run to 1.25×10^{6} cycles or failure, and those that ranout without failure were residual strength tested.

e. Strain levels used in set-up were converted to related load levels for load controlled fatigue testing.

_____

* Within this laboratory the Support Service Laboratory performed the testing.

TABLE 4.1   PROGRAM TEST MATRIX FOR STATIC AND FATIGUE TESTING

Test Series	Environmental Condition	Type of Loading	Static Test Cond.	Fatigue Test Cond.*	No. of Replicates	No. Specs to be Strain Gaged**	No. of M.C. Travelers	Type of Mechanical Test Spec.	Discontinuity Configuration	ACL No. Ref.	Sub-Assy No.	Specimen Numbers	To be Performed by
I	Wet	Static	-65FW	--	3	3	1	Compression Per Fig.3.6	Plain ©	4210	A-1	1,6,17,22	ETL
II		Fatigue		-65FW	9	9	1				A-2	2-5,12-16	
III				218FW	10	10	1					7-11,18-21	
Subtotal					22	22	3						
IV	Wet	Static	-65FW	--	3	3	1	Compression Per Fig 3.7	©-©'PDO#1	4210	A-4	1,3,5	ETL
V	Dry		RTD	--	3	3	1				A-4/A-5	12,14,16	
VI	Wet		RTW	--	2	2	1			4210/4211	A-5/B-10	23,25,27	
VII	Wet		218FW	--	2	2	1			4211	B-10/B-11	34,36,38	
VIII		Fatigue		-65FW	8	8	1			4210	A-4	2,4,6-11	
IX	Dry			RTD	8	8	1				A-5	13,15,17-21	
X	Wet			RTW	8	8	1			4210/4211	A-5/B-10	24,26,28-33	
XI	Wet			218FW	8	8	1			4211	B-10/B-11	35,37,39-44	
Subtotal					42	42	8						
XII	Wet	Static	-65FW	--	2	2	1	Compression Per Fig 3.7	©-"©PDO#2	4210	A-7	1,3,5	ETL
XIII	Dry		RTD	--	3	3	1				A-7/A-8	12,14,16	
XIV	Wet		RTW	--	2	2	1			4210/4211	A-8/B-12	23,25,27	
XV	Wet		218FW	--	3	3	1			4211	B-12/B-13	34,36,38	
XVI		Fatigue		-65FW	8	8	1			4210	A-7	2,4,6-11	
XVII	Dry			RTD	8	8	1				A-8	13,15,17-22	
XVIII	Wet			RTW	8	8	1			4210/4211	A-8/B-12	24,26,28-33	
XIX	Wet			218FW	8	8	1			4211	B-12/B-13	35,37,39-44	
Subtotal					42	42	8						
XX	Dry	Static	RTD	--	3	3	1	Tension per Figure 3.8B	Plain ©	4210	A-3	1-3	MRL
XXI	Dry			--	3	3	1	Tension per Figure 3.8A	©-©'PDO#1		A-6	1-3	
XXII				--	3	3	1		©-"©PDO#2		A-9	1-1	
Subtotal					9	9	3						
TOTAL					115	115	22						

* Surviving specimens will be residual strength static tested at same temp. as that at which the fatigue test is run
** All static specimens will have back-to-back bi-axial gages, all fatigue specimens will have back-to-back longitudinal gages.

4.7

TABLE 4.2   TEST SERIES AND SPECIMEN/FIXTURE MATCH-UP

Item	Test Series No. and Description	Test Specimen and Fixture Description
1.	Static Test Series I	Specimen per Figure 3.6 Fixture per Figure 4.3
2.	Residual Strength Test Series II, III	Specimens Per Figure 3.6 Fixture Per Figure 4.3
3.	Static Test Series IV, V, VI, VII	Specimens per Figure 3.7 Fixture per Figure 4.3
4.	Residual Strength Test Series VIII, IX, X, XI	Specimens Per Figure 3.7 Fixture Per Figure 4.3.
5.	Static Test Series XII, XIII, XIV, XV	Specimen per Figure 3.7 Fixture per Figure 4.3
6.	Residual Strength Test Series XVI, XVII, XVIII, XIX	Specimen Per Figure 3.7 Fixture Per Figure 4.3.
7.	Static Test Series XX, XXI, XXII	ASTM D 3039 Fixture and Specimen Per Figure 3.8
8.	Fatigue Test Series II, III, VIII, IX, X, XI, XVI, XIX	Specimen for Figure 3.7 Fixtures Per Figures 4.3 4.4, and 4.5

TABLE 4.3   STRAIN LEVELS FOR SET-UP

Fatigue Test Condition	Strain Level Setting In 10^3 μ-in/inch												
	5.0	5.5	6.0	6.5	7.0	7.5	8.0	8.5	9.0	9.5	10.0	10.5	11.0
-65W			X			X			X			X	
RTD			X			X			X			X	
RTW			X		X		X		X				
218FW	X		X		X		X						

4.5 MOISTURE CONDITIONING

In order to simulate the severe environmental conditions to which Navy aircraft are exposed, a one-percent by weight moisture absorption requirement was imposed on many (see Table 4.1 for wet specimens) specimens tested in this program. The three laminates (plain laminate, ply drop-off No. 1, and ply drop-off No. 2) were exposed to the same procedure for moisture conditioning. From Table 4.1, edge taped (aluminum foil tape) specimens for test series I-IV, VI-VIII, X-XII, XIV through XVI, and XVIII through XIX were moisture conditioned as follows:

a.   63 days at 170°F and 95% RH plus

b.   36 days at 170°F and 80% RH

The predicted moisture distribution in the 30 ply section of the three laminates is presented in Figure 4.5.
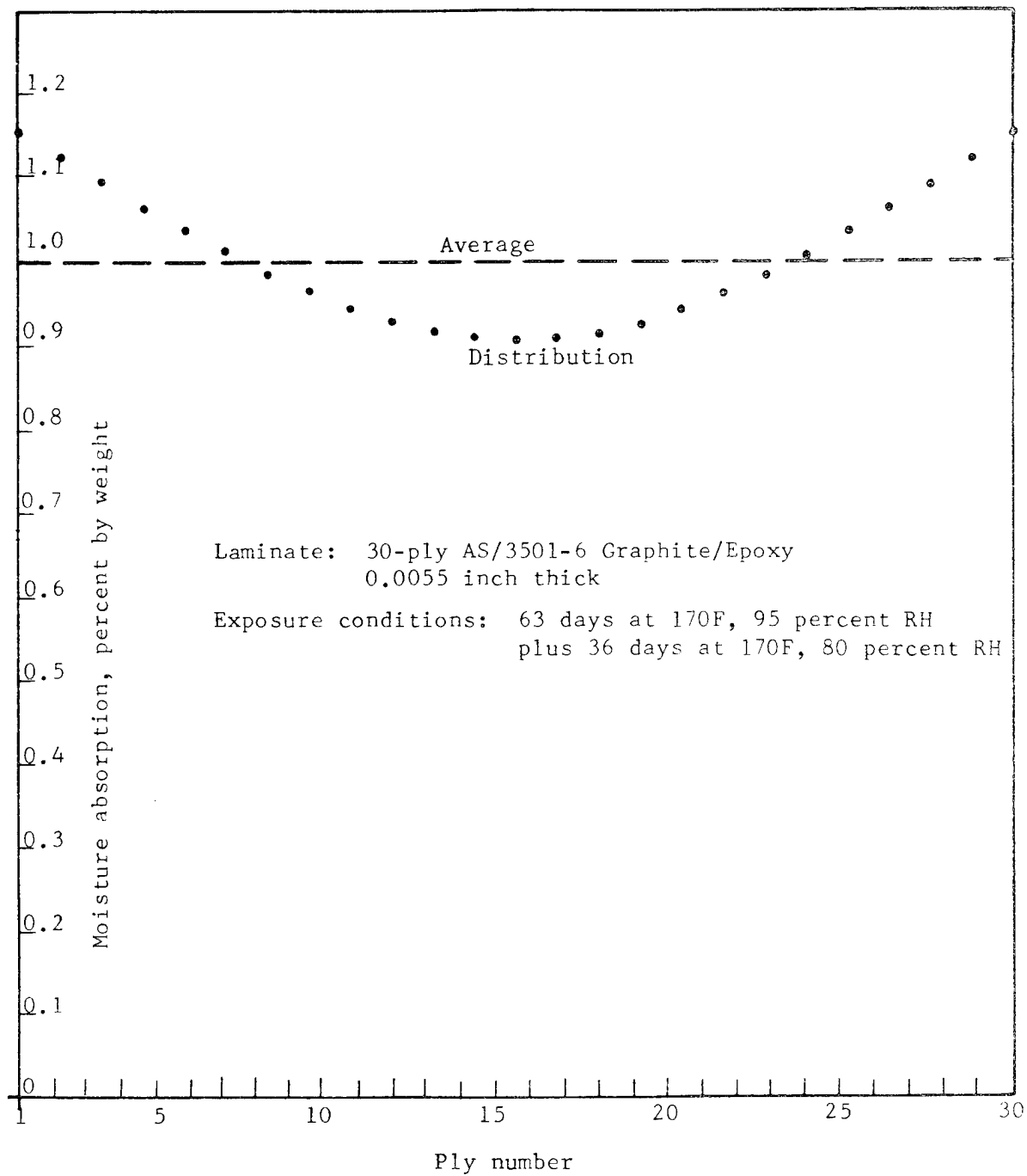
Figure 4.5. Moisture Distribution, 30-Ply Laminate

4.10

SECTION 5

TEST DATA

5.1 GENERAL

The program experimental data generated are presented in this section. All static (compression and tension) and R=10, compression-compression fatigue test data for the plain 30-ply laminate are presented in Section 5.2. Similarly, Section 5.3 presents test data for the two ply drop-off No. 1 laminate configuration and Section 5.4 presents the test data for the four ply drop-off No. 2 laminate configuration. Gross failure modes of the static and fatigue test specimens are discussed in Section 5.5. While residual strength data are presented in Section 5.6, Section 5.7 presents the moisture absorption data on the wet specimens.

5.2 PLAIN LAMINATE

5.2.1 Static Test Data

5.2.1.1 RTD Static Tension Test Data

Static tension tests at RTD conditions were performed by the Materials Research Lab (MRL) on plain laminate specimens ACL 4210A-3-1, -2, and -3 from Test Series XX. Appendix E, pages E.2 through E.11, present the detailed experimental measurements from these tests. The reduced data yielded the mechanical properties presented in Table 5.1.

From Test Series XX, Table 5.1, the mean values of mechanical properties are 105.7 Ksi strength, 10,000 μ-in/in failure strain, 10.48×10^6 psi modulus of elasticity, and 0.347 Poisson's Ratio. The three specimen scatter exhibited by the strength and strain to failure are reasonable, while it is low for the elastic properties.

TABLE 5.1 – 0° STATIC TENSION TEST DATA, RTD

Test Series/ Specimen ID	Discontinuity Configuration	Width (in)	Thick-ness (in)	Area (in²)	Maximum Load (kips)	Ultimate Stress* (ksi)	Failure Strain** (x10⁶)	Modulus of Elasticity (x10⁶ psi)	Poisson's Ratio
XX –ACL 4210A-3-1	Plain Laminate, 30 plies	0.997	0.178	0.1775	19.394	109.262	10298	10.48	0.352
-2		1.015	0.180	0.1827	21.446	117.384	11135	10.40	0.352
-3		1.009	0.178	0.1796	16.250	90.479	8575	10.55	0.337
Mean					19.030	105.708	10003	10.48	0.347
S.D.					2.617	13.800	1355	0.075	0.009
C.V.					0.138	0.131	0.130	0.007	0.025
XXI–ACL 4210A-6-1	PDO #1, Thin Section, 28 plies	1.008	0.167	0.1683	18.490	109.863	10883	10.19	0.357
-2		1.009	0.167	0.1685	18.466	109.590	10783	10.01	0.347
-3		1.012	0.166	0.1680	17.440	103.809	10224	10.05	0.352
Mean					18.132	107.754	10630	10.08	0.352
S.D.					0.599	3.419	355	0.095	0.005
C.V.					0.033	0.032	0.033	0.009	0.014
XXI–ACL 4210A-6-1	PDO #1, Thick Section, 30 plies	1.008	0.178	0.1794	18.490	103.066	--	--	--
-2		1.009	0.178	0.1796	18.466	102.817	--	--	--
-3		1.012	0.178	0.1801	17.440	96.835	--	--	--
Mean					18.132	100.906	--	--	--
S.D.					0.599	3.528	--	--	--
C.V.					0.033	0.035	--	--	--
XXII–ACL 4210A-9-1	PDO #2, Thin Section, 26 plies	1.014	0.149	0.1511	20.090	132.958	10755	12.05	0.272
-2		1.017	0.149	0.1515	20.774	137.122	11584	11.99	0.271
-3		1.011	0.149	0.1496	17.269	115.434	9608	11.80	0.274
Mean					19.378	128.505	10649	11.95	0.272
S.D.					1.858	11.509	942	0.131	0.001
C.V.					0.096	0.089	0.093	0.011	0.006
XXII–ACL 4210A-9-1	PDO #2, Thick Section, 30 plies	1.014	0.180	0.1825	20.090	110.882	--	--	--
-2		1.017	0.181	0.1841	20.774	112.841	--	--	--
-3		1.011	0.180	0.1820	17.269	94.885	--	--	--
Mean					19.378	106.203	--	--	--
S.D.					1.858	9.850	--	--	--
C.V.					0.096	0.093	--	--	--

*Specimens failed at thin section
**Strain gages located on thin section only

Pages E.5, E.8 and E.11 in Appendix E present the stress-strain curves for the specimens. Note that the curves are linear with negligible flatwise bending. Other curves (see page E.4) present Load vs. Derived Stroke. These curves must not be interpretated as load-strain curves since the derived stroke (the distance the load cells move in testing) does not correspond exactly with the strain deformation of the specimen.

5.2.1.2 -65°FW, Static Compression Test Data

Static Compression tests at -65 FW conditions were performed by the Engineering Test Lab (ETL) on plain laminate Specimens ACL 4210A-1-1, -1-6, and -2-17 from Test Series I. The results of these tests are presented in Table 5.2. The mean modulus for the three specimens is 10.37 msi and the mean Poisson's Ratio is 0.312. Figures 5.1, 5.2 and 5.3 present the stress-strain curves for the three test specimens. The curves are slightly nonlinear above the proportional limit. The proportional limit stress (-33.6 ksi) is 30% of the ultimate value (-113.6 ksi) whereas, the proportional limit strain (-3533 µ-in/in) is 26% of the failure strain (-13,533 µ-in/in).

5.2.2 Fatigue Test Data

5.2.2.1 -65°FW Compression Fatigue Test Data

The R=10 compression-compression fatigue tests were conducted at -65°FW conditions at constant frequency (10 Hz) on specimens from Test Series II with results presented in Table 5.3. Curves of stress versus number of cycles and strain versus number of cycles are presented in Figures 5.4 and 5.5. The stress versus number of cycles curve (Figure 5.4) is gradually decreasing with a decreasing slope from the static value of -114 ksi to runout (1.25×10^6 cycles) at -83 ksi. The stress at runout is 73% of the static value. The strain versus number of cycles curve is a horizontal straight line from the static strain value of -13,300 µin/in to 10^4 cycles from which the curve slopes to the strain value of -11,100 µ-in/in. at runout. The strain at runout is 83% of the static strain.

5.2.2.2 218°FW Compression Fatigue Test Data

At the 218°FW condition the R=10, constant frequency (10 Hz), compression-compression fatigue test results on specimens from Test Series III

TABLE 5.2 STATIC COMPRESSION TEST DATA

Test Series/ Specimen ID	Discontinuity Configuration	Width (in)	Thickness (in)	Area (in²)	Ultimate			Proportional Limit		Modulus (10⁶ psi)	Poisson's Ratio	Test Condition
					Load (lbs)	Stress (ksi)	Strain (μin/in)	Stress (ksi)	Strain (μin/in)			
I-4210A-1-1	Plain Laminate, 30 plies	2.0282	0.1784	0.3618	-34700	- 95.909	-10650	-33.167	- 3350	10.00	0.328	-65FW
-6		2.0228	0.1754	0.3548	-39700	-111.894	-14300	-33.820	- 3550	10.00	0.310	
-2-17		2.0220	0.1747	0.3532	-47000	-133.069	-15650	-33.975	- 3700	11.11	0.297	
Mean					-40467	-113.624	-13533	-33.654	- 3533	10.37	0.312	
S.D.					- 6186	- 18.640	- 2587	- 0.429	-175.6	0.641	0.016	
C.V.					0.153	0.164	0.191	0.013	0.050	0.062	0.050	
IV-4210A-4-1	PDO #1, Thin Section, 28 plies	2.2039	0.1622	0.3283	-44000	-134.024	-18000	-36.552	- 4100	9.09	0.317	-65FW
-3		2.0270	0.1630	0.3304	-48000	-145.278	-18000	-48.426	- 5000	9.75	0.310	
-5		2.0264	0.1633	0.3309	-39000	-117.860	-15300	-36.260	- 3800	9.38	0.250	
Mean					-43667	-132.287	-17100	-40.413	- 4300	9.41	0.292	
S.D.					- 4509	- 13.782	- 1559	- 6.941	-624.5	0.331	0.037	
C.V.					0.103	0.104	0.091	0.172	-0.145	0.035	0.126	
IV-4210A-4-1	PDO #1, Thick Section, 30 plies	2.2039	0.1756	0.3554	-44000	-123.804	---	---	---	---	---	-65FW
-3		2.0270	0.1760	0.3567	-48000	-134.567	---	---	---	---	---	
-5		2.0264	0.1775	0.3597	-39000	-108.423	---	---	---	---	---	
Mean					-43667	-122.245	---	---	---	---	---	
S.D.					- 4509	- 13.140	---	---	---	---	---	
C.V.					0.103	0.108	---	---	---	---	---	
V-4210A-4-12	PDO #1, Thin Section, 28 plies	2.0170	0.1595	0.3217	-35000	-108.797	-13100	-37.300	- 4100	9.38	0.232	RTD
5-14		2.0254	0.1608	0.3257	-34000	-104.390	-13100	-36.840	- 4150	9.09	0.313	
5-16		2.0254	0.1630	0.3301	-36000	-109.058	-13450	-36.350	- 4050	8.82	0.234	
Mean					-35000	-107.415	-13217	-36.830	- 4100	9.10	0.260	
S.D.					- 1000	- 2.623	-202.1	- 0.475	50	0.275	0.046	
C.V.					0.029	0.024	0.015	0.013	0.012	0.030	0.178	
V-4210A-4-12	PDO #1, Thick Section, 30 plies	2.0170	0.1760	0.35550	-35000	- 98.592	-11150	-33.800	- 3600	9.38	0.167	RTD
5-14		2.0254	0.1722	0.3488	-34000	- 97.477	-10950	-28.000	- 2700	10.59	0.296	
5-16		2.0254	0.1780	0.3605	-36000	- 99.861	-11800	-44.380	- 4900	9.38	0.194	
Mean					-35000	- 98.643	-11300	-35.393	- 3733	9.78	0.218	
S.D.					- 1000	- 1.193	-444.4	- 8.305	-1106	0.700	0.068	
C.V.					0.029	0.012	0.039	0.245	0.296	0.072	0.311	

(CONT'D)

TABLE 5.2 STATIC COMPRESSION TEST DATA, CONTINUED

Test Series/ Specimen ID	Discontinuity Configuration	Width (in)	Thickness (in)	Area (in²)	Ultimate Load (lbs)	Ultimate Stress (ksi)	Ultimate Strain (μin/in)	Proportional Limit Stress (ksi)	Proportional Limit Strain (μin/in)	Modulus (10⁶ psi)	Poisson's Ratio	Test Condition
VI-4210A-5-23	PDO #1, Thin Section, 28 plies	2.0269	0.1617	0.3277	-35000	-106.805	-12700	-36.619	- 3750	10.00	0.167	RTW
VI-4211B-10-25		2.0189	0.1670	0.3372	-35500	-105.279	-13800	-35.093	- 3900	9.52	0.231	
Mean					-35250	-106.042	-13250	-35.856	- 3825	9.76	0.199	
S.D.					-353.5	- 1.079	- 778	- 1.079	-106.1	0.339	0.045	
C.V.					0.010	0.010	0.059	0.030	0.028	0.035	0.227	
VI-4210A-5-23	PDO #1, Thick Section, 30 plies	2.0269	0.1756	0.3559	-35000	- 98.342	--	--	--	--	--	
4211B-10-25		2.0189	0.1831	0.3697	-35500	- 96.024	--	--	--	--	--	
Mean					-35250	- 97.183	--	--	--	--	--	
S.D.					-353.5	- 1.639	--	--	--	--	--	
C.V.					0.010	0.017	--	--	--	--	--	
VII-4211B-10-36	PDO #1, Thin Section, 28 plies	2.0174	0.1695	0.3419	-27500	- 80.433	- 9150	-35.098	- 3450	10.25	0.391	218FW
11-38		2.0219	0.1698	0.3433	-24000	- 69.910	- 7450	-34.955	- 3500	10.00	0.228	
Mean					-25750	- 75.171	- 8300	-35.026	- 3475	10.13	0.310	
S.D.					- 2475	7.441	- 1202	- 0.101		0.177	0.115	
C.V.					0.096	0.099	0.145	0.003	0.012	0.017	0.372	
VII-4211B-10-36	PDO #1, Thick Section, 30 plies	2.0174	0.1772	0.3575	-27500	- 76.923	--	--	--	--	--	
11-38		2.0219	0.1793	0.3625	-24000	- 66.207	--	--	--	--	--	
Mean					-25750	- 71.565	--	--	--	--	--	
S.D.					- 2475	7.577	--	--	--	--	--	
C.V.					0.096	0.106	--	--	--	--	--	
XII-4210A-7-1	PDO #2, Thin Section, 26 plies	2.0217	0.1482	0.2996	-42000	-140.187	-14950	-53.404	- 4950	11.11	0.237	-65FW
-3		2.0267	0.1478	0.2995	-36500	-121.870	-12350	-53.422	- 4850	11.11	0.247	
Mean					-39250	-131.028	-13650	-53.413	- 4900	11.11	0.242	
S.D.					- 3889	- 12.952	-1838.5	- 0.013	-70.71	0	0.007	
C.V.					0.099	0.099	0.135	0	0.014	0	0.029	

TABLE 5.2   STATIC COMPRESSION TEST DATA – CONTINUED

Test Series/ Specimen ID	Discontinuity Configuration	Width (in)	Thickness (in)	Area (in²)	Ultimate			Proportional Limit		Modulus (10⁶psi)	Poisson's Ratio	Test Condition
					Load (lbs)	Stress (ksi)	Strain (μ in/in)	Stress (ksi)	Strain (μ in/in)			
XII-4210A-7-1	PDO #2,	2.0217	0.1750	0.3538	-42000	-118.711	--	--	--	--	--	-65FW
-3	Thick Section,	2.0267	0.1752	0.3551	-36500	-102.788	--	--	--	--	--	
Mean	30 plies				-39250	-110.749	--	--	--	--	--	
S.D.					-3889	-11.259	--	--	--	--	--	
C.V.					0.099	0.102	--	--	--	--	--	
XIII-4210A-7-12	PDO #2,	2.0203	0.1497	0.3024	-36000	-119.048	-11900	-39.680	-3600	11.74	0.222	RTD
8-14	Thin Section,	2.0247	0.1735	0.3513	-35000	-99.630	-12300	-45.540	-5350	8.82	0.149	
8-16	26 plies	2.0254	0.1729	0.3502	-36000	-102.798	12350	-34.270	-3850	9.09	0.208	
Mean					-35667	-107.159	-12183	-39.830	-4267	9.88	0.193	
S.D.					-577.3	-10.417	-246.6	-5.636	-946.5	1.61	0.039	
C.V.					0.016	0.097	0.020	0.141	0.222	0.163	0.201	
XIII-4210A-7-12	PDO #2,	2.0203	0.1758	0.3552	-36000	-101.351	-12850	-45.050	-5250	8.82	0.200	RTD
8-14	Thick Section,	2.0247	0.1769	0.3582	-35000	-97.711	-12000	-33.500	-3700	9.52	0.149	
8-16	30 plies	2.0254	0.1744	0.3532	-36000	-101.925	-12300	-33.970	-3450	10.00	0.232	
Mean					-35667	-100.329	-12383	-37.510	-4133	9.45	0.194	
S.D.					-577.3	-2.285	-431.1	-6.539	-975.1	0.593	0.042	
C.V.					0.016	0.023	0.035	0.174	0.236	0.063	0.216	
XIV-4210A-8-23	PDO #2,	2.0294	0.1475	0.2993	-32000	-106.916	-10600	-53.458	-3700	11.54	0.176	RTW
4211B-12-25	Thin Section,	2.0236	0.1512	0.3060	-33000	-107.843	-10750	-52.287	-4700	11.43	0.128	
Mean	26 plies				-32500	-107.379	-10675	-52.872	-4200	11.49	0.152	
S.D.					-707.1	-0.655	-106.1	-0.828	-707.1	0.078	0.034	
C.V.					0.022	0.006	0.010	0.168	0.168	0.007	0.223	
XIV-4210A-8-23	PDO #2,	2.2094	0.1787	0.3626	-32000	-88.252	--	--	--	--	--	
4211B-12-25	Thick Section,	2.0236	0.1798	0.3638	-33000	-90.709	--	--	--	--	--	
Mean	30 plies				-32500	-89.480	--	--	--	--	--	
S.D.					-707.1	1.737	--	--	--	--	--	
C.V.					0.022	0.019	--	--	--	--	--	

5.6

TABLE 5.2 STATIC COMPRESSION TEST DATA – CONCLUDED

Test Series/ Specimen ID	Discontinuity Configuration	Width (in)	Thickness (in)	Area (in²)	Ultimate Load (lbs)	Ultimate Stress (ksi)	Ultimate Strain (μin/in)	Proportional Limit Stress (ksi)	Proportional Limit Strain (μin/in)	Modulus (10⁶psi)	Poisson's Ratio	Test Cond.
XV-4211B-12-34	PDO #2, Thin Section, 26 plies	2.0294	0.1525	0.3095	-29500	-95.315	- 9850	-38.770	- 3800	10.71	0.224	218FW →
→ 12-36		2.0226	0.1558	0.3151	-24000	-76.166	- 7450	-38.083	- 3600	10.53	0.236	
13-38		2.0226	0.1546	0.3127	-30200	-96.578	- 10050	-38.375	- 3700	10.34	0.270	
Mean					-27900	-89.353	- 9117	-38.409	- 3700	10.53	0.243	
S.D.					- 3396	-11.438	-1446.8	- 0.345	- 100	0.185	0.024	
C.V.					0.122	0.128	0.159	0.009	0.027	0.018	0.098	
XV-4211B-12-34	PDO #2, Thick Section, 30 plies	2.0294	0.1775	0.3602	-29500	-81.899	--	--	--	--	--	218FW →
→ 12-36		2.0226	0.1811	0.3663	-24000	-65.520	--	--	--	--	--	
13-38		2.0226	0.1800	0.3641	-30200	-82.944	--	--	--	--	--	
Mean					-27900	-76.788	--	--	--	--	--	
S.D.					- 3396	- 9.77	--	--	--	--	--	
C.V.					0.122	0.127	--	--	--	--	--	

5.7

Figure 5.1 0° Static Compression Test Series 1, Specimen ACL 4210A-1-1 Stress-Strain Curves
-65FW, Plain Laminate

Figure 5.2 0° Static Compression Test Series I, Specimen ACL 4210A-1-6 Stress-Strain Curves, -65FW, Plain Laminate

5.9
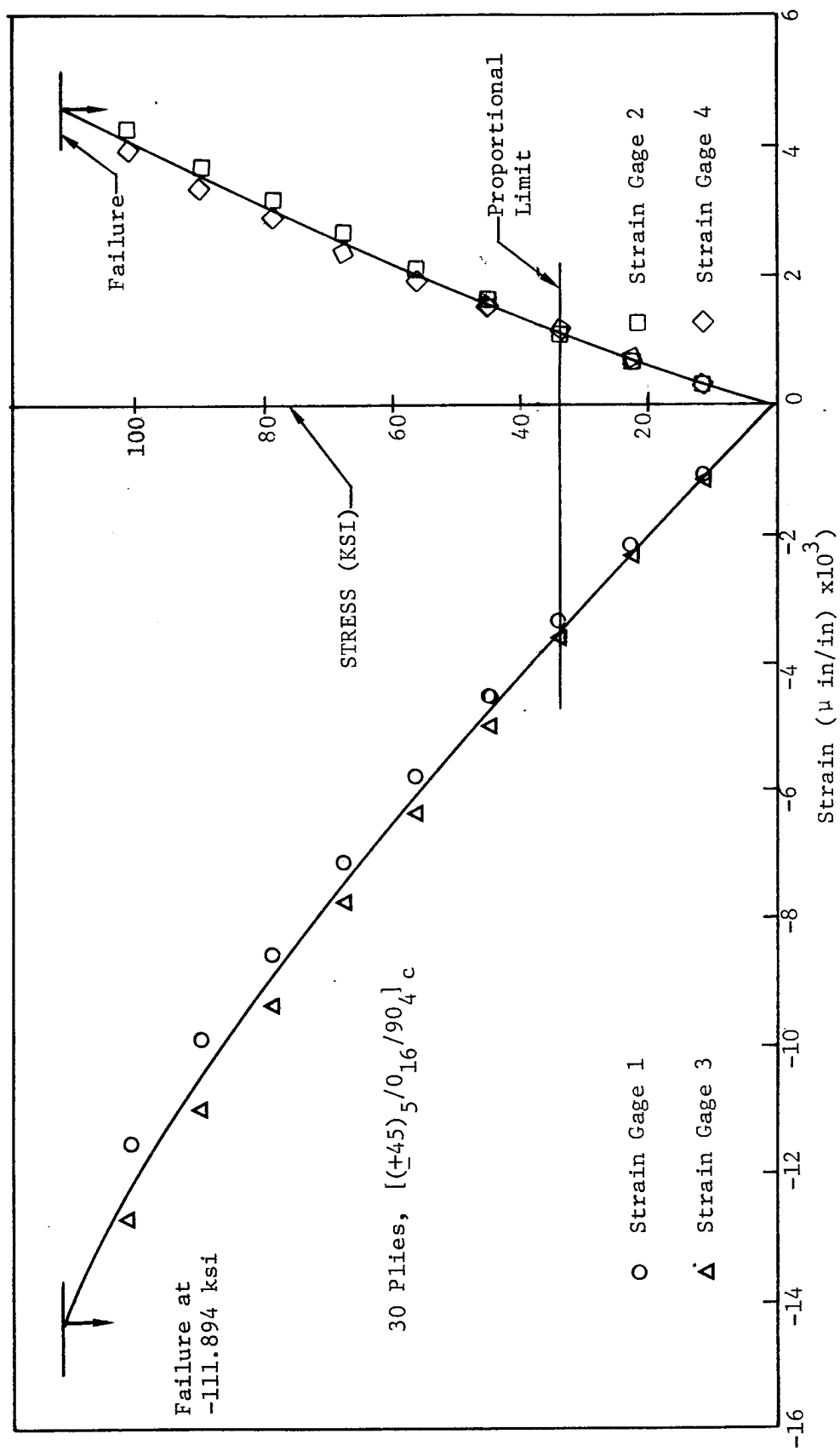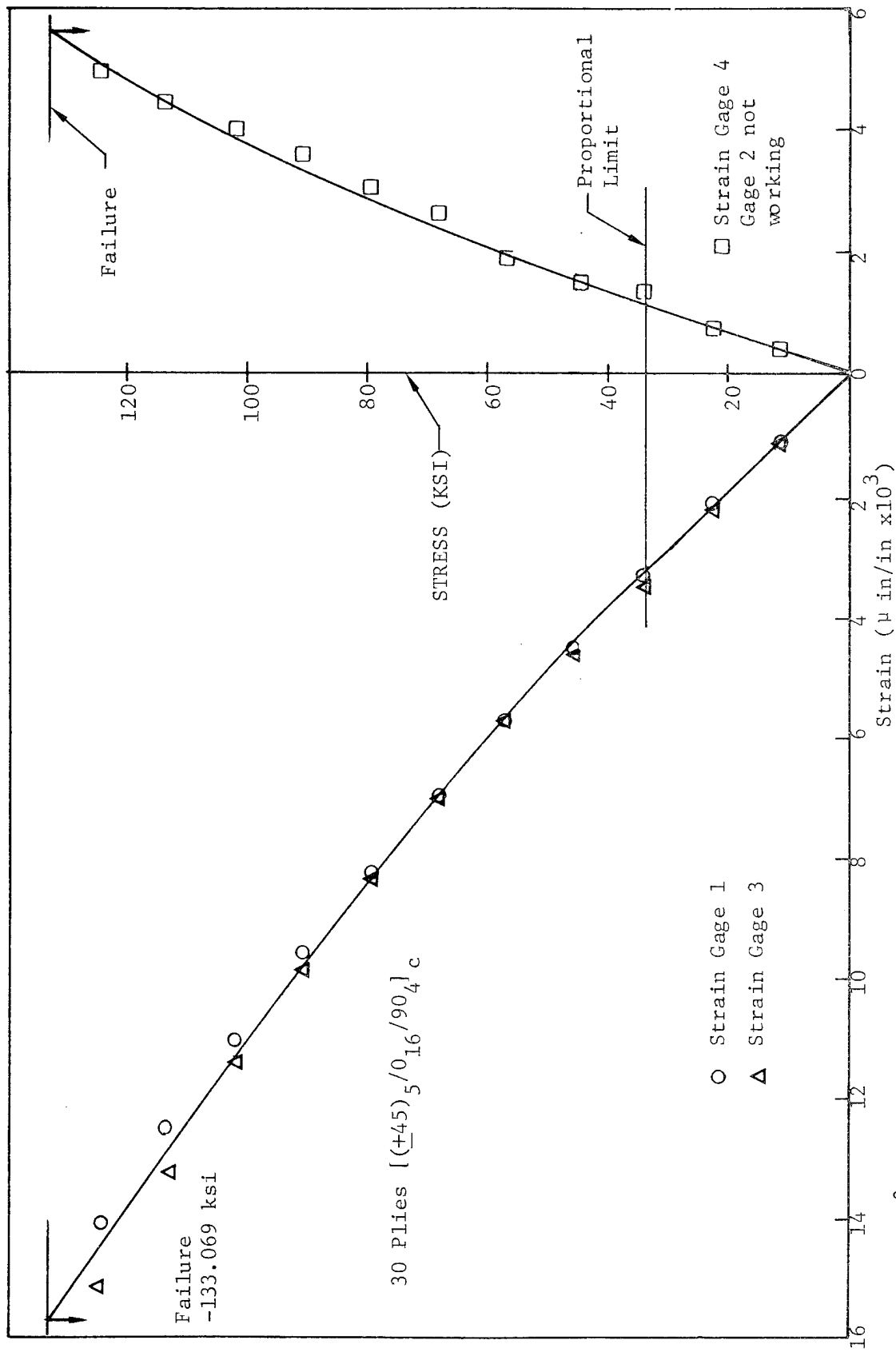
Figure 5.3 0° Static Compression Test Series I, Specimen ACL 4210A-2-17 Stress-Strain Curves, -65FW, Plain Laminate

TABLE 5.3   R=10,   COMPRESSION-COMPRESSION FATIGUE TEST DATA

Test Series/ Specimen ID	Discontinuity Configuration	Width (in)	Thickness (in)	Area (in²)	Maximum Comp. Load(lbs)	Maximum Comp. Stress (ksi)	Maximum Fatigue Strain Goal (μin/in)	Actual Maximum Fatigue Strain (μ in/in)	Residual Strength (lbs)	Cyclic Rate (Hz)	No. of Cycles to fail or Runout	Test Condition
II-4210A-1-2	Plain Laminate, 30 plies	2.0278	0.1804	0.3658	-20000	- 54.675	- 6000	- 6429	-35200	10	1.25×10^6	-65FW
-3		2.0271	0.1770	0.3588	-24200	- 67.447	- 7500	- 8098	-41000		1.25×10^6	
-4		2.0256	0.1745	0.3535	-28400	- 80.339	- 9000	- 9143	-43400		1.25×10^6	
-5		2.0244	0.1752	0.3547	-39200	-110.516	-13000	-13392	--		130	
-12		2.0160	0.1776	0.3580	-29700	- 82.961	- 9500	-11089	-51600		1.25×10^6	
II-4210A-2-13		2.0247	0.1765	0.3573	-32000	- 89.560	-10500	-10803	--		48530	
-14		2.0241	0.1787	0.3617	-34300	- 94.830	-11250	-11524	--		131450	
-15		2.0208	0.1761	0.3559	-36000	-101.152	-12000	-12686	--		163110	
-16		2.0200	0.1751	0.3537	-36700	-103.760	-12500	-12986	--		11780	
III-4210A-1-7	Plain Laminate, 30 plies	2.0210	0.1776	0.3589	-18200	- 50.710	- 4100	- 4997	-34500	10	1.25×10^6	218FW
-8		2.0217	0.1788	0.3615	-19700	- 54.495	- 6000	- 6293	-35350		1.25×10^6	
-9		2.0237	0.1759	0.3560	-22550	- 63.343	- 7000	- 7069	-36500		1.25×10^6	
-10		2.0229	0.1743	0.3526	-25700	- 72.887	- 8000	- 7620	-24000*		1	
-11		2.0217	0.1765	0.3568	-26000	- 72.870	- 8500	- 8277	--		230	
III-4210A-2-18		2.0262	0.1759	0.3564	-26000	- 72.952	- 8000	- 8264	*		1	
-19		2.0267	0.1783	0.3614	-24000	- 66.408	- 7500	- 7485	--		35190	
-20		2.0232	0.1789	0.3619	-24700	- 68.251	- 7500	- 7685	--		743880	
-21		2.0210	0.1757	0.3551	--	--	- 8250	--	**		0	
-22		2.0284	0.1770	0.3590	--	--	- 8250	--	**		0	
VIII-4210A-4-2	PDO#1, Thin Section, 28 plies	2.0249	0.1616	0.3272	-17700	- 54.095	- 6000	- 6165	-49300	10	1.25×10^6	-65FW
-4		2.0271	0.1652	0.3349	-23000	- 68.677	- 7500	- 7531	-38600		1.25×10^6	
-6		2.0265	0.1643	0.3329	-26200	- 78.702	- 9000	- 9132	-33000		1.25×10^6	
-7		2.0259	0.1622	0.3286	-30000	- 91.296	-10500	-10636	--		11380	
-8		2.0265	0.1640	0.3323	-29100	- 87.571	-10000	-10500	--		106050	
-9		2.0278	0.1623	0.3291	-31500	- 95.715	-11000	-11155	--		**	
-10		2.0274	0.1618	0.3280	-32000	- 97.561	-11000	-11455	--		410	
-11		2.0263	0.1612	0.3266	-29500	- 90.324	-10750	-11149	--		12220	

(Continued)

*Failed when taking data before fatigue @ 218FW
**Auto-Stop not operational, 1000 < no. of cycles < 10000

5.11

TABLE 5.3   R=10, COMPRESSION-COMPRESSION FATIGUE TEST DATA - CONT'D.

Specimen ID	Discontinuity Configuration	Width (in)	Thickness (in)	Area (in²)	Maximum Comp. Load (lbs)	Maximum Comp. Stress (ksi)	Maximum Fatigue Strain Goal (μ in/in)	Actual Maximum Fatigue Strain (μ in/in)	Residual Strength (lbs)	Cyclic Rate (Hz)	No. of Cycles to fail or Runout	Test Condition
VIII-4210A-4-2	PDO #1, Thick Section, 30 plies	2.0249	0.1757	0.3558	-17700	-49.747	--	--	-49300	10	1.25x10⁶	-65FW
-4		2.0271	0.1751	0.3549	-23000	-64.807	--	--	-38600		1.25x10⁶	
-6		2.0265	0.1783	0.3613	-26200	-72.516	--	--	-33000		1.25x10⁶	
-7		2.0259	0.1759	0.3563	-30000	-84.199	--	--	--		11380	
-8		2.2065	0.1748	0.3542	-29100	-82.157	--	--	--		106050	
-9		2.0278	0.1733	0.3514	-31500	-89.641	--	--	--		*	
-10		2.0274	0.1766	0.3508	-32000	-91.220	--	--	--		410	
-11		2.0263	0.1769	0.3584	-29500	-82.310	--	--	--		12220	
IX-4210-A-5-13	PDO #1, Thin Section, 28 plies	2.0234	0.1619	0.3276	-18000	-54.945	-6000	-6493	-37000	10	1.25x10⁶	RTD
-15		2.0250	0.1603	0.3246	-27000	-83.179	-9000	-10191	--		9980	
-17		2.0246	0.1639	0.3318	-23000	-69.319	-7500	-8233	--		602920	
-18		2.0248	0.1633	0.3306	-30000	-90.744	-10000	-11390	--		2230	
-19		2.0273	0.1674	0.3394	-30500	-89.864	-10500	-11625	--		400	
-20		2.0275	0.1643	0.3331	-23500	-70.549	-7500	-8381	--		229940	
-21		2.0293	0.1626	0.3300	-26500	-80.303	-9000	-9961	--		9200	
-22		2.0291	0.1640	0.3328	-30000	-90.144	-10000	-11048	--		1670	
IX-4210-A-5-13	PDO #1, Thick Section, 30 plies	2.0234	0.1768	0.3577	-18000	-50.322	-6000	-5737	-37000	10	1.25x10⁶	RTD
-15		2.0250	0.1770	0.3584	-27000	-75.335	-9000	-8896	--		9980	
-17		2.0246	0.1745	0.3533	-23000	-65.100	-7500	-7246	--		602920	
-18		2.0248	0.1754	0.3552	-30000	-84.460	-10000	-9920	--		2230	
-19		2.0273	0.1742	0.3532	-30500	-86.353	-10500	-10188	--		400	
-20		2.0275	0.1769	0.3587	-23500	-65.514	-7500	-7400	--		9200	
-21		2.0293	0.1764	0.3580	-26500	-74.022	-9000	-8761	--		9200	
-22		2.0291	0.1746	0.3543	-30000	-84.674	-10000	-9748	--		1670	

*Auto-Stop not operational, 1000< no. of cycles < 10000

TABLE 5.3. R=10, COMPRESSION-COMPRESSION FATIGUE TEST DATA – CONT'D.

Test Series/ Specimen ID	Discontinuity Configuration	Width (in)	Thickness (in)	Area (in²)	Maximum Comp. Load (lbs)	Maximum Comp. Stress (ksi)	Maximum Fatigue Strain Goal (μ in/in)	Actual Maximum Fatigue Strain (μ in/in)	Residual Strength (lbs)	Cyclic Rate (Hz)	No. of Cycles to fail or Runout	Test Condition
X-4210A-5-24	PDO #1, Thin Section, 28 plies	2.0191	0.1636	0.3303	-17600	-53.285	- 6000	- 6088	-38000	10	1.25×10^6	RTW
4211B-10-26		2.0237	0.1685	0.3410	-20000	-58.651	- 7000	- 7074	-35700		1.25×10^6	
-28		2.0247	0.1656	0.3353	-23200	-69.192	- 8000	- 6963	--		205060	
-29		2.0259	0.1661	0.3365	-25500	-75.780	- 9000	- 8501	--		129010	
-30		2.0254	0.1656	0.3354	-28000	-83.482	-10000	-10476	--		1420	
-31		2.0268	0.1674	0.3393	-26750	-78.839	- 9500	- 9656	--		9470	
-32		2.2067	0.1687	0.3419	-29000	-84.280	-10500	-11023	--		21760	
-33		2.0252	0.1641	0.3323	-30000	-90.280	-11000	-11688	--		5770	
X-4210A-5-24	PDO #1, Thick Section, 30 plies	2.0191	0.1769	0.3572	-17600	-49.272	--	--	-38000	10	1.25×10^6	RTW
4211B-10-26		2.0237	0.1823	0.3689	-20000	-54.215	--	--	-35700		1.25×10^6	
-28		2.0247	0.1800	0.3644	-23200	-63.666	--	--	--		205060	
-29		2.2059	0.1799	0.3644	-25500	-69.978	--	--	--		129010	
-30		2.0254	0.1788	0.3621	-28000	-77.327	--	--	--		1420	
-31		2.0268	0.1802	0.3652	-26750	-73.247	--	--	--		9470	
-32		2.2067	0.1816	0.3680	-29000	-78.804	--	--	--		21760	
-33		2.0252	0.1809	0.3663	-30000	-81.900	--	--	--		5770	
XI-4211B-10-35	PDO #1, Thin Section, 28 plies	2.2059	0.1708	0.3460	-15200	-43.931	- 5000	- 5112	-28700	10	1.25×10^6	218FW
-11-37		2.2019	0.1672	0.3381	-17500	-51.760	- 6000	- 6161	-24000		1.25×10^6	
-39		2.0220	0.1677	0.3391	-21000	-61.929	- 7000	- 7571	--		5440	
-40		2.0224	0.1695	0.3428	-22800	-66.511	- 8000	- 8170	--		10310	
-41		2.0239	0.1706	0.3453	-20000	-57.921	- 6500	- 6695	--		89360	
-42		2.0238	0.1717	0.3475	-19000	-54.676	- 6250	- 6161	--		90050	
-43		2.0253	0.1682	0.3406	-25700	-75.455	- 9000	- 9149	--		50	
-44		2.0235	0.1681	0.3401	-27000	-79.388	- 8500	- 8472	--		470	
XI-4211B-10-35	PDO #1, Thick Section 30 plies	2.2059	0.1808	0.3663	-15200	-41.496	--	--	-28700	10	1.25×10^6	218FW
-11-37		2.0219	0.1800	0.3639	-17500	-48.090	--	--	-24000		1.25×10^6	
-39		2.0220	0.1828	0.3696	-21000	-56.818	--	--	--		5440	
-40		2.0224	0.1798	0.3636	-22800	-62.706	--	--	--		10310	
-41		2.0239	0.1818	0.3679	-20000	-54.362	--	--	--		89360	
-42		2.0238	0.1872	0.3788	-19000	-50.158	--	--	--		90050	
-43		2.0253	0.1790	0.3625	-25700	-70.896	--	--	--		50	
-44		2.0235	0.1791	0.3624	-27000	-74.503	--	--	--		470	

TABLE 5.3   R=10, COMPRESSION-COMPRESSION FATIGUE TEST DATA – CONT'D.

Specimen ID	Discontinuity Configuration	Width (in)	Thickness (in)	Area (in^2)	Maximum Comp. Load (lbs)	Maximum Comp. Stress (ksi)	Maximum Fatigue Strain Goal (μ in/in)	Actual Maximum Fatigue Strain (μ in/in)	Residual Strength (lbs)	Cyclic Rate (Hz)	No. of Cycles to fail or Runout	Test Condition
XVI-4210A-7-2	PDO #2, Thin Section 26 plies	2.0260	0.1508	0.3055	-2000	- 65.466	- 6000	- 6030	-45000	10	1.25×10^6	-65FW
-4		2.0273	0.1495	0.3031	-24000	- 79.182	- 7500	- 7352	-41400		1.25×10^6	
-6		2.0282	0.1510	0.3062	-29500	- 96.342	- 9000	- 9441	-47350		1.25×10^6	
-7		2.0268	0.1482	0.3004	-33500	-111.518	-10500	-10595	--		4060	
-8		2.0287	0.1492	0.3027	-34500	-113.974	-11000	-11234	--		790	
-9		2.0307	0.1490	0.3026	-30600	-101.124	- 9750	- 9840	--		750	
-10		2.0286	0.1498	0.3039	-29600	- 97.400	- 9250	- 9530	--		756950	
-11		2.0312	0.1512	0.3071	-32000	-104.200	-10000	-10136	--		33350	
XVI-4210A-7-2	PDO #2, Thick Section 30 plies	2.0260	0.1802	0.3651	-20000	- 54.779	--	--	-45000	10	1.25×10^6	-65FW
-4		2.0273	0.1750	0.3548	-24000	- 67.644	--	--	-41400		1.25×10^6	
-6		2.0282	0.1828	0.3708	-29500	- 79.558	--	--	-47350		1.25×10^6	
-7		2.0268	0.1758	0.3563	-33500	- 94.022	--	--	--		4060	
-8		2.0287	0.1753	0.3556	-34500	- 97.019	--	--	--		790	
-9		2.0307	0.1756	0.3566	-30600	- 85.810	--	--	--		750	
-10		2.0286	0.1759	0.3568	-29600	- 82.960	--	--	--		756960	
-11		2.0312	0.1781	0.3618	-32000	- 88.447	--	--	--		33350	
XVII-4210-A-8-13	PDO #2, Thin Section 26 plies	2.0210	0.1506	0.3044	-18000	- 59.133	- 6000	- 6044	-34000	10	1.25×10^6	RTD
-15		2.0252	0.1482	0.3001	-22000	- 73.309	- 7500	- 7585	-36000		1.25×10^6	
-17		2.0256	0.1460	0.2957	-26000	- 87.927	- 9000	- 9196	--		261140	
-18		2.0253	0.1472	0.2981	-29000	- 97.283	-10000	-10346	--		12630	
-19		2.0242	0.1503	0.3042	-31500	-103.550	-11000	-11348	--	1	30	
-20		2.0242	0.1506	0.3048	-26000	- 85.302	- 9000	- 9176	--	10	305490	
-21		2.0260	0.1485	0.3009	-29000	- 96.378	-10000	-10467	--		72620	
-22		2.0276	0.1476	0.2993	-31000	-103.575	-10500	-10982	--	8	1050	

TABLE 5.3 R=10, COMPRESSION-COMPRESSION FATIGUE TEST DATA – CONT'D.

Specimen ID	Discontinuity Configuration	Width (in)	Thickness (in)	Area (in²)	Maximum Comp. Load (lbs)	Maximum Comp. Stress (ksi)	Maximum Fatigue Strain Goal (μin/in)	Actual Maximum Fatigue Strain (μ in/in)	Residual Strength (lbs)	Cyclic Rate (Hz)	No. of Cycles to fail or Runout	Test Condition
XVII-4210-A-8-13	PDO #2, Thick Section, 30 plies	2.0210	0.1756	0.3549	-18000	- 50.718	- 6000	- 5773	-34000	10	1.25×10^6	RTD
-15		2.0252	0.1755	0.3554	-22000	- 61.902	- 7500	- 7344	-36000		1.25×10^6	
-17		2.0256	0.1750	0.3545	- 26000	- 73.343	- 9000	- 8799	--	1	261140	
-18		2.0253	0.1766	0.3577	- 29000	- 81.074	-10000	- 9965	--	10	12630	
-19		2.0242	0.1768	0.3579	- 31500	- 88.013	-11000	-10783	--	8	30	
-20		2.0242	0.1779	0.3601	- 26000	- 72.202	- 9000	- 8806	--		305490	
-21		2.0260	0.1740	0.3525	- 29000	- 82.270	-10000	- 9908	--		72620	
-22		2.0276	0.1743	0.3534	- 31000	- 87.719	-10500	-10443	--		1050	
XVIII-4210A-8-24	PDO #2, Thin Section, 26 plies	2.0188	0.1494	0.3016	- 17600	- 58.355	- 6000	- 6055	-35400	10	1.25×10^6	RTW
4211B-12-26		2.0246	0.1541	0.3120	-22600	- 72.436	- 7000	- 7077	--		249890	
-28		2.0245	0.1528	0.3093	- 24300	- 78.564	- 8000	- 8005	-35200		1.25×10^6	
-29		2.0260	0.1569	0.3179	- 26800	- 84.303	- 9000	- 9254	--		85460	
-30		2.0253	0.1551	0.3141	- 29600	- 94.237	-10000	-10163	--		1580	
-31		2.0258	0.1589	0.3219	- 25500	- 79.217	- 8500	- 8653	--		90850	
-32		2.0262	0.1563	0.3167	- 25800	- 81.465	- 8250	- 8457	--		159870	
-33		2.0268	0.1523	0.3087	- 34650	-112.245	-11000	-11440	--		110	
XVIII-4210A-8-24	PDO #2, Thick Section, 30 plies	2.0188	0.1760	0.3553	- 17600	- 49.535	--	--	-35400	10	1.25×10^6	RTW
4211B-12-26		2.0246	0.1802	0.3648	-22600	- 61.952	--	--	--		249890	
-28		2.0245	0.1788	0.3620	- 24300	- 67.127	--	--	-35200		1.25×10^6	
-29		2.0260	0.1829	0.3706	- 26800	- 72.315	--	--	--		85460	
-30		2.0253	0.1820	0.3686	- 29600	- 80.304	--	--	--		1580	
-31		2.0258	0.1802	0.3650	- 25500	- 69.863	--	--	--		90850	
-32		2.0262	0.1791	0.3629	- 25800	- 71.094	--	--	--		159870	
-33		2.0268	0.1793	0.3634	- 34650	- 95.349	--	--	--		110	

TABLE 5.3   COMPRESSION–COMPRESSION FATIGUE TEST DATA – CONCLUDED

Specimen ID	Discontinuity Configuration	Width (in)	Thickness (in)	Area (in²)	Maximum Comp. Load (lbs)	Maximum Comp. Stress (ksi)	Maximum Fatigue Strain Goal (μ in/in)	Actual Maximum Fatigue Strain (μ in/in)	Residual Strength (lbs)	Cyclic Rate (Hz)	No. of Cycles to fail or Runout	Test Condition
XIX-4211B-12-35	PDO #2, Thin Section, 26 plies	2.0278	0.1560	0.3163	-16100	-50.901	-5000	-5266	-30700	10	1.25×10^6	218FW
4211B-13-37		2.0268	0.1558	0.3158	-19400	-61.431	-6000	-6438	-30300		1.25×10^6	
-39		2.0226	0.1531	0.3097	-22300	-72.005	-7000	-6980	--		21940	
-40		2.0224	0.1535	0.3104	-25700	-83.022	-8000	-8558	--		1500	
-41		2.0221	0.1554	0.3142	-28000	-89.115	-9000	-9447	--		2080	
-42		2.0223	0.1555	0.3145	-21300	-67.726	-6500	-6836	--		150000	
-43		2.0233	0.1560	0.3156	-28000	-88.720	-9250	-9130	--		20	
-44		2.0205	0.1550	0.3132	-28200	-90.038	-9500	-9541	--		10	
XIX-4211B-12-35	PDO #2, Thick Section, 30 plies	2.0278	0.1822	0.3695	-16100	-43.572	--	--	-30700	10	1.25×10^6	218FW
4211B-13-37		2.0268	0.1820	0.3689	-19400	-52.588	--	--	-30300		1.25×10^6	
-39		2.0226	0.1798	0.3637	-22300	-61.314	--	--	--		21940	
-40		2.0224	0.1791	0.3622	-25700	-70.955	--	--	--		1500	
-41		2.0221	0.1780	0.3599	-28000	-77.799	--	--	--		2080	
-42		2.0223	0.1798	0.3636	-21300	-58.581	--	--	--		150000	
-43		2.0233	0.1820	0.3682	-28000	-76.045	--	--	--		20	
-44		2.0205	0.1798	0.3633	-28200	-77.622	--	--	--		10	

Figure 5.4. Constant Cycle Fatigue Stress Behavior for Plain Laminate, -65FW.

R=10, 10 HZ
30 Ply, $[(\pm 45)_5/0_{16}/90_4]_c$

5.17

MAXIMUM COMPRESSIVE STRAIN (μIN/IN)

NUMBER OF CYCLES, N

R = 10, 10 Hz

30 Ply, $\overline{[(\pm 45)_5/0_{16}/90_4]}_c$
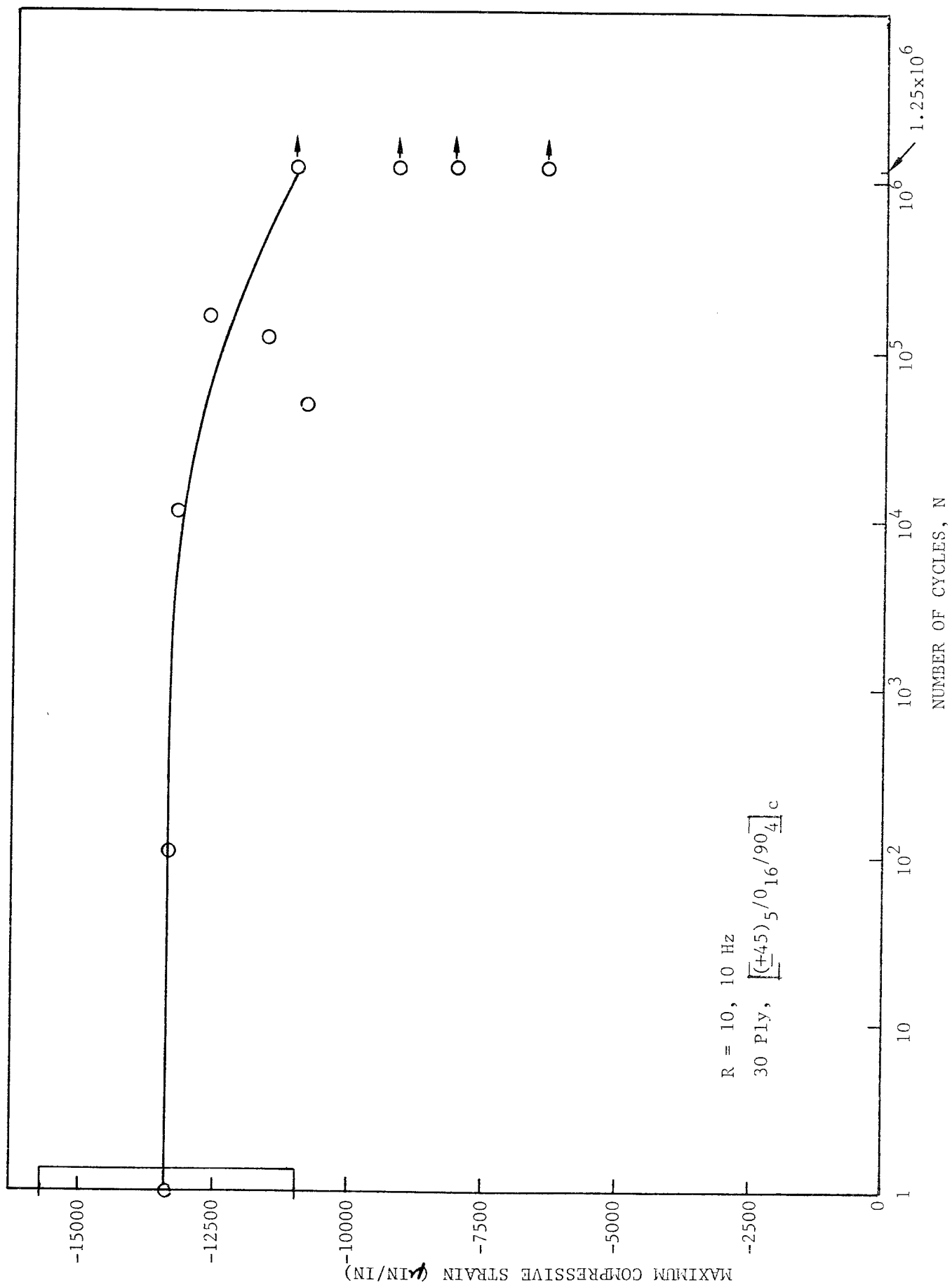
Figure 5.5. Constant Cycle Fatigue Strain Behavior, Plain Laminate, -65FW.

are presented in Table 5.3. These test data are plotted versus number of
cycles and presented in Figures 5.6 and 5.7. From the figures, note that
for both the stress and strain curves the slopes are near horizontal from
the static values* (76 ksi/8400μ-in/in) to approximately the 3.5×10^4 cycle
point from which the curves slope down to their runout values (63 ksi/7100
ksi). Note that, Figure 5.6, the stress at runout is 84% of the static
value and, from Figure 5.7, the strain at runout is also 80% of the static
strain value. Also, note that four specimens failed before data was taken
at 218° FW. Two specimens were damaged upon placement in the test fixture
(specimens associated with "0 cycles to fail") while two specimens failed
under initial loading (specimens associated with "1 cycle to fail").

5.3 PLY DROP-OFF NO. 1

5.3.1 Static Data

5.3.1.1 RTD Static Compression Test Data

Static compression tests were performed on Test Series V Specimens ACL
4210A-4-12, -5-14, and -5-16. Each specimen had two longitudinal and two
transverse strain gages mounted on both its thick and its thin sections.
The test results are presented in Table 5.2. The test data is separated
into thick and thin section data with related strain data plotted and
presented in Figures 5.8-5.13. From Table 5.2, note that the mean modulus
for the thick section differs by approximately 7% from the mean modulus
for the thin section. The difference between thick section and thin section
data for mean Poisson's Ratio and mean ultimate stress are much larger.
Also, note that the thick section ultimate stress is approximately 92% of the
thin section ultimate stress. Examination of the curves in Figures 5.8 -
5.13 shows that there is little difference in the shape of the curves
between thick and thin section data for the same specimen. The thin
section curves, however, always reach a higher stress and higher strain
at failure. The proportional limits of the thin and thick section specimens
are, on average, approximately 34 -36% of their ultimate stresses.

---

* See Reference (1) page 153, Table 5.17 for these static data
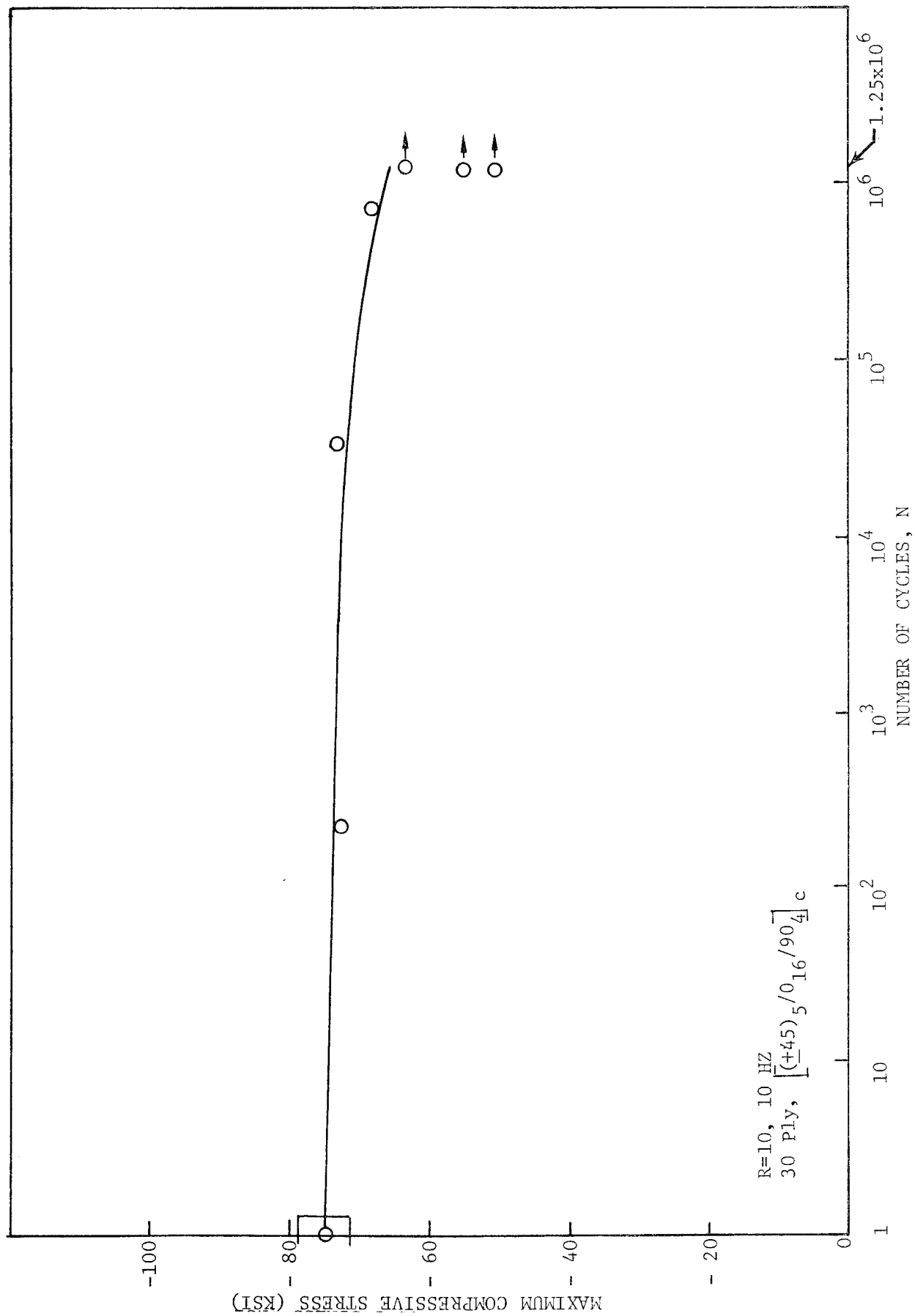
Figure 5.6. Constant Cycle Stress Fatigue Behavior for Plain Laminate, 218°Fw.

R=10, 10 HZ
30 Ply, $[(\pm 45)_5/0_{16}/90_4]c$

MAXIMUM COMPRESSIVE STRESS (KSI)

NUMBER OF CYCLES, N

1.25×10^6
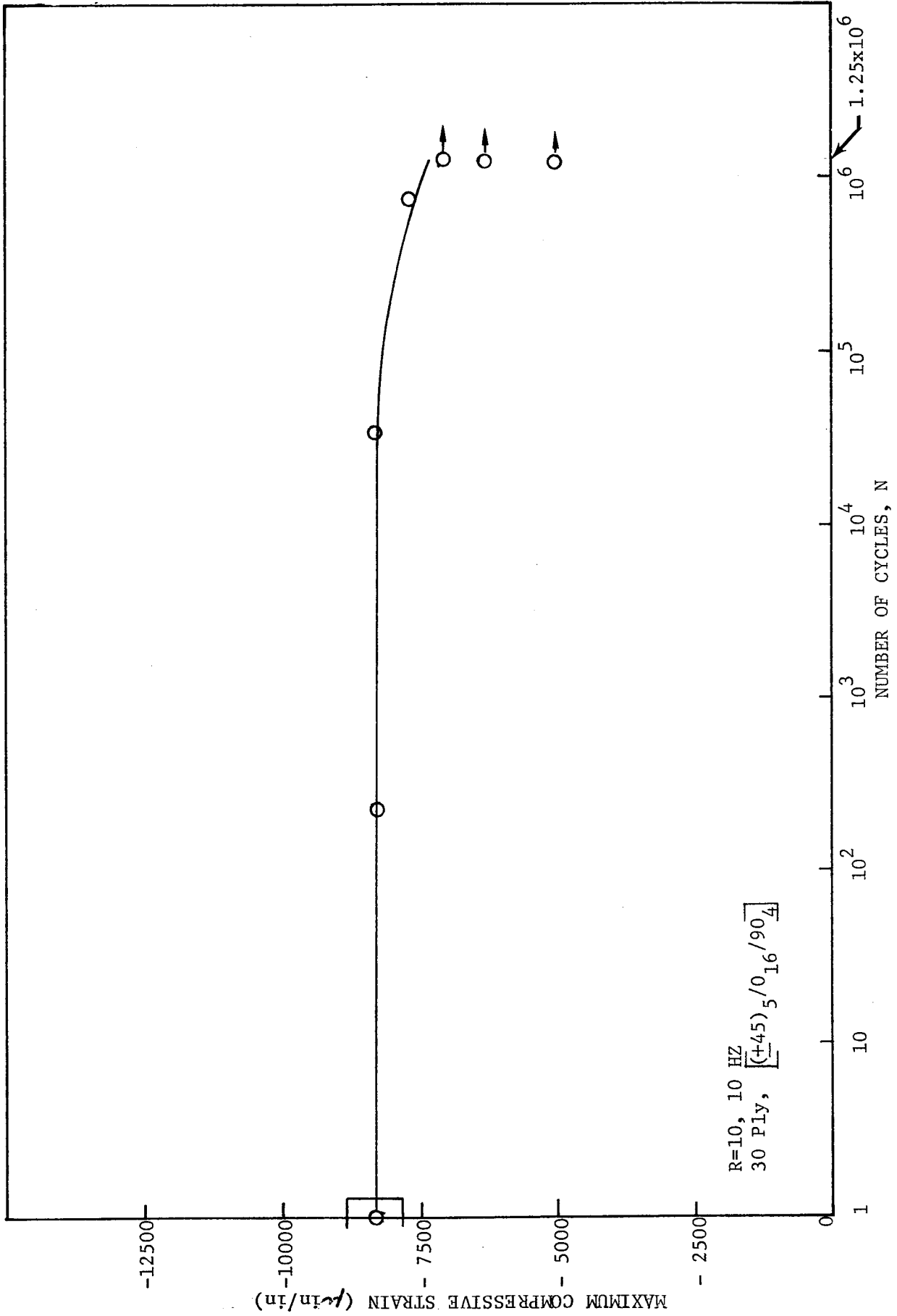
Figure 5.7. Constant Cycle Strain Fatigue Behavior for Plain Laminate, 218°FW.

Figure 5.8. 0° Static Compression Test Series V, Specimen ACL 4210A-4-12 Stress-Strain Curves, RTD, (PDO) #1, Thin Section.

Figure 5.9-0° Static Compression Test Series V, Specimen ACL 4210A-4-12 Stress-Strain Curves, RTD, (PDO) #1, Thick Section

Figure 5.10 0° Static Compression Test Series V, Specimen ACL 4210-5-14 Stress Strain Curves, RTD, (PDO) #1, Thin Section

STRESS (KSI)

Failure

Proportional Limit

□ Strain Gage 4

◇ Strain Gage 8

○ Strain Gage 3

△ Strain Gage 7

Strain (μ in/in x 10^3)

30 Plies, $[(\underline{+45})_5/0_{16}/90_4]_c$

Failure at -97.477 ksi

Figure 5.11 0° Static Compression Test Series V, Specimen ACL 4210A-5-14 Stress-Strain Curves, RTD, (PDO) #1, Thick Section

Figure 5.12 0° Static Compression Test Series V, Specimen ACL 4210A-5-16 Stress-Strain Curves, RTD, (PDO) #1, Thin Section.

Figure 5.13 0° Static Compression Test Series V, Specimen ACL 4210A-5-16 Stress-Strain Curves, RTD, (PDO) #1, Thick Section

Thin section proportional limit value (-36.8 ksi/-4100μ-in/in) is 34%
of the ultimate stress (-107.4 ksi) and 31% of the ultimate strain value
(-13,217 μ-in/in) with a modulus of elasticity of 9.10×10^6 psi and a
Poisson's Ratio of 0.260.

The 30-ply, thick section data shown in Table 5.2 were compared with
previous* test data from a 30-ply, $[(\pm 45)_5/0_{16}/90_4]_c$ test series tested under
similar environmental conditions. Differences in mean Poisson's Ratio are
large (33%) although, scatter for the PDO#1 specimens is large. However,
the differences between ultimate stresses and moduli are smaller (approxi-
mately 6% each).

5.3.1.2 RTD Static Tension Test Data

Static tension tests at RTD conditions were performed on Specimens ACL
4210A-6-1, -2, and -3 from Test Series XXI. The results of the tests are
presented in Appendix E, pages E.12 through E.23 with reduced data presented
in Table 5.1. Note that the mean ultimate stress for the thick section
is approximately 93.6% of the thin section ultimate stress. The figures on
pages E.14, E.19, and E.23 are the stress-strain curves for the specimens.
The curves are linear to failure and show a small amount of flatwise bending.
For thin section tension data, the scatter is low, showing an ultimate
stress of 107.8 ksi with a strain to failure of 10,630 μ-in/in, a modulus
of elasticity of 10.08×10^6 psi, and a Poisson's Ratio of 0.352.

5.3.1.3 RTW Static Compression Test Data

Static Compression tests at RTW conditions were performed on Specimens
ACL 4210A-5-23 and ACL 4211B-10-25 from Test Series VI with results pre-
sented in Table 5.2. The mean modulus is 9.76×10^6 psi and the mean Poisson's
Ratio is 0.199 taken on the thin section. The _thick section
ultimate stress compares well with 30-ply data from previous data**. Note
that the mean ultimate stress from previous data** (Test Series XX) is only
1.3% less than the measured thick section ultimate stress of Test Series
VI in Table 5.2.

---

*See Reference (1), Table 5.16, page 145
**Reference (1) Table 5.17, page 153

Figures 5.14 and 5.15 present the stress-strain curves for the thin
section test data. Note that for specimens 4210A-5-23 and 4211B-10-25
the proportional limit is 33- 34% of the ultimate stress. The ultimate
stress for the thick section is 92% of the thin section ultimate stress.
For the thin section, the proportional limit values (-35.9 ksi/-3825 μ-in/in)
are 34% of the ultimate stress value (106.0 ksi) and 29% of the ultimate
strain value. Modulus of elasticity was 9.76×10^6 psi with Poisson's Ratio
being 0.199.

5.3.1.4 -65°FW Static Compression Test Data

The results of -65°FW condition static compression tests on Specimens
ACL 4210A-4-1, -3, and -5 of Test Series IV are presented in Table 5.2.
The ultimate stress for the thick section is approximately 91.6% of the
ultimate stress in the thin section. Figures 5.16, 5.17, and 5.18 present
the stress-strain curves for the thin section of the specimens. Note
that for the thin section the mean proportional limit (-40.4 ksi/-4300 μin/
in) for these specimens is 31% of the ultimate stress and 25% of the
failure strain. Modulus of elasticity is 9.41×10^6 with Poisson's Ratio
being 0.292.

5.3.1.5 218°FW Static Compression Test Data

The 218°FW specimens ACL 4211B-10-36 and -11-38 from Test Series VII
were tested in static compression. The results of the tests are presented
in Table 5.2. Note that the thick section ultimate stress is 95% of the
thin section ultimate stress. The 30-ply thick section data from Table
5.2 can be compared with data obtained from under similar environmental
conditions,Reference (1)*. Note that the difference between the
mean ultimate stress in Table 5.2 and the mean ultimate stress from
Reference (1) is less than 6%. Figures 5.19 and 5.20 present the stress-
strain curves for the thin section data shown in Table 5.2. Note that the
proportional limit stress (-35.0 ksi) is 47% of the ultimate stress (-75.2
ksi) for Test Series VII, whereas, the proportional limit strain (-3476
μ-in/in) is 41% of the failure strain (-8300 μ-in/in). Modulus of Elasti-

---

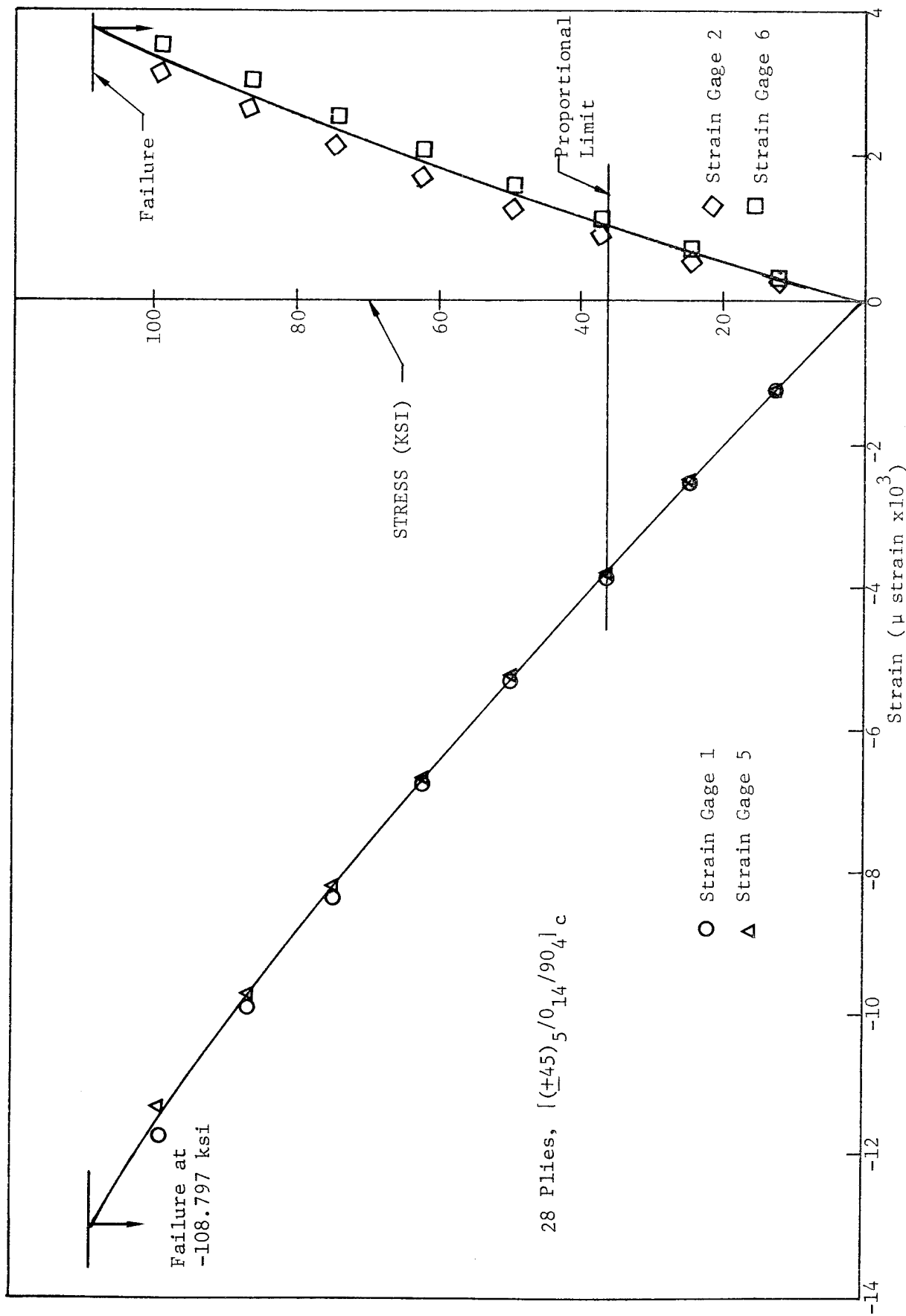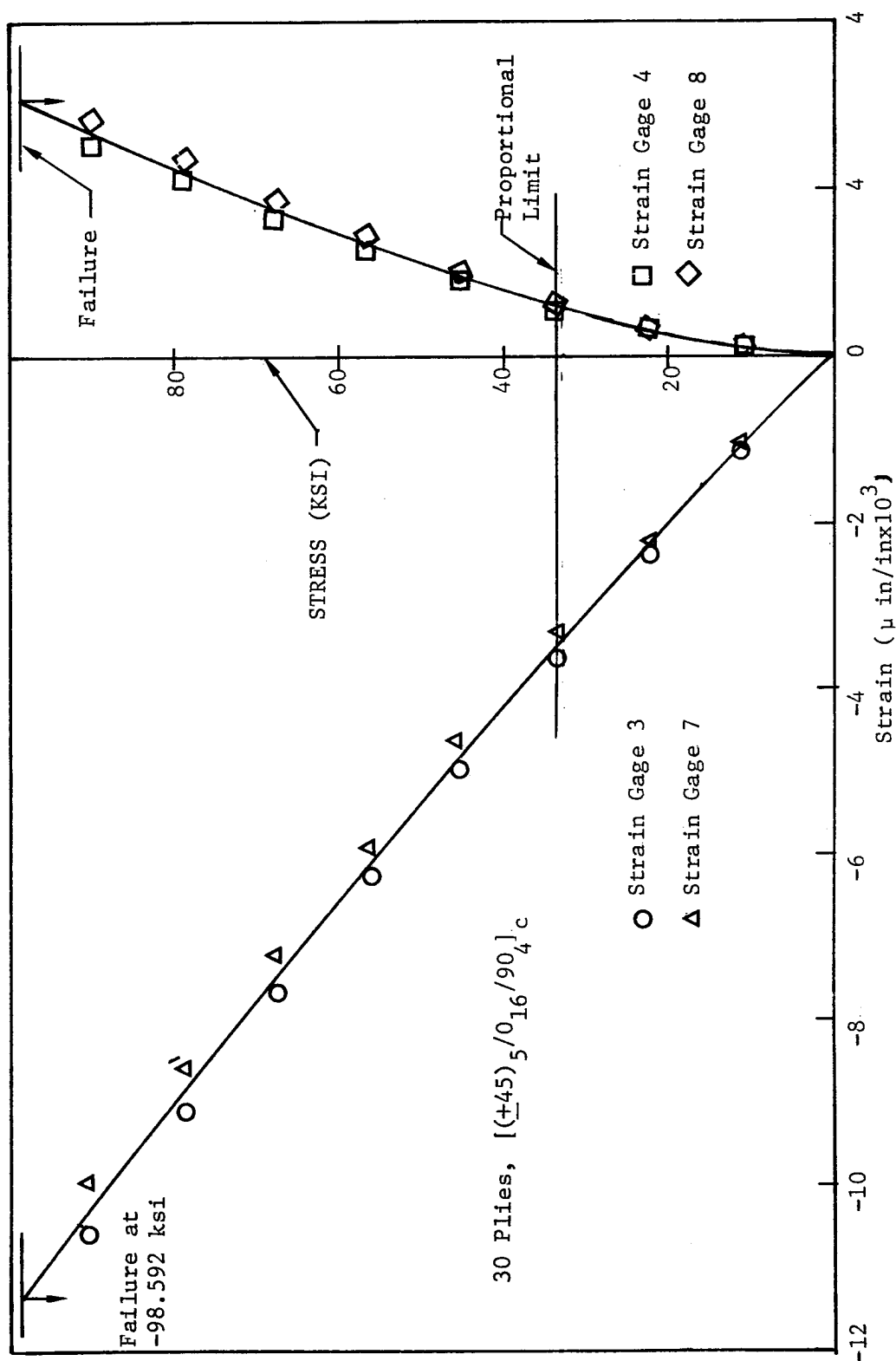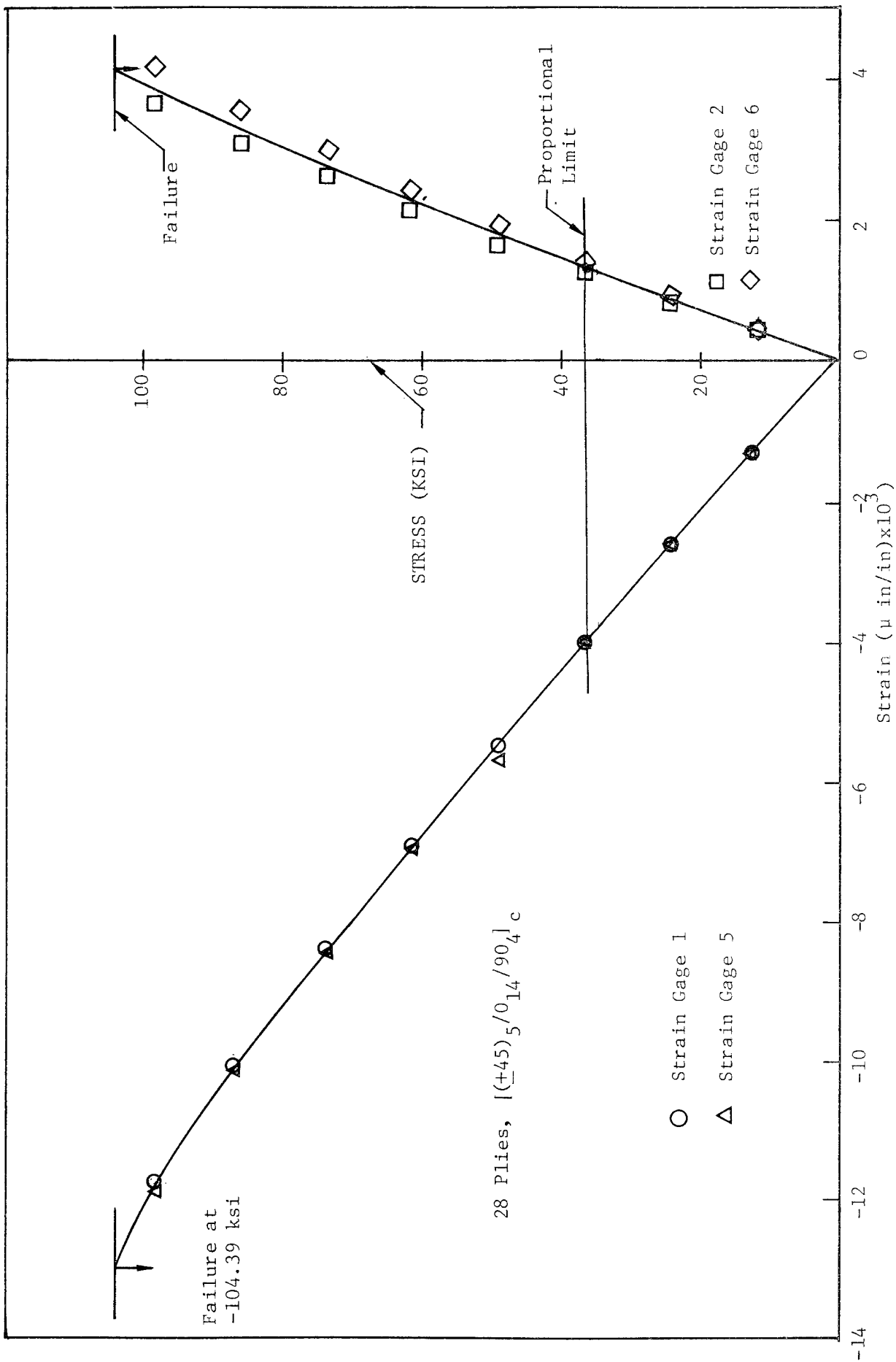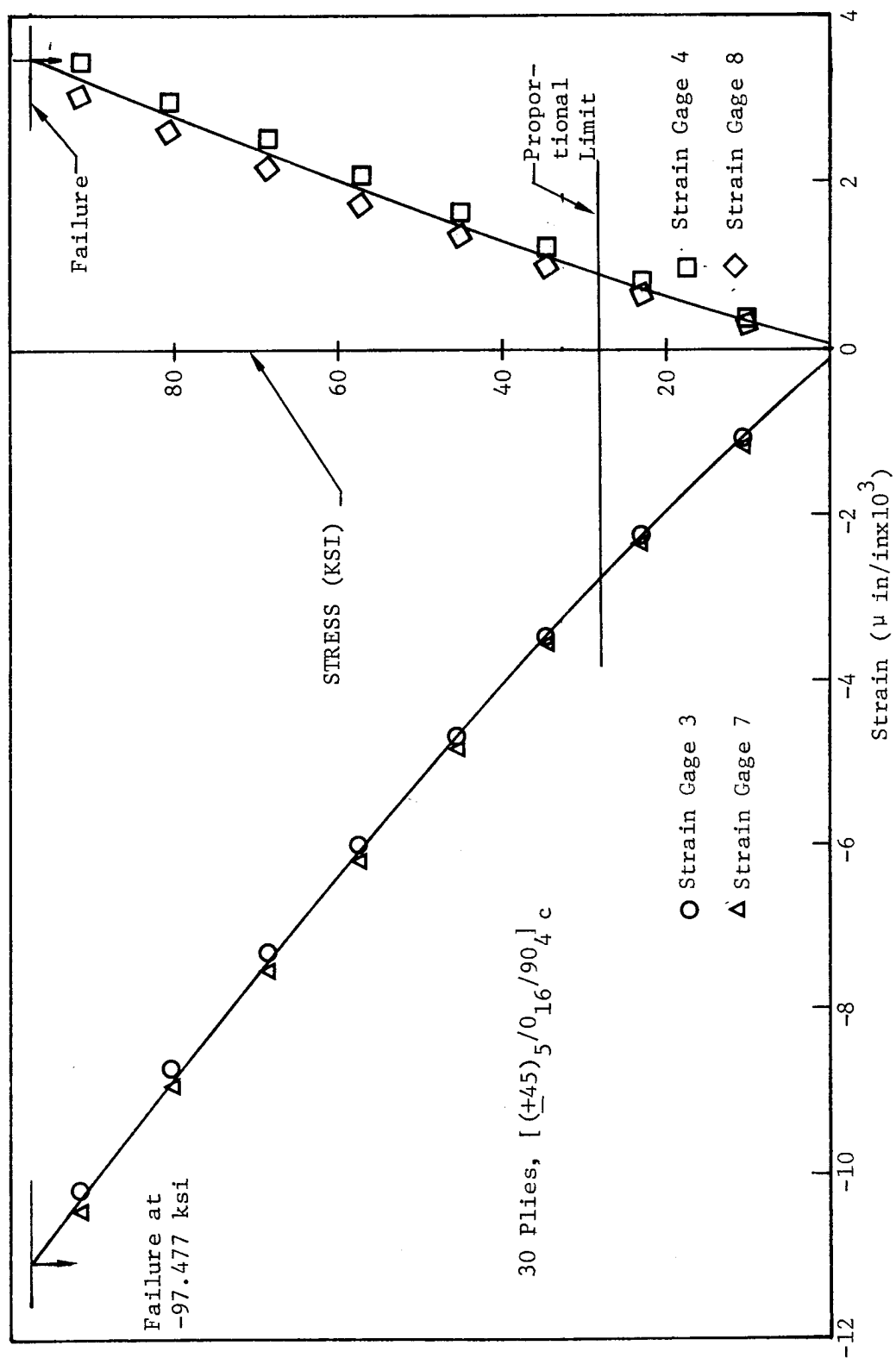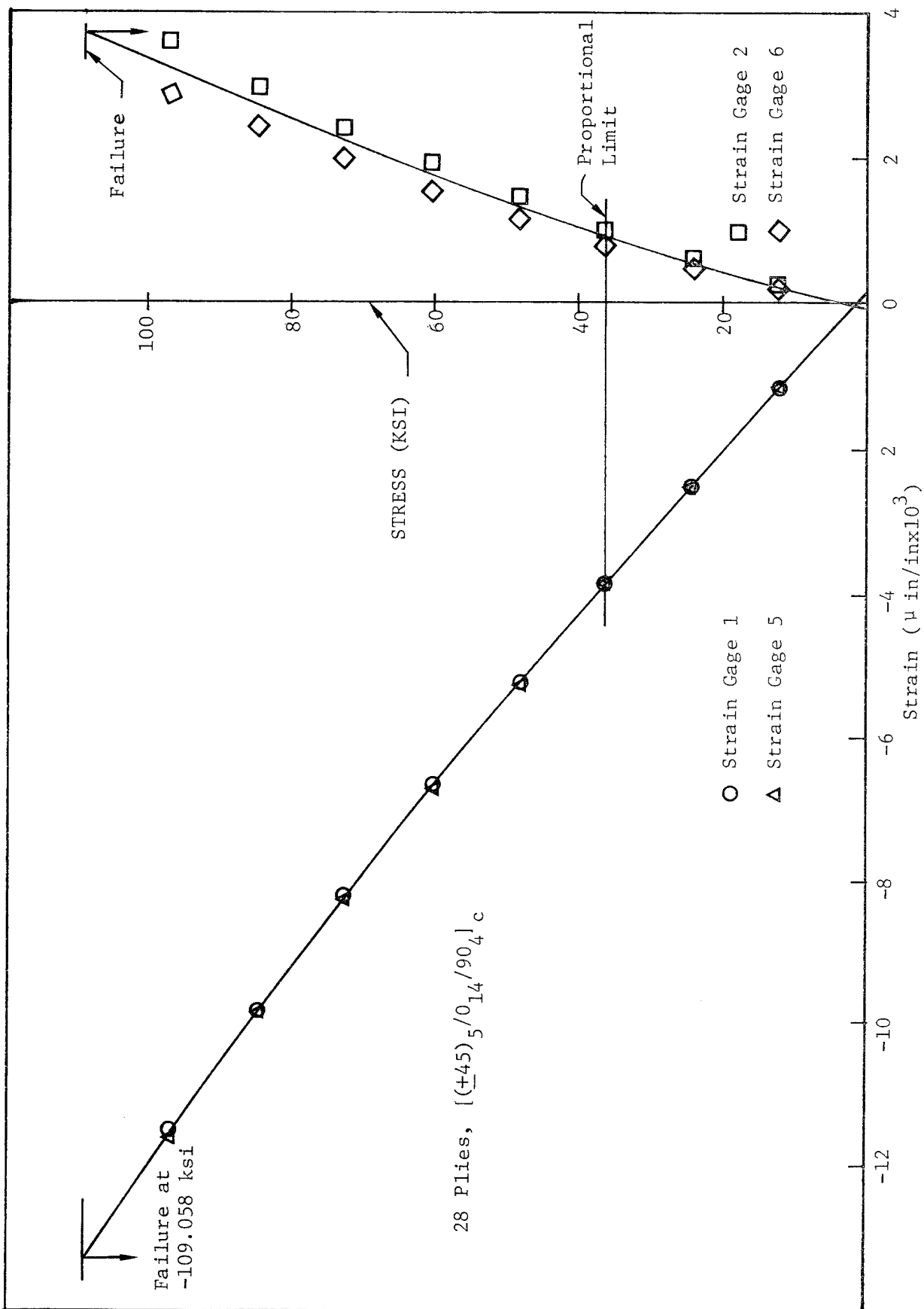*Page 153, Table 5.17, Test Series XXII
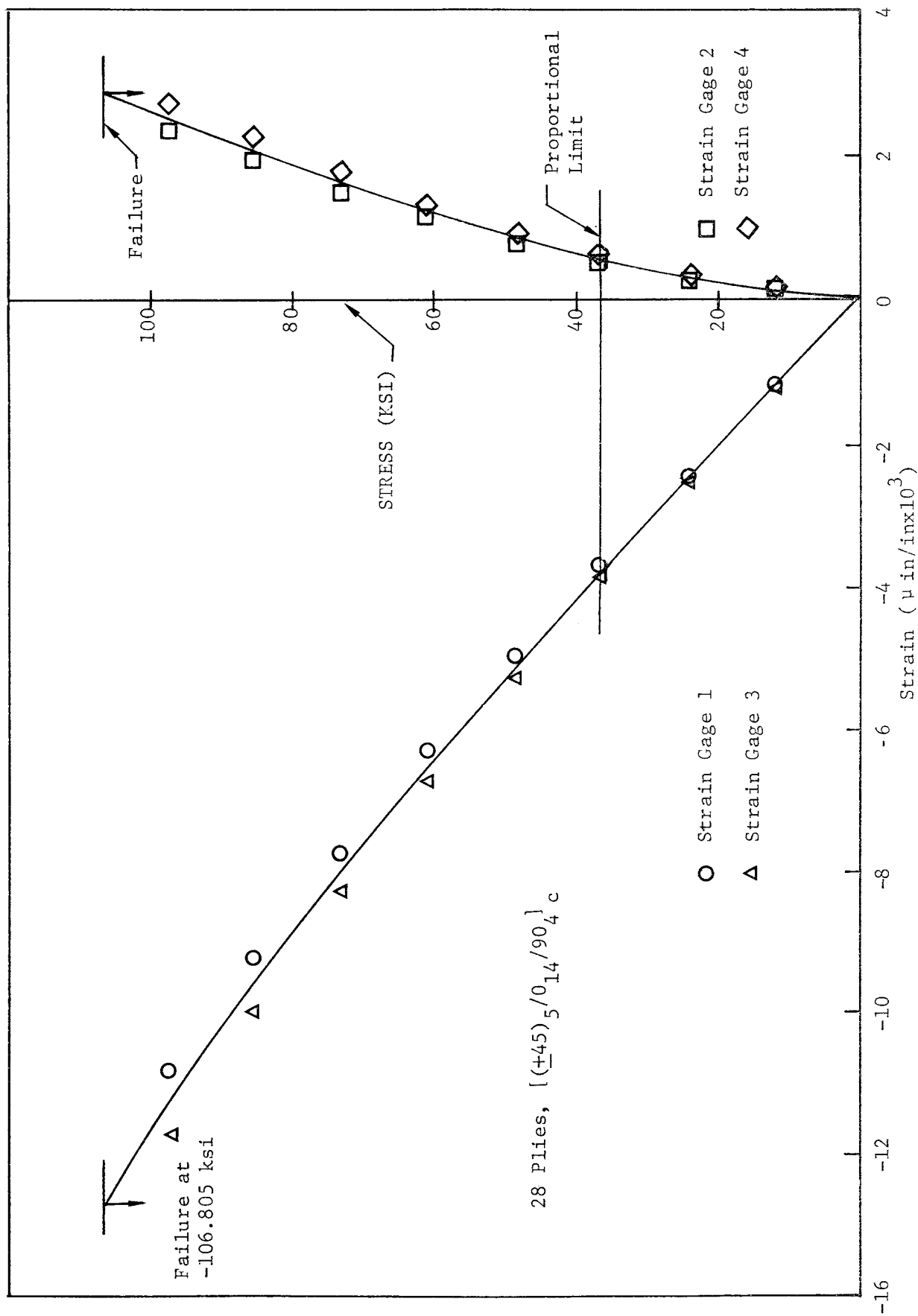
Figure 5.14 0° Static Compression Test Series VI, Specimen ACL 4210A-5-23 Stress-Strain Curves, RTW, (PDO) #1, Thin Section
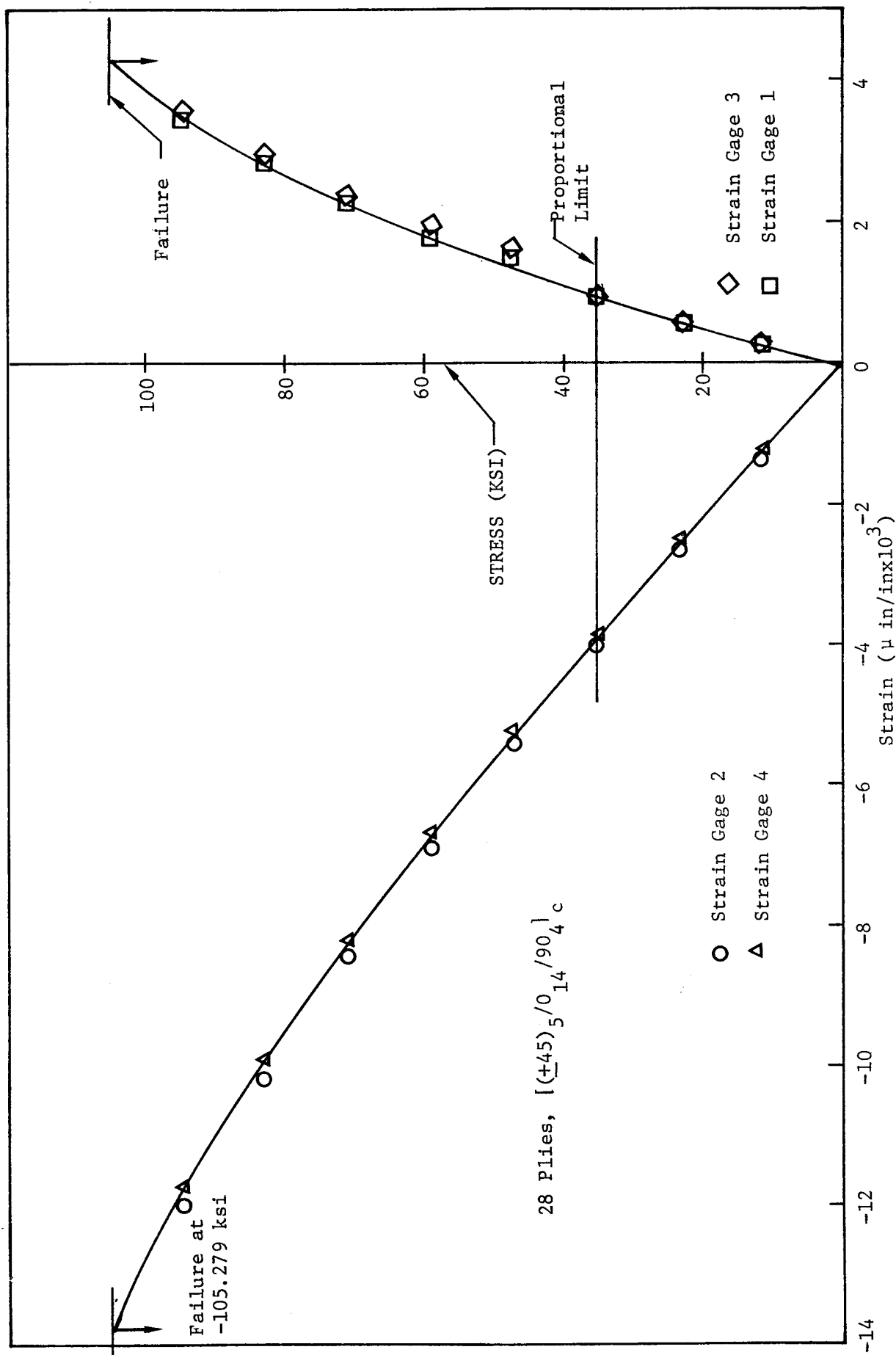
Figure 5.15 0° Static Compression Test Series VI, Specimen ACL 4211B-10-25 Stress-Strain Curves, RTW, (PDO) #1, Thin Section
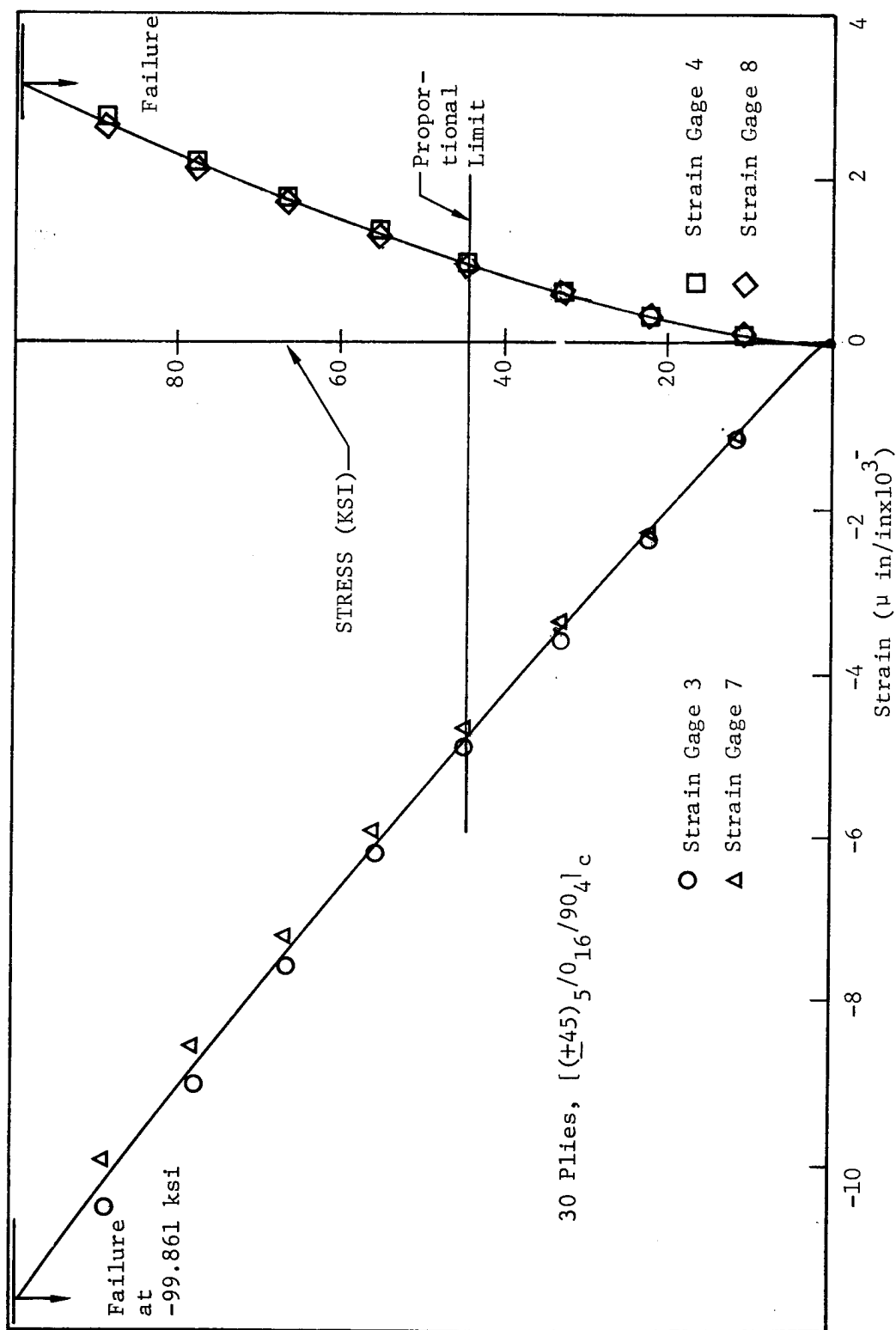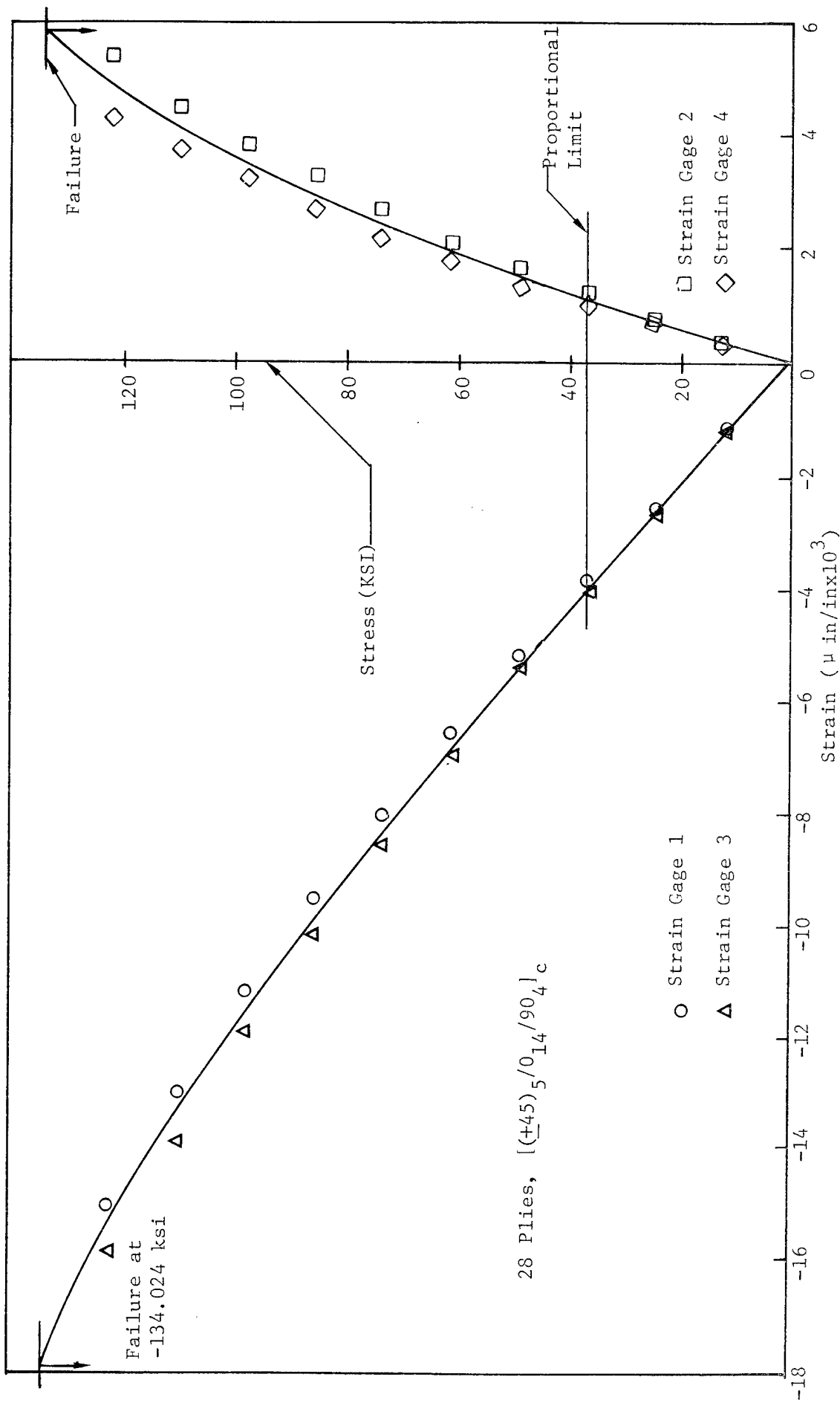
Figure 5.16 0° Static Compression Test Series IV, Specimen ACL 4210A-4-1 Stress-Strain Curves, -65FW, (PDO) #1, Thin Section

28 Plies, $[(\underline{+45})_5/0_{14}/90_4]_c$

Failure at -134.024 ksi

Proportional Limit

Failure

Stress (KSI)

Strain (μ in/in x 10^3)

○ Strain Gage 1
△ Strain Gage 3

□ Strain Gage 2
◇ Strain Gage 4
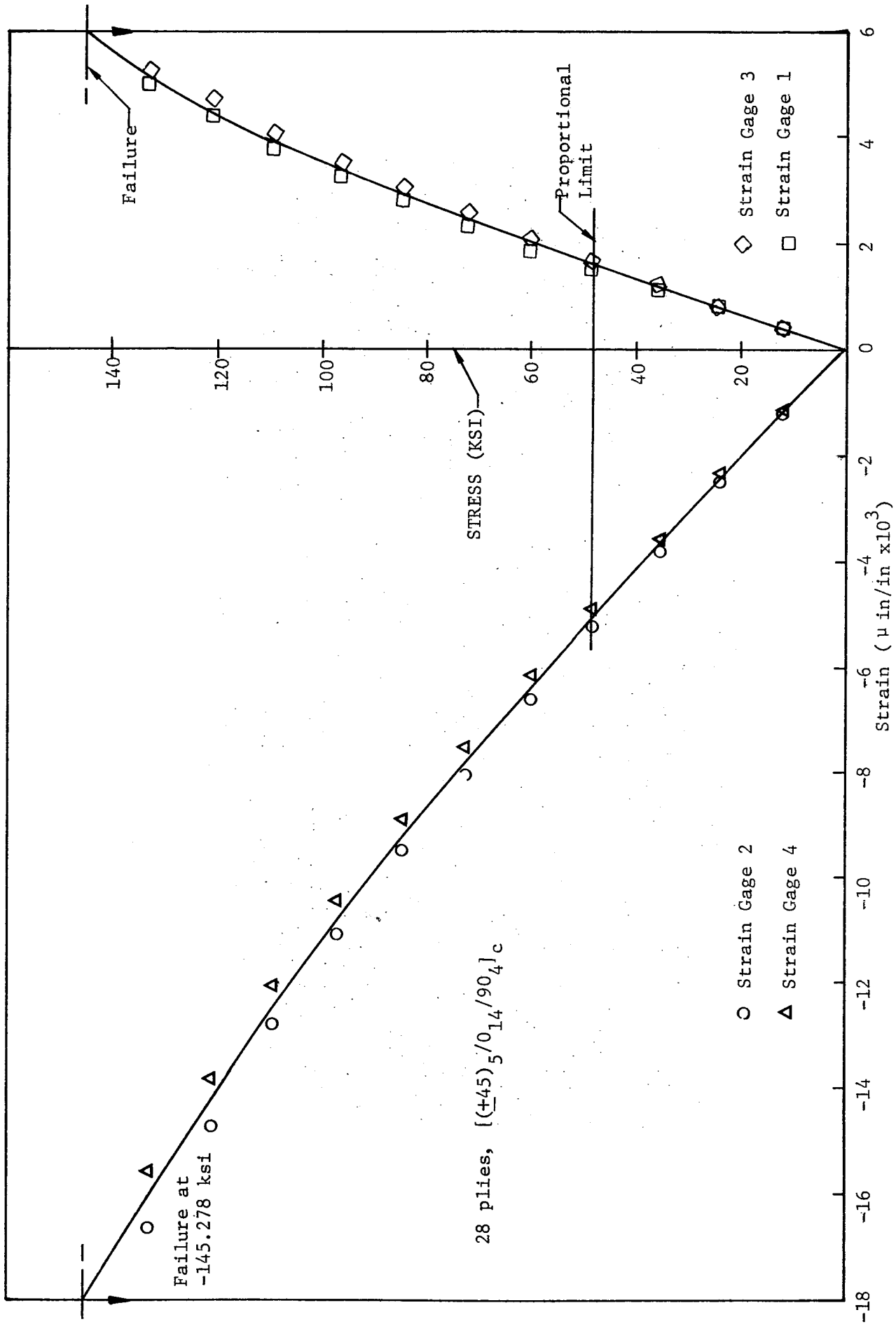
Figure 5.17 0° Static Compression Test Series IV, Specimen ACL 4210A-4-3 Stress-Strain Curves, -65FW, (PDO) #1, Thin Section

5.33
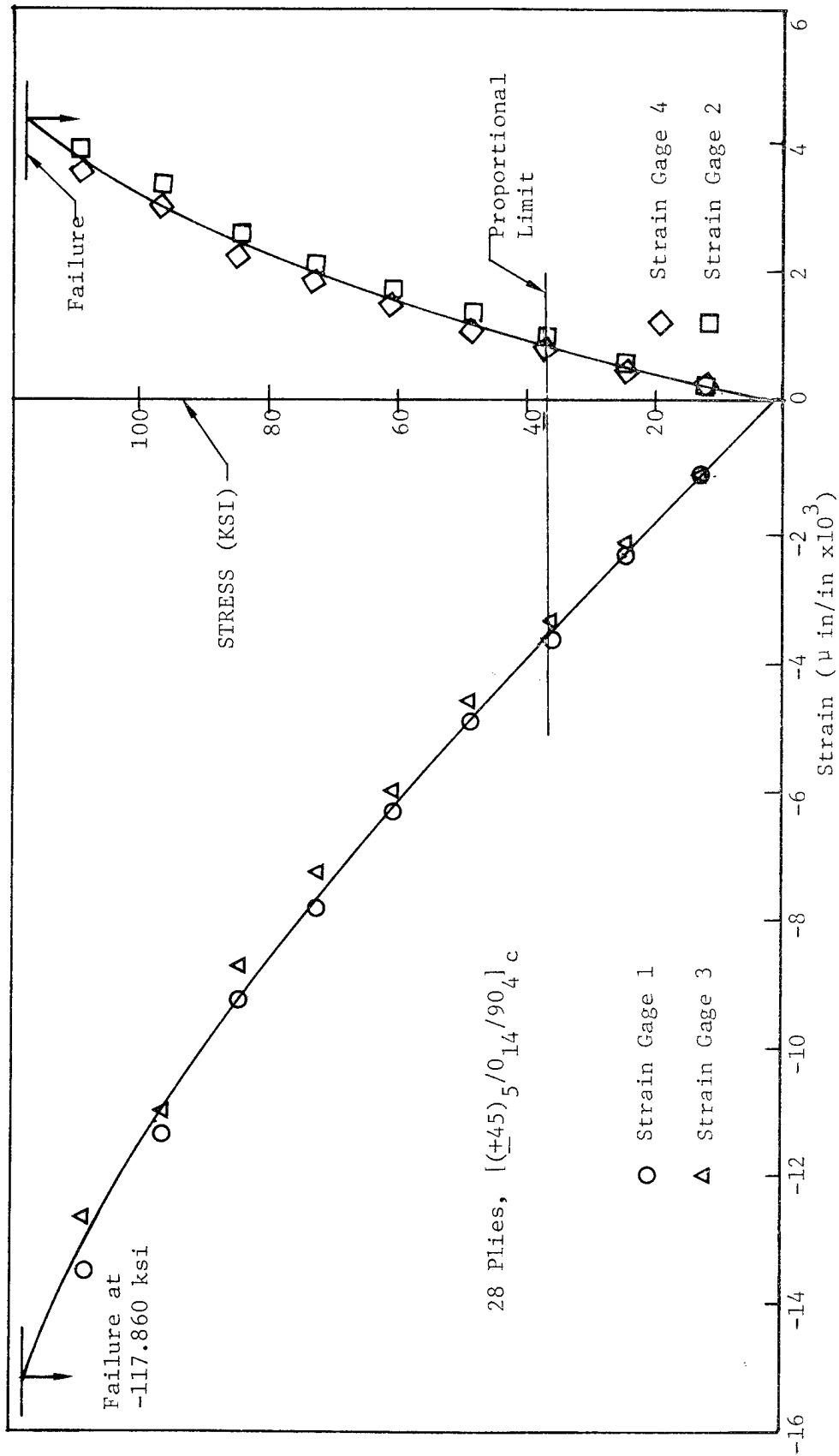
Figure 5.18 0° Static Compression Test Series IV, Specimen ACL 4210A-4-5 Stress-Strain Curves, -65FW, (PDO) #1, Thin Section
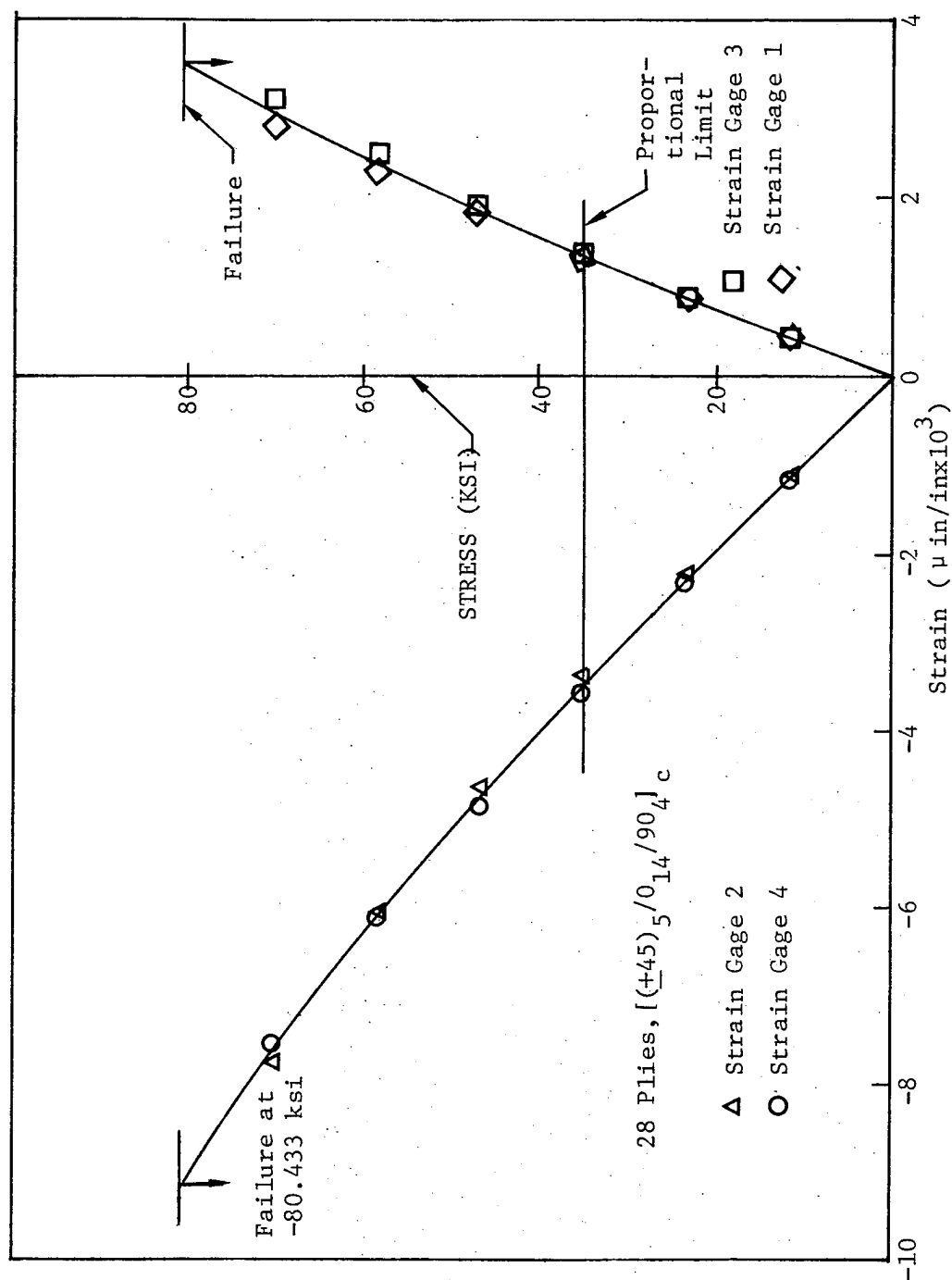
Figure 5.19 0° Static Compression Test Series VII, Specimen ACL 4211B-10-36
Stress-Strain Curves, 218FW, (PDO)#1, Thin Section
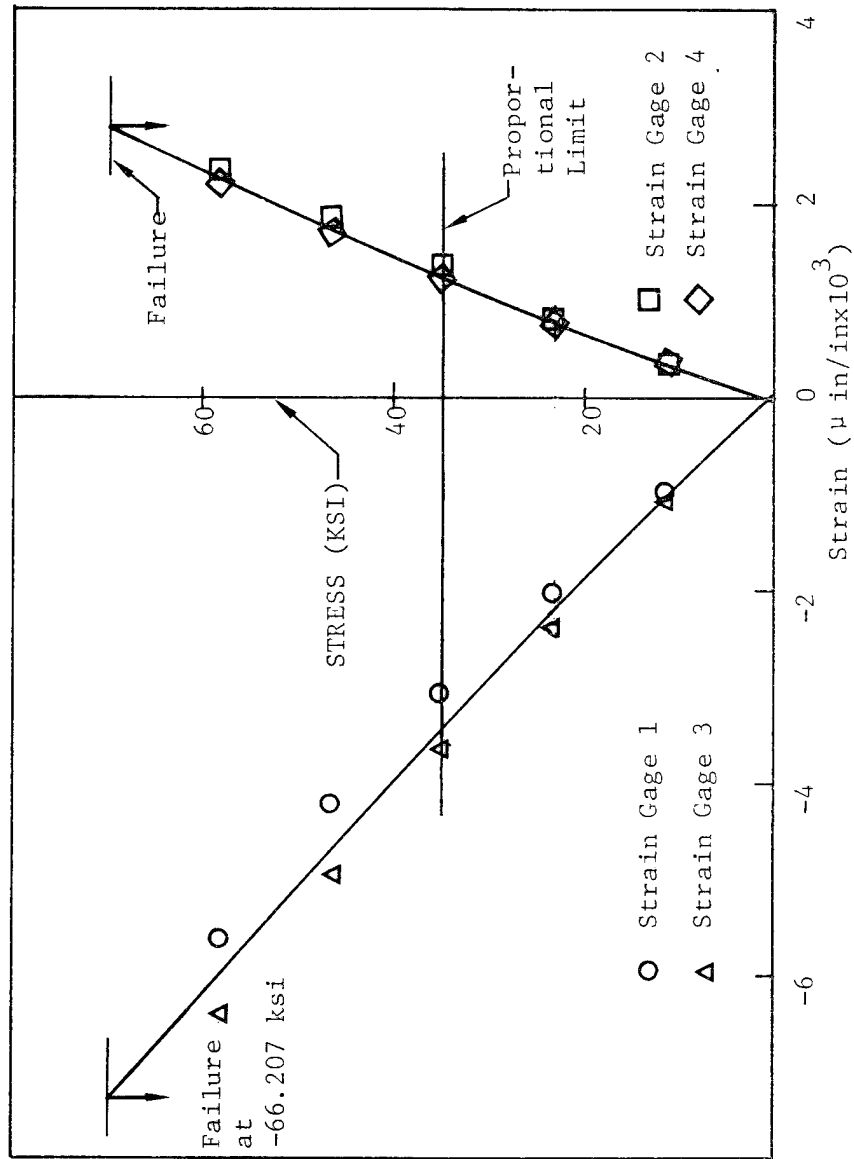
Figure 5.20 0° Static Compression Test Series VII, Specimen ACL 4211B-11-38
Stress-Strain Curves, 218FW. (PDO) #1, Thin Section

city is 10.13×10^6 psi and Poisson's Ratio is 0.310.

5.3.2 Fatigue Test Data

5.3.2.1 RTD Compression Fatigue Test Data

RTD condition, R=10, constant frequency (10 Hz), compression-compression fatigue testing was performed on specimens from Test Series IX with results presented in Table 5.3. Gages were mounted on both the thick and thin sections. Figures 5.21 and 5.22 present the RTD test data S vs. N curves. On each figure are two curves; one being the thick section curve and the other being the thin section curve. Figure 5.21 shows that the thin and thick section curves parallel one another from their static stress values to the stress values at runout (1.25×10^6 cycles). It is observed that the minimum* stresses at runout (projected curve) for both the thin and thick sections are approximately 62% of the static stress values, respectively. From Figure 5.22, note that the strains (6500 μ-in/in and 5700 μ in/in) at runout (projected curve on both the thin and thick sections are approximately 50% of the static strain values.

5.3.2.2 RTW Compression Fatigue Test Data

RTW condition, R=10, constant frequency (10 Hz), compression-compression fatigue testing was performed on specimens from Test Series X with results presented in Table 5.3. Strain gages were mounted on the thin section only. Figures 5.23 and 5.24 present the RTW fatigue test data. Figure 5.23 presents maximum compressive stress versus number of cycles (f vs N) curves. The maximum compressive stress (-58.6 ksi and -54.2 ksi) at runout for both the thin and thick sections is 55% of the static value. Figure 5.24 presents maximum compressive strain versus number of cycles for the thin section. Note that the strain (-7074 μ-in/in) at runout is 53% of the static failure strain value.

5.3.2.3 -65°FW Compression Fatigue Test Data

-65°FW condition, R=10, constant frequency (10 Hz), compression-compression fatigue testing was performed on specimens from Test Series VIII with results presented in Table 5.3. There were gages mounted on the thin section only. Figures 5.25 and 5.26 are the stress versus number of cycles

---

*Peak compressive stress in cycles

Figure 5.21. Constant Cycle Fatigue Stress Behavior, (PDO #1), RTD.
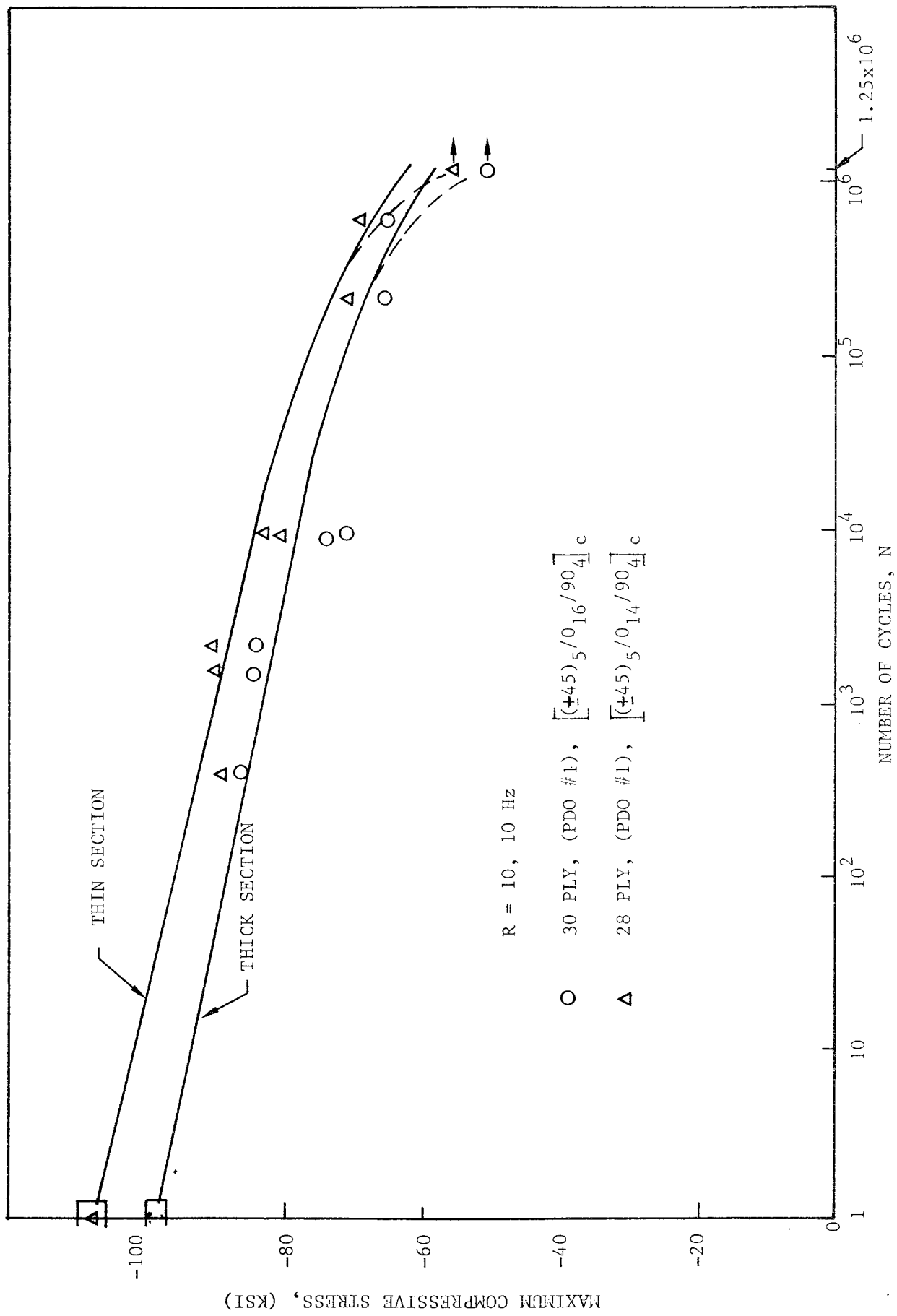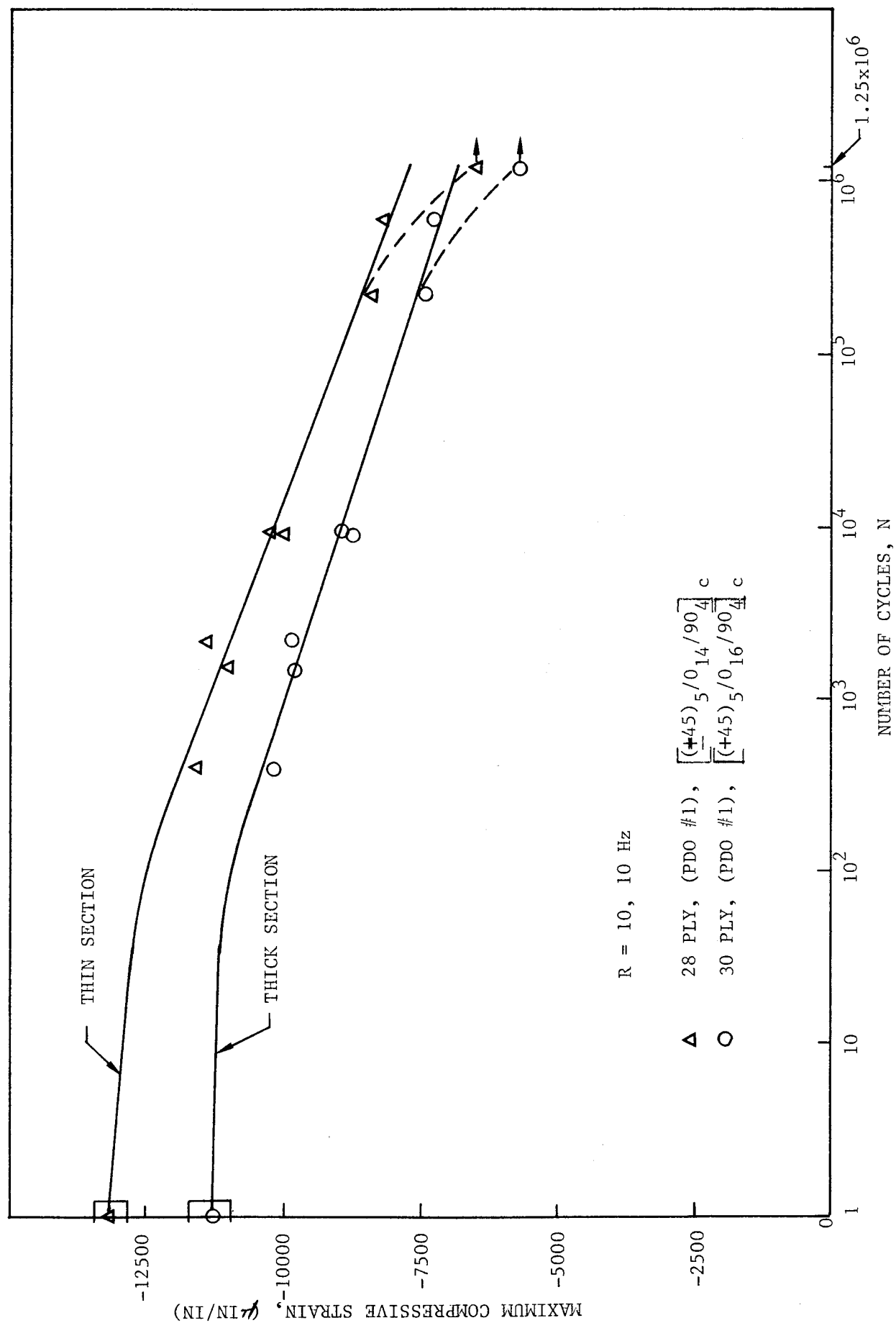
Figure 5.22. Constant Cycle Fatigue Strain Behavior, (PDO #1), RTD.
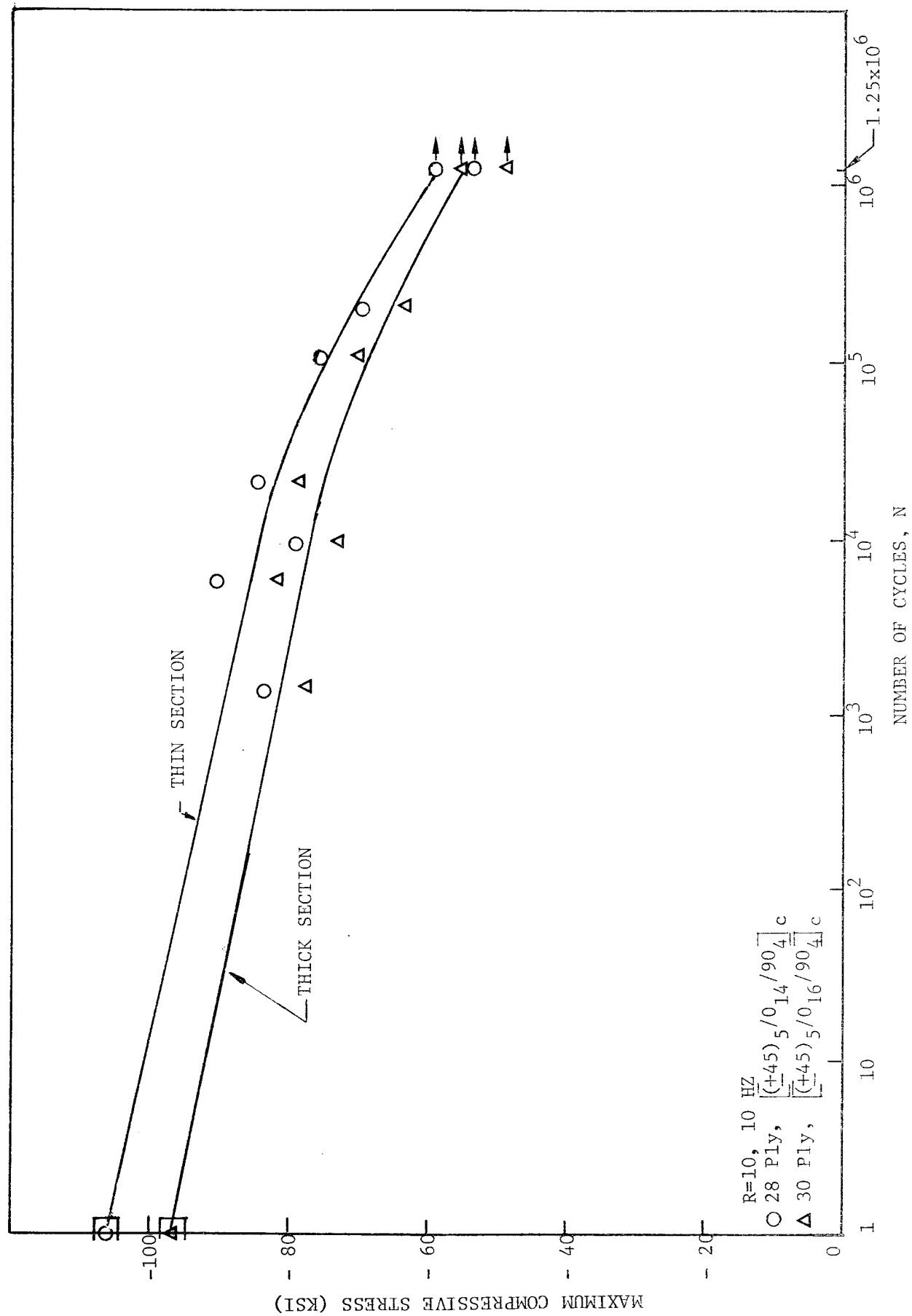
Figure 5.23. Constant Cycle Fatigue Stress Behavior, (PDO #1), RTW.

5.40
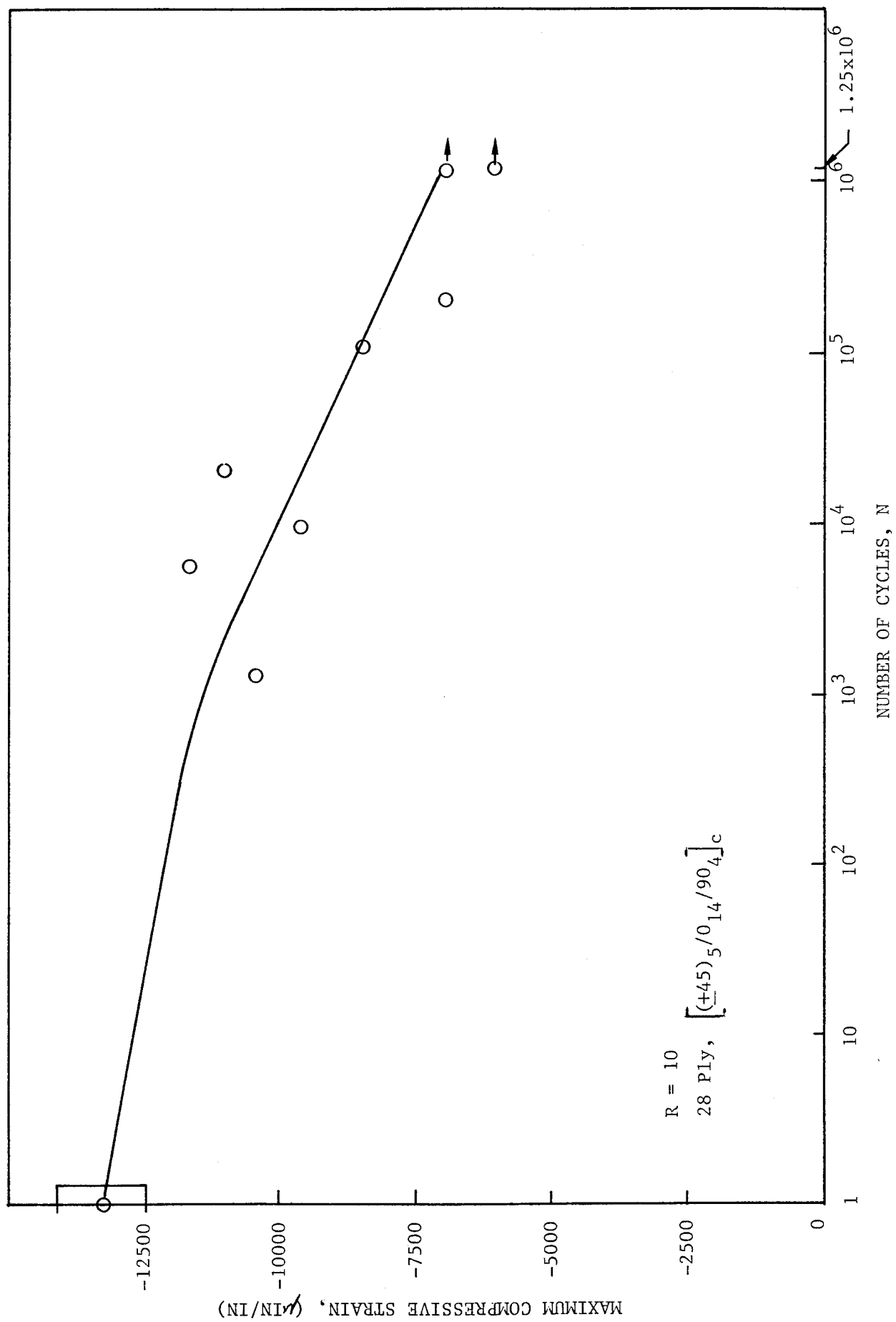
Figure 5.24. Constant Cycle Fatigue Strain Behavior. (PDO #1), RTW.

R = 10

$\left[(\pm 45)_5/0_{14}/90_4\right]_c$

28 Ply,

NUMBER OF CYCLES, N

MAXIMUM COMPRESSIVE STRAIN, (μIN/IN)
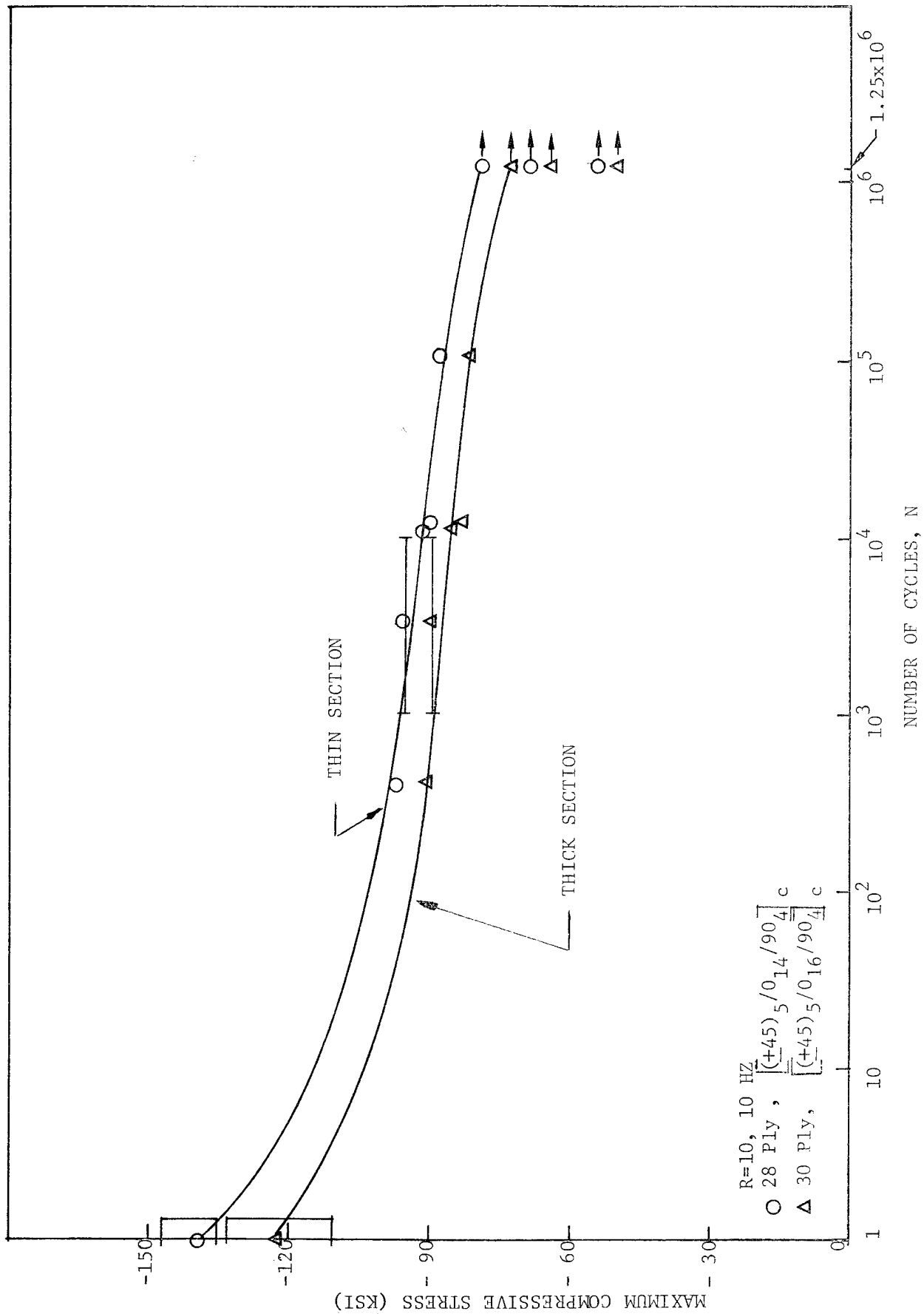
Figure 5.25. Constant Cycle Fatigue Stress Behavior for (PDO #1), −65°FW.
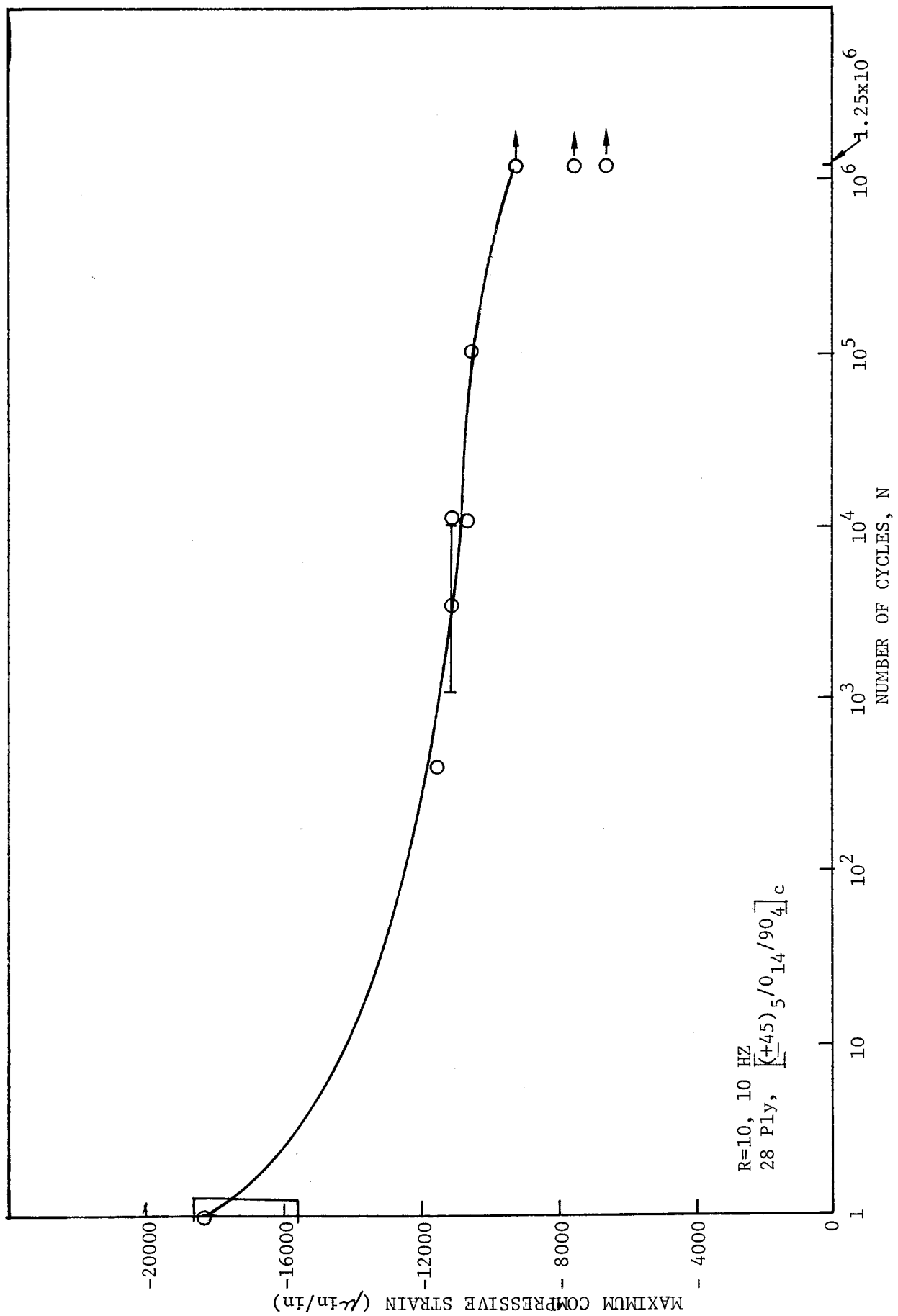
Figure 5.26. Constant Cycle Fatigue Strain Behavior, (PDO #1) -65°FW, Thin Section.

R=10, 10 HZ
28 Ply, $[(\pm 45)_5/0_{14}/90_4]_c$

NUMBER OF CYCLES, N

MAXIMUM COMPRESSIVE STRAIN (μin/in)

(f vs N) and strain versus number of cycles (ε vs N) plots. On both curves,
note that there is one point at which the actual number of cycles could not
be accurately determined. At this point, the auto-stop on the test
monitoring equipment failed to operate. The point is known to be between
1,000 and 10,000 cycles, however, and this is reflected on the plots. From
Figure 5.25, note that the stress (-78.7 ksi and -72.5 ksi) at runout on
both the thick and thin sections is 59% of the static stress value while
the strain at runout (see Figure 5.26) is 53% of the static strain value.

5.3.2.4 218°FW Compression Fatigue Test Data

218°FW condition, R=10, constant frequency (10 Hz), compression-compres-
sion fatigue tests were performed on specimens from Test Series XI with
results presented in Table 5.3. Figures 5.27 and 5.28 present the stress
(f) and strain (ε) data plotted versus number of cycles (N). From Figure
5.27, note that the compressive stresses for both the thin and thick
section at runout (-51.8 ksi and -48.1 ksi) are 67% and 69%, respectively, of
the static compressive stress.

5.4 PLY DROP-OFF NO. 2

5.4.1 Static Test Data

5.4.1.1 RTD Static Compression Test Data

Static compression tests were performed on specimens ACL 4210A-7-12,
-8-14, and -8-16 from Test Series XIII with the results presented in
Table 5.2. On the specimens, gages were mounted on both the thick and
thin sections. From Table 5.2, note that the mean ultimate stress (-100.3
ksi) for the thick section is 94% of the mean thin section ultimate
stress (-107.2 ksi). The mean ultimate strain (-12,383 μ-in/in) of the
thick section is 102% of that of the thin section (-12,183 μ-in/in), the
mean proportional limit for the thin section is -39.8 ksi or 37% of the
mean ultimate stress with the mean proportional limit strain (-4267 μ in/in)
being 35% of the mean ultimate strain. The mean modulus of elasticity
is 9.88x10^6 psi with Poisson's Ratio being 0.193. The difference in modu-
lus and Poisson's Ratio values for the thick and thin sections is   not
significant. The thick section properties from Table 5.2 can be compared
to 30-ply data from Reference (1). The mean ultimate stress from Reference
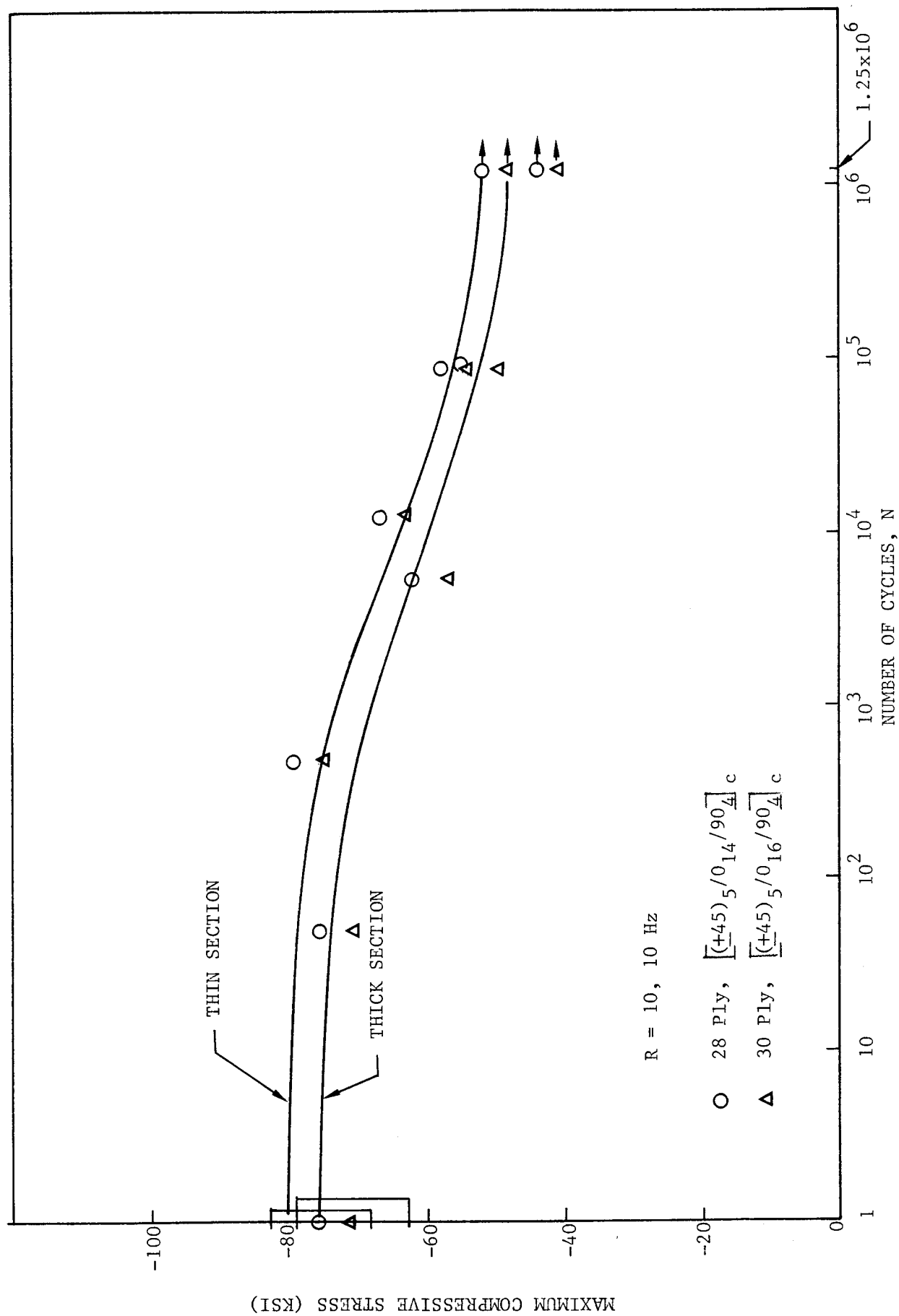
Figure 5.27.   Constant Cycle Fatigue Stress Behavior, (FDO #1), 218°FW.
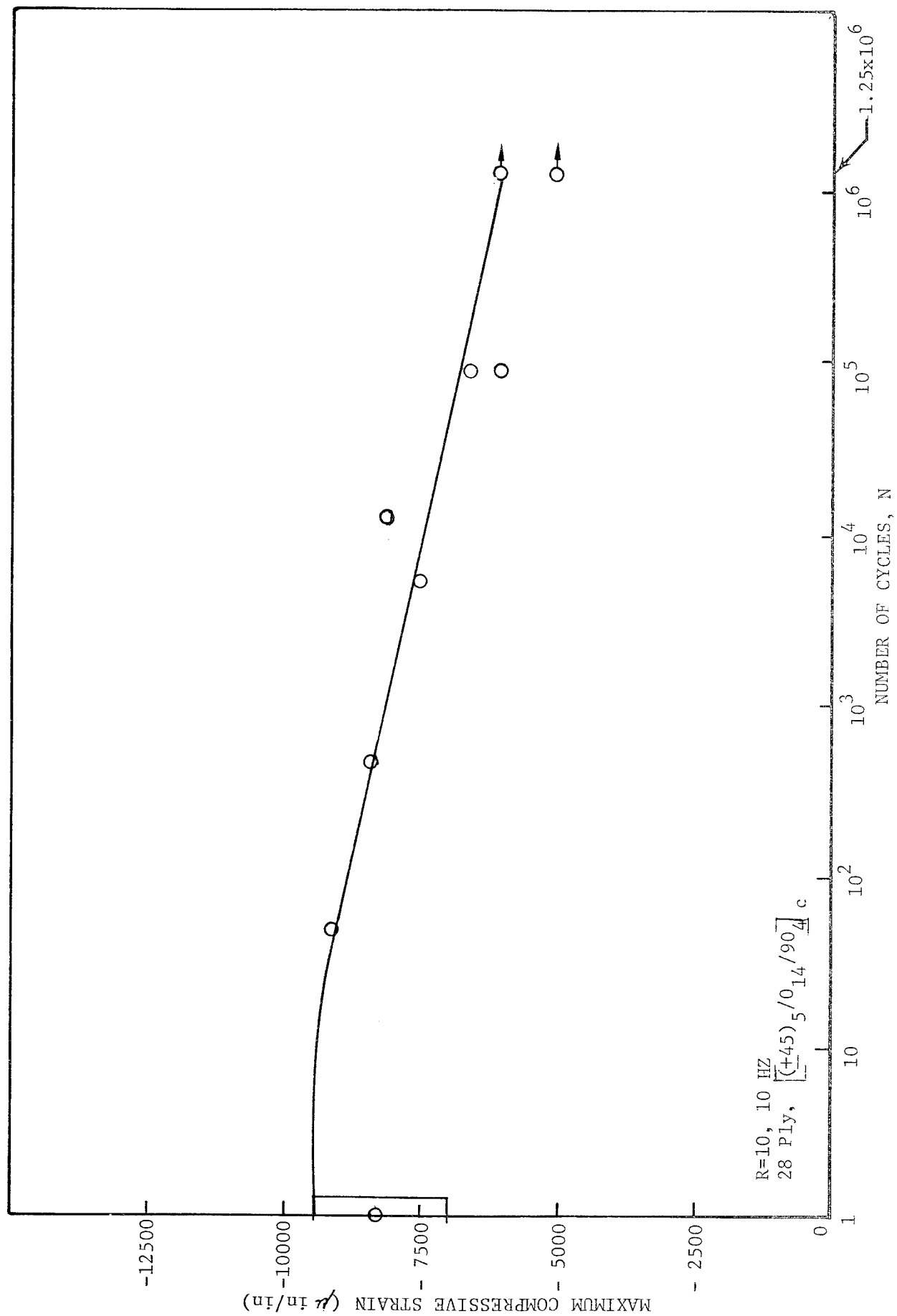
Figure 5.28. Constant Cycle Fatigue Strain Behavior, (PDO #1), 218°FW, Thin Section.

R=10, 10 HZ
28 Ply, $[(\underline{+}45)_5/0_{14}/90_4]_c$

MAXIMUM COMPRESSIVE STRAIN (μ in/in)

NUMBER OF CYCLES, N

5.46

(1) differs from the mean thick section ultimate stress of Table 5.2 by
less than 4.5% and the mean moduli differ by approximately 9%. However,
the differences in proportional limits and Poisson's Ratios are much
greater. Stress and Strain test data for the thick and thin sections was
plotted and is presented in Figures 5.29 through 5.34. There is little
difference in the shape of the curves between the thick and thin sections
but the thin section curves always reach slightly higher stress and
strain levels at failure.

5.4.1.2 RTD Static Tension Test Data

Static tension tests at RTD conditions were performed on Specimens
ACL 4210A-9-1, -2, and -3 from Test Series XXII. The results of the tests
are presented in Appendix E, pages E.26 through E.35, with reduced data
presented in Table 5.1. From Table 5.1, note that the mean thick section
ultimate stress is approximately 83% of the mean thin section ultimate
stress. The figures on pages E.27, E.30, and E.35 are the stress-strain
curves for Specimens ACL 4210A-9-1, -2, and -3. Note that the curves are
linear with little longitudinal strain gage bending. The curves associated
with Specimen ACL 4210A-9-2 (see page E.30) show a discontinuity at a high
stress level just before failure. The surface on one side of the test speci-
men cracked, introducing additional strain in the gages on that side of the
specimen (gages 1 and 3) with no increase in the stress. For the thin
section the ultimate stress is 128.5 ksi with a failure strain of 10,649
μ-in/in, a modulus of elasticity of 11.95×10^6 psi, and a Poisson's Ratio
of 0.272.

5.4.1.3 RTW Static Compression Test Data

Static compression tests were performed on Specimens ACL 4210A-8-23
and ACL 4211B-12-25 from Test Series XIV with results presented in Table
5.2. From Table 5.2, note that the mean ultimate stress for the thick
section is 83% of that of the thin section. The mean ultimate stress of
-95.9 ksi from Reference (1)[*], and the mean thick section ultimate stress
from Table 5.2 of -89.5 ksi, differ by approximately 7%. Figures 5.35
and 5.36 are the stress-strain curves from these specimens. Test Series XIV

---

[*]Page 153, Table 5.17

Figure 5.29 0° Static Compression Test Series XIII Specimen ACL 4210A-7-12 Stress-Strain Curves, RTD, (PDO) #2, Thin Section
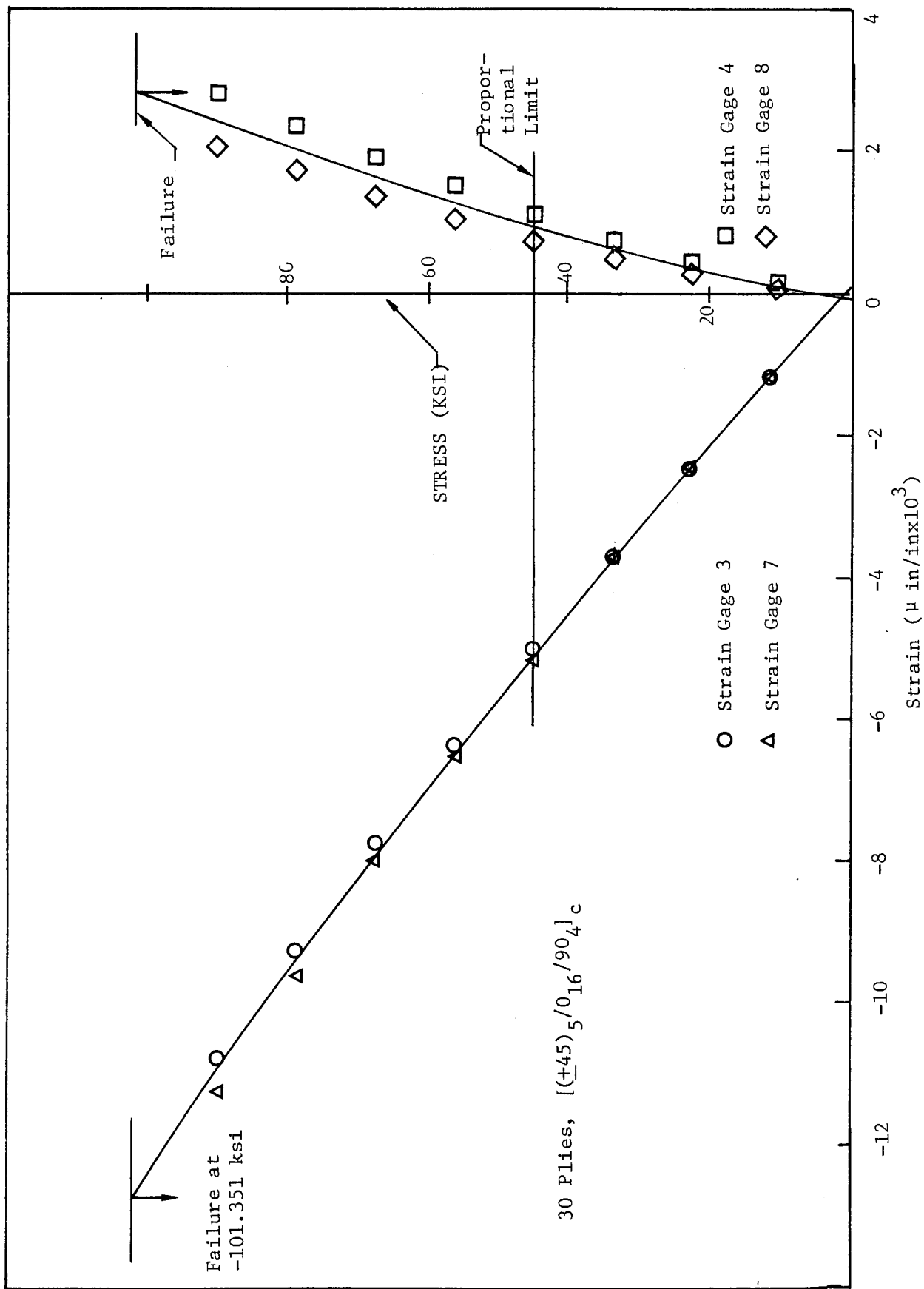
Figure 5.30 0° Static Compression Test Series XIII, Specimen ACL 4210A-7-12 Stress-Strain Curves, RTD, (PDO) #2, Thick Section
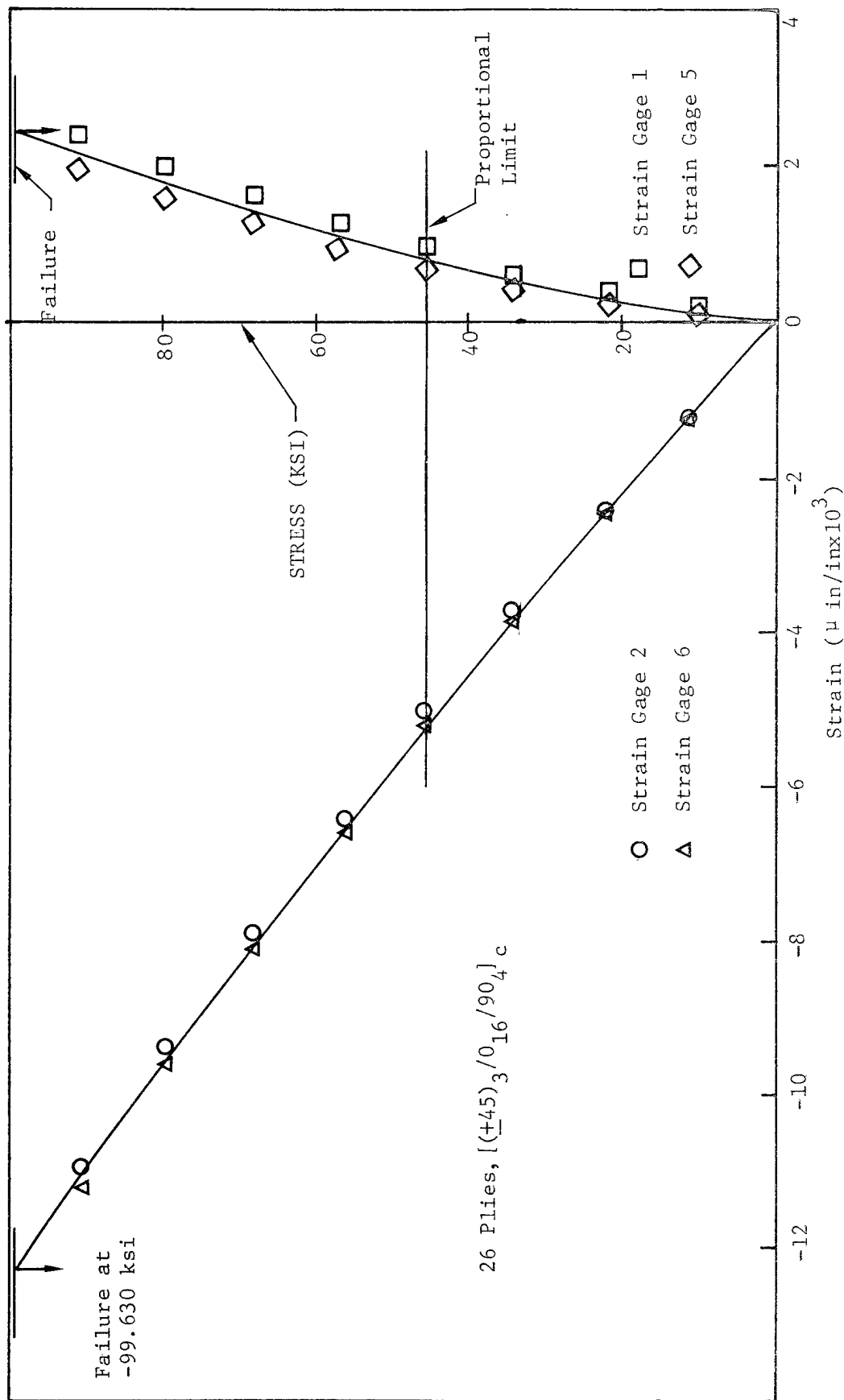
Figure 5.31 0° Static Compression Test Series XIII, Specimen 4210A-8-14 Stress-Strain Curves, RTD, (PDO) #2, Thin Section
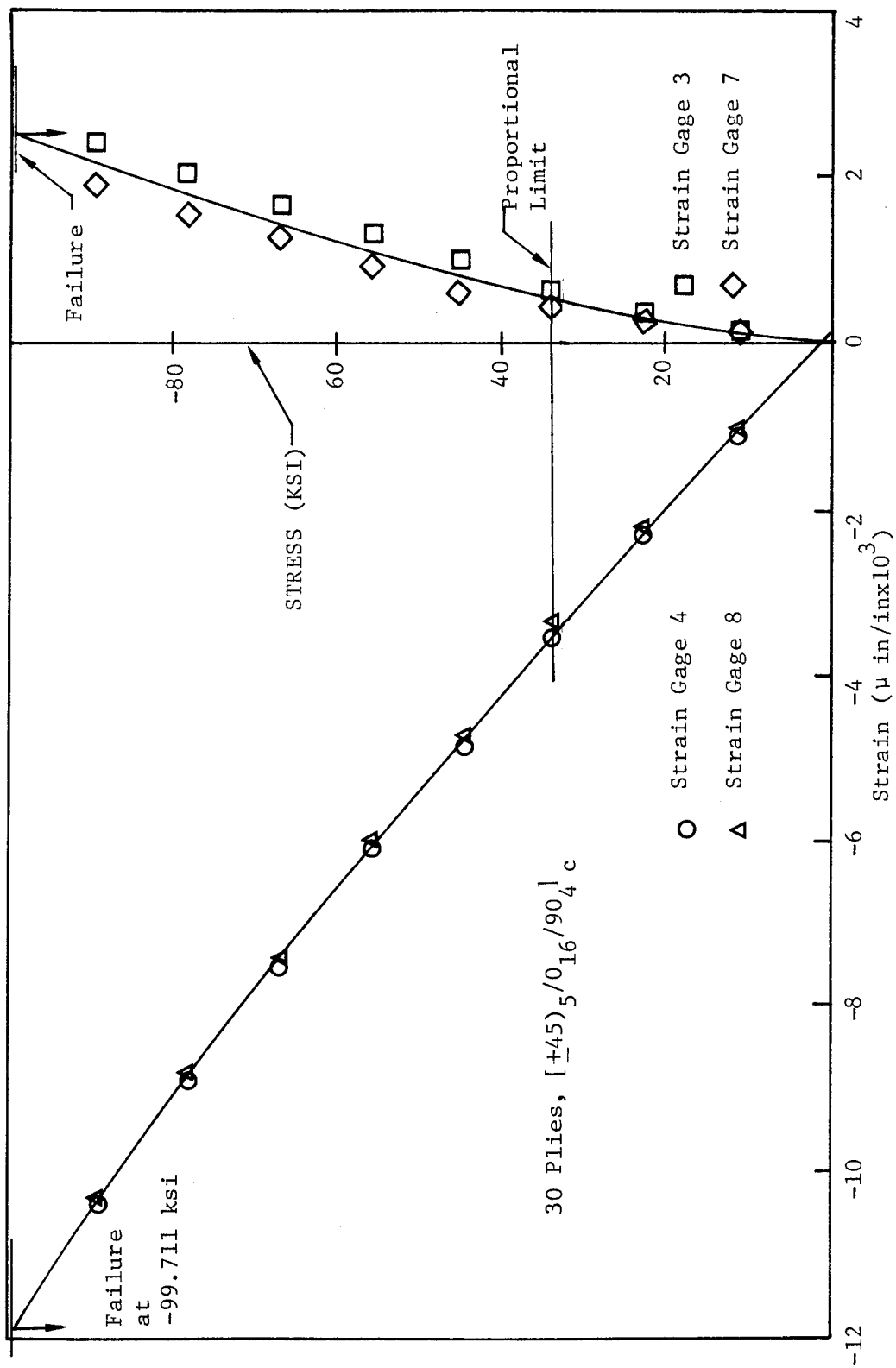
Figure 5.32 0° Static Compression Test Series XIII, Sepcimen ACL 4210A-8-14 Stress-Strain Curves, RTD, (PDO) #2, Thick Section
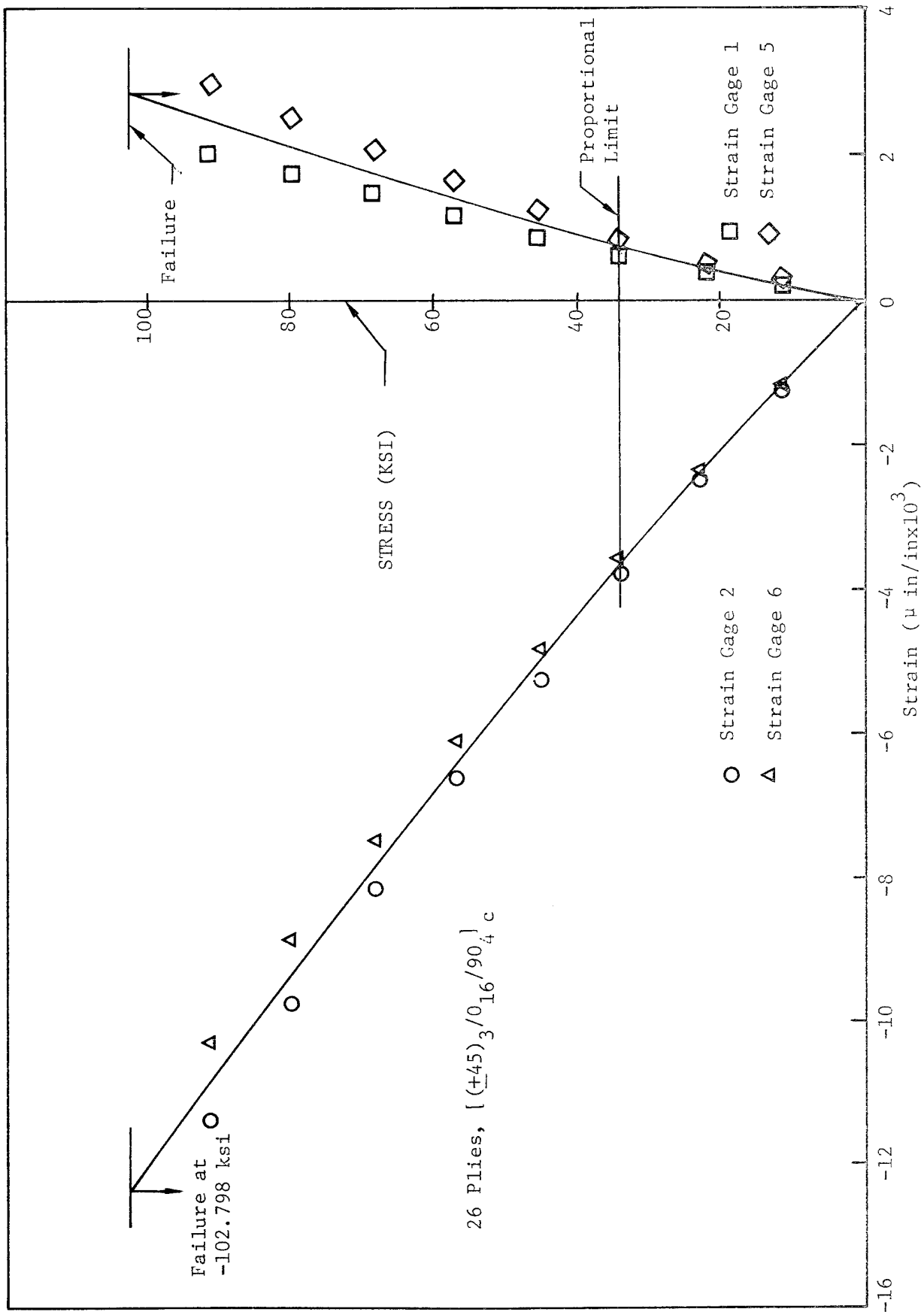
Figure 5.33 0° Static Compression Test Series XIII Specimen ACL 4210A-8-16 Stress-Strain Curves, RTD,(PDO) #2, Thin Section
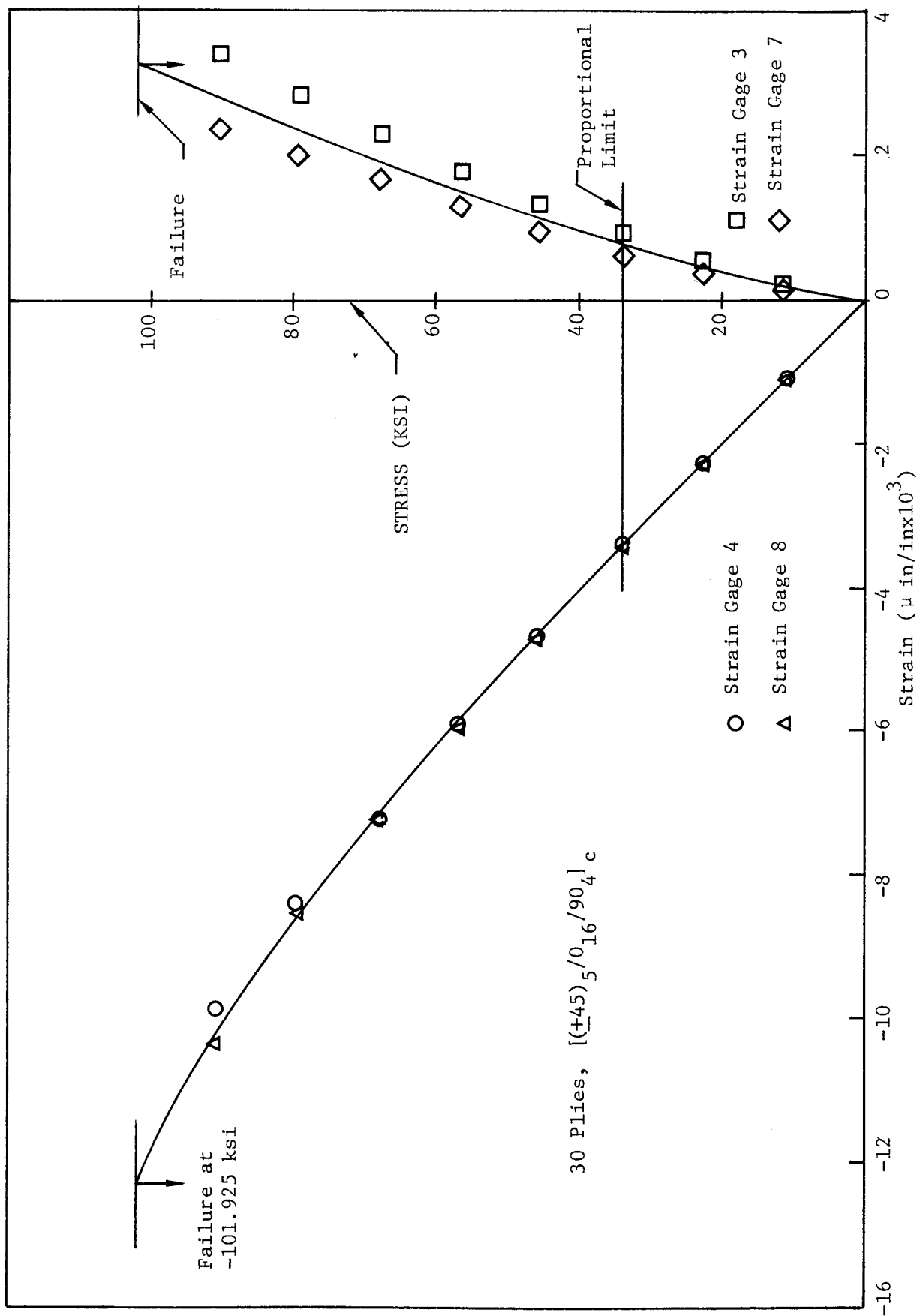
Figure 5.34 0° Static Compression Test Series XIII, Specimen ACL4210A-8-16 Stress-Strain Curves, RTD, (PDO) #2, Thick Section
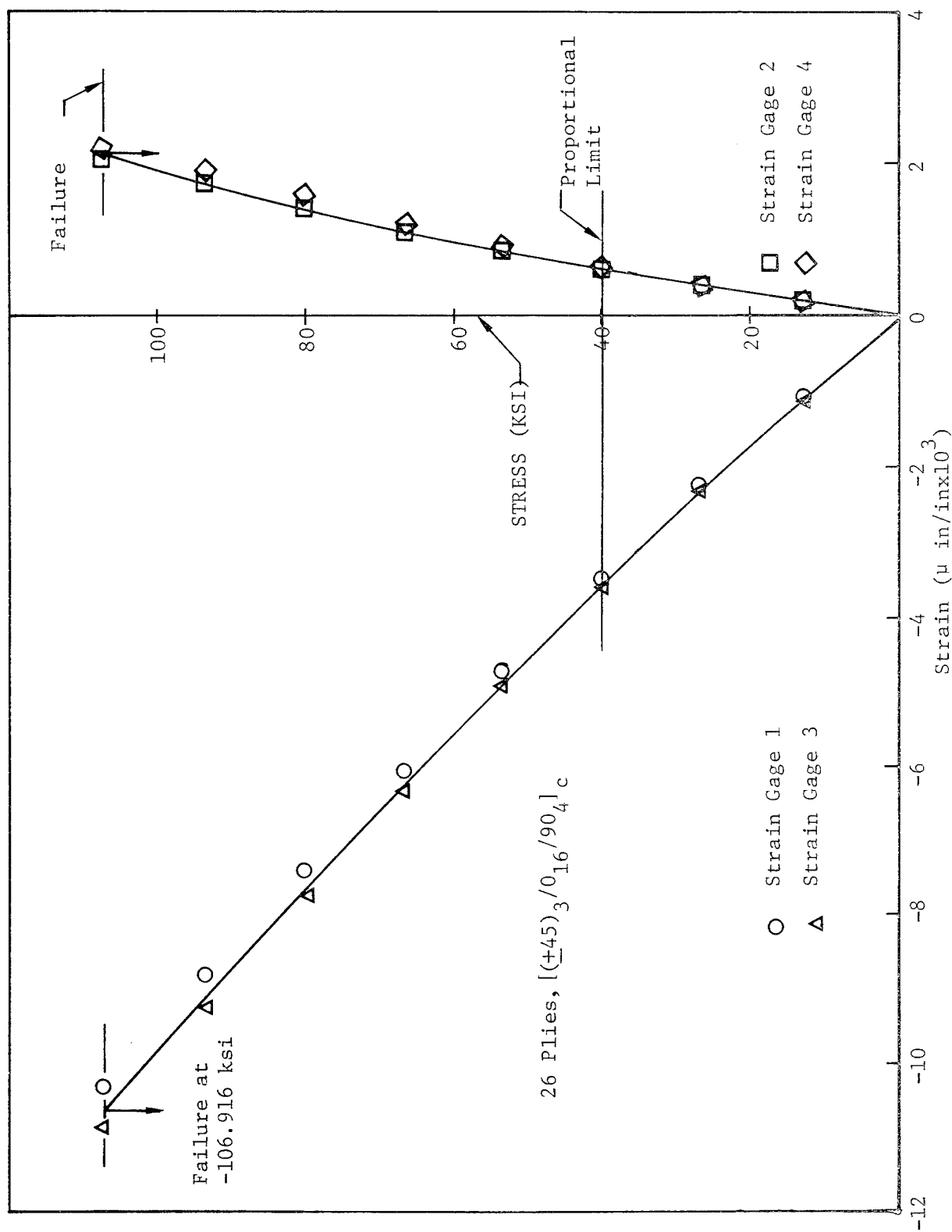
Figure 5.35 0° Static Compression Test Series XIV, Specimen ACL 4210A-8-23 Stress-Strain Curves RTW, (PDO) #2, Thin Section
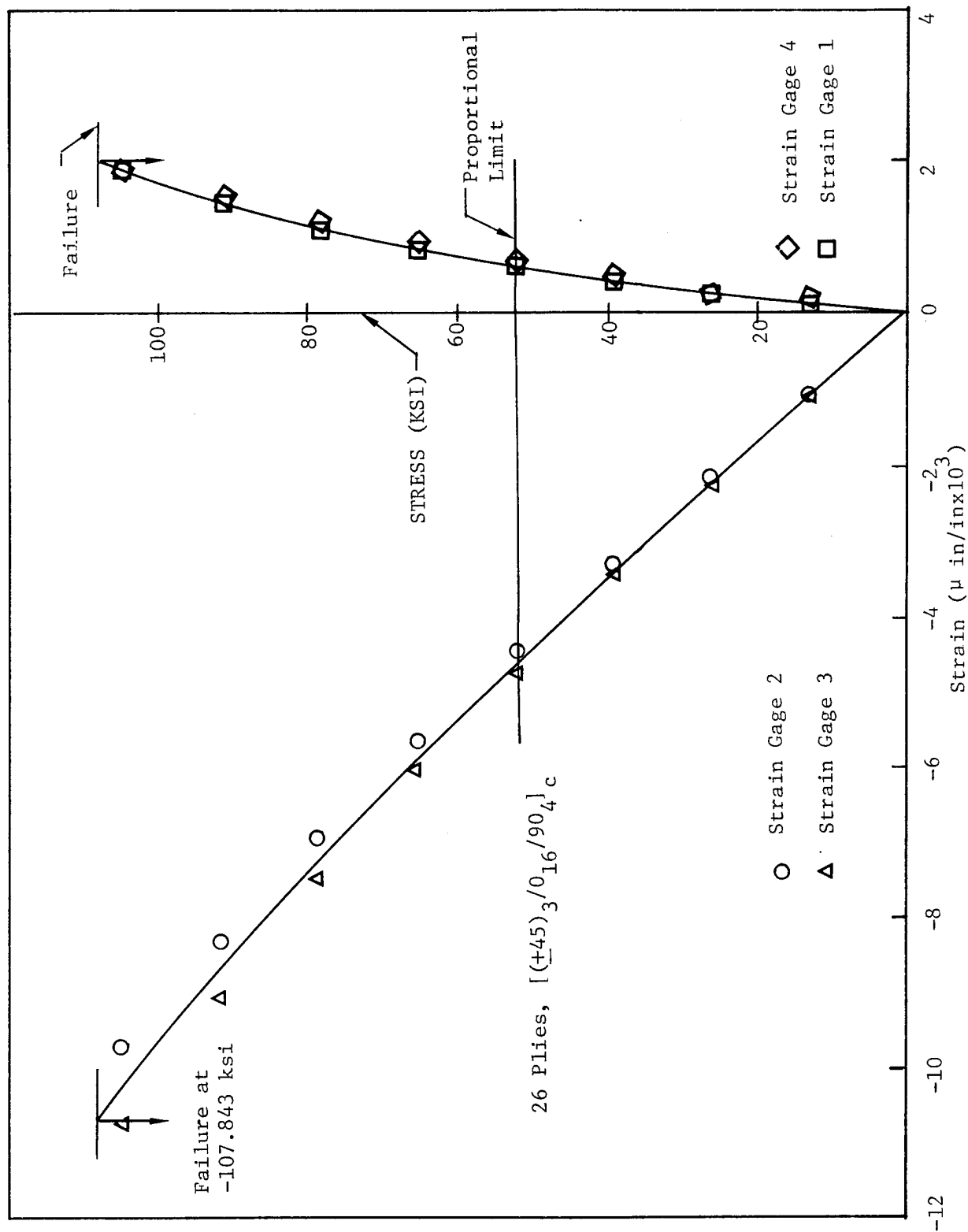
Figure 5.36 0° Static Compression Test Series XIV, Specimen ACL 4211B-12-25 Stress-Strain Curves, RTW, (PDO) #2, Thin Section

proportional limit stress (-52.9 ksi) is 49% of the ultimate stress (-107.4 ksi), whereas, the porportional limit strain (-4200 μ-in/in) is 39% of the failure strain (-10,675 μ-in/in). Modulus of elasticity is 11.49×10^6 psi and the Poisson's Ratio is 0.152.

5.4.1.4 -65°FW Static Compression Test Data

Static compression tests at -65°FW conditions were performed on Specimens ACL 4210A-7-1 and -3 from Test Series XII with results presented in Table 5.2. From Table 5.2, note that the predicted mean thick section ultimate stress is 84% of the mean thin section value. Figures 5.37 and 5.38 present the test data stress-strain curves. Test Series XII proportional limit stress (-53.4 ksi) is 41% of the ultimate stress (-131.028 ksi) for the thin section, whereas, proportional limit strain (-4900) is 36% of the failure strain (-13,650 μ-in/in). Modulus of elasticity is 11.11×10^6 psi and Poisson's Ratio is 0.242.

5.4.1.5 218°FW Static Compression Test Data

Static compression tests at 218°FW conditions were performed on Specimens ACL 4211B-12-34, -12-36, and -13-38 from Test Series XV with results presented in Table 5.2. From Table 5.2, note that the mean thick section ultimate stress is 86% of the mean thin section ultimate stress. Data from Table 5.2 can be compared to the 218°FW data from $[(\pm 45)_5/0_{16}/90_4]_c$ specimens presented in Reference (1).* Note that the predicted mean ultimate stress from Table 5.2 , -76.8 ksi, and the mean ultimate stress from Reference (1)* differ by approximately 1%. Figures 5.39, 5.40 and 5.41 present the thin section data as stress strain curves. Thin section proportional limit stress (-38.4 ksi) is 43% of the ultimate stress (-89.4 ksi), whereas, proportional limit strain (-3700 μ-in/in) is 41% of the strain at failure. Modulus of elasticity is 10.53×10^6 psi and the Poisson's Ratio is 0.243.

---

*Page 153, Table 5.17
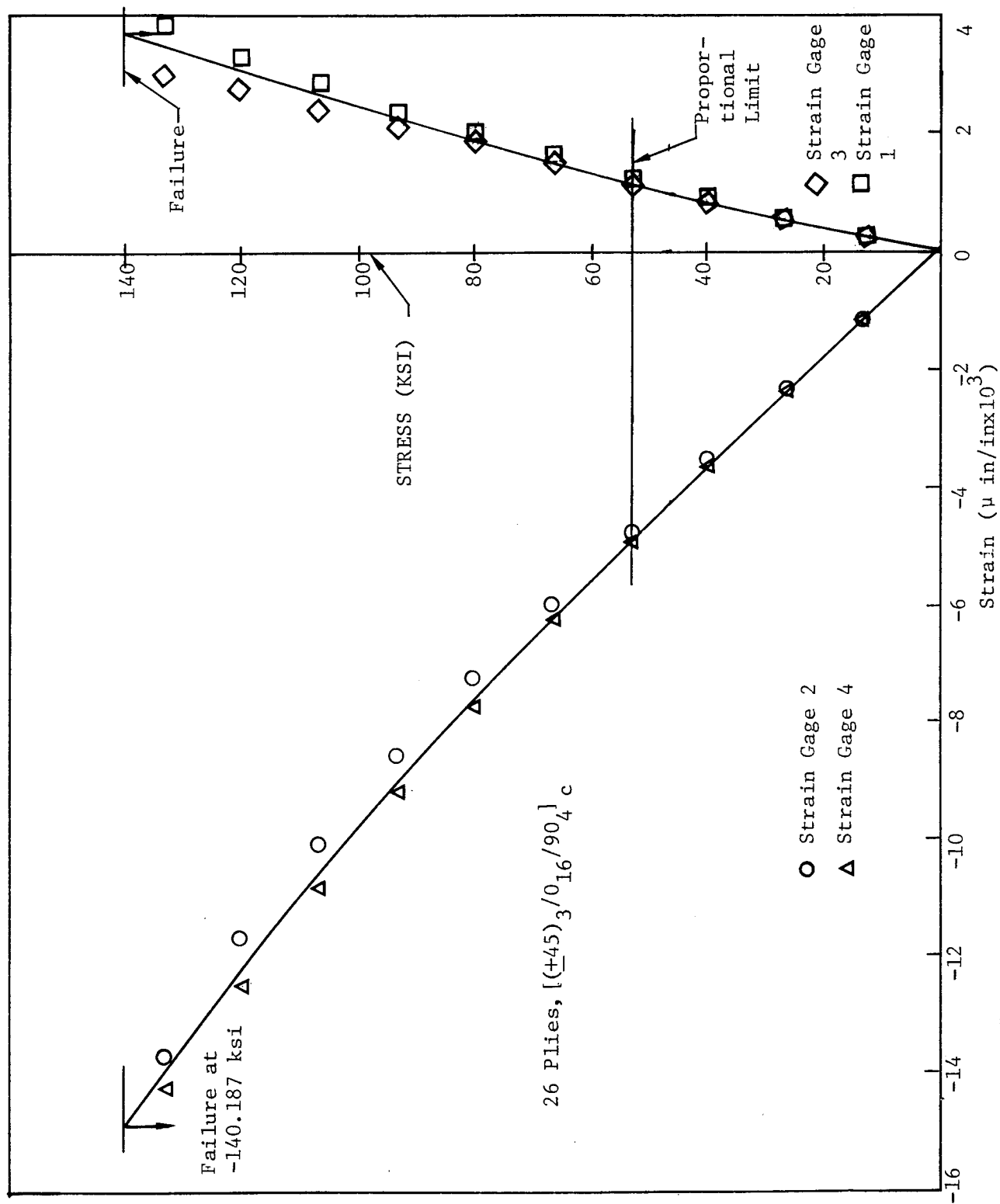
Figure 5.37 0° Static Compression Test Series XII, Specimen ACL4210A-7-1 Stress-Strain Curves, -65FW, (PDO) #2, Thin Section
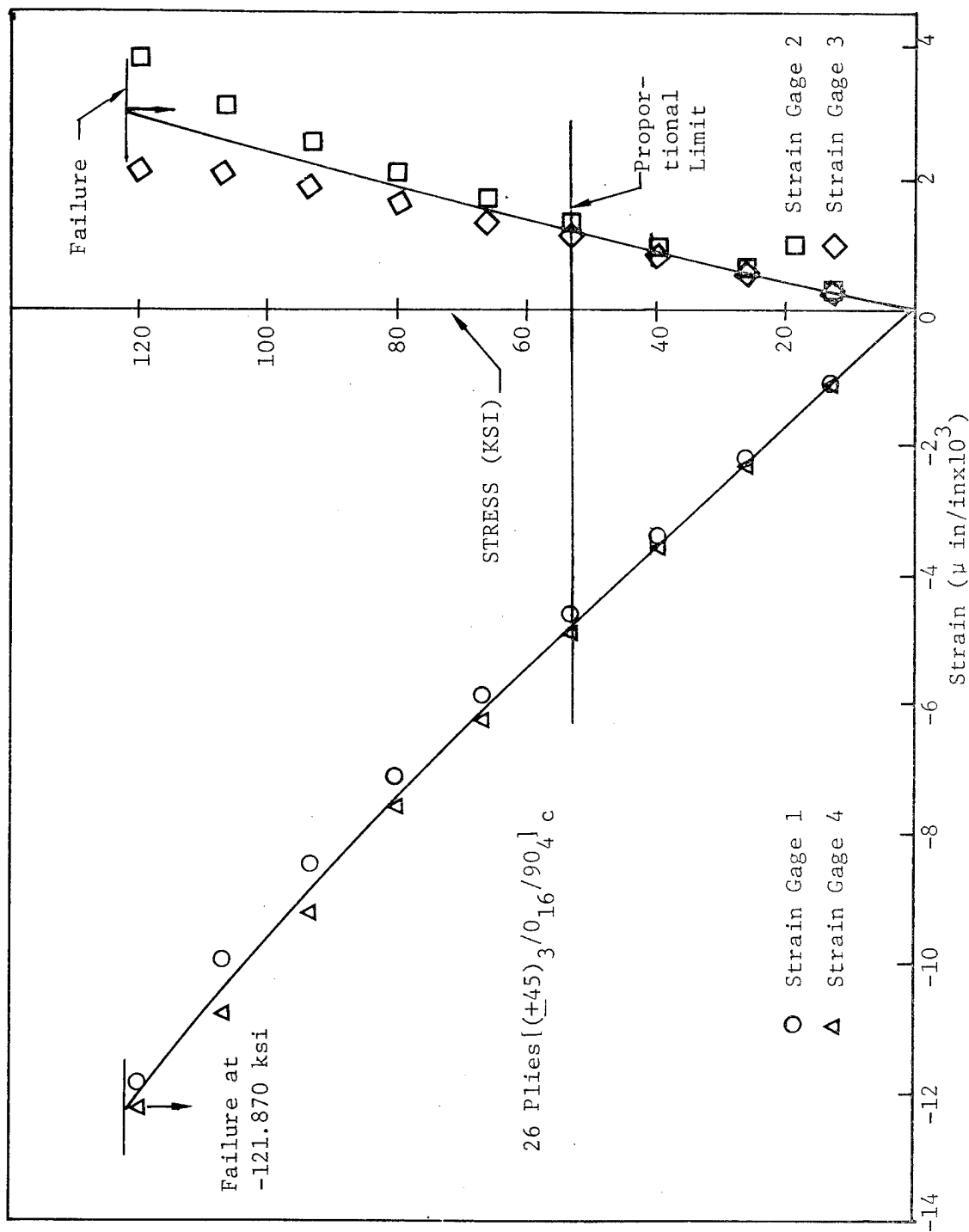
Figure 5.38 C° Static Compression Test Series XII, Specimen ACL 4210A-7-3 Stress-Strain
Curves, -65FW, (PDO) #2, Thin Section
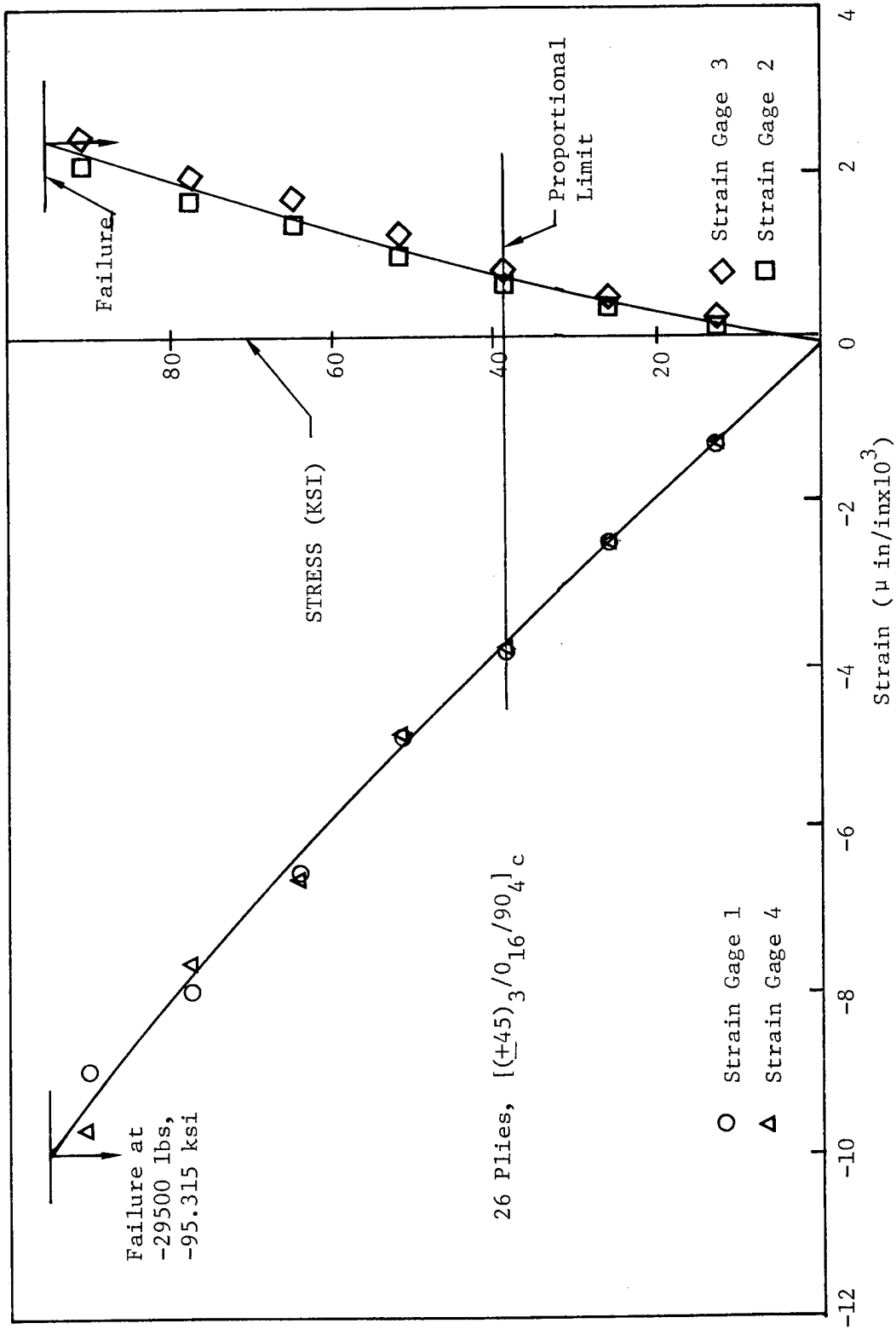
Figure 5.39 0° Static Compression Test Series XV, Specimen ACL 4211B-12-34 Stress-Strain Curves, 218FW, (PDO) #2, Thin Section
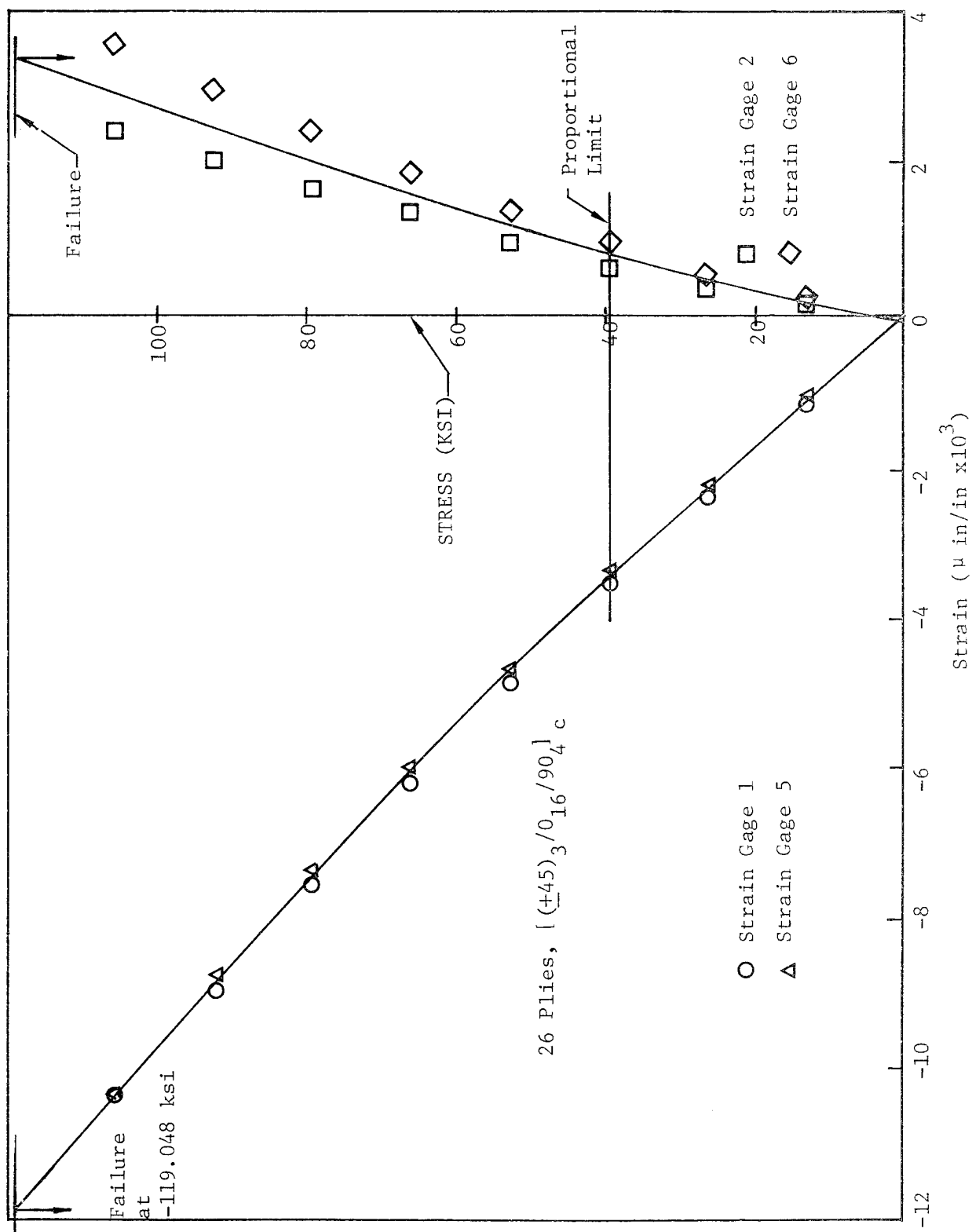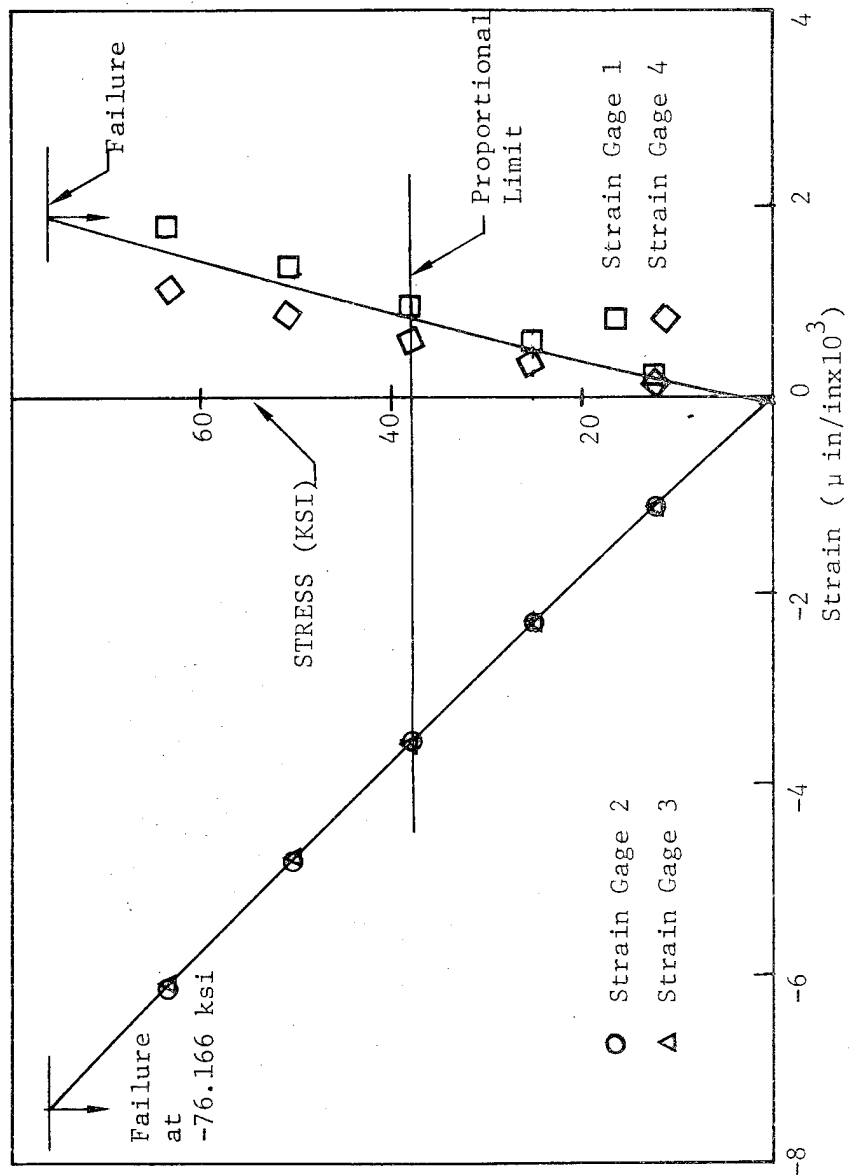
Figure 5.40 0° Static Compression Test Series XV Specimen ACL 4211B-12-36 Stress-Strain Curves, 218FW, (PDO) #2, Thin Section
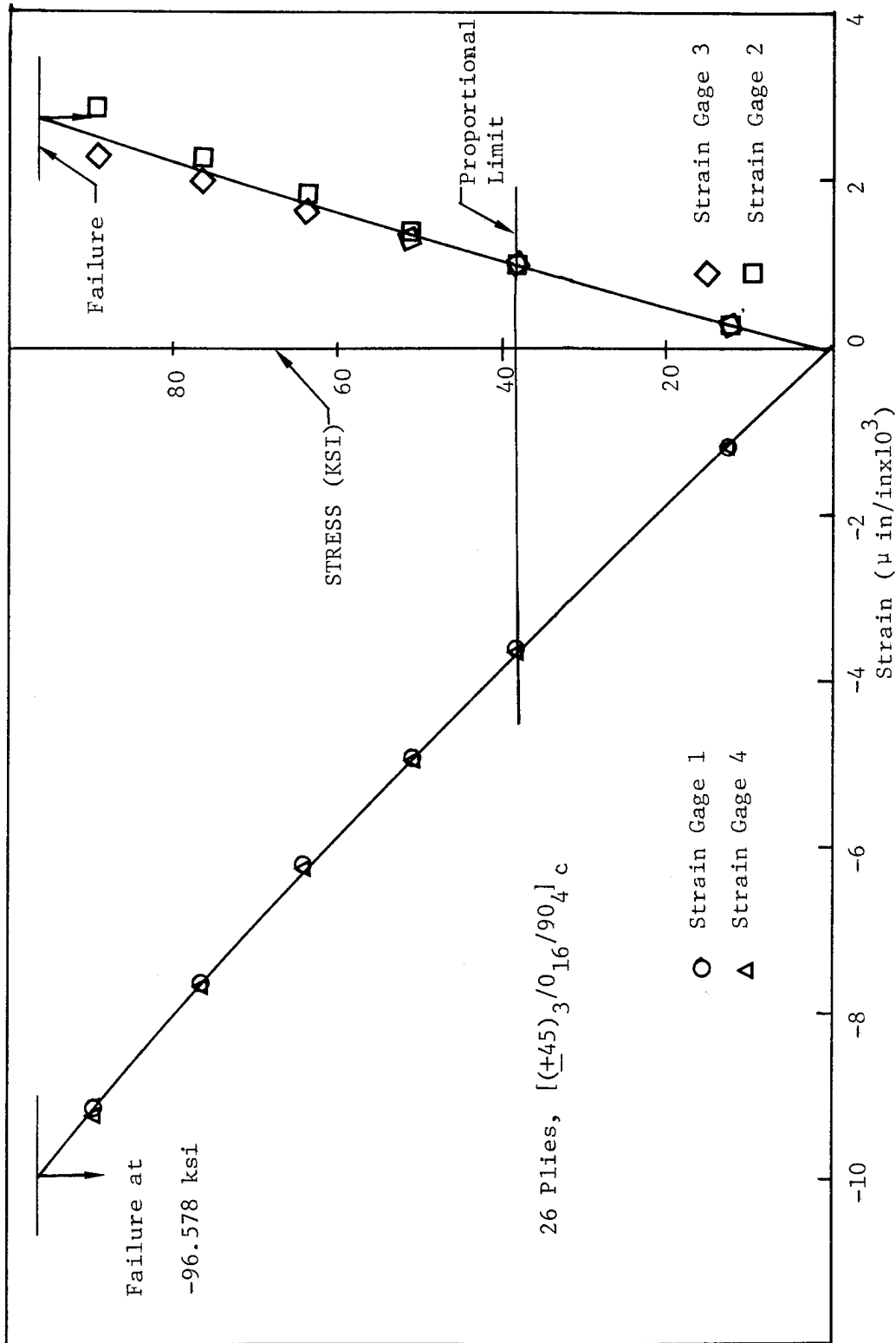
Figure 5.41 0° Static Compression Test Series XV, Specimen ACL 4211B-13-38 Stress-Strain Curves, 218FW, (PDO) #2, Thin Section

5.4.2 Fatigue Test Data

5.4.2.1 RTD Compression Fatigue Test Data

RTD condition, R=10, constant frequency (1, 8, or 10 Hz), compression-compression fatigue testing was performed on specimens from Test Series XVII with results presented in Table 5.3. Strain gages were mounted on both the thick and the thin sections of the specimen. Figures 5.42 and 5.43 present the RTD test data. On each figure are two curves; one being the thick section curve and the other being the thin section curve. Figures 5.42 and 5.43 show the thin and thick section curves virtually parallel to one another from the first non-static data point (30 cycles) to runout (1.25×10^6 cycles). From Figure 5.42, note that the runout stress (-73.3 ksi) for the thin section is 68% of the static stress value while, for the thick section, the stress (-61.9 ksi) at runout is 62% of the static stress value. From Figure 5.43 it is observed that the strain (-7585 μ-in/in) at runout for the thin section is 62% of the static strain value while, for the thick section, the strain (-7344 μ-in/in) at runout is 59% of the static strain value.

5.4.2.2 RTW Compression Fatigue Test Data

RTW condition, R=10, constant frequency (10 Hz), compression-compression fatigue testing was performed on specimens from Test Series XVIII with results presented in Table 5.3. Strain gages were mounted on the thin section only. Figures 5.44 and 5.45 present the RTW test data. Thin section 1.25×10^6 cycles runout maximum compressive stress (-78.6 ksi) is 73% the static value, whereas, the related strain value (-8005 μ-in/in) is 75% of the static value. Thick section runout maximum compressive stress (-67.1 ksi) is 75% of the static value.

5.4.2.3 -65 FW°Compression Fatigue Test Data

The -65°FW condition, R=10, constant frequency (10 Hz), compression-compression fatigue testing was performed on specimens from Test Series XVI with results presented in Table 5.3. There were gages mounted on the thin section only. Figures 5.46 and 5.47 are the stress versus number of cycles and strain versus number of cycles plots. From Figure 5.46, note

5.62
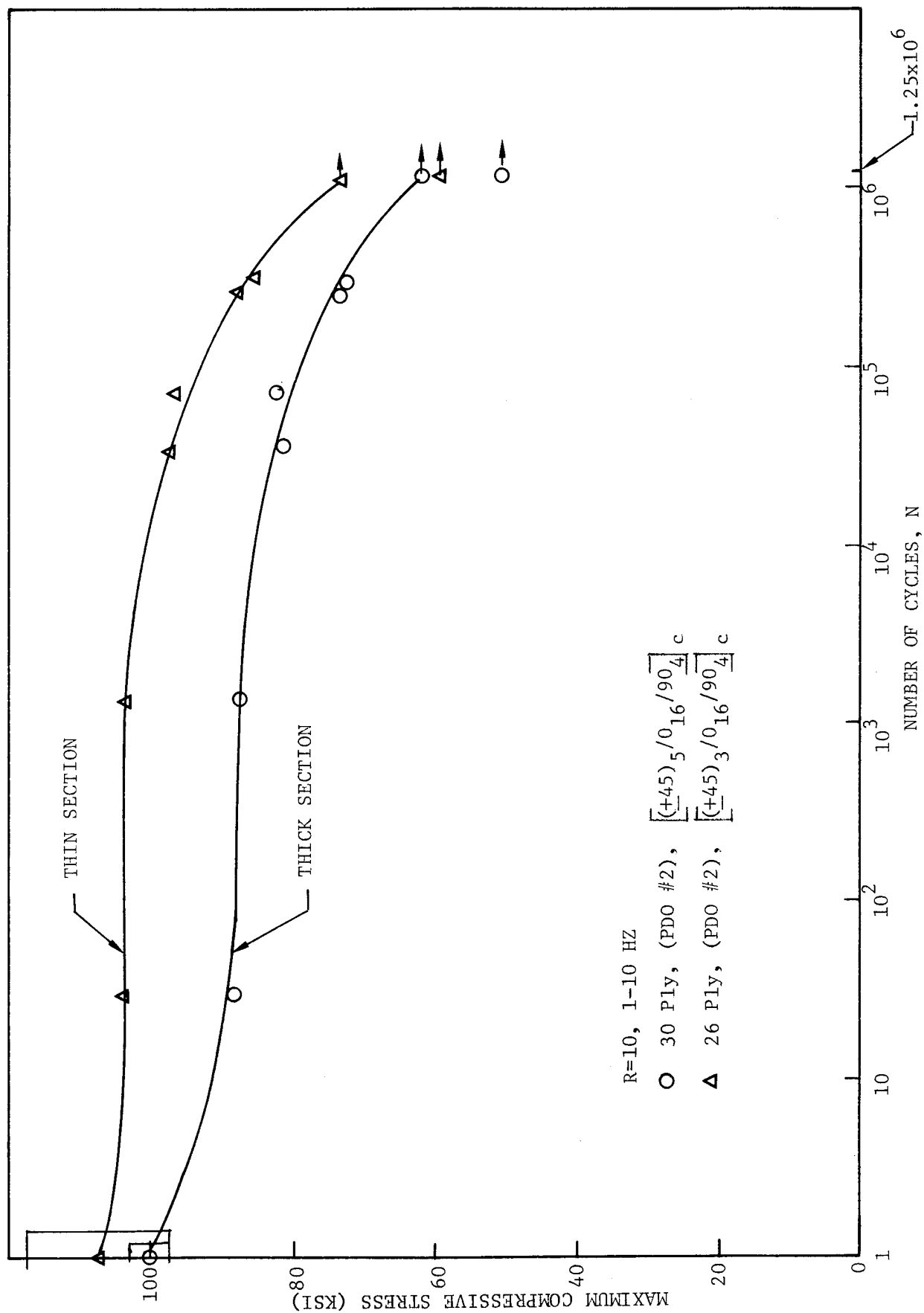
Figure 5.42. Constant Cycle Fatigue Stress Behavior, (PDO #2), RTD.
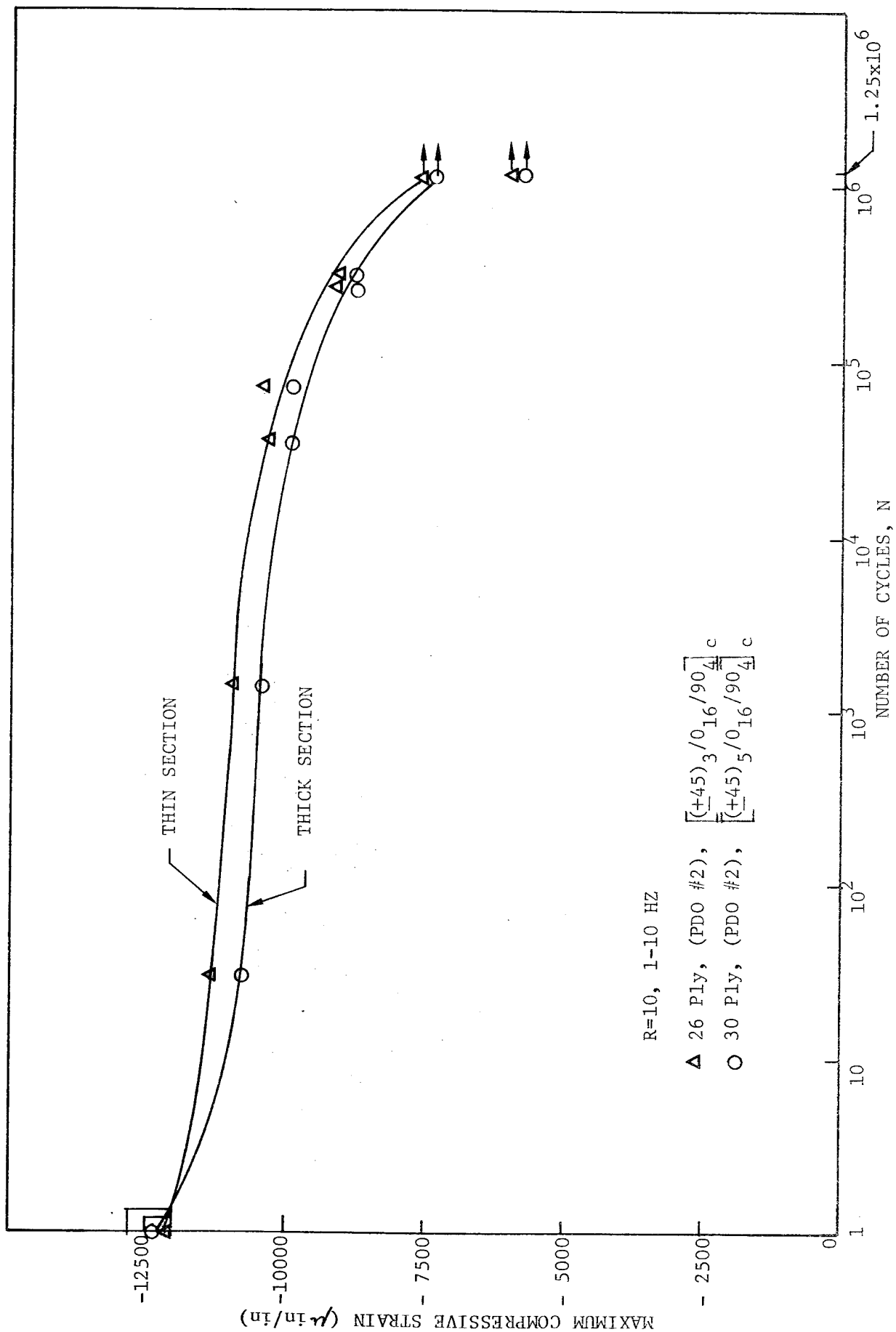
Figure 5.43. Constant Cycle Fatigue Strain Behavior, (PDO #2), RTD.
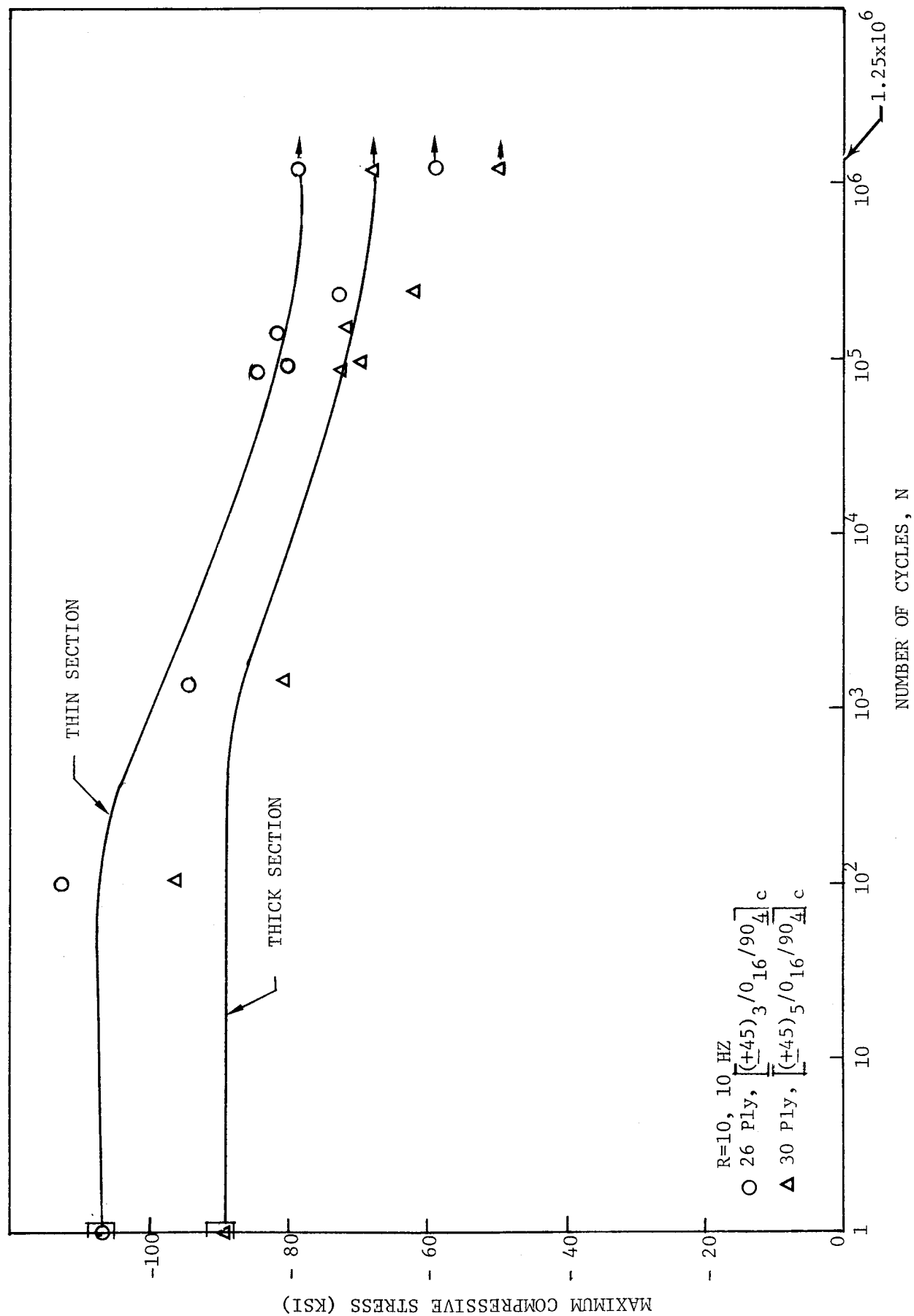
Figure 5.44. Constant Cycle Fatigue Stress Behavior. (PDO #2), RTW.
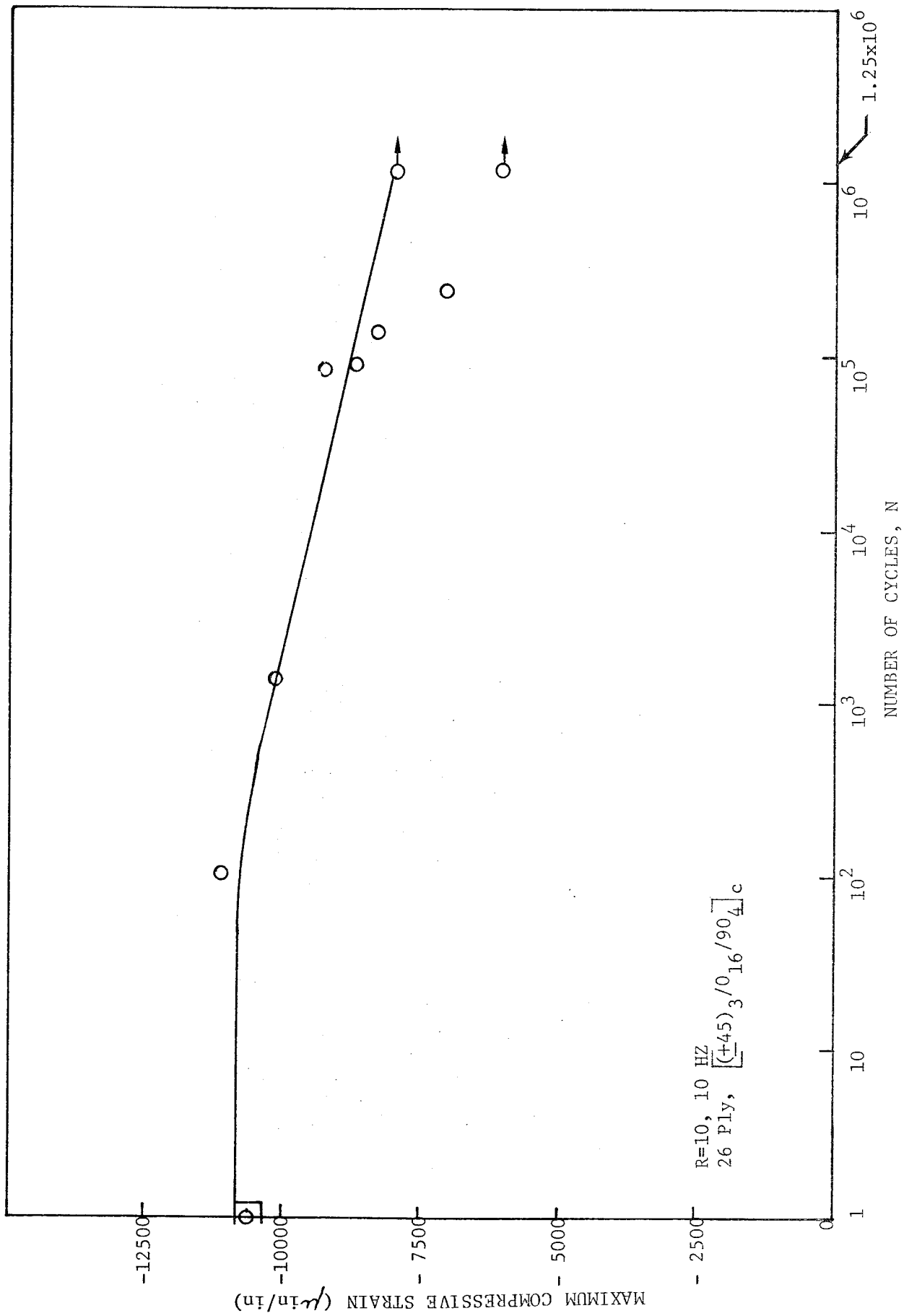
Figure 5.45. Constant Cycle Fatigue Strain Behavior (PDO #2), RTW, Thin Section.

R=10, 10 HZ
26 Ply, $[(\pm 45)_3/0_{16}/90_4]_c$

MAXIMUM COMPRESSIVE STRAIN (μin/in)

NUMBER OF CYCLES, N
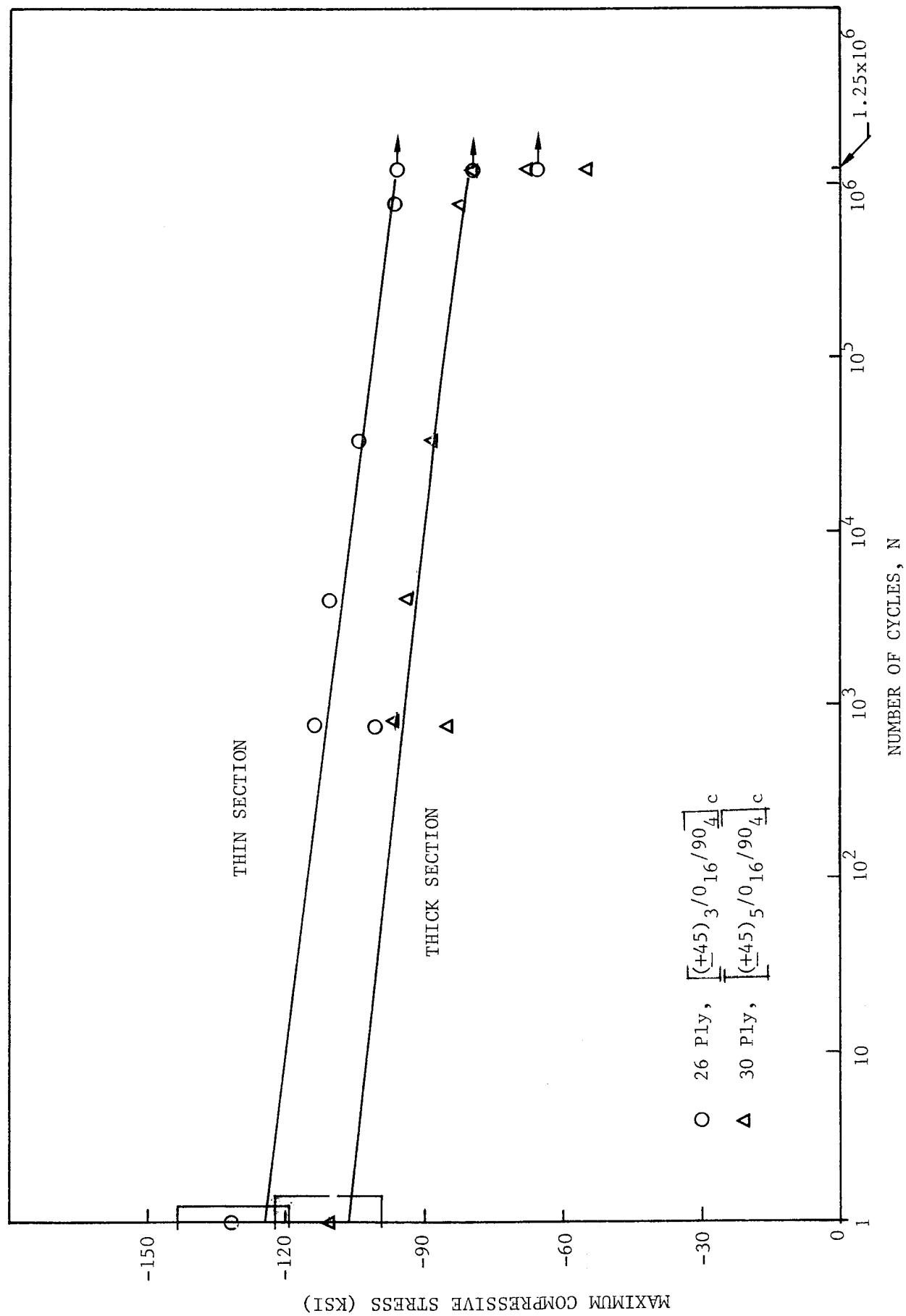
Figure 5.46. Constant Cycle Fatigue Stress Behavior, (PDO #2), -65°FW.

5.67
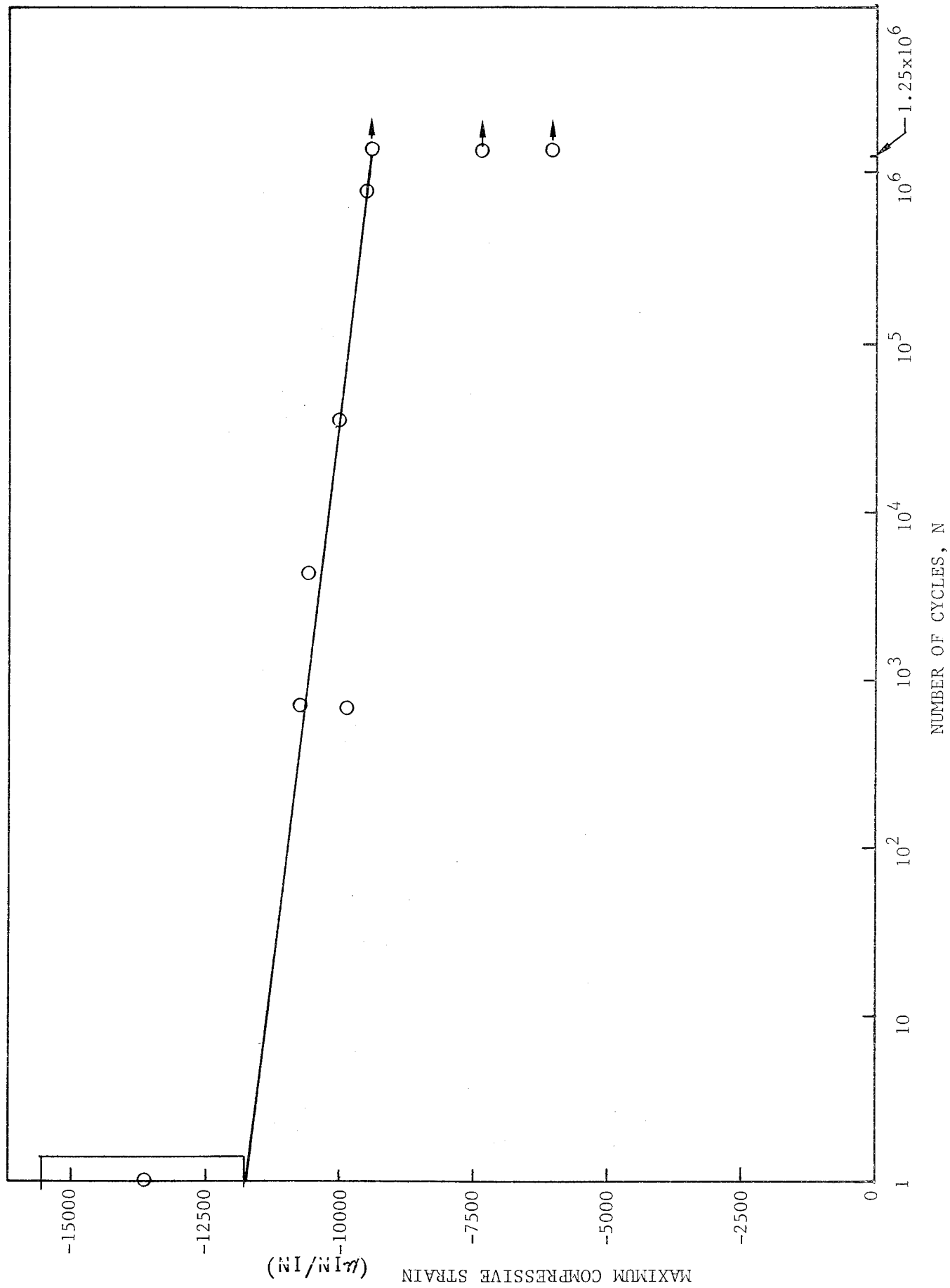
Figure 5.47. Constant Cycle Fatigue Strain Behavior, (PDO #2), -65°FW, Thin Section.

5.68

that the maximum compressive stress at runout is 74% of the static stress value for the thin section while for the thick section it is 72%. From Figure 5.47 the maximum compressive strain at runout is 69% of the static strain value.

5.4.2.4 218°FW Compression Fatigue Test Data

The 218°FW condition, R=10, constant frequency (10 Hz), compression-compression fatigue tests were performed on specimens from Test Series XIX with results presented in Table 5.3. Figures 5.48 and 5.49 present the stress and strain data plotted versus number of cycles. From Figure 5.48, note that the maximum compressive stress (61.4 ksi) for the thin section at runout is 69% of the static ultimate stress, whereas for the thick section the compressive stress (-52.6 ksi) at runout is 68% of the static ultimate stress. From Figure 5.48, the maximum compressive strain at runout is 71% of the static ultimate strain value.

5.5 RESIDUAL STRENGTH

Residual strength test results are presented in Table 5.4 for each Test Series, ply drop-off or plain laminate configuration and test environment. Plain laminate residual strength data at -65°FW and 218°FW varied directly with the maximum cyclic compressive stress applied during the 1.25×10^6 cycles of fatigue. This trend is similar to the results obtained on the same laminate in Reference (1)* RTD and RTW fatigue conditions with residual strength testing at 218°F. For ply drop-off No. 1 the residual strength under -65°FW, RTW, and 218°FW varies indirectly with the maximum cyclic compressive stress applied during the 1.25×10^6 cycles of fatigue. At -65°FW, RTW, and 218°FW conditions, for ply drop-off No. 2 configuration, no clear trend or relationship is evident for the residual strength results as related to the maximum cyclic compression fatigue stress applied for 1.25×10^6 cycles.

5.6 FAILURE MODES

5.6.1 Static Failure Modes

Static compression failure modes at various environmental conditions for the various plain and discontinuity configuration laminates are detailed

---

*Page 215, Table 5.24
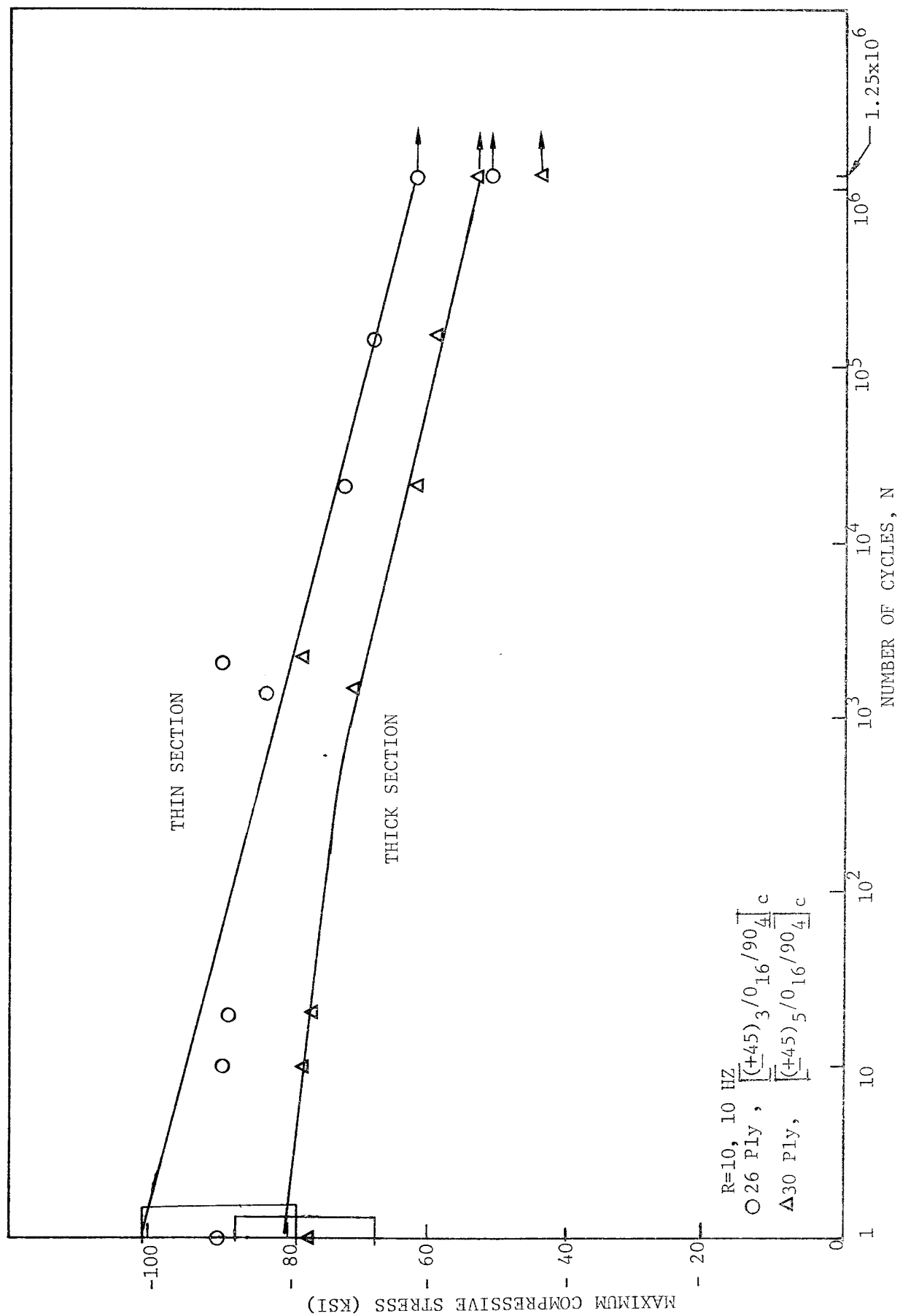
Figure 5.48. Constant Cycle Fatigue Stress Behavior, (PDO #2), 218°FW.

5.70
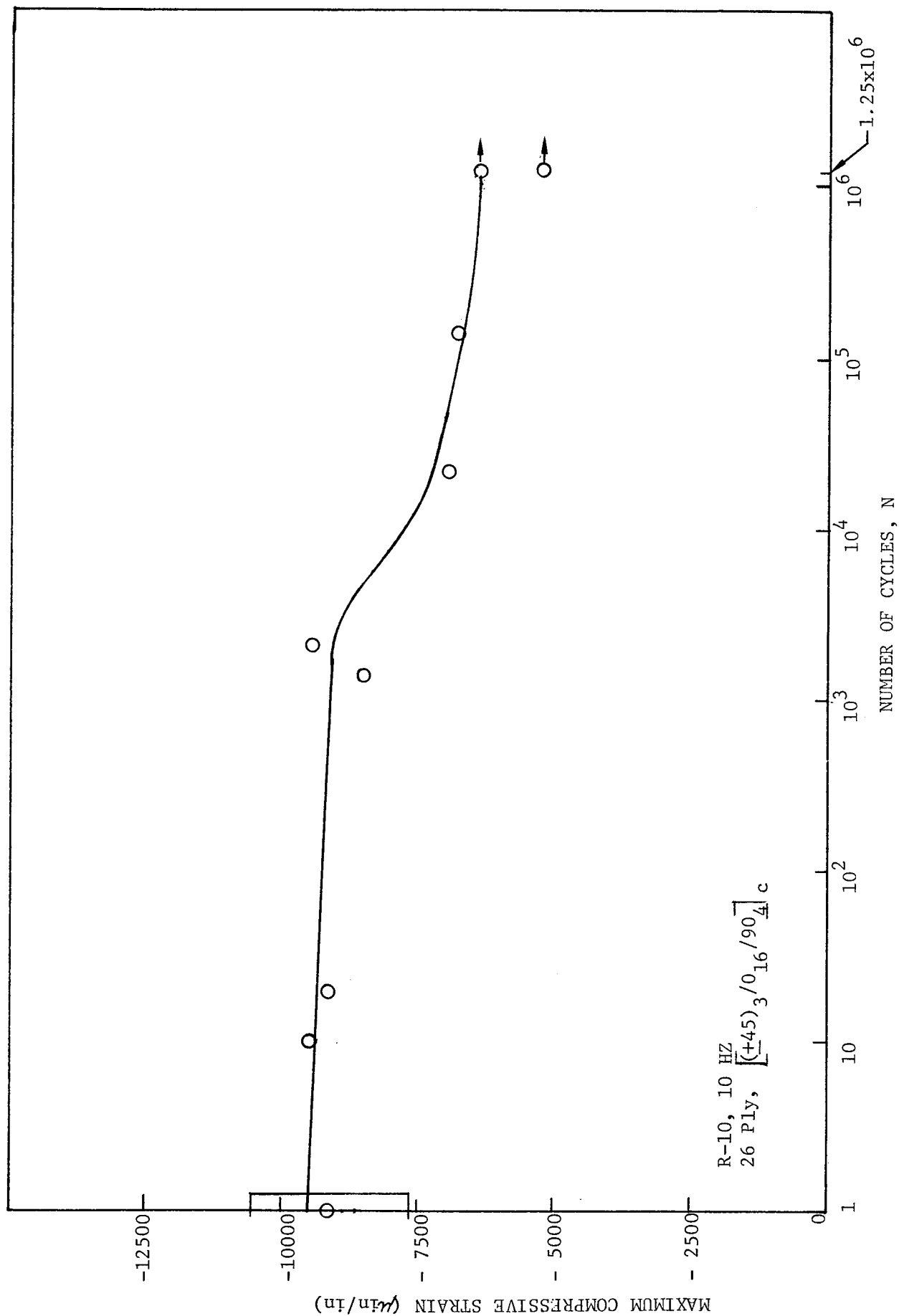
Figure 5.49. Constant Cycle Fatigue Strain Behavior, (PDO #2), 218°FW, Thin Section.

R-10, 10 HZ
26 Ply, $[(\pm 45)_3 / 0_{16} / 90_4]_c$

NUMBER OF CYCLES, N

MAXIMUM COMPRESSIVE STRAIN (μin/in)

Test Series	Specimen No.	Residual Strength Ksi	Cyclic Max.Stress Ksi		Discontinuity Configuration		Test Condition
II	4210A-1-2	-96.227	-54.675		Plain Lam, 30 plies		-65°FW
	-3	-114.270	-67.477				
	-4	-122.772	-80.339				
	-12	-144.134	-82.961		↓	↓	↓
III	4210A-1-7	-96.127	-50.170		Plain Lam, 30 plies		218°FW
	-8	-97.787	-54.495				
	-9	-102.528	-63.343		↓	↓	↓
VIII	4210-A-4-2	-150.672	-54.095		PDO#1,	28 plies	-65°FW
	-4	-115.258	-68.677				
	-6	-99.129	-78.702		↓	↓	↓
VIII	4210A-4-2	-138.561	-49.747		PDO#1,	30 plies	-65°FW
	-4	-108.763	-64.807				
	-6	-91.337	-72.516		↓	↓	↓
IX	4210A-5-13	-112.943	-54.945		PDO#1,	28 plies	RTD
IX	4210A-5-13	-103.439	-50.322		PDO#1,	30 plies	RTD
X	4210A-5-24	-115.047	-53.285		PDO#1,	28 plies	RTW
	4211B-10-26	-104.692	-58.651		↓	↓	↓
X	4210A-5-24	-106.383	-49.272		PDO#1,	30 plies	RTW
	4211B-10-26	-96.774	-54.215		↓	↓	↓
XI	4211B-10-35	-82.948	-43.931		PDO#1,	28 plies	218°FW
	-11-37	-70.985	-51.760		↓	↓	↓
XI	4211B-10-35	-75.894	-41.496		PDO#1	30 plies	218°FW
	-11-37	-65.952	-48.090		↓	↓	↓

TABLE 5.4. RESIDUAL STRENGTH TEST RESULTS (SPECIMENS SURVIVING
1.25 x 10^6 CYCLES R = 10 FATIGUE) (Concluded).

Test Series	Specimen No.	Residual Strength Ksi	Cyclic Max.Strength Ksi		Discontinuity Configuration		Test Condition
XVI	4210A-7-2	-147.300	-65.466		PDO#2,	26 plies	-65°FW
	-4	-136.589	-79.182				
	-6	-154.637	-96.342		↓	↓	↓
XVI	4210A-7-2	-123.254	-54.779		PDO#2,	30 plies	-65°FW
	-4	-116.685	-67.644				
	-6	-127.697	-79.558		↓	↓	↓
XVII	4210A-8-13	-111.695	-59.133		PDO#2	26 plies	RTD
	-15	-119.960	-73.309		↓	↓	↓
XVII	4210A-8-13	-95.802	-50.718		PDO#2,	30 plies	RTD
	-15	-101.294	-61.902		↓	↓	↓
XVIII	4210A-8-24	-117.374	-58.355		PDO#2,	26 plies	RTW
	4211B-12-28	-113.805	-78.564		↓	↓	↓
XVIII	4210A-8-24	-99.634	-49.535		PDO#2,	30 plies	RTW
	4211B-12-28	-97.237	-67.127		↓	↓	↓
XIX	4211B-12-35	-97.060	-50.901		PDO#2,	26 plies	218°FW
	-13-37	-95.947	-61.431		↓	↓	↓
XIX	4211B-12-35	-83.085	-43.572		PDO#2,	30 plies	218°FW
	-13-37	-82.136	-52.588		↓	↓	↓

in Table 5.5 with failure photographs shown in Appendix G. Dominant failure mode in all specimens was diagonal shear and straight across compression fracture with some delamination. In some cases the diagonal shear was through the thickness, in others it was across the width, and in still others it occurred both ways. With two exceptions, all 23 specimens failed in the middle of the specimen length in the thinner section, sometimes away from the discontinuity and sometimes closely adjacent to the discontinuity. While failure mode of the two exceptions was about the same, the location was at or under the end of the tab.

Failure load, stress, strain, and elastic properties data are also given for comparison of these properties at various environments and discontinuity configurations with the failure modes.

5.6.2 R=10 Compression-Compression Fatigue Failure Modes

Fatigue failure modes are detailed in Table 5.6 with failure photographs given in Appendix G. Basic failure mode was similar in all specimens consisting of diagonal shear, delamination, and straight across compression fracture. However, 19 of the 84 specimens had failure locations in the end of tab area with some bondline or tab delamination in evidence. These end of tab failures occurred most often at 218°FW and next most often at RTW. For the other 65 specimens failure was in the middle length part of the specimen and the majority of the ply drop-off specimens showed fatigue failures at the discontinuity.

Failure load and stress and cycles to failure are given for comparison of the various environments and discontinuity configurations with the failure modes.

5.7 MOISTURE DATA

Detail moisture data by test series is given in Table 5.7. At least one moisture control traveler was dried and used with each test series for moisture absorption measurement. For selected test series, additional "as manufactured" specimens were used for monitoring moisture pickup. These specimens were about three months old (from laminate assembly manufacturing data) at test series make-up and first weighing. Dried specimens showing moisture losses from -0.053% to -0.238%, (average:-0.159%) had slightly

TABLE 5.5   STATIC COMPRESSION TEST DATA – FAILURE MODES[1]

Specimen ID	Discontinuity Configuration	Failure Load (lbs)	Failure Stress* (ksi)	Strain @ Failure (μ-in/in)	Proportional Limit (ksi)	Strain At Prop. Limit	Failure Modes	Modulus (x10⁶ psi)	Poisson's Ratio	Test Condition
I-ACL-4210A-1-1	Plain Laminate 30 Plies	-34700	- 95.909	-10,650	-31.970	-3350	DS,SACF,DL(MOS)	10.00	0.328	-65FW
-1-6		-39700	-111.894	-14,300	-37.298	-3550	SACF,DS,DL(MOS)	10.00	0.329	
-2-17		-47000	-133.069	-15,650	-44.356	-3700	DS,SACF,DL(MOS)	11.11	0.341	
IV-ACL-4210A-4-1	PDO #1	-44000	-134.024	-18,000	-44.675	-4100	SACF,DS,DL(MOS)	9.09	0.323	-65FW
-4-3		-48000	-145.278	-18,000	-48.426	-5000	DS,SACF,DL(MOS)	9.75	0.310	
-4-5		-39000	-117.860	-15,300	-39.286	-3800	DS,DL,SACF-(MOS)	9.38	0.232	
V-ACL-4210A-4-12	PDO #1	-35000	-108.797	-13,100	-36.266	-4100	DL,DS@MOS ON THIN PART	9.38	0.255	RTD
-5-14		-34000	-104.390	-13,100	-34.797	-4150	SACF,DS,DL@MOS ON THIN PART	9.09	0.308	
-5-16		-36000	-109.058	-13,450	-36.353	-4050	SACF,DS,DL@MOS ON THIN PART	8.82	0.247	
VI-ACL-4210A-5-23	PDO #1	-35000	-106.805	-12,200	-35.602	-3750	DL,DS,SACF(MOS)	10.00	0.181	RTW
4211B-10-25		-35500	-105.279	-13,800	-35.093	-3900	SACF,DS(MOS)	9.52	0.231	
VII-ACL-4211B-10-36	PDO #1	-27500	- 80.433	- 9,150	-26.811	-3450	DS(THRU THICK@EOT),SACF,DL	10.25	0.385	218FW
-11-38		-24000	- 69.910	- 7,450	-23.303	-3500	DS(THRU THICK),SACF-(MOS)	10.00	0.362	
XII-ACL-4210A-7-1	PDO #2	-42000	-140.187	-14,950	-46.729	-4850	DS,SACF,DL(MOS)	11.11	0.241	-65FW
-3		-36500	-121.870	-12,350	-40.623	-4850	DS,SACF,DL(MOS)	11.11	0.250	
XIII-ACL-4210A-7-12	PDO #2	-36000	-119.048	-11,900	-39.683	-3600	DS,SACF,DL@MOS ON THIN PART	11.74	0.317	RTD
-8-14		-35000	- 99.630	-12,300	-33.210	-5350	DS,SACF,DL@MOS ON THIN PART	8.82	0.149	
-8-16		-36000	-102.798	-12,350	-34.266	-3850	DS,SACF,DL@MOS ON THIN PART	9.09	0.203	
XIV-ACL-4210A-8-23	PDO #2	-32000	-106.916	-10,600	-35.639	-3700	SACF,DS,DL(UTEOT)	11.54	0.182	RTW
4211B-12-25		-33000	-107.843	-10,750	-35.948	-4700	DS,SACF,DL(MOS)	11.43	0.119	
XV-ACL-4211B-12-34	PDO #2	-29500	- 95.315	- 9,850	-31.772	-3800	SACF,DS(BOTH WAYS),DL-MOS	10.71	0.241	218FW
-12-36		-24000	- 76.166	- 7,450	-25.388	-3600	SACF,DS(BOTH WAYS),DL-MOS	10.53	0.229	
-13-38		-30200	- 96.578	-10,050	-32.193	-3700	SACF,DS(BOTH WAYS),DL-MOS	10.34	0.274	

LEGEND: DS- diagonal shear   SACF - straight across compression fracture
          DL- delamination   UTEOT - under tapered edge of tab
          MOS - middle of specimen

[1]-See Appendix G for failure photographs
*failure stress at thin section
[2]-DS(both ways): diagonal shear thru the thickness and across the width

TABLE 5.6 R=10 COMPRESSION FATIGUE TEST DATA – FAILURE MODES ①

Specimen ID	Discontinuity Configuration	Failure Modes	Cycles to runout or Failure	Test Condition	Max. Cyclic Strain (μin/in)	Max. Cyclic Load (lbs)	Max. Cyclic Stress (ksi)	Residual Strength (lbs)
II-ACL-4210A-1-2	Plain Laminate	SACF,DS,DL-MOS(1" FROM END)	1.25×10^6	-65FW	- 6429	-20000	- 54.675	-35200
1-3		DS(THRU THICK),SACF,DL-UTEOP	1.25×10^6		- 8098	-24200	- 67.447	-41000
1-4		DS(BOTH WAYS),SACF,DL-MOS	1.25×10^6		- 9143	-28400	- 80.339	-43400
1-5		DS(THRU THICK),DL,SACF,-UTEOP	130		-13392	-39200	-110.516	—
1-12		DS(BOTH WAYS),DL,SACF,-MOS(1"FROM END)	1.25×10^6		-11089	-29700	- 82.961	-51600
2-13		DL,DS(BOTH WAYS),DL-MOS	48530		-10803	-32000	- 89.560	---
2-14		SACF,DS(BOTH WAYS),DL(-MOS)	131450		-11524	-34300	- 94.830	---
2-15		SACF,DS(BOTH WAYS)DL(MOS)	163110		-12686	-36000	-101.152	---
2-16		SACF,DS(BOTH WAYS)DL(MOS)	11780	↓	-12986	-36700	-103.760	---
III-ACL-4210A-1-7	Plain Laminate	DS,TB,DL(UTEOT)	1.25×10^6	218FW	- 4997	-18200	- 50.710	-34500
-8		TB,DS,SAC,DL(UTEOT)	1.25×10^6		- 6293	-19700	- 54.495	-35350
-9		DS,DL,SAC,TB(UTEOR)	1.25×10^6		- 7069	-22500	- 63.343	-36500
-10		DS,DL,SAC,TB(UTEOR)	10		- 7620	-25700	- 72.887	---
-11		SACF,DS(THRU THICK),EOT	230**		- 8277	-26000	- 72.869	---
2-18		DS,TB,SAC(UTEOT)	35190		- 8264	-26000	- 71.962	---
2-19		DS,SAC,(1" FROM END OF TAB)	10		- 7485	-24000	- 66.408	---
2-20		DS,DL(UTEOT)	743880		- 7685	-24700	- 68.251	---
2-21		SACF,DS(THRU THICK),DL(MOS)	0***		--	--	--	---
2-22		DL(UTEOP),SACF(UTEOP)	0***	↓	--	--	--	---
VIII-ACL-4210A4-2	PDO #1	SACF,DS,DL-MOS(1" FROM END)	1.25×10^6	-65FW	- 6165	-17700	-54.095	-49300
4-4		DS,DL,SACF,-MOS	1.25×10^6		- 7531	-23000	-68.677	-38600
4-6		DS,DL,SACF,-MOS	1.25×10^6		- 9132	-26200	-78.702	-33000
4-7		DS,DL,SACF-MOS	11380		-10636	-30000	-91.296	---
4-8		DS,DL,SACF-MOS	106050		-10500	-29100	-87.571	---
4-9		DS,DL,SACF-MOS	>1000<10000**		-11155	-31500	-95.715	---
4-10		DS,DL,SACF,-MOS	410		-11455	-32000	-97.561	---
4-11		DS,DL,SACF-MOS	12220	↓	-11149	-29500	-90.324	---

(Continued)

5.76

TABLE 5.6 (CONTINUED)

Specimen ID	Discontinuity Configuration	Failure Modes	Cycles to runout or Failure	Test Condition	Max. Cyclic Strain (μin/in)	Max. Cyclic Load (lbs)	Max. Cyclic Stress (ksi)	Residual Strength (lbs)
IX-ACL-4210A-5-13	PDO #1	DL,DS@MOS ON THIN PART	1.25×10^6	RTD	- 6493	-18000	- 54.945	37000
-15			9980		-10191	-27000	- 83.179	--
-17			602920		- 8233	-23000	- 69.319	--
-18			2230		-11390	-30000	- 90.744	--
-19			400		-11625	-30500	- 89.864	--
-20			229940		- 8381	-23500	- 70.549	--
-21			9200		- 9961	-26500	- 80.303	--
-22			1670		-11048	-30000	- 90.144	--
X-ACL-4211B-10-26	PDO #1	SACF,DS,DL(MOS)	1.25×10^6	RTW	- 7074	-20000	- 58.651	35700
4210A-5-24		DS,DL,SAC(UTEOT)	1.25×10^6		- 6088	-17600	- 53.285	38000
4211B-10-28		TB,DS,DL(1" UTEOT)	205060		- 6963	-23200	- 69.192	--
4211B-10-29		DS,SACF,DL(MOS)	129010		- 8501	-25500	- 75.780	--
-30		DL,SACF,DS(MOS)	1420		-10476	-28000	- 83.482	--
-31		DS,SACF,DL(MOS)	9470		- 9656	-26750	- 78.839	--
-32		SACF,DS(BOTH WASY),DL(MOS)	21760		-11023	-29000	- 84.820	--
-33		DL,DS,SACF,MOS TO UTEOP)	5770		-11688	-30000	- 90.280	--
XI-ACL-4211B-10-35	PDO #1	DS,SAC(MOS)	1.25×10^6	218FW	- 5112	-15200	- 43.930	28700
11-37		DS,SAC,DL(MOS)	1.25×10^6		- 6161	-17500	- 51.760	24000
-39		DS,SAC,DL(MOS)	5440		- 7571	-21000	- 61.929	--
-40		DS,SAC,DL(MOS)	10310		- 8170	-22800	- 66.511	--
-41		DS,SAC,DL(MOS)	89360		- 6695	-20000	- 57.920	--
-42		DS,SAC,DL(MOS)	90050		- 6161	-19000	- 54.676	--
-43		DS(BOTH WAYS),SACF,DL(MOS)	50		- 9149	-25700	- 75.455	--
-44		DS(BOTH WAYS),SACF,DL(MOS)	470		- 8472	-27000	- 79.388	--

TABLE 5.6 (CONTINUED)

Specimen ID	Discontinuity Configuration	Failure Modes	Cycles to runout or Failure	Test Condition	Max. Cyclic Strain (μin/in)	Max. Cyclic Load (lbs)	Max. Cyclic Stress (ksi)	Residual Strength (lbs)
XVI-ACL-4210A-7-2	PDO #2	SACF,DS(BOTH WAYS),DL-MOS(1"FROM END)	1.25×10^6	-65FW	- 6030	-20000	- 65.466	-45000
7-4		SACF,DS(BOTH WAYS),DL-MOS(1"FROM END)	1.25×10^6		- 7352	-24000	- 79.182	-41400
7-6		SACF,DS(BOTH WAYS),DL-MOS(1"FROM END)	1.25×10^6		- 9441	-29500	- 96.342	-47350
7-7		DS(BOTH WAYS),DL,SACF-MOS	4060		-10595	-33500	-111.518	--
7-8		DS(BOTH WAYS),SACF,DL-MOS	790		-11234	-34500	-113.974	--
7-9		DS(BOTH WAYS),DL,SACF,-MOS	750		- 9840	-30600	-101.124	--
7-10		DS(BOTH WAYS),DL,SACF-MOS	756950		- 9530	-29600	- 97.400	--
7-11		DS(BOTH WAYS),SACF,DL-MOS	33350		-10136	-32000	-104.200	--
XVII-ACL-4210A-8-13	PDO #2	DS,DL@UTEOT ON THIN PART	1.25×10^6	RTD	- 6044	-18000	- 59.133	-34000
-15		DS,SACF@MOS ON THIN PART	1.25×10^6		- 7585	-22000	- 73.309	-36000
-17		DS,DL@MOS ON THIN PART	261140		- 9196	-26000	- 87.927	--
-18		DS,DL@MOS ON THIN PART	12630		-10346	-29000	- 97.283	--
-19		DL,DS@MOS	30		-11348	-31500	-103.550	--
-20		DS,SCAF,DL@MOS ON THIN PART	305490		- 9176	-26000	- 85.302	--
-21		DS,SACF,DL@MOS ON THIN PART	72620		-10467	-29000	- 96.378	--
-22		DS,DL,SACF@MOS ON THIN PART	1050		-10982	-31000	-103.575	--
XVIII-ACL-4210A-8-24	PDO #2	SAC,DS,DL(1" FROM EOT)	1.25×10^6	RTW	- 6055	-17600	- 58.355	-35400
4211B-12-26		TB,DS,SAC,DL(1"UTEOT)	249890		- 7077	-22600	- 72.346	--
-28		DS,DL,SAC,(1"UTEOT)	1.25×10^6		- 8005	-24300	- 78.564	-35200
-29		DS,DL,SAC(AT EOT)	85460		- 9254	-26800	- 84.303	--
-30		SAC,DS,DL(1" FROM EOT)	1580		-10163	-29600	- 94.237	--
-31		DS,TB,DL(AT EOT)	90850		- 8653	-25500	- 79.217	--
-32		DS(BOTH WASY),SACF,DL(MOS)	159870		- 8457	-25800	- 81.465	--
-33		DS,(BOTH WAYS),SACF,DL(MOS)	110		-11440	-34650	-112.245	--

TABLE 5.6 (CONCLUDED)

Specimen ID	Discontinuity Configuration	Failure Modes	Cycles to runout or Failure	Test Condition	Max. Cyclic Strain (μin/in)	Max. Cyclic Load (lbs)	Max. Cyclic Stress (ksi)	Residual Strength (lbs)
XIX-ACL-4211B-12-35	PDO #2	DS,SACF@MOS	1.25×10^6	218FW	-5266	-16100	-50.901	-30700
13-37		DS,SACF@MOS	1.25×10^6		-6438	-19400	-61.431	-30300
-39		DS,SACF,DL@MOS	21940		-6980	-22300	-72.005	--
-40		DS,SACF,@MOS	1500		-8558	-25700	-83.022	--
-41		SACF,DS@MOS	2080		-9447	-28000	-89.115	--
-42		DS,DL,SACF@MOS	150000		-6836	-21300	-67.726	--
-43		SACF,DS@MOS ON THIN PART	20		-9130	-28000	-88.720	--
-44		DS,SACF@UTEOP	10		-9541	-28200	-90.038	--

1 See Appendix G for failure photographs

*Taken at Thin Section
**Auto Stop Did Not Work
***Broke While Positioning In Test Fixture

LEGEND: DS – Diagonal Shear
          DL – Delamination
          EOT – Edge of Tab
          MOS – Middle of Specimen
          SAC – Straight Across Compression Fracture
          TB – Tab Bond
          UTEOT – Under Tapered Edge of Tab

TABLE 5.7. TEST SERIES MOISTURE DATA.

Test Series & Date/Cum. Time	Coupon I.D.	No. of Plies	% Wt. Loss in Drying	% Wt. Gain After Moisture Conditioning	% Wt. After Test Series Testing Complete	Coupon Condition	Test Condition
Basic Date: 1/9/80 = 0 Time							
Cumulative Time: Days I	MC-6	– 30	2 -0.134	132 1.065	180 1.108	– Dried*	– -65°FW
Cumulative Time: Days II	MC-8	– 30	2 -0.176	132 1.098	204 1.119	– Dried*	– -65°FW
Cumulative Time: Days III	MC-17B	– 30	2 -0.218	132 1.106	195 1.021	– Dried*	– 218°FW
Cumulative Time: Days IV	MC'-10	– 28	2 -0.174	132 1.091	180 1.139	– Dried*	– -65°FW
Cumulative Time: Days V	MC'-11	– 28	2 -0.175	– –	30 0.125	– Dried*	– RTD
Cumulative Time: Days VI	MC'-13 MC'-1	– 28 30	2 -0.175 –	132 1.100 0.920	147 1.100 0.920	– Dried* Not Dried	– RTW RTW
Cumulative Time: Days VII	MC-2 MC-18B	– 30 30	2 – – -0.133	132 1.003 1.146	212 0.938 1.125	– Not Dried Dried*	– 218°FW 218°FW
	MC'-14	28	-0.149	1.042	0.993	Dried	218°FW
Cumulative Time: Days VIII	MC'-9 MC'-24	– 28 28	2 – – -0.174	132 0.940 1.165	223 0.892 1.117	– Not Dried Dried*	– -65°FW -65°FW
	MC-3	30	– –	1.002	0.979	Not Dried	-65°FW
Cumulative Time: Days IX	MC'-25	– 28	2 -0.150	– –	55 0%	– Dried*	– RTD

TABLE 5.7. TEST SERIES MOISTURE DATA (Continued).

Test Series & Date/Cum. Time	Coupon I.D.	No. of Plies	% Wt. Loss in Drying	% Wt. Gain After Moisture Conditioning	% Wt. After Test Series Testing Complete	Coupon Condition	Test Condition
Cumulative Time: Days X		-	2	49	192	-	-
	MC'-12	28	-	0.926	0.876	Not Dried	RTW
	MC'-27	28	-0.122	1.096	1.072	Dried*	RTW
	MC-4	30	-	0.945	0.923	Not Dried	218°FW
Cumulative Time: Days XI		-	2	49	196	-	-
	MC'-26	28	-	0.951	0.903	Not Dried	218°FW
	MC'-28	28	-0.073	1.135	1.064	Dried*	218°FW
	MC-5	30	-	1.031	0.944	Not Dried	218°FW
	MC-21	30	-0.137	1.179	1.114	Dried*	218°FW
Cumulative Time: Days XII		-	2	132	180	-	-
	MC"-16A	26	-0.110	1.119	1.119	Dried*	-65°FW
Cumulative Time: Days XIII		-	2	-	35	-	-
	MC"-17A	26	-0.189	-	0%	Dried*	RTD
Cumulative Time: Days XIV		-	2	132	154	-	-
	MC"-15A	26	-	0.756	0.783	Not Dried	RTW
	MC"-19A	26	-0.189	0.979	0.979	Dried*	RTW
	MC-7	30	-	0.986	1.008	Not Dried	RTW
Cumulative Time: Days XV		-	2	132	154	-	-
	MC"-18A	26	-	0.935	0.962	Not Dried	218°FW
	MC"-20A	26	-0.188	1.052	1.131	Dried*	218°FW
	MC-15B	30	-	0.956	0.935	Not Dried	218°FW

TABLE 5.7.   TEST SERIES MOISTURE DATA (Continued).

Test Series & Date/Cum. Time	Coupon I.D.	No. of Plies	% Wt. Loss in Drying	% Wt. Gain After Moisture Conditioning	% Wt. After Test Series Testing Complete	Coupon Condition	Test Condition
Cumulative Time: Days XVI	-	-	2	132	173	-	-
	MC'-23	26	-	0.951	0.951	Not Dried	-65°FW
	MC"-30	26	-0.134	1.095	1.095	Dried*	-65°FW
	MC-16B	30	-	0.883	0.861	Not Dried	-65°FW
Cumulative Time: Days XVII	-	-	2	-	47	-	-
	MC"-31	26	-0.053	-	0.027	Dried*	RTD
Cumulative Time: Days XVII	-	-	2	35	173	-	-
	MC"-29	26	-	0.915	0.889	Not Dried	RTW
	MC"-33	26	-0.210	1.079	1.079	Dried*	RTW
	MC-19B	30	-	1.032	1.032	Not Dried	RTW
Cumulative Time: Days XIX	-	-	2	35	209	-	-
	MC"-32	26	-	0.928	0.876	Not Dried	218°FW
	MC"-34	26	-0.238	1.214	1.189	Dried*	218°FW
	MC-20B	30	-	1.040	0.996	Not Dried	218°FW
	MC-22	30	0.088	1.144	1.101	Dried*	218°FW

*Drying Conditions: 48 Hrs. @170°F in air.

higher moisture weight gains than the ones that were not dried. For all dried coupons (30,28, and 26 plies) that went through the 99 day, two stage, moisture conditioning the mean amount of moisture absorbed was 1.106% with a standard deviation of 0.055% and a coefficient of variation of 0.049. Coupons (30,28, and 26 plies) that were not dried but moisture conditioned gave a moisture weight gain mean value of 0.950%, a standard deviation of 0.066%, and a coefficient of variation of 0.069. The difference in mean moisture contents between the dried and undried coupons was 0.156% or very close to the average weight loss of the dried coupons of -0.159%. This indicates that the dried specimens picked up an additional amount of moisture almost equal to the weight lost during drying.

Moisture weight gain for the specimens described above after each test series testing was complete is shown in Table 5.7. After test series testing completion the moisture conditioned (wet) coupons that had been dried had a mean moisture content of 1.092% with a standard deviation of 0.052% and a coefficient of variation of 0.048. For the coupons that were not dried the mean moisture content was 0.926% with a standard deviation of 0.060% and a coefficient of variation of 0.065 after test series testing. Differences between the dried and undried coupons in moisture absorption were 0.166%, or close to the -0.159% weight loss in the dried coupons.

Since the coupon weight loss (-0.159%) in drying is an indication of the moisture pickup during specimen fabrication, the dried coupons are a better indication of the total specimen moisture content than are the ones that are not dried. Moisture content of coupons is about 10% higher than that predicted for 30 ply specimens. The fact that these coupons of 30, 26, and 28 plies were all exposed to the same moisture conditioning may be a causative factor.

SECTION 6

ANALYSIS OF EXPERIMENTAL DATA

6.1 SCOPE OF WORK

As in the first-year effort [1], emphasis during the present second-year program has been on the analysis of the static test data. This is a necessary first step toward the goal of predicting fatigue life of composites.

A detailed literature survey was presented in the first-year report [1]. Only a limited amount of additional literature has been published since that time. However, a good up-to-date summary of fatigue analyses of composite materials has recently been compiled by Saff [2] for the Navy. As he states, "modeling of fatigue damage in composites is in its infancy." Also, "much work needs to be done to determine the mechanisms of damage growth and the significance of matrix cracking and delamination on residual strength and fatigue life." Saff concludes that detailed analyses based upon physically realistic models, rather than empirical data fits, appear to be the most promising approaches. The present work is in full accord with this conclusion.

During the past year, two new analytical tools have been developed by the Composite Materials Research Group at the University of Wyoming which have a direct impact on the goals of the present program. These include the addition of longitudinal shear loading capability to the existing micromechanics analysis [3], and the development of an entirely new three-dimensional finite element analysis of laminated composites [4]. Although both of these developments were funded primarily by other sources, the needs of the present program were a strong factor in their development. Unfortunately, since both of these analyses have just been completed, there has been insufficient time yet to fully utilize them to analyze the experimental data generated by Northrop during this second-year study. However, preliminary results are presented here to demonstrate these new analytical capabilities. It is anticipated that many more correlations between theory and experiment will be attempted during the third-year effort.

As in the first-year study [1], extensive use was also made of the scanning electron microscope (SEM) in studying failure modes. This SEM work and each of the above analyses are discussed in detail in the following sections.

6.2 SCANNING ELECTRON MICROSCOPY

The scanning electron microscope (SEM) is a very useful tool for examining fracture surfaces in composite materials, because of its wide range of magnification and excellent depth of field. The latter feature was particularly important in the present study because of the very disrupted nature of the compression failure surfaces. During the past year the University of Wyoming has purchased a new scanning electron microscope, a JEOL JSM-35C unit, which is an improved version of the JSM-U3 unit used to obtain the SEM photographs presented in the first-year report [1]. Both units are now available; the new unit was used in the present work.

6.2.1 Specimen Preparation and Examination

A total of 71 specimens were mounted and examined, representing all of the various environmental conditions considered. The specimen mounts for the new JSM-35C are one inch in diameter, four times larger in area than the one-half inch diameter mounts used with the older JSM-U3 unit, permitting much larger specimen pieces to be examined. Typically, three pieces were cut from each test specimen to be examined. A longitudinal sawcut was made through the fracture surface, perpendicular to the surface of the specimen. This exposed the inside of the laminate at the fracture surface, and also as much as one-half to one inch in from the fracture surface. In this matter, the extent of the damage could be determined. In addition, a fracture surface as observed looking parallel to the direction of loading (the axial or longitudinal direction), and a fracture surface parallel to the surface of the specimen were mounted. In this manner, three orthogonal surfaces could be studied for each test specimen. As in the first-year study [1], a Buehler No. 10-4150 silicon carbide cutoff disk was used as required. All specimens were ultrasonically cleaned to remove debris, then vapor coated with gold to increase electrical conductivity in the SEM.

6.2.2 Discussion of SEM Observations

Although a total of 71 specimens were examined, not all were photographed, either because they contained nothing of special interest, or because they exhibited failure modes already photographed on other specimens.

In general, little was observed in the present set of specimens that had not already been seen in the fractures exhibited in those specimens examined in the prior study [1]. While it was felt that the failures were being influenced by the ply drop-offs, the influence was not dominant. Most unexpectedly, the presence of the ply drop-offs could not be readily detected in the SEM. At the fracture surface, the specimens were too extensively shattered. Thus, the presence of the ply drop-offs is not evident in the SEM photographs to be shown.

All of the photographs included here are of fatigue specimens; the observed failure modes of the static compression specimens were very similar, just as in the first-year study [1]. The information across the bottom of each photograph is as follows. The first item is the electron beam acceleration voltage, in kilovolts (not of particular significance to the present discussion). The second item is the magnification, the third is the photograph number. The solid horizontal bar is a scale marker, its length being given, in micrometers, immediately below. The last item, UW 80, identifies the SEM unit used.

The figure caption for each photograph is written in the same format, for ease of comparison. The specimen no. is the Northrop number, as defined and used in Sections 3, 4, and 5. The C-C, C-C', and C-C" designations indicate plain (no ply drop-offs present), ply drop-off No. 1 (two 0° plies dropped off – see Figure 3.1), and ply drop-off No. 2 (four 45° plies dropped off, in a staggered pattern – see Figure 3.2) configurations. The designations RTW, -65FW, etc. also follow the experimental notation established by Northrop to identify the test conditions of temperature and moisture. The final item in the figure caption identifies the view shown by the photograph, as previously defined.

All specimens were examined and photographed by the author directly. The brief description given beneath each photograph is based upon the notes made during the actual observation. The region photographed was selected as being representative of the failure mode observed. These observations are summarized in the following paragraphs.

6.3

Figure 6.1 is a low magnification (13X) view of a sawcut section through the thickness of the laminate parallel to the direction of compressive fatigue loading. The left end of the specimen is the actual gross fracture. The secondary ply delaminations extending well into the laminate are readily visible, as are the several regions of transverse cracking of individual plies, associated with individual fiber microbuckling. This was a typical room temperature, wet failure mode.

Figure 6.2 is a similar photo, but for a ply drop-off No. 2 (C-C") configuration, and at the low test temperature (-65°F). The ply delaminations are more distinct, and somewhat more extensive than for the room temperature condition. A corresponding photograph for an elevated temperature (218°F) test would have indicated little delamination. Both Figures 6.1 and 6.2 represent low cycle fatigue tests (9470 and 33,350 cycles to failure, respectively). However, the failure mode did not appear to be particularly sensitive to this parameter.

In comparison to Figures 6.1 and 6.2, Figure 6.3 represents an elevated temperature, wet fatigue test. As noted above, delamination is minimal. However, the general disruption and crushing of the specimen well away from the gross fracture surface is obvious. Suggestions of shear failures are exhibited. However, when examined at higher magnifications, it appeared that these shear failures were initiated by local regions of fiber microbuckling.

Figure 6.4 is also a photograph of a longitudinal sawcut section of a 218FW fatigue specimen, but for a C-C" ply drop-off configuration. The photograph is of the region in the one-half inch interval between the outer and inner 45° ply drop-offs (see Figure 3.2). The exact location of each individual ply drop-off could not be determined; apparently the material was totally disrupted in these local regions, completely obscuring the original geometry. The apparent gross shear failure is more pronounced in this C-C" configuration (with four ply drop-offs occurring in one local area) than in the C-C' configuration of Figure 6.3, where only two plies were discontinuous. Again however, it is probable that this gross shear failure was in fact precipitated by local fiber microbuckling, primarily of the 0° plies.
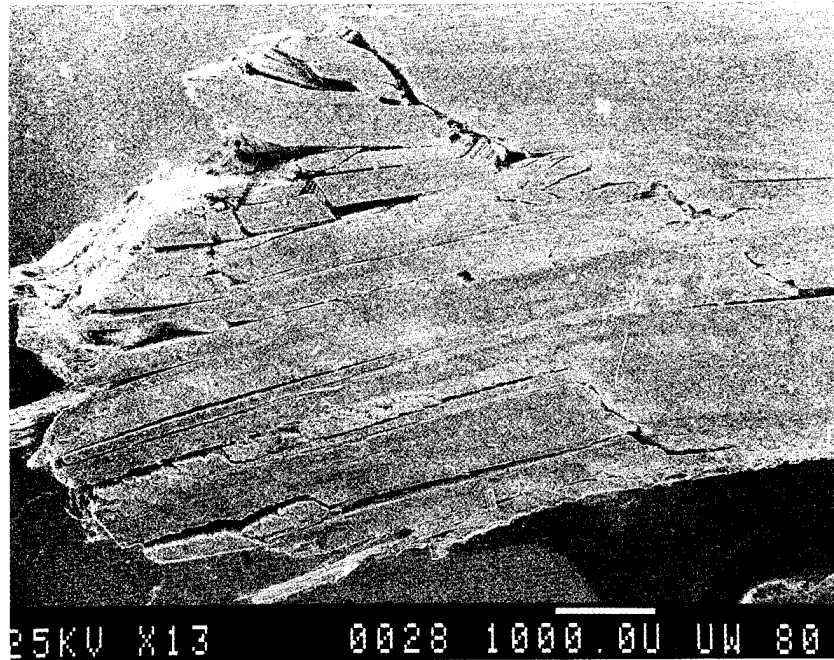
Figure 6.1 Specimen No. X-ACL-4211B-10-31, C-C', RTW; Longitudinal Sawcut Section.

A low magnification overall view of the 30-ply side of the fracture near one edge of the specimen is shown. The 0° ply drop-offs are believed to end at the fracture surface, but could not be distinguished. The considerable amount of ply delamination typically evident is shown, along with compressive failures well below the actual fracture surface.

Figure 6.2   Specimen No. XVI-ACL-4210A-7-11, C-C", -65FW; Longitudinal
Sawcut Section

This low magnification overall view of the 30-ply side of

the fracture is at the center of the specimen. The inner

(+45°) ply drop-offs are believed to be at the fracture

surface, but could not be distinguished.

The extensive ply delaminations were probably caused in

large part by the high energy release at fracture, due to

the high maximum cyclic stress (-104.2 ksi). More extensive

delaminations close to the gross fracture surface did appear

to occur at the low test temperature, as represented here.

Figure 6.3 Specimen No. XI-ACL-4211B-11-42, C-C', 218FW; Longitudinal Sawcut Section

This overall view is in the region of the 0° ply drop-offs; however, they could not be distinguished. The gross fracture occurred well to the right of the field of view shown here. That is, although local failures are evident in the regions of the ply drop-offs, as shown here, the primary failure occurred in the thin section of the specimen.

The extent of ply delamination was much less in this elevated temperature, wet condition than indicated in Figures 6.1 and 6.2 for the lower temperatures.
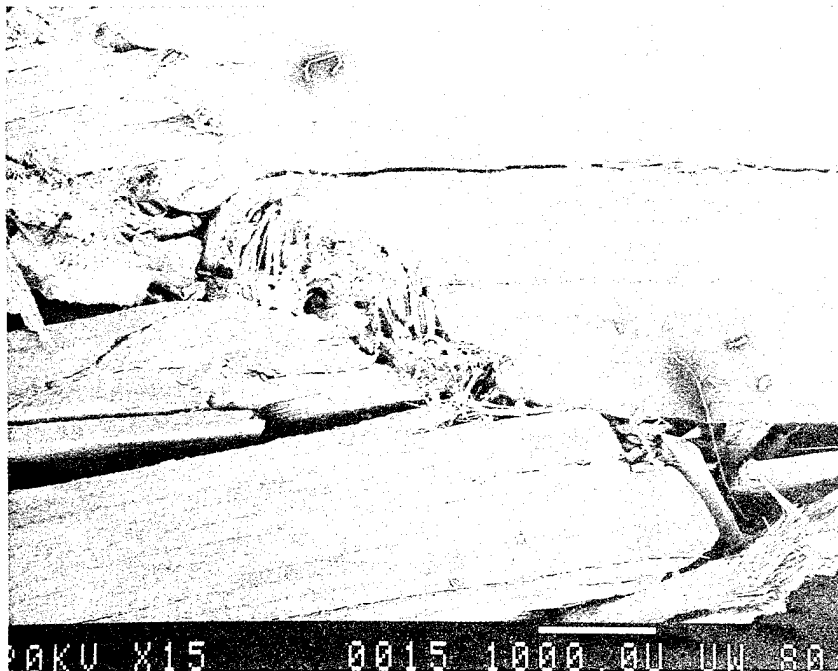
Figure 6.4   Specimen No. XIX-ACL-4211B-13-42, C-C", 218FW; Longitudinal
Sawcut Section

The drop-off of the outer (-45°) plies is slightly to the

left of the field of view; the drop-off of the inner (+45°)

plies is to the right. The gross failure occurred in the

general region of the outer ply drop-offs. Obviously, the

material in the region between ply drop-offs was well disrupted.

Evidence of a gross shear failure can be seen. As in Figure

6.3, extensive ply delaminations did not occur.

In contrast to Figures 6.3 and 6.4, Figure 6.5 indicates the considerably different fracture surface exhibited by the low temperature specimens. The fracture surface is relatively clean, with few disrupted regions, and extensive delamination. In this view, the delaminations are parallel to the line of sight. The number of cycles to failure, 150,000 and 131,450 for the specimens of Figures 6.4 and 6.5, respectively, were about the same.

All of the specimens tested had $\mp$ 45° plies on the outer surfaces. (See Figures 3.1 and 3.2.) Figure 6.6 indicates the buckling of these outer two plies after delaminating from the adjacent 0° ply. This is a view looking parallel to the direction of compressive loading, into the gross fracture surface. The small region of fiber microbuckling in the extreme upper left of the photograph indicates the high stresses these 45° plies were carrying before they delaminated and buckled. This specimen failed at 305,490 cycles; perhaps a fatigue crack propagation was responsible for this delamination.

Figure 6.7 represents a specimen which survivied 1.25×10^6 cycles and was subsequently residual strength tested. The sawcut surface has been smeared, so that fractures can be readily distinguished from the unfractured material. Figure 6.8 represents a specimen which survived only 1670 cycles. Both are C-C' configurations. As can be seen, in spite of the totally different fatigue lives, the failure modes exhibited by these two specimens are very similar. That is, as noted also in the first-year study [1], there is not an observable difference between the static, low cycle, and high cycle fracture modes. This is significant in terms of attempting to use static or quasi-static analyses to study fatigue response, as is being done in the present investigation. The SEM observations suggest that this may be a very reasonable approach.

A significant failure mode, particularly in the room temperature and elevated temperature fatigue specimens in the wet condition, was fiber microbuckling. Figure 6.9 presents a typical example. Although the gross failure occurred at the ply drop-off cross section at the extreme left of the photograph, the presence of extensive fiber microbuckling is evident well inward from this fracture surface. These regions will be examined more closely in
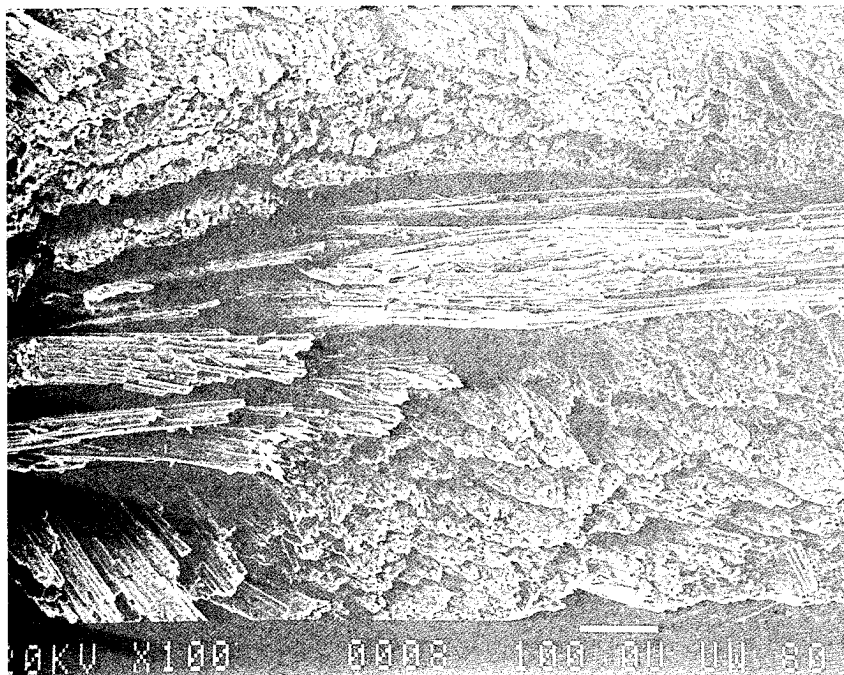
Figure 6.5   Specimen No. II-ACL-4210A-2-14, C-C, -65FW; Fracture Surface
at 45° to Load Direction

The fractured ends of fibers are shown, indicating a relatively

clean fracture, with minimal crushing.   Longitudinal cracks

(ply delaminations) are apparent, although not as extensive

in this plain specimen as in the ply drop-off specimens at

the low test temperature, as shown, for example, in Figure 6.2.
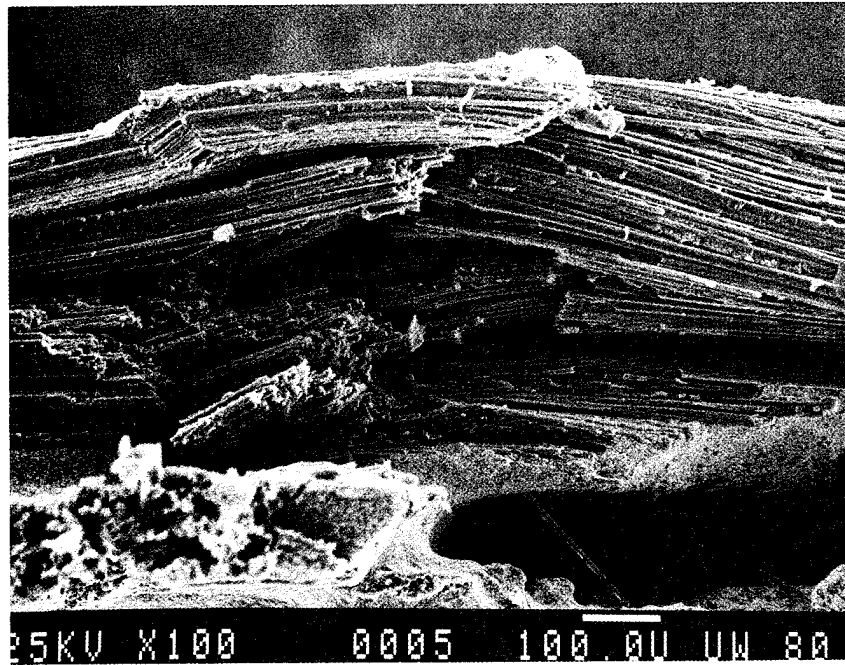
Figure 6.6   Specimen No. XVII-ACL-4210A-8-20, C-C", RTD; Fracture
Surface, Viewed Along Axis of Loading

The $\mp$ 45° plies on the outer surface of the specimen in the
region of the ply drop-offs are shown. They delaminated from
the adjacent 0° ply, and buckled outward. A local microbuckle
can also be seen in the outermost ply, at the extreme top
left corner of the photograph. The general appearance of the
fracture surface indicated a considerable amount of crushing.

Figure 6.7   Specimen No. VIII-ACL-4210A-4-4, C-C', -65FW; Longitudinal
Sawcut Section

This specimen survived 1.25×10^6 cycles at a -68.7 ksi

stress level, and was residual strength tested to -115.3 ksi.

An extensive amount of fragmentation was observed, as indicated

in this photograph. In general, however, the overall failure

mode was similar to those observed in the specimens which

failed during fatigue cycling.

6.12
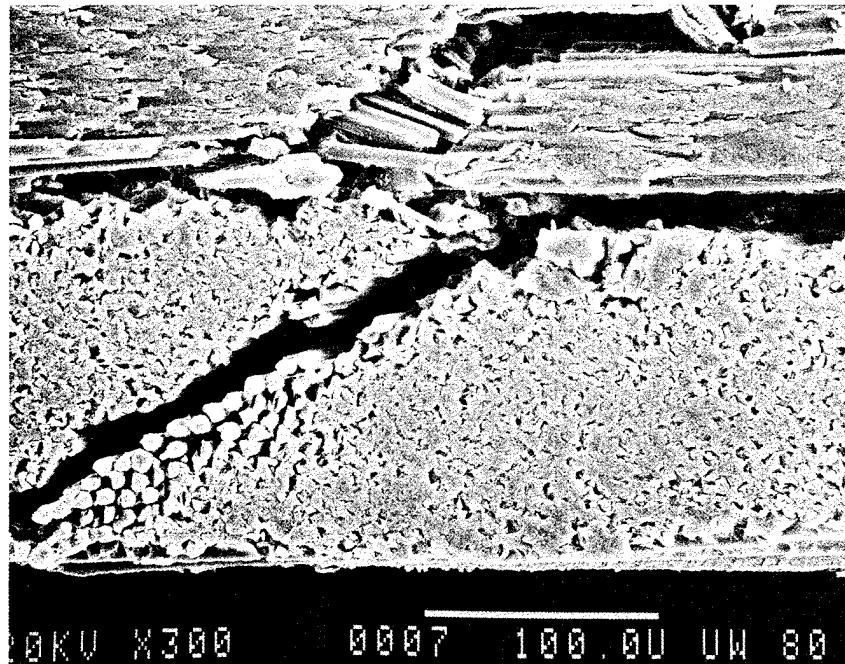
Figure 6.8   Specimen No. IX-ACL-4210A-5-22, C-C', RTD; Longitudinal
             Sawcut Section

This room temperature, dry specimen, like that represented

in Figure 6.7, indicated more delamination and general

disruption than the corresponding wet specimens. Evidence

of shear failures of the 0° plies, and debonding of individual

fibers in the 90° plies, can be seen. This was in the general

area of the 0° ply drop-offs, the gross fracture surface

being well to the right of the region shown.
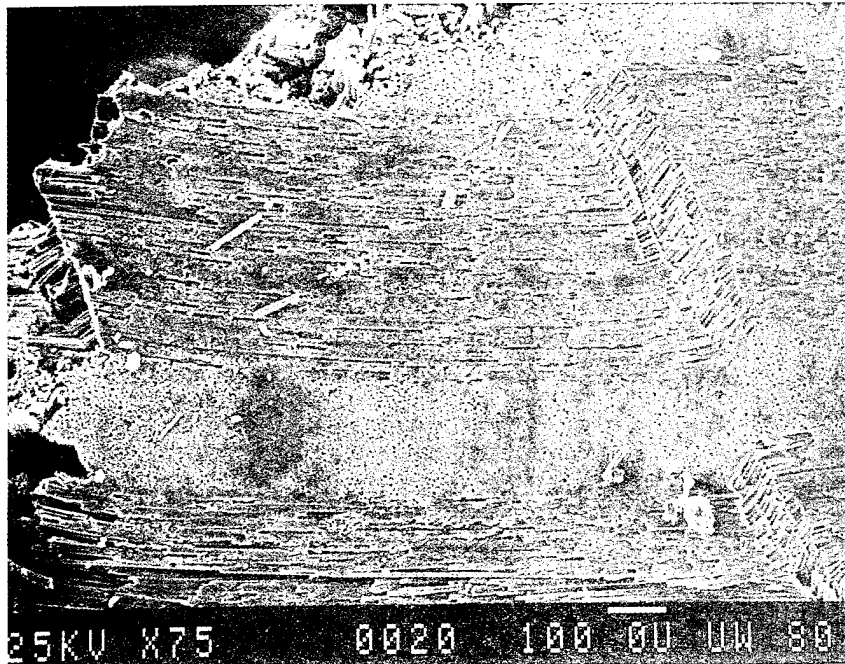
Figure 6.9   Specimen No. XI-ACL-4211B-11-44, C-C', 218FW; Longitudinal
Sawcut Section

A view of the 28-ply end (thin end) near one edge of the
specimen is shown. The ply drop-off is believed to be right
at the fracture surface, although not evident.

Minimal delamination at the fracture surface is apparent at
this high temperature, wet test condition, even though the
applied stress was high (-79.4 ksi), the specimen failing at
only 470 cycles. This is in contrast to the extensive delamina-
tion evident in Figures 6.1 and 6.2, the RTW and -65FW condi-
tions, respectively.

Extensive zones of fiber microbuckling of the 0° plies are
also shown, many fiber diameters in from the gross fracture
surface.

6.14

the next two photographs. However, this Figure 6.9 also verifies the prior statement that minimal delaminations occurred in the elevated temperature specimens. This view is similar to those of Figures 6.1 and 6.2 (although at a higher magnification), and does not show the extensive delaminations exhibited by those specimens. It was relatively certain that the 0° ply drop-offs were located right at the gross fracture plane. However, positive indications of their presence could not be found. It is believed that one of the ply drop-offs was right at the center of the fracture region shown along the left edge of the photograph.

Figure 6.10 is a higher magnification view of a local region of the buckled fibers shown in Figure 6.9. The lateral shifting or shearing of the entire 0° ply can be seen.

Figure 6.11 shows another region of the specimen of Figure 6.9. Again the gross distortion of the 0° ply is obvious. This in turn caused the 90° ply above to break up; the matrix material surrounding individual fibers is totally fragmented. The fibers of the + 45° ply directly under the 0° ply apparently were also fractured, perhaps by a buckling failure as well. When the laminate was sectioned for examination, some of these broken fibers fell out. The next ply down, the -45° ply, is also well-disrupted, as the absence of matrix surrounding individual fibers indicates.

Figure 6.12 shows a close-up of a zone of buckled 0° ply fibers in a C-C" laminate, near the gross fracture surface, exhibiting a failure much similar to that of the C-C' laminate of Figure 6.10.

In the first-year report [1], a number of photographs of delamination interfaces were shown. Two features were noted, fiber replication and matrix lacerations [1]. These features were again commonly observed, one example being shown in Figure 6.13.

6.2.3 Summary of SEM Observations

In general, in spite of the extensive amount of work done, the results of the SEM investigation were disappointing. It had been expected that the two different types of ply drop-offs would be clearly visible, and their influence

6.15
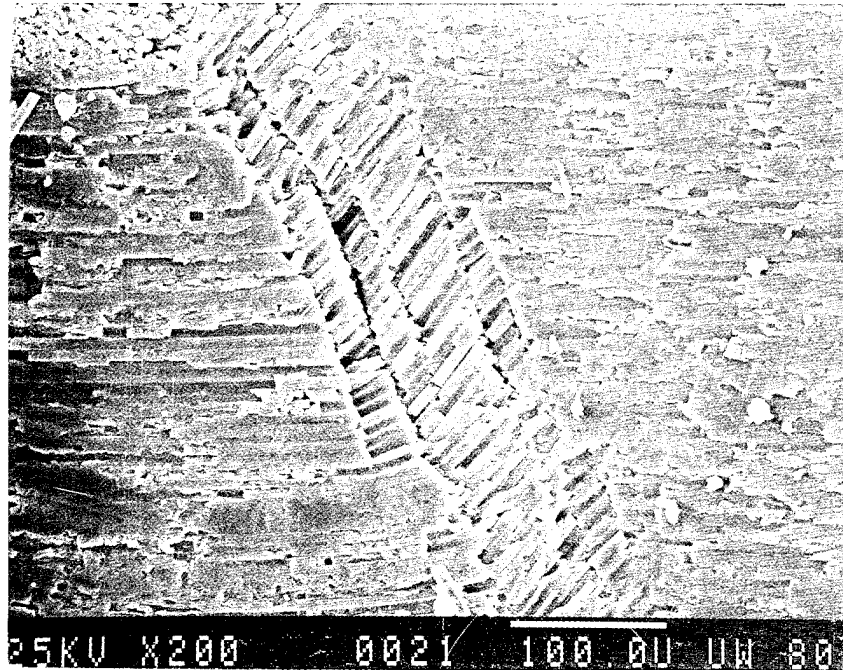
Figure 6.10   Specimen No. XI-ACL-4211B-11-44, C-C', 218FW; Longitudinal
Sawcut Section

This is a higher magnification view of a portion of the
region of buckled 0° fibers at the right-center of the photo-
graph of Figure 6.9.   The exact location can readily be
identified by the debris on the surface.

The break-up of the individual fibers into multiple lengths
can be seen.   The adjacent 90° ply is visible in the extreme
upper left corner of the photograph.

Figure 6.11   Specimen No. XI-ACL-4211B-11-44, C-C', 218FW; Longitudinal Sawcut Section

Another region of the same specimen presented in Figure 6.9 is shown. The buckled 0° ply is at the bottom of the thin section of the laminate (ply no. 26 at the C' side in Figure 3.1). The single 90° ply above this ply is correspondingly deformed, the matrix surrounding individual fibers being totally fragmented.

A portion of the +45° ply below the buckled ply has broken off below the sawcut surface and has fallen out.
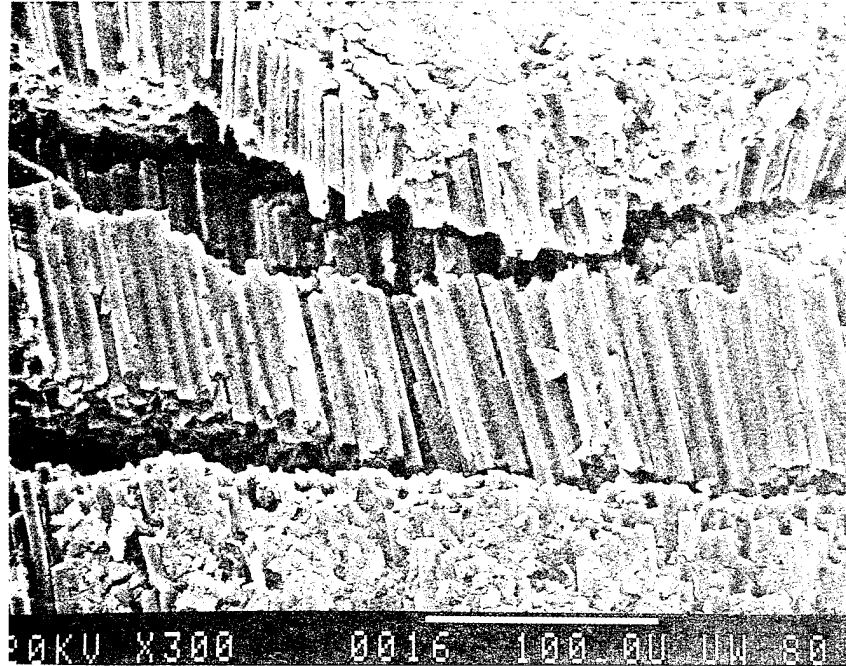
Figure 6.12   Specimen No. XIX-ACL-4211B-13-42, C-C", 218FW; Delaminated
Fracture Surface

This is a view looking perpendicular to the plies of the
laminate, very near the gross transverse fracture surface,
in the region of the outer (-45°) ply drop-off. Unlike the
previous photographs, the applied compressive loading was in
the vertical direction in this view.

The depth of the zone of buckled fibers is evident.
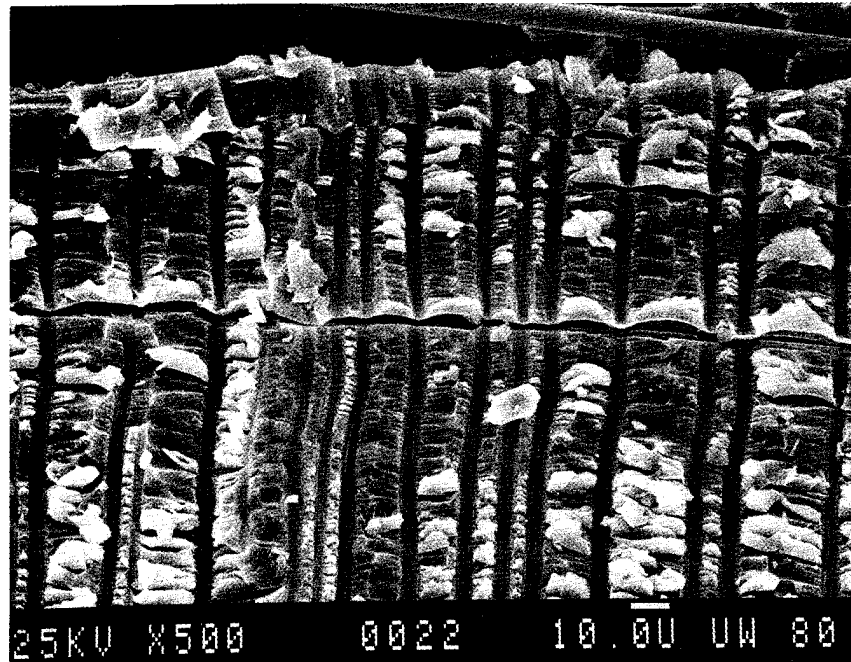
Figure 6.13   Specimen No. XI-ACL-4211B-11-44, C-C', 218FW; Delaminated
Fracture Surface

As in Figure 6.12, the applied compressive loading was in

the vertical direction. The interface between a 0° ply

and a 90° ply (indicated by the single fiber at the top of

the photograph) is shown. Only replicates of the 0° ply

are present, the actual ply material having delaminated and

fallen away.

The edge of the gross transverse fracture surface is shown

at the top of the photograph. The "matrix lacerations"

shown, for example, in Figure 6.1 of Reference [1] are clearly

evident here also, being typically observed.

6.19

on the failure obvious. This was not the case. In no SEM observation was a ply drop-off clearly discernable. Apparently the laminate was well-disrupted in these regions, the fractures obscuring the original geometry.

One goal of the present analytical work is to be able to model the ply drop-off geometries using the three-dimensional finite element analysis [4]. The local geometry of the laminate in the region of the ply drop-off is required for this purpose. It was necessary to rely on the macrophotography discussed in Section 6.4 to obtain this information.

On the positive side, the extensive SEM work clearly verified the consistently high quality of the laminates fabricated and tested by Northrop. No voids, inclusions or other defects were found in any of the specimens.

In the first-year study [1] it was found that there was little if any difference between the room temperature and elevated temperature fatigue failures, whether the specimens were tested wet or dry. Thus, it might have been expected that there would also be relatively little difference for the -65°F test conditions of the present study. There were differences, however; the -65° F specimens tended to fail in a more brittle manner than the room or elevated temperature specimens. This is probably the primary reason for the higher strengths and strains to failure exhibited by these specimens (see, for example, Table 2.5). That is, the matrix exhibited less ductility at the low temperature, thus better supporting the individual fibers against the occurrence of microbuckling, a dominate failure mode of the 0° plies. When the low test temperature specimens did fail, the large amount of stored energy which was suddenly released could not be absorbed as readily by the less ductile matrix, resulting in the more extensive delaminations indicated by the SEM photographs presented in Section 6.2.2.

Confirming the Northrop observations of gross failure modes (see, for example, Tables 5.5 and 5.6 and the related discussion in Section 5.6), no major differences were observed in the local failure modes of the plain, 0° ply drop-off, and ± 45° ply drop-off configurations. With the possible

6.20

exception of the 0° ply drop-off endurance limit values being low (see Table 2.5), the lack of distinct differences in failure modes, on both the macro and micro levels, was also reflected in the mechanical properties data. This is, of course, a very desirable response from a design aspect, since it is very efficient to utilize ply drop-offs to vary the laminate configuration from one region to another in the structure. The minimal influence of ply drop-offs again points out the very forgiving nature of composite materials with respect to ply discontinuities and other stress concentration effects.

One near term goal of the present study is to be able to use the three-dimensional finite element analysis described in Section 6.4 to analyze specific discontinuity geometries, to permit the quantitative prediction of the extent and type of degradation of properties induced by these discontinuities.

6.3 COMBINED MICROMECHANICS/POINT STRESS ANALYSIS OF LAMINATE RESPONSE

In the first-year study [1], particular attention was given to the unidirectional composite experimental data when performing the analytical correlations. Primarily, this was because the unidirectional material represents the basic building block of any laminate; an understanding of laminate response must start with an understanding of the response of the individual plies. Since local failure modes were of special interest, a micromechanics analysis could be utilized directly. This proved to be very informative.

A brief study was also made of the $[\pm45]_{4S}$ and F-18 laminates, using a classical point stress analysis to predict gross response. While also quite informative, it did not provide information on local failure modes. The micromechanics analysis could not be used since in-plane shear stresses are induced in the individual plies of a laminate, due to the interaction or coupling between plies. The micromechanics analysis existing at that time could not handle in-plane (longitudinal) shear loadings.

During the past year, a longitudinal shear loading capability has been added to the micromechanics analysis [3]. In the following subsections, this new analytical capability will first be briefly described, then applied to some of the $[\pm45]_{4S}$ laminate data generated in the first-year study for various environmental conditions [1], and finally, applied to the much more complex F-18 laminate experimental data of the present effort.

6.3.1 Description of Micromechanics Analysis with Addition of Longitudinal Shear Loading Capability

The changes in theory associated with the addition of a longitudinal (out-of-plane) shear loading capability to the generalized plane strain formulation used in the first-year study [1], which included only a normal stress in the out-of-plane direction, were significant. In addition, major changes were required in the finite element solution technique and associated computer program. The added stress and strain components required revisions in the elastoplastic constitutive equations. In addition, the

special treatment of the compatibility of additional boundary conditions resulted in a special strain-displacement relation. Implementing these changes into the existing finite element analysis, although following classical developments, was a major effort. In many cases, where before a plane stress state was the only consideration, a stress tensor was involved in developing suitable failure criteria, principal stress calculations, etc.

A brief description of these considerations is presented in the following paragraphs. Complete details are given in Reference [3], the basic work being performed under an Army Materials and Mechanics Research Center contract.

Although generalized plane strain can be defined in a very general manner, it has been simplified for purposes of the present analysis. This treatment allows displacements to occur in all three coordinate directions, yet retains the advantages of the plane strain assumption. Specifically, each displacement is dependent upon the x- and y-coordinate (in-plane) directions, and the displacement in the z-direction (the fiber direction) has an added linear dependence on the z-coordinate, the axial coordinate of the composite in the present analysis. In the previous version of the micromechanics analysis [5], the generalized plane strain assumption was used to simplify the expression for the z-displacement, by assuming it to be dependent only on the axial coordinate position. Eliminating the functional dependence on the x- and y-coordinates essentially eliminated axial shear deformations, while allowing only constant axial normal displacements. Including the x and y dependence of the z-displacement allows a special form of axial shear deformation corresponding to the generalized plane strain treatment.

The key element of the relationship between load and displacement of a continuum is the constitutive equation. Each constituent material of a composite has unique properties represented in its own constitutive equation. In the present analysis, the fiber material is considered to be isotropic and transversely isotropic in order to model fibers such as graphite, but can be reduced to a simple elastic, isotropic material for the purpose of characterizing fibers such as boron and glass. The matrix material is considered to be isotropic and elastoplastic, the plastic response being modeled by the Prandtl-Reuss flow rule.

A constitutive equation involving only four stress and strain components has been derived in detail [5], but the two additional longitudinal shear components require additional consideration. The two additional shear stress-shear strain equations are

$$\tau_{xz} = G' \gamma_{xz}$$
$$\tau_{yz} = G' \gamma_{yz} \tag{6.1}$$

where G' is the longitudinal shear modulus, τ represents shear stress, and γ is shear strain. When Eqs. (6.1) are included in the complete set of constitutive equations for transversely isotropic elastic behavior, a material properties matrix $[D]$ is generated as

$$[D] = \frac{E}{Q}
\begin{bmatrix}
1 - \dfrac{E\nu'^2}{E} & \nu + \dfrac{E\nu'^2}{E'} & 0 & 0 & 0 & (1+\nu)\nu' \\[2mm]
 & 1 - \dfrac{E\nu'^2}{E'} & 0 & 0 & 0 & (1+\nu)\nu' \\[2mm]
 & & \dfrac{Q}{2(1+\nu)} & 0 & 0 & 0 \\[2mm]
 & & & \dfrac{E'Q}{2E(1+\nu')} & 0 & 0 \\[2mm]
 & & & & \dfrac{E'Q}{2E(1+\nu')} & 0 \\[2mm]
\text{Symmetric} & & & & & 1 - \dfrac{E\nu'^2}{E'}
\end{bmatrix} \tag{6.2}$$

where

$$Q = (1+\nu)(1 - \nu - \frac{2E\nu'^2}{E'})$$

ν = in-plane Poisson's ratio

ν' = major Poisson's ratio

E = transverse elastic modulus

E' = longitudinal elastic modulus

6.24

In obtaining Eq. (6.2), the relation $G = E/2(1 + \nu)$ has been utilized. The constitutive equation for isotropic material behavior is merely a simplification of Eq. (6.2), where the longitudinal and transverse moduli, and the Poisson's ratios, are equal.

The constitutive equation must also represent elastoplastic material behavior in the matrix after yielding occurs. An octahedral shear stress yield criterion has been employed, and plastic strain is assumed to be proportional to the deviatoric stress tensor, using the Prandtl-Reuss flow rule. Reference [5] discusses sources of more information related to these two criteria. The resulting constitutitve equation is

$$
[D] = \frac{E}{(1+\nu)}
\begin{bmatrix}
\frac{1-\nu}{1-2\nu} - \frac{S_{11}^2}{B} & \frac{\nu}{1-2\nu} - \frac{S_{11}S_{22}}{B} & \frac{-S_{11}S_{12}}{B} & \frac{-S_{11}S_{13}}{B} & \frac{-S_{11}S_{23}}{B} & \frac{\nu}{1-2\nu} - \frac{S_{11}S_{33}}{B} \\[6pt]
 & \frac{1-\nu}{1-2\nu} - \frac{S_{22}^2}{B} & \frac{-S_{22}S_{12}}{B} & \frac{-S_{22}S_{13}}{B} & \frac{-S_{22}S_{23}}{B} & \frac{\nu}{1-2\nu} - \frac{S_{22}S_{33}}{B} \\[6pt]
 & & 1 - \frac{S_{12}^2}{B} & \frac{-S_{12}S_{13}}{B} & \frac{-S_{12}S_{23}}{B} & \frac{-S_{12}S_{33}}{B} \\[6pt]
 & & & 1 - \frac{S_{13}^2}{B} & \frac{-S_{13}S_{23}}{B} & \frac{-S_{13}S_{33}}{B} \\[6pt]
 & & & & 1 - \frac{S_{23}^2}{B} & \frac{-S_{23}S_{33}}{B} \\[6pt]
\text{Symmetric} & & & & & \frac{1-\nu}{1-2\nu} - \frac{S_{33}^2}{B}
\end{bmatrix}
\qquad (6.3)
$$

where

S_{ij} = the deviatoric stress tensor

$B = \frac{3\tau_0^2}{E}\, 2M_T(1 + \nu) + E$

$\tau_0 = (\frac{1}{3}\, S_{ij}\, S_{ij})^{\frac{1}{2}}$ = octahedral shear stress

$2M_T$ = tangent modulus of the octahedral shear stress – octahedral shear strain curve

A major consideration in the finite element formulation is the desire to have a combined loading capability, where any combination of loads can be applied simultaneously. This leads to the seemingly impossible task of applying separate and contradictory boundary conditions simultaneously. It is possible to apply the two shear boundary conditions separately by adjusting

the element strain-displacement relation. The derivation of this relation
for a regular treatment of generalized plane strain is outlined in Reference
[3]. The resulting equation must be adapted to manage the shear boundary
conditions separately. Since the boundary conditions are concerned with
displacements, the shear displacements must be considered to be separate
and unique entities at each node point rather than combined into a general
z-displacement. Thus, a τ_{xz} shear stress induces a z-displacement w_{xz}, and
τ_{yz} shear stress induces a z-displacement w_{yz}. These separate displacements
can be arbitrarily specified without affecting other boundary conditions if
the strain-displacement matrix equation is expanded slightly as follows:

$$
\begin{Bmatrix} \varepsilon_x \\ \varepsilon_y \\ \gamma_{xy} \\ \gamma_{xz} \\ \gamma_{yz} \\ \varepsilon_z \end{Bmatrix} = \frac{1}{2A}
\begin{bmatrix}
b_i & 0 & 0 & 0 & b_j & 0 & 0 & 0 & b_k & 0 & 0 & 0 & 0 \\
0 & c_i & 0 & 0 & 0 & c_j & 0 & 0 & 0 & c_k & 0 & 0 & 0 \\
c_i & b_i & 0 & 0 & c_j & b_j & 0 & 0 & c_k & b_k & 0 & 0 & 0 \\
0 & 0 & b_i & 0 & 0 & 0 & b_j & 0 & 0 & 0 & b_k & 0 & 0 \\
0 & 0 & 0 & c_i & 0 & 0 & 0 & c_j & 0 & 0 & 0 & c_k & 0 \\
0 & 0 & 0 & 0 & 0 & 0 & 0 & 0 & 0 & 0 & 0 & 0 & 2A
\end{bmatrix}
\begin{Bmatrix} u_i \\ v_i \\ w_{xzi} \\ w_{yzi} \\ u_j \\ v_j \\ w_{xzj} \\ w_{yzj} \\ u_k \\ v_k \\ w_{xzk} \\ w_{yzk} \\ w_n \end{Bmatrix}
\qquad (6.4)
$$

where i, j, and k represent the three respective nodes of an element, and w_n
represents the constant normal axial displacement. It will be noted that
the three extra columns in the matrix and the added zeros effectively prevent
the longitudinal shear strains from influencing each other and the remainder
of the strains. The added terms in the displacement vector will also be noted.

The remaining finite element formulation follows a three-dimensional
formulation by Zienkiewicz [6], as shown in abbreviated form in the following
equations:

$$[K]^e = \int_{vol} [B]^T [D][B] \; d(vol) \qquad (6.5)$$

$$\{\delta\} = [K]^{-1}\{F\} \qquad (6.6)$$

$$\{\varepsilon\} = [B] \; \{\delta\} \qquad (6.7)$$

$$\{\sigma\} = [D][B] \; \{\delta\} \qquad (6.8)$$

where

$\{\delta\}$ = nodal displacements

$\{\varepsilon\}$ = element strains

$[B]$ = strain-displacement matrix

$[D]$ = constitutive equation

$\{\sigma\}$ = element stresses

$[K]^e$ = element stiffness matrix

$\{F\}$ = nodal force vector

$[K]^{-1}$ = inverse of the global stiffness matrix.

Element stiffness matrices are developed in Eq. (6.5), which combined together for the entire model form a global stiffness matrix. This is inverted for use in Eq. (6.6), to solve for nodal displacements. Element strains and stresses are calculated from the displacement vector in Eqs. (6.7) and (6.8), respectively. Two differences from Zienkiewicz's formulation are the nodal force vector and, of course, the nodal displacement vector. The displacement vector was previously defined; the nodal force vector proves to be very similar, due to the fact that there are five force components and displacement components possible at each node of the finite element grid.

The finite element analysis computer program developed by Miller and Adams [5] has been adapted for the modified form of generalized plane strain. The additional components of stress and strain result in the necessity of a thorough revision of the basic solution technique. The Branca technique [7] for applying loads and boundary conditions, and the specialized Gaussian elimination solution of the stiffness matrix, are the major burdens in the

revision. Developing these new techniques revealed a more efficient procedure for storing the stiffness matrix [3].

The special stiffness formulation discussed above caused complexities in the Gaussian elimination procedure. Branca first developed the special Gaussian elimination scheme, and testified that it required intricate book-keeping. Bookkeeping complexities are compounded in the present analysis due to the added boundary conditions, but the theory upon which Gaussian elimination is based remains unchanged. Thus the Gaussian elimination procedure degenerates into an involved exercise in bookkeeping and programming.

Implementing the preceding theory into the FORTRAN computer program of Reference [5] results in a new generalized plane strain, finite element micro-mechanics analysis. The incremental procedure utilized by Miller and Adams [5] remains intact in the present analysis except for the calculation of octahedral shear stress, which now includes the two added shear stress terms. This tangent modulus method enables highly inelastic materials to be managed easily.

In developing the analysis, another consideration was found to be essential for an efficient computer program. Designing the finite element mesh effi-ciently has a profound effect on the size of the stiffness matrix. The highest difference in node numbers in any one element determines the bandwidth of the stiffness matrix, i.e.,

$$BW = 4(R + 1) + 5 \tag{6.9}$$

where

BW = bandwidth of stiffness matrix

R = highest node number difference

The addition of 5 is due to the special boundary condition columns. The finite element mesh, besides the requirement to have a fine mesh in areas of high stress gradients, is also required to have a minimum R value. Additionally, due to the loading technique, the highest node number is also required to be located at the upper right-hand corner of the mesh. A model was developed as shown in Figure 6.14 that fulfilled these requirements, by arranging node
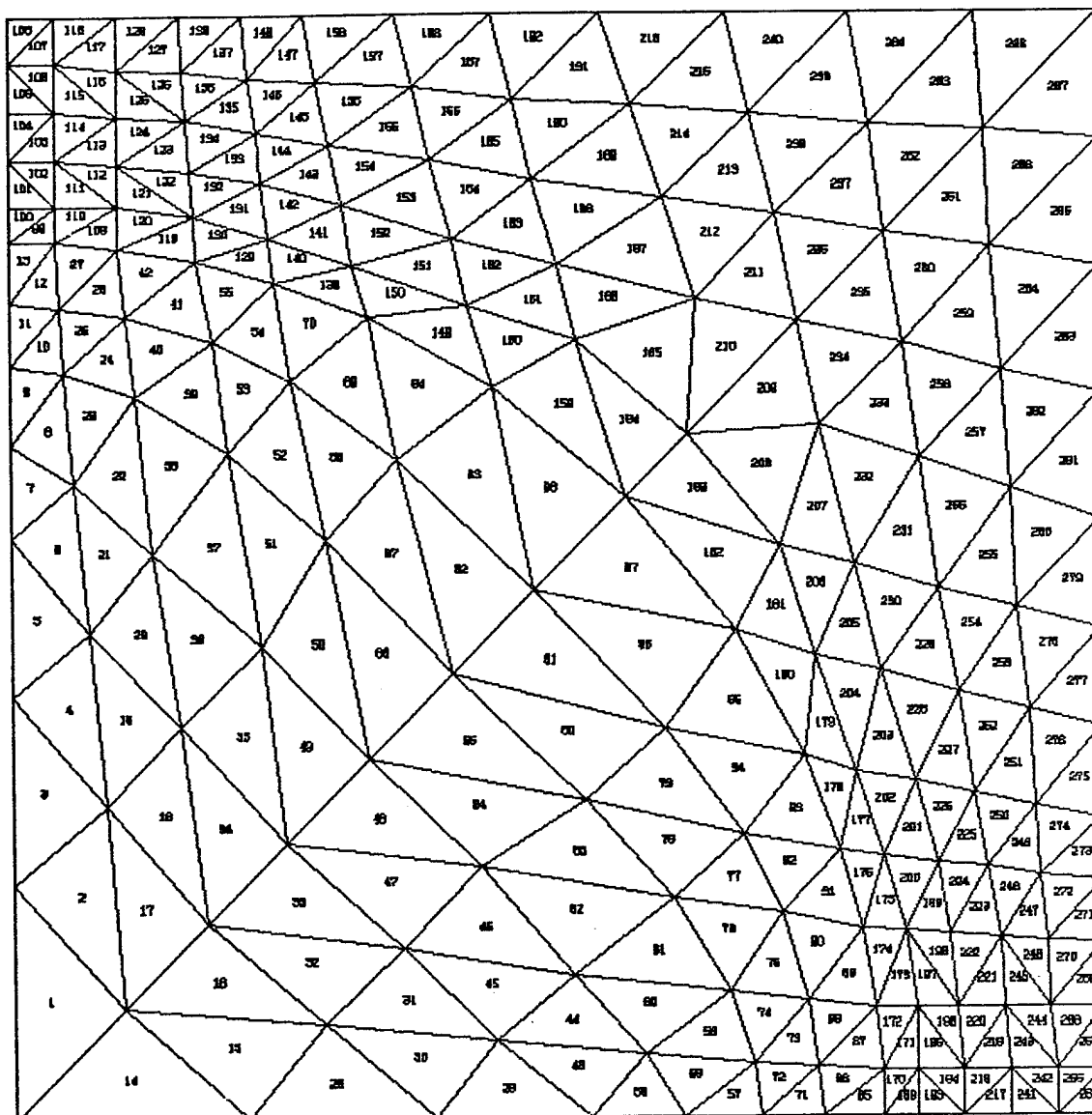
FINITE ELEMENT MESH
50.0 PERCENT FIBER BY VOLUME

Figure 6.14. Typical Finite Element Model of Quadrant to be Analyzed.

points in rows and columns (although obscure), and numbering the nodes one row at a time in successive columns. There are 13 rows and 13 columns resulting in 169 nodes and 288 elements. The resulting R value is 14, making the bandwidth 65, as calculated from Eq. (6.9).

In a typical program run, utilizing the finite element model of Figure 6.14, the stiffness matrix alone requires 37,180 words (60 bits per word) of central memory on the CDC Cyber 760 computer system. This amount is over 40 percent of the entire central memory necessary, which is approximately 90,000 words. An average time used by the central processor to run the program for each increment is 5.57 seconds. This value varies between 5 seconds and 8 seconds per increment, depending on the number of increments, for the applications in this investigation and most investigations.

Increment sizes were selected to be in the range of 500 psi for in-plane normal stresses and longitudinal shear stresses, while axial normal stresses were taken as about 1000 psi. During highly inelastic behavior, increments should be decreased accordingly; values on the order of 100 psi were used.

There are three failure theories necessary for a comprehensive prediction of failure in the present micromechanics analysis. An octahedral shear stress criterion is used to define failure of the matrix. This is a measure of the distortional energy stored in the matrix. The limitation of this criterion is that it is not suitable for a hydrostatic stress state, since there is no distortional component present. Therefore, a hydrostatic criterion is also invoked by testing for a hydrostatic stress state higher than the ultimate value.

In the prior analysis [5], the fiber was tested for failure by a simple maximum stress criterion. Since only three normal stresses existed, a more complicated criterion was not needed. Because shear stresses also exist in the present analysis, a new criterion must be invoked. The fact that the graphite fiber is an orthotropic (transversely isotropic) material increases the complexity of the problem. A criterion specifically designed for orthotropic materials, and which considers the entire stress tensor, is the

6.30

Tsai-Wu [8] failure criterion. Experimental results show that the Tsai-Wu criterion predicts failure far better than a maximum stress or maximum strain criterion [9]. The Tsai-Wu tensor form is also of a more general character than the Tsai-Hill criterion [9]. The only awkward characteristic of the Tsai-Wu criterion is the F_{12} term. This has been discussed widely in the literature, but Narayanswami and Adelman [10] show that neglecting this term rarely causes an error greater than 10 percent. This is the so-called "Modified Tsai-Wu" failure criterion. Assuming tensile and compressive allowable stresses to be equal, the form of the equation becomes:

$$F_1 \sigma_1 + F_2 \sigma_2 + F_3 \sigma_3 + F_4 \sigma_4 + F_5 \sigma_5 + F_6 \sigma_6$$
$$+ F_{11} \sigma_1^2 + F_{22} \sigma_2^2 + F_{33} \sigma_3^2 + F_{44} \sigma_4^2 + F_{55} \sigma_5^2 + F_{66} \sigma_6^2 = 1 \qquad (6.10)$$

where σ represents the actual stress components, and the F terms represent stress allowables as defined by Tsai and Wu [8].

6.3.2 Constituent Material Properties

The matrix system used in the present investigation was Hercules 3501-6 epoxy resin. Because longitudinal shear loading is a major consideration in the present study, it is appropriate to employ matrix constituent material properties derived from longitudinal shear experimental data. Solid rod torsion test shear data were developed for this matrix material [11]. This test method has been shown to be a viable means of determining shear moduli and shear strengths [12]. Each test specimen was approximately 4 inches long, with a diameter of ¼ inch, fabricated in a mold similar to those shown in Reference [12]. These tests were performed on dry specimens and specimens saturated with moisture, at three temperature conditions, viz., 70°F (room temperature) 212°F, and 320°F.

Data from either shear tests or tensile tests can be readily converted to octahedral shear stress-octahedral shear strain expressions for input to the analysis. Tensile test data were used to obtain the octahedral shear stress-octahedral shear strain behavior of the epoxy matrix for use in the

6.31

first-year study. These curves are repeated here as Figure 6.15. Similar results reduced from solid rod torsion test data are shown in Figure 6.16. The tensile test specimens were of a "dog-bone" configuration; approximate dimensions were 1/10 inch thick, ½ inch width, 2½ inch gage length, and 5 inch overall length. To use either of these sets of data in the micromechanics computer program, they must be expressed in equation form, with temperature and moisture as independent variables. A curve-fitting method, developed by Richard and Blacklock [13], was used to fit each data curve (at each test condition). Incorporating these equations directly into the computer program enables the calculation of tangent modulus values for each load increment, as needed for the inelastic material properties matrix defined by Eq. (6.3). The ultimate octahedral shear stress is also calculated, for use in the octahedral shear stress failure criterion.

Comparing the octahedral shear stress-octahedral shear strain curves generated from tensile and from shear test data, Figures 6.15 and 6.16, respectively, the shear test data show modulus values slightly higher, but close enough to attest to the general accuracy of the experimental data. Another observation is the significant extent of inelastic behavior of the epoxy resin when subjected to shear test conditions (Figure 6.16), in contrast to the limited plastic response exhibited by the uniaxial tensile data. A possible reason for this difference is the unique effect of flaws in each type of specimen. The thin, "dog-bone," tensile specimen is more susceptible to stress concentrations due to flaws such as voids or microcracks than the shear specimen. That is, the shear specimen is more stable in the presence of flaws because only the material on the surface of the rod is highly stressed. This surface is smooth and has a low number of flaws because the specimen is fabricated in a carefully polished steel mold. Internal flaws in the rod specimens have a reduced influence compared to these in the tensile specimens, which are subjected to a uniformly high stress throughout their volume.

AS graphite fiber properties were mainly obtained from the Hercules technical literature. Shear moduli and shear stress allowables, necessary

6.32

OCTAHEDRAL SHEAR STRESS (KSI)

OCTAHEDRAL SHEAR STRAIN (X 1000)

(Wt %M; °C)

0.00 | 21.0
3.40 21.0
6.80 21.0
0.00 150.0
3.40 150.0
6.80 150.0
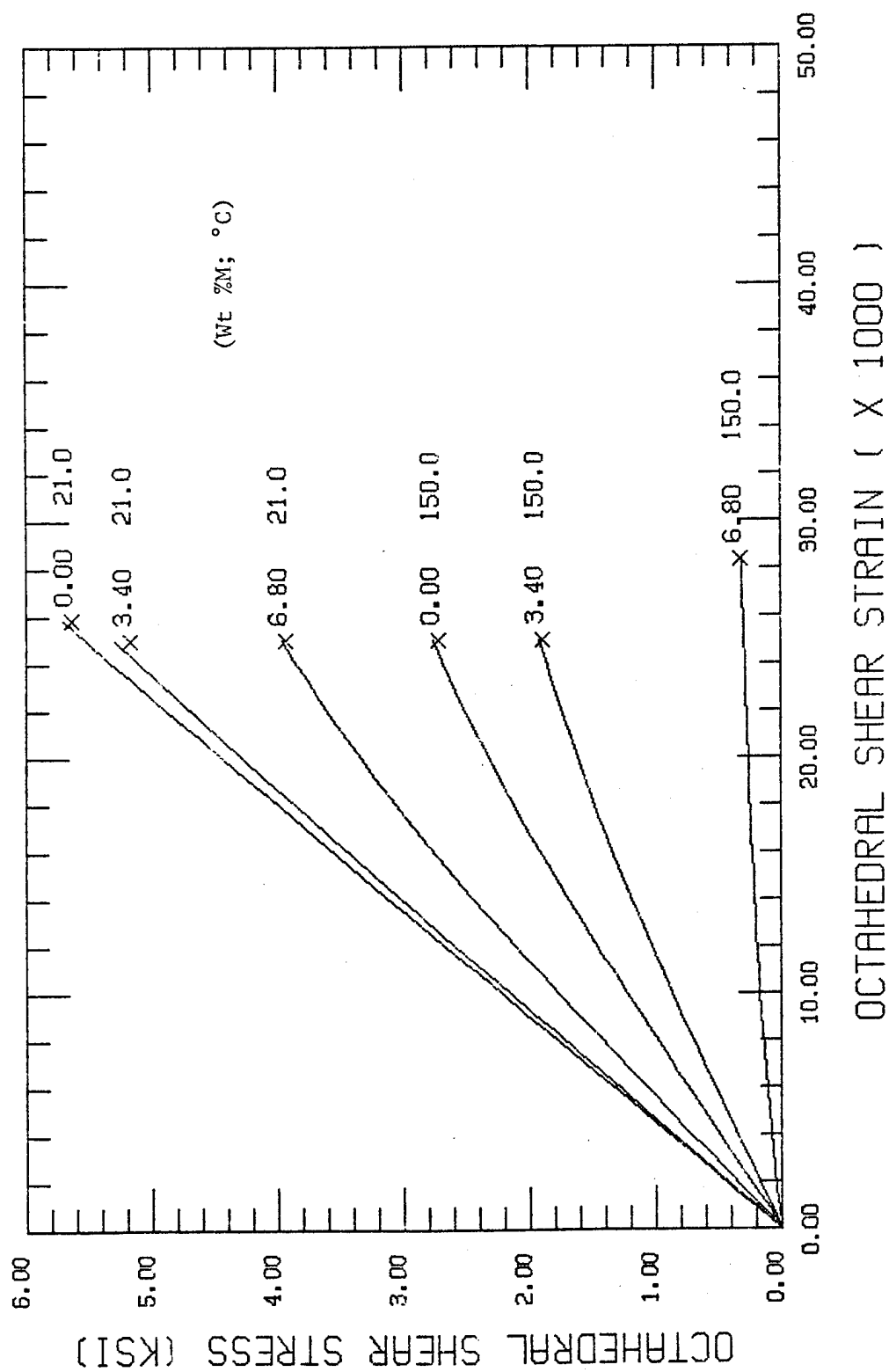
Figure 6.15.   Hercules 3501-6 Epoxy Matrix Octahedral Shear Stress-Strain Curves as Generated from Uniaxial Tensile Tests.
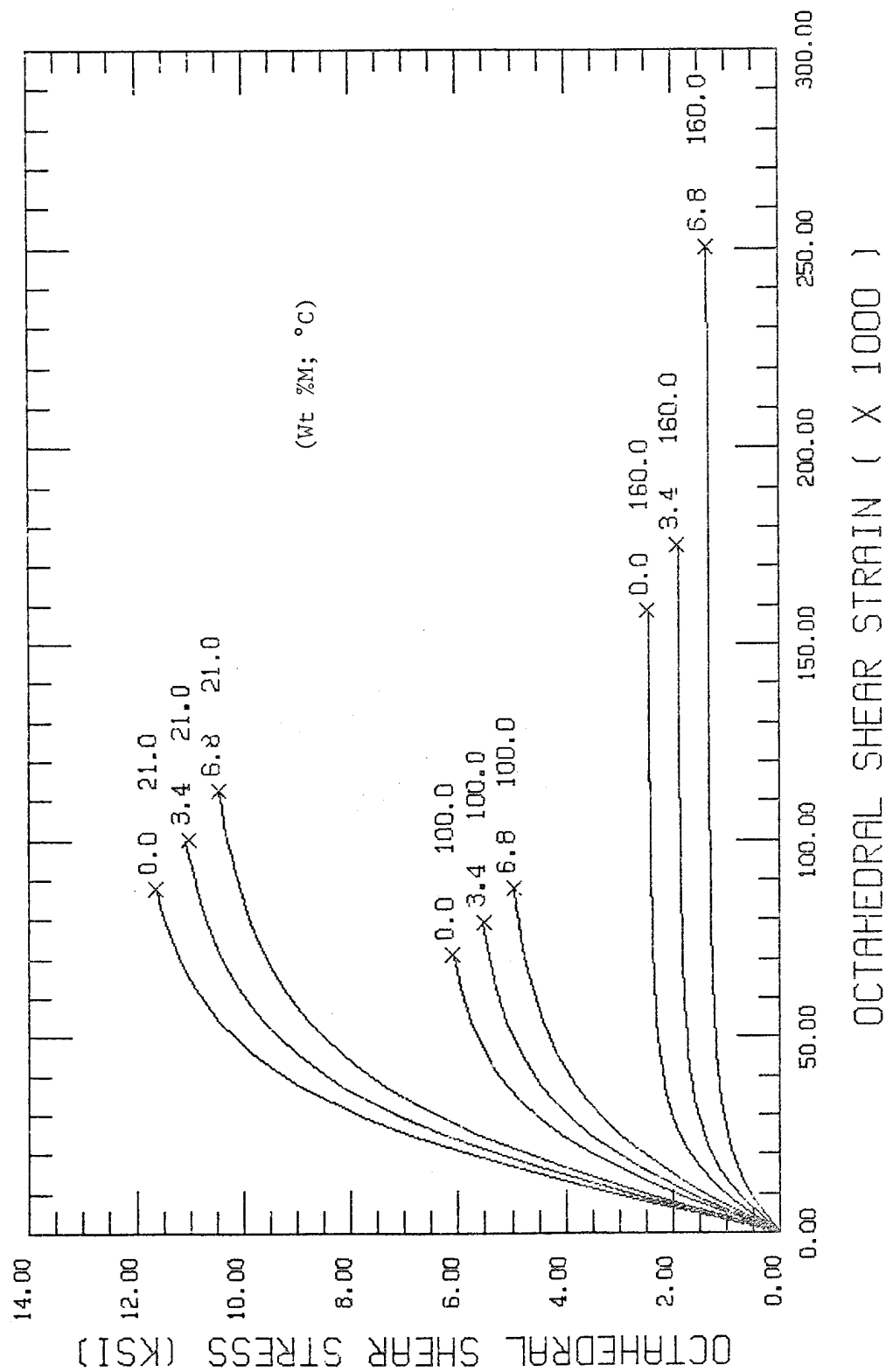
Figure 6.16. Hercules 3501-6 Epoxy Matrix Octahedral Shear Stress-Strain Curves as Generated From Solid Rod Torsion Tests.

for stiffness calculations and the fiber failure criterion, were not available from the Hercules literature. The in-plane and longitudinal shear tests required to determine these properties are not commonly performed on a fiber, due to its small diameter. Instead, a shear modulus value was calculated in the transverse plane of symmetry from the respective values of Young's modulus and Poisson's ratio. It was necessary to estimate values of longitudinal shear modulus and longitudinal shear ultimate stress from data for other similar graphite fibers [14]. The values were 5.0 Msi and 225 ksi, respectively, as shown in Table 6.1. The transverse shear stress being relatively unimportant because of the inability of the analysis to directly apply transverse shear loads, a value of 25 ksi transverse shear allowable was chosen. Microscopically the graphite fiber is much like a composite due to the longitudinally arranged graphite crystal structure. Thus, a low transverse allowable shear stress is a viable approximation.

Properties of the constituent materials are presented in Table 6.1, with estimated values denoted by an asterisk. Two sets of epoxy matrix material properties at room temperature, dry conditions are also shown, generated from tensile and shear experimental data (Figures 6.15 and 6.16), respectively.

TABLE 6.1. CONSTITUENT MATERIAL PROPERTIES FOR AS-GRAPHITE FIBER
          AND 3501-6 EPOXY RESIN

| PROPERTY | HERCULES AS-GRAPHITE FIBER | HERCULES 3501-6 EPOXY MATRIX (ROOM TEMPERATURE, DRY) | |
		(FROM TENSILE TEST DATA)	(FROM SHEAR TEST DATA)
Longitudinal Modulus, E_L (Msi)	32.0	0.62	0.84
Transverse Modulus, E_T (Msi)	2.0	0.62	0.84
Longitudinal Shear Modulus, G_{LT} (Msi)	5.0*	0.23	0.31
Transverse Shear Modulus, G_{TT} (Msi)	0.80	0.23	0.31
Major Poisson's Ratio ν_{LT}	0.20	0.34	0.34*
In-Plane Poisson's Ratio ν_{TT}	0.25	0.34	0.34*
Longitudinal Tensile Strength, σ_L^u (ksi)	450.0	12.0	24.6
Transverse Tensile Strength, σ_T^u (ksi)	50.0*	12.0	24.6
Longitudinal Shear Strength, τ_{LT}^u (ksi)	225.0	6.0	12.3
Transverse Shear Strength, τ_{TT}^u (ksi)	25.0	6.0	12.3
Longitudinal Coefficient of Thermal Expansion α_L (10^{-6}/°C)	−0.36	40.0	40.0
Transverse Coefficient of Thermal Expansion α_T (10^{-6}/°C)	18.0	40.0	40.0
Coefficient of Moisture Expansion	0	2.0	2.0

*Estimated

6.3.3 Correlations with $[\pm 45]_{4S}$ Laminate Experimental Data

As a first step in attempting to correlate the combined micromechanics/ point stress analysis procedure with actual laminate experimental data, the simpler $[\pm 45]_{4S}$ configuration tested extensively by Northrop in the first-year study [1] was selected. The results to be presented here were also included in Reference [3], as a demonstration of the accuracy of the basic analysis procedure, the correlations being quite good, as will be seen.

The method of combining the two analyses to do this, and the scheme of arriving at an inelastic stress-strain curve for a particular laminate, is described by the following four steps:

1. Calculate ply properties from the micromechanics analysis.

2. Apply the laminate point stress analysis to the prescribed laminate, loaded in the prescribed manner, to obtain the stress state induced in each ply.

3. Use the micromechanics analysis to analyze each unique ply of the laminate, holding loads in the same ratios as the laminate analysis predicted. This will result in inelastic stresses and strains in each ply when loaded to high levels.

4. Transform the stress and strain states back to laminate coor- dinates to obtain a laminate stress-strain curve. This curve can be used for comparisons with laminate experimental data.

The Northrop experimental data were available for a 57.5 percent fiber volume, $[\pm 45]_{4S}$ laminate at four combinations of temperature and moisture conditions [1], viz, room temperature, dry (RTD); room temperature, one percent moisture by weight (RTW); elevated temperature (218°F), dry (ETD); and elevated temperature (218°F), one percent moisture (ETW). These conditions will hence be referred to using the abbreviations in parentheses; i.e., RTD, RTW, ETD, ETW, similar to the notation of Reference [1].

To begin the analysis, unidirectional ply properties are calculated using the micromechanics analysis, to be consistent with the properties utilized later when inelastic strains are to be calculated. Constituent

properties for the Hercules AS graphite fiber and the Hercules 3501-6 epoxy matrix are given in Table 6.1 and Figure 6.16. Composite properties are shown in Table 6.2; the stiffness values correspond closely to properties used in the first-year study (see Table 6.4 of Reference [1]). However, thermal and moisture coefficients of expansion differ considerably. It is important to be mutually consistent in the present development from one analysis to the other, i.e., properties used initially in the laminate analysis must correspond to values (see Table 6.2) used later in the micromechanics analysis.

The ply properties as calculated using the micromechanics analysis are used in the laminate point stress analysis, where ply stress states due to temperature, moisture and/or applied loads are obtained. In applying a thermal or moisture load to the laminate, the laminate analysis assumes the input elastic properties to remain constant throughout the temperature or moisture change. Because the matrix modulus is actually not constant, but decreases significantly with increasing temperatures, the predicted curing stresses will be higher than they actually are. To more accurately estimate the curing stresses, an effective temperature change can be used which is smaller than

TABLE 6.2. PROPERTIES CALCULATED FROM MICROMECHANICS ANALYSIS FOR USE IN LAMINATE ANALYSIS

PROPERTY	RTD	RTW	ETD	ETW
E_L (Msi)	18.700	18.690	18.563	18.554
E_T (Msi)	1.467	1.450	1.172	1.147
G_{LT} (Msi)	0.918	0.897	0.611	0.589
ν_{LT}	0.2573	0.2571	0.2544	0.2542
α_L $(10^{-6}/°F)$	0.265	0.253	0.092	0.080
α_T $(10^{-6}/°F)$	18.00	17.97	17.61	17.61
β_L $(10^{-6}/\%M)$	0.042	0.041	0.026	0.025
β_T $(10^{-3}/\%M)$	1.082	1.078	1.031	1.027

the actual temperature change. For cooling from 350°F to 70°F, an effective temperature change of -200°F was used rather than the actual -280°F. In

cooling from 350°F to 218°F only a 75°F effective temperature change was used. These assumed effective temperature changes are the same as previously [1]. Actual loads to be applied to model stresses induced in the individual plies during each case of curing and conditioning are shown in Table 6.3, along with actual load ratio increments due to the subsequently applied axial compressive load. To arrive at these values, the laminate analysis uses the composite ply properties that were calculated by the micro-mechanics analysis. The resulting stress state is calculated in both ply coordinates and laminate coordinates by the laminate analysis, thus eliminating the necessity of transforming the stress state by hand for subsequent input to the micromechanics analysis.

TABLE 6.3. LOAD RATIOS CALCULATED FROM LAMINATE ANALYSIS FOR USE IN MICROMECHANICS ANALYSIS FOR $[\pm 45]_{4s}$ LAMINATE

HYGROTHERMAL LOADS

STRESSES (ksi)	RTD (-200°F)	RTW (1%M,-200°F)	ETD(-75°F)	ETW (1%M,-75°F)
$\bar{\sigma}_z$	-4.65	-3.23	-1.41	-0.33
$\bar{\sigma}_x$	4.65	3.23	1.41	0.33
$\bar{\tau}_{xz}$	0.0	0.0	0.0	0.0

APPLIED LOAD RATIOS FOR -1000 psi AXIAL COMPRESSIVE STRESS

STRESSES (psi)	RTD	RTW	ETD	ETW
$\bar{\sigma}_z$	-912	-912	-928	-930
$\bar{\sigma}_x$	- 88	- 88	- 72	- 70
$\bar{\tau}_{xz}$	500	500	500	500

The micromechanics analysis is now used to model a single unidirectional ply of the laminate in ply coordinates. The entire curing and conditioning history of each ply is simulated, as well as the applied load increments. The resulting inelastic strains at each incremental applied load are in ply coordinates and must be transformed back to laminate coordinates. This done,

longitudinal stress and strain at various increments for each condition
are the final results needed to compare with experimental data.

Figures 6.17 through 6.20 show the predicted incremental stress-strain
points compared to the experimental data curves. The complete experimental
data curves to failure are not shown here, although they are available in
Reference [1]. A very slight overprediction error is seen for both of the
room temperature conditions, while the elevated temperature condition
predictions are in excellent agreement with experiment. Although the differences
between theory and experiment are perhaps not significant, the most likely
explanation for slight differences is based on flaws in the matrix or flaws
in the fiber-matrix bond. The stress concentrations caused by these flaws
reduce the strength of the material. The RTD case (Figure 6.17) does show
this discrepancy. Any softening of the matrix should reduce the stress
concentrating effect of flaws. When moisture is added in the RTW case,
(Figure 6.18) it serves as a plasticizer that tends to negate the thermal
curing stresses. Now the actual composite behavior is slightly closer to
the predicted curve for a composite with no material flaws. This theory is
further supported in the elevated temperature test cases (Figures 6.19 and
6.20), where the predicted incremental values are in very close agreement with
the experimental data. The elevated temperature and moisture in the ETW test
case (Figure 6.20) softens the matrix, reducing the effect of defects, and
narrowing the gap between experiment and theory.

The reason for the excellent accuracy of the analysis can be investi-
gated by observing the loading history recorded in the stress contour
plots. Also, insight into other possible sources of error may be attained.
Normalized octahedral shear stress contours for the RTD test case are shown
in Figure 6.21, ranging from curing stresses to the stress state at failure.
Referring back to the original step-by-step description of the laminate
analysis presented earlier in this subsection, it will be noted that hygro-
thermal effects are considered in separate steps. First, there are stresses
induced by hygrothermally-influenced consistuent material properties (see
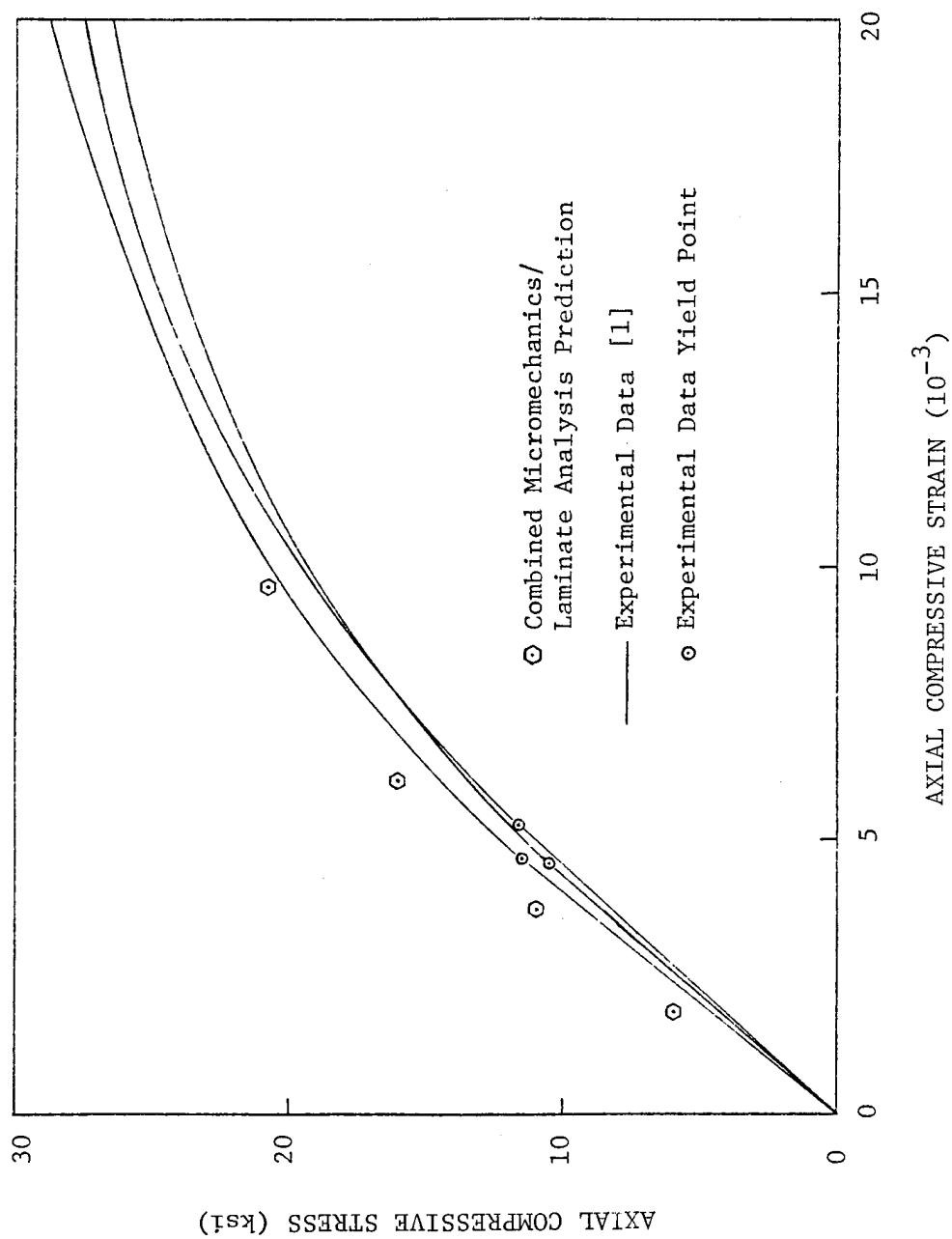
Figure 6.17 Comparison of room temperature, dry (RTD) experimental data [1] for a $[\pm 45]_{4s}$ laminate with combined micromechanical and laminate analysis predictions.
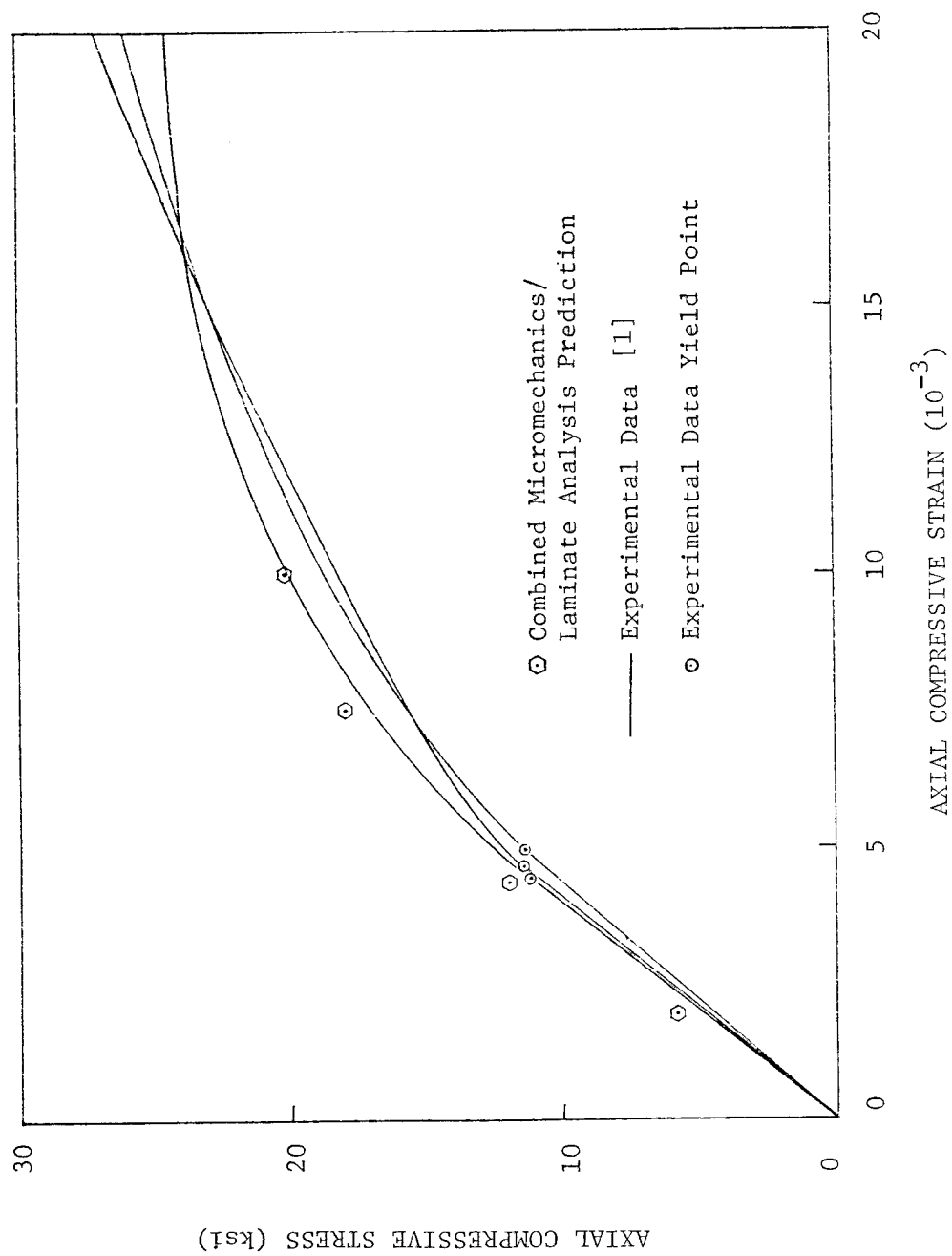
Figure 6.18 Comparison of room temperature, wet (RTW) experimental data [1] for a $[\pm 45]_{4s}$ laminate with combined micromechanical and laminate analysis predictions.

⊙ Combined Micromechanics/ Laminate Analysis Prediction

— Experimental Data [1]

⊙ Experimental Data Yield Point

Axis labels:

AXIAL COMPRESSIVE STRESS (ksi) — vertical axis, with values 0, 10, 20, 30

AXIAL COMPRESSIVE STRAIN (10^{-3}) — horizontal axis, with values 0, 5, 10, 15, 20
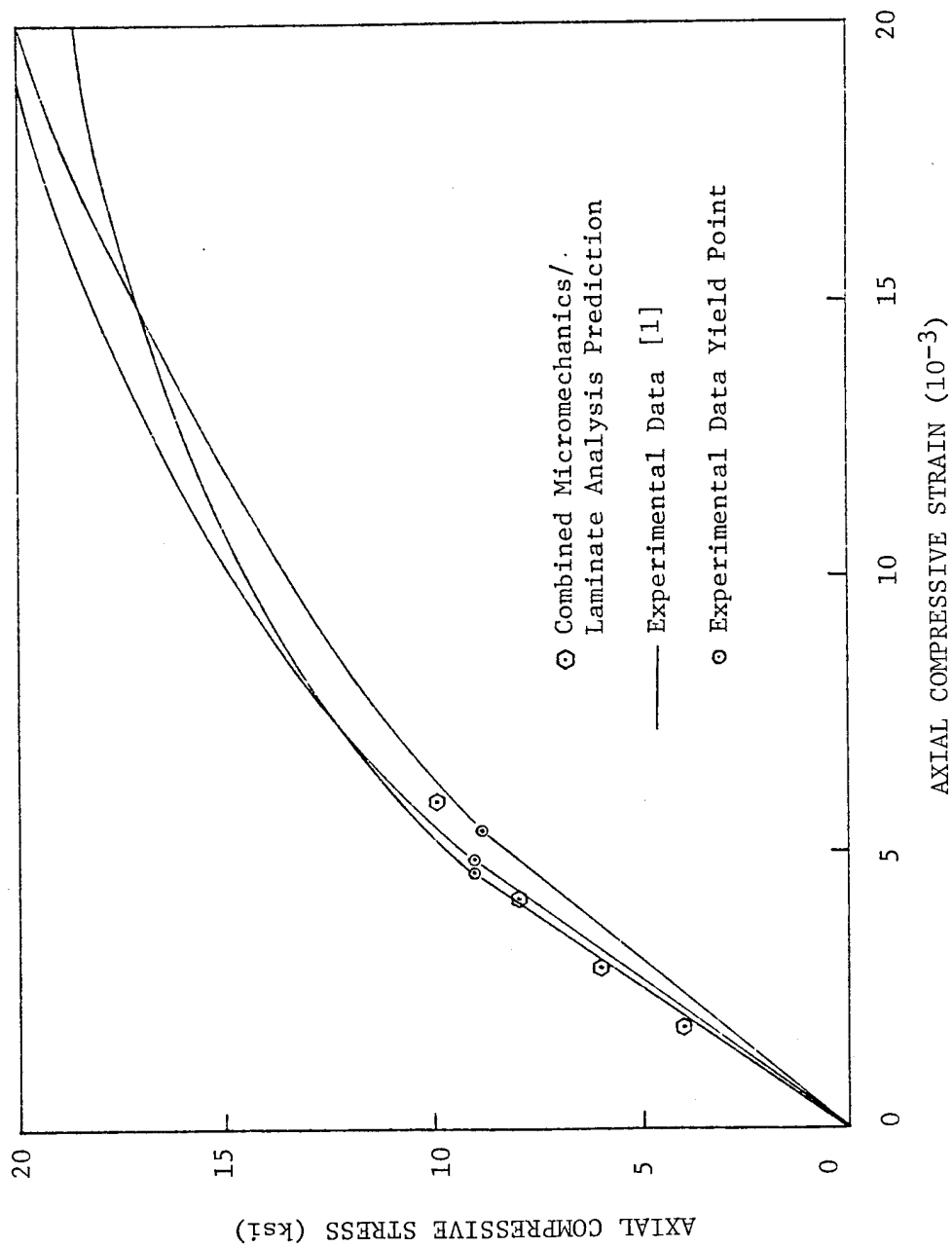
Figure 6.19. Comparison of elevated temperature, dry (ETD) experimental data [1] for a [±45]₄s laminate with combined micromechanical and laminate analysis predictions.
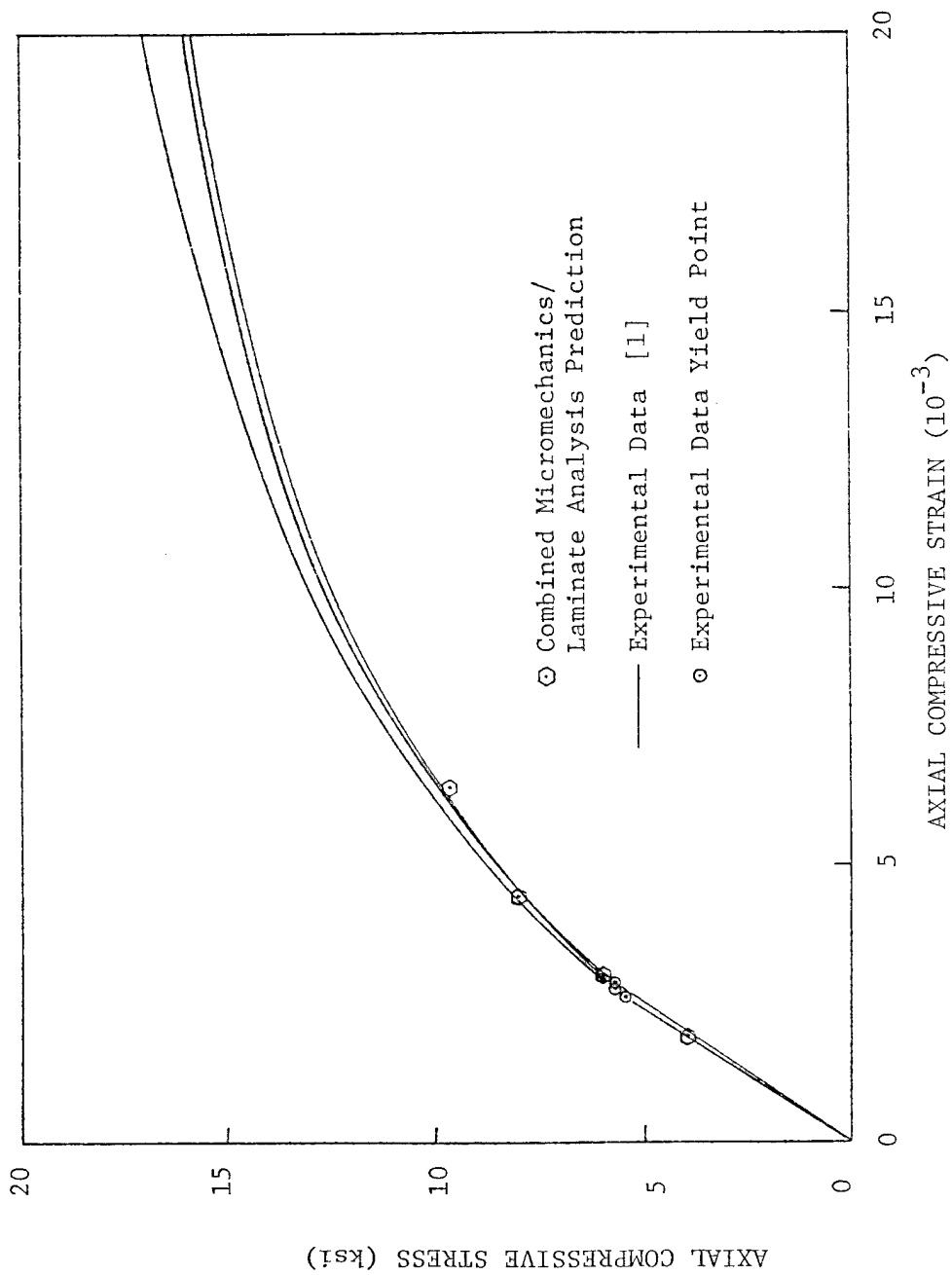
Figure 6.20 Comparison of elevated temperature, wet (ETW) experimental data [1] for a [±45]₄s laminate with combined micromechanical and laminate analysis predictions.
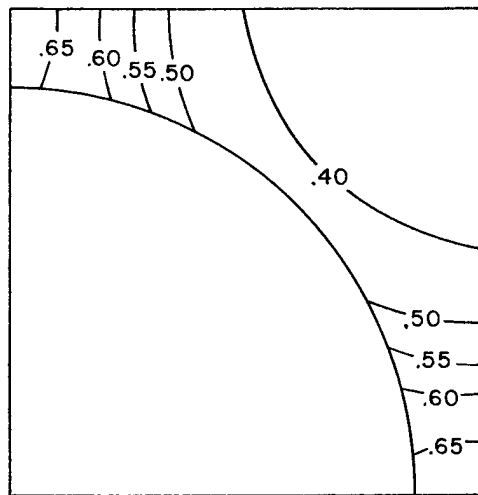
a) Octahedral shear stress
of ply alone after cool-
down from 350°F cure tem-
perature to room tempera-
ture (70°F)
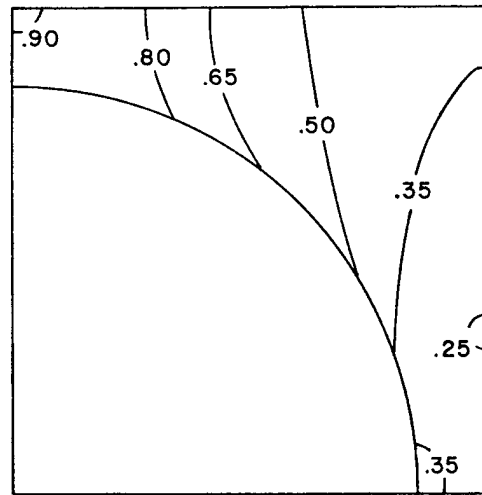
b) Octahedral shear stress
after laminate cooldown
effects are included
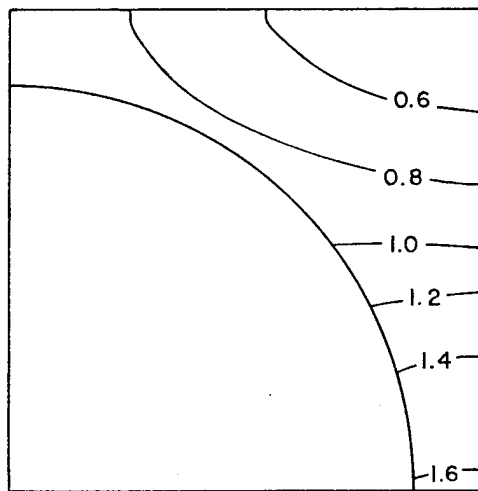
c) Octahedral shear stress at
experimentally determined
composite yield stress;
applied axial stress, $\bar{\sigma}_x$ =
-11.5 ksi
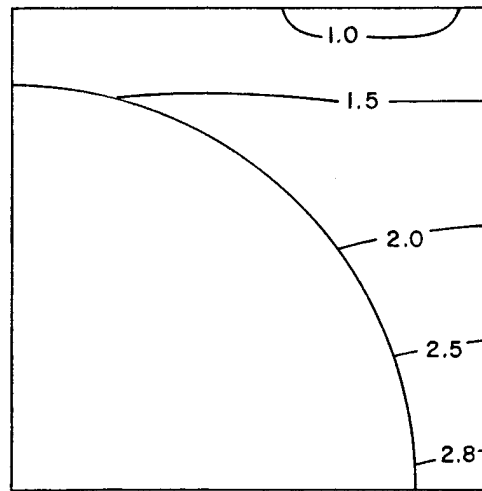
d) Octahedral shear stress at
predicted first element
failure; applied axial stress
$\bar{\sigma}_x$ = -21.0 ksi

Figure 6.21   Contour plots of octahedral shear stress (normalized with
respect to matrix yield stress, 4.18 ksi), and interface
normal and interface shear stresses with an AS/3501-6
graphite/epoxy $[\pm45]_{4s}$ laminate ply at room temperature,
dry conditions (RTD).
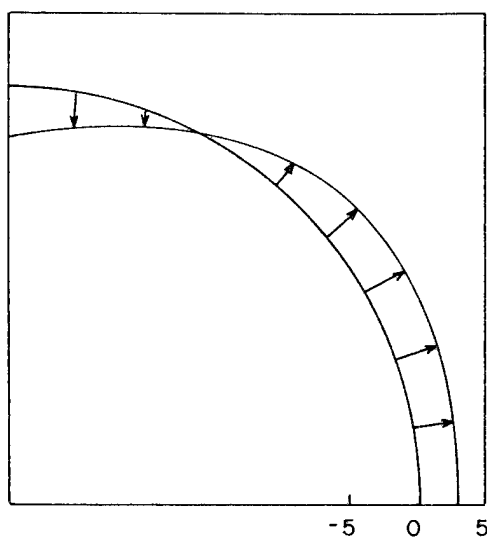
6.45

e) Interface normal stress
    (ksi) after laminate cure,
    cooldown, and moisture
    absorption effects
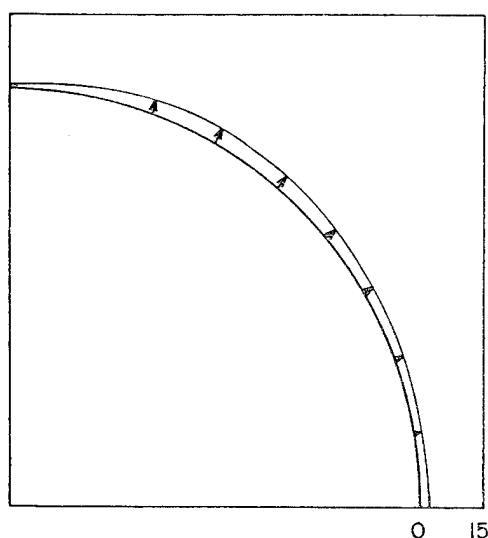
f) Interface shear stress
    (ksi) after laminate cure,
    cooldown, and moisture
    absorption effects
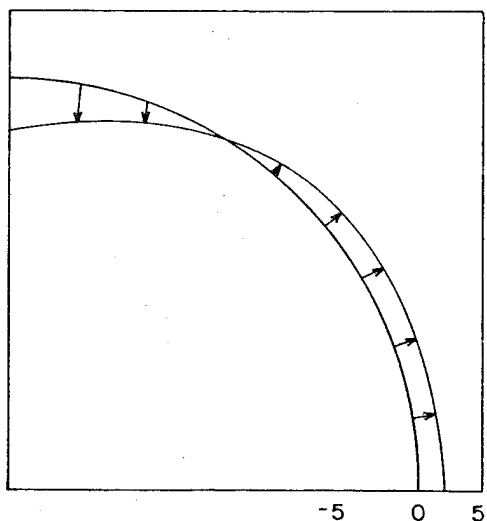
g) Interface normal stress
    (ksi) at predicted first
    element failure
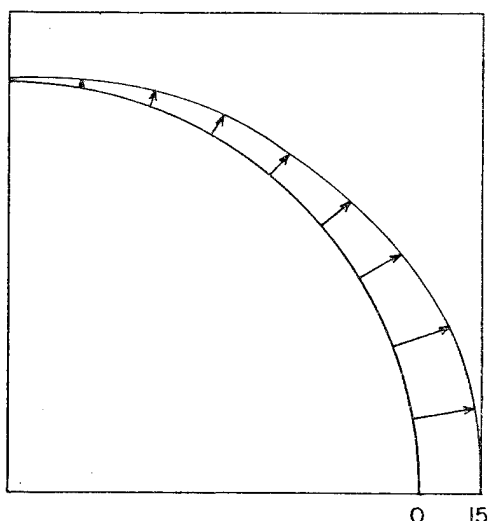
h) Interface shear stress
    (ksi) at predicted first
    element failure

(applied axial stress, $\bar{\sigma}_x$ = -21.0 ksi)

Figure 6.21 (continued) Contour plots of octahedral shear stress
             (normalized with respect to matrix yield stress, 4.18 ksi),
             and interface normal and interface shear stresses within
             an AS/3501-6 graphite/epoxy $[\pm 45]_{4s}$ laminate ply at room
             temperature, dry conditions (RTD).

Figure 6.21a). Second, other plies are influenced by hygrothermal effects, which in turn influence the stresses in the representative ply now being considered (see Figure 6.21b). These will be termed "ply curing effects" and "laminate curing effects," respectively. Because Figure 6.21a is also representative of stresses in a unidirectional composite, contrasting Figures 6.21a and 6.21b show curing stress differences between a unidirectional laminate and a [±45] laminate. But, for the present purposes, it is important to note the additional curing effects of the ply configuration in Figure 6.21b and the magnitude of them. Any material defect which might exist in a local region of high stress will cause a severe stress concentration, which in turn can cause premature matrix yielding and failure. This is a possible reason for the lower stiffness exhibited by the experimental data at room temperature conditions. Figure 6.21c shows the amount of matrix that has already yielded locally when the overall composite response first indicates a yield point experimentally. While the tangent modulus of the yielded matrix is still close to the initial modulus, the nonlinearity is not apparent in the composite response. Only after the yielded region has propagated upward a distance equal to half the width of the quadrant, do the experimental data begin to suggest an elastic limit. When the micromechanics analysis predicts first element failure, this implies the initiation of a crack. To prevent this damage initiation, the composite should thus not be loaded past the stress represented by the final predicted point in Figure 6.17. After curing, the composite experiences large normal stresses along the interface, as shown in Figure 6.21e, suggesting a high probability of debonding behavior. There are also fairly high shear stresses along the interface in this as-cured condition, which grow rapidly as load is applied and increased to predicted first failure (Figures 6.21f and 6.21h). This shear stress is the combined effect of the applied longitudinal shear stress and the transverse normal stress, which are acting in weak directions of the material, and which eventually lead to failure. It will also be noted in Figure 6.21g that the normal inter-face stress has been reduced by the applied loads. This is further evidence of how applied loads can relieve some of the stresses induced during cooldown; it is an inelastic coupling effect.

The ETW test case involves two separate forms of curing and conditioning stresses. First, stresses are induced independently in each ply by thermal and moisture changes due to the differences in properties between the fiber and matrix. Secondly, since the individual plies, exhibiting the aforementioned hygrothermal strains, are bonded to each other, they mutually affect each other because of their differing ply orientations. The combination of thermal and moisture loads has far-reaching consequences because of the opposing effects in cooldown and moisture absorption. The temperature drop during cooldown causes the matrix to contract by a relatively large amount, the fiber to contract transversely by a lesser amount, and the fiber to actually expand slightly in its axial direction (see Table 6.1). The composite axial strain is predicted to be negative, as can be seen by the positive composite thermal coefficient of expansion in Table 6.2. Figure 6.22a, when compared to Figure 6.22b and 6.22c, indicates that the octahedral shear stresses induced by curing are almost fully negated by the absorption of one weight percent moisture by the composite. The small hygrothermal stresses which result are the reason for the low average laminate hygrothermal stresses shown in the last column of Table 6.3. However, the shifting of the octahedral shear stress contours in Figure 6.22c due to the application of the induced loads will be noted. This is depicted more clearly at first failure, as represented by Figure 6.22d. The detrimental effect of unfavorable temperature and moisture combinations is clearly shown in comparing the octahedral shear stress contours at first failure of the ETW test case compared to the RTD case. An octahedral first element failure stress of approximately 11.6 ksi (shown normalized in Figure 6.21d for the RTD case as the 2.8 contour) is reduced to 5.2 ksi in the ETW case (shown normalized in Figure 6.22d as the 2.2 contour). This is a significant change, considering that it is due to a relatively modest temperature change.

Interface normal stresses induced during cooldown and one percent moisture absorption are relatively small tensile stresses (see Figure 6.22e), but subsequent mechanical loading of the laminate counteracts the induced tensile stresses, so that near the x-axis of symmetry a small negative value exists
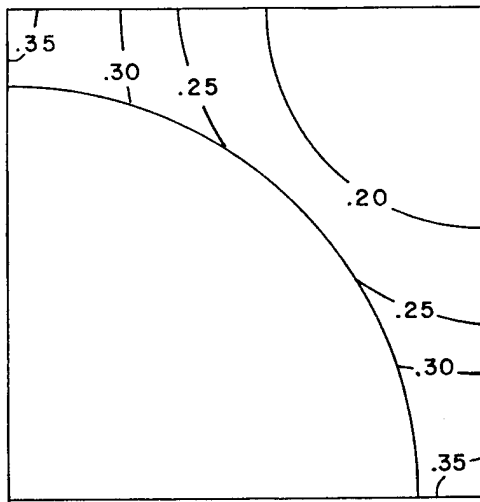
a) Octahedral shear stress of
    ply alone after cooldown
    from 350°F cure temperature
    to 218°F (normalized with
    respect to 218°F, dry matrix
    yield stress, 2.74 ksi)
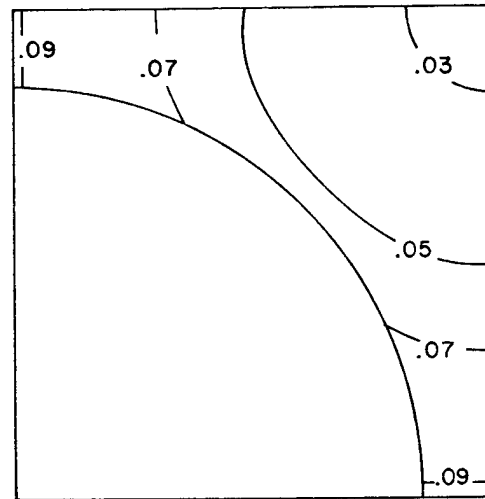
b) Octahedral shear stress of
    ply alone after 1% mois-
    ture absorption (normalized
    with respect to 218°F, 1%M
    matrix yield stress, 2.58
    ksi)
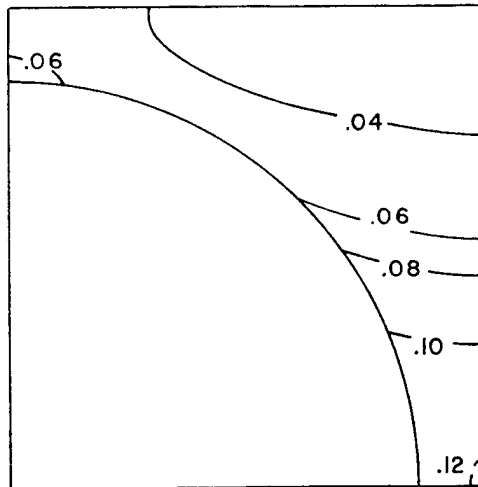
c) Octahedral shear stress
    after laminate hygrothermal
    effects are included
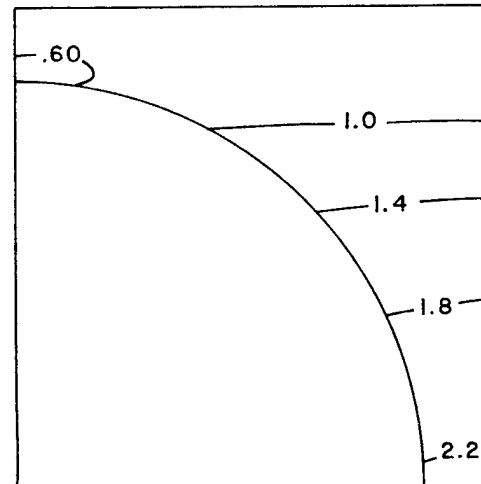
d) Octahedral shear stress at
    predicted first element
    failure, applied axial stress,
    $\bar{\sigma}_x$ = -9.6 ksi

(normalized with respect to 218°F, 1%M matrix yield stress, 2.58 ksi)

Figure 6.22   Contour plots of octahedral shear stress, and interface normal
              and interface shear stresses within an AS/3501-6 graphite/epoxy
              $[\pm45]_{4s}$ laminate ply at 218°F, 1% moisture by weight conditions
              (ETW).

6.49
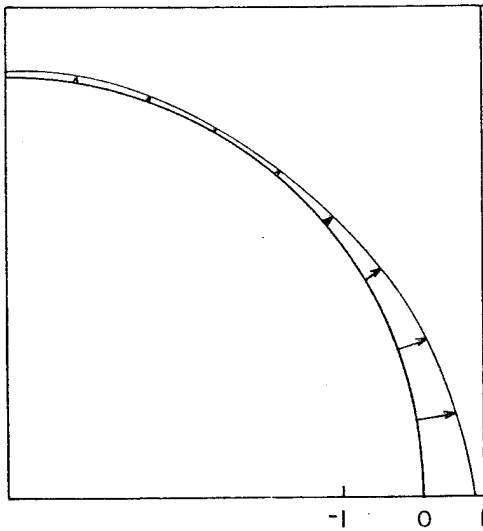
e)   Interface normal stress
     (ksi) after laminate cure,
     cooldown, and moisture
     absorption effects
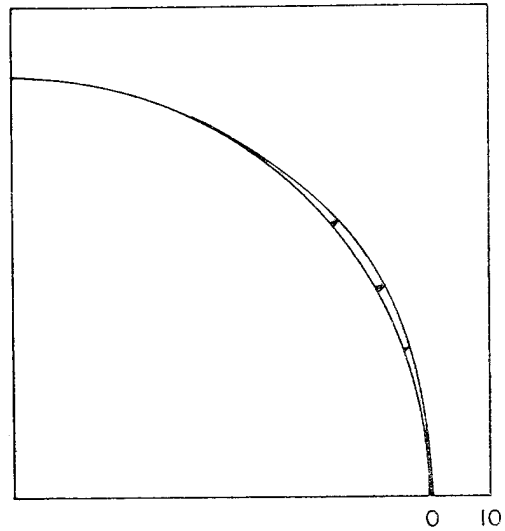
f)   Interface shear stress
     (ksi) after laminate cure,
     cooldown, and moisture
     absorption effects
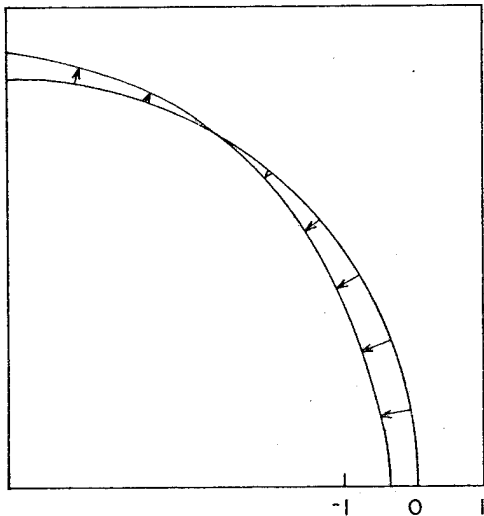
g)   Interface normal stress
     (ksi) at predicted first
     element failure

h)   Interface shear stress
     (ksi) at predicted first
     element failure

(applied axial stress, $\bar{\sigma}_x$ = -9.6 ksi)

Figure 6.22   (continued)   Contour plots of octahedral shear stress, and
              interface normal and interface shear stresses within an
              AS/3501-6 graphite/epoxy $[\pm45]_{4s}$ laminate ply at 218°F,
              1% moisture by weight conditions (ETW).

at first element failure (Figure 6.22g). Small tensile stresses are induced near the y-axis of symmetry at first element failure, but are small enough that they have no noticeable effect on subsequent laminate behavior. Although the interface shear stress after curing and moisture conditioning (Figure 6.22f) is small (four percent of the ultimate stress), the subsequently applied mechanical loads result in shear stresses along the interface which are relatively high at first element failure (Figure 6.22h).

6.3.4 Correlations with F-18 Laminate Experimental Data

The combined micromechanics/point stress analysis was also correlated with the static compression stress-strain experimental data generated in the present study. This included both Ply Drop-off No. 1 and No. 2 specimens, as well as a plain laminate, at the various test temperature and moisture preconditioning combinations. A total of 11 combinations were simulated, viz, all of those for which experimental stress-strain curves are presented in Section 5. These combinations are summarized in Table 6.4.

The same procedure as used in correlating the $[\pm45]_{4s}$ laminate data of the first-year study [1], presented in Section 6.3.3, was used. In obtaining the ply stress ratios from the laminate analysis, the ply properties of Table 6.2 were again used, as applicable. Since the -65FW condition did not exist for the previous correlations, the ply properties for this condition were calculated using the micromechanics analysis. Results are given in Table 6.5.

In addition to the effective temperature changes discussed in Section 6.3.3 for the 218°F and room temperature states, an effective temperature change $\Delta T = -250°F$ was used to simulate the -65°F test temperature condition.

Comparisons of the analytical predictions of the stress-strain response with the available experimental data, for all 11 combinations listed in Table 6.4, are presented in Figures 6.23 through 6.33. The corresponding ply stress ratios calculated from the laminate analysis for use in the micromechanics analysis are given in Tables 6.6 through 6.16. These tables have the same meaning as Table 6.3, previously described in Section 6.3.3. That is, they

6.51

TABLE 6.4. F-18 LAMINATE COMBINATIONS USED IN EXPERIMENTAL/ANALYTICAL CORRELATIONS

FIGURE NUMBER	ENVIRONMENTAL CONDITION	LAMINATE CONFIGURATION	SECTION MODELED	FIGURE NOS. OF EXPERIMENTAL DATA CURVES AVAILABLE FOR CORRELATIONS
6.17	-65FW	Plain	-	5.1, 5.2, 5.3
6.18		PDO#1	thin	5.16, 5.17, 5.18
6.19		PDO#2	thin	5.37, 5.38
6.20	RTD	PDO#1	thin	5.8, 5.10, 5.12
6.21			thick	5.9, 5.11, 5.13
6.22		PDO#2	thin	5.29, 5.31, 5.33
6.23			thick	5.30, 5.32, 5.34
6.24	RTW	PDO#1	thin	5.14, 5.15
6.25		PDO#2	thin	5.35, 5.36
6.26	218FW	PDO#1	thin	5.19, 5.20
6.27		PDO#2	thin	5.39, 5.40, 5.41

define the average ply stresses for use as loading conditions in the micro-
mechanics analysis, these values being obtained from the laminate analysis.

As can be seen in Figures 6.23 through 6.33, the combined micromechanics/
laminate analysis consistently overpredicted the stress-strain response as
experimentally determined. There is, of course, some scatter of the experi-
mental data as well. This overprediction, while not extremely large, is
greater than that observed in the analytical/experimental correlations for

TABLE 6.5. PLY PROPERTIES AT -65FW CALCULATED FROM MICROMECHANICS ANALYSIS FOR USE IN LAMINATE ANALYSIS

$$E_L = 18.550 \text{ Msi}$$

$$E_T = 1.208 \text{ Msi}$$

$$G_{LT} = 0.556 \text{ Msi}$$

$$\nu_{LT} = 0.279$$

$$\alpha_L = 0.089 \times 10^{-6}/°F$$

$$\alpha_T = 18.49 \times 10^{-6}/°F$$

$$\beta_L = 0.028 \times 10^{-3}/\%M$$

$$\beta_T = 1.729 \times 10^{-3}/\%M$$

the $[\pm 45]_{4s}$ laminates of Figures 6.17 through 6.20. The degree of nonlinearity of the stress-strain response is also much less for the F-18 laminates, as expected, because of the dominance of the 0° plies. As discussed in the first-year report [1], the unidirectional ply stiffness in the axial (0°) direction was also overpredicted, suggesting that the fiber axial stiffness may actually be slightly lower than assumed in the analysis. This would result in an overprediction of the stiffness of 0° ply dominated configurations such as the F-18 laminates, while having much less influence on the $[\pm 45]_{4s}$ laminates, which are shear dominated. This aspect will be explored further in subsequent studies.

As discussed in Section 6.3.3 also, the analysis presently predicts only first failure and not ultimate strength. In future work, the addition of a crack propagation capability will permit such predictions. Also, the use of a 3-D nonlinear laminate analysis will permit the inclusion of interlaminar stress ratios with increasing extent of elastoplastic response.

6.53

TABLE 6.6. PLY STRESS RATIOS CALCULATED FROM LAMINATE ANALYSIS FOR USE
IN MICROMECHANICS ANALYSIS FOR PLAIN LAMINATE AT -65°FW
CONDITION, 30 PLY (UNIFORM) SECTION

HYGROTHERMAL LOADS ($\Delta T = -250°F$, $\Delta M = 1\%$)

STRESSES (ksi)	0° PLIES	+45° PLIES	-45° PLIES	90° PLIES
$\bar{\sigma}_z$	-0.580	-5.610	-5.610	-10.650
$\bar{\sigma}_x$	3.450	3.690	3.690	3.930
$\bar{\tau}_{zx}$	0.0	-0.310	0.310	0.0

-1 KSI AXIAL COMPRESSIVE STRESS LOADING

STRESSES (ksi)	0° PLIES	+45° PLIES	-45° PLIES	90° PLIES
$\bar{\sigma}_z$	-1.628	-0.540	-0.540	0.540
$\bar{\sigma}_x$	0.008	-0.045	-0.045	-0.098
$\bar{\tau}_{zx}$	0.0	0.068	-0.068	0.0
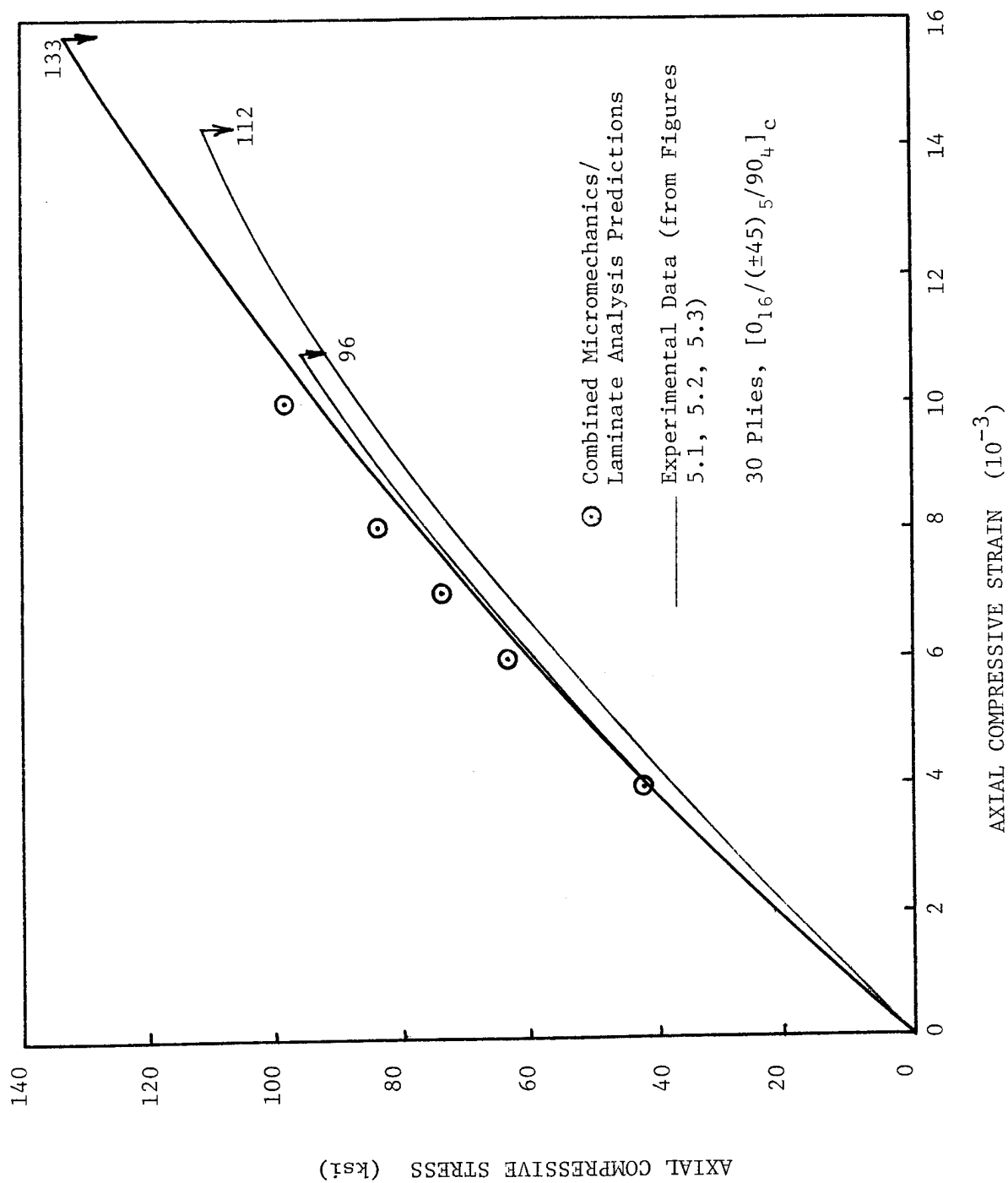
Figure 6.23 Comparison of -65°F, 1 percent moisture (-65FW) experimental data for three plain laminates with combined micromechanics/laminate analysis prediction.

TABLE 6.7 PLY STRESS RATIOS CALCULATED FROM LAMINATE ANALYSIS FOR USE IN MICROMECHANICS ANALYSIS FOR PLY DROP-OFF NO. 1 LAMINATE AT -65FW CONDITION, 28 PLY (THIN) SECTION

HYGROTHERMAL LOADS ($\Delta T = -250°F$, $\Delta M = 1\%$)

STRESSES (ksi)	0° PLIES	+45° PLIES	-45° PLIES	90° PLIES
$\bar{\sigma}_z$	-0.78	-5.24	-5.24	-9.71
$\bar{\sigma}_x$	3.51	3.72	3.72	3.94
$\bar{\tau}_{zx}$	0.0	-0.27	0.27	0.0

-1 KSI AXIAL COMPRESSIVE STRESS LOADING

STRESSES (ksi)	0° PLIES	+45° PLIES	-45° PLIES	90° PLIES
$\bar{\sigma}_z$	-1.699	-0.566	-0.566	0.566
$\bar{\sigma}_x$	0.006	-0.049	-0.049	-0.098
$\bar{\tau}_{zx}$	0.0	0.070	-0.070	0.0

TABLE 6.8. PLY STRESS RATIOS CALCULATED FROM LAMINATE ANALYSIS FOR USE IN MICROMECHANICS ANALYSIS FOR PLY DROP-OFF NO. 2 LAMINATE AT -65°FW CONDITION, 26 PLY (THIN) SECTION

HYGROTHERMAL LOADS ($\Delta T = -250°F$, $\Delta M = 1\%$)

STRESSES (ksi)	0° PLIES	+45° PLIES	-45° PLIES	90° PLIES
$\bar{\sigma}_z$	-0.66	-6.01	-6.01	-11.36
$\bar{\sigma}_x$	3.40	3.66	3.66	3.92
$\bar{\tau}_{zx}$	0.0	-0.32	0.32	0.0

-1 KSI AXIAL COMPRESSIVE STRESS LOADING

STRESSES (ksi)	0° PLIES	+45° PLIES	-45° PLIES	90° PLIES
$\bar{\sigma}_z$	-1.467	-0.550	-0.550	0.370
$\bar{\sigma}_x$	0.0	-0.045	-0.045	-0.091
$\bar{\tau}_{zx}$	0.0	0.058	-0.058	0.0
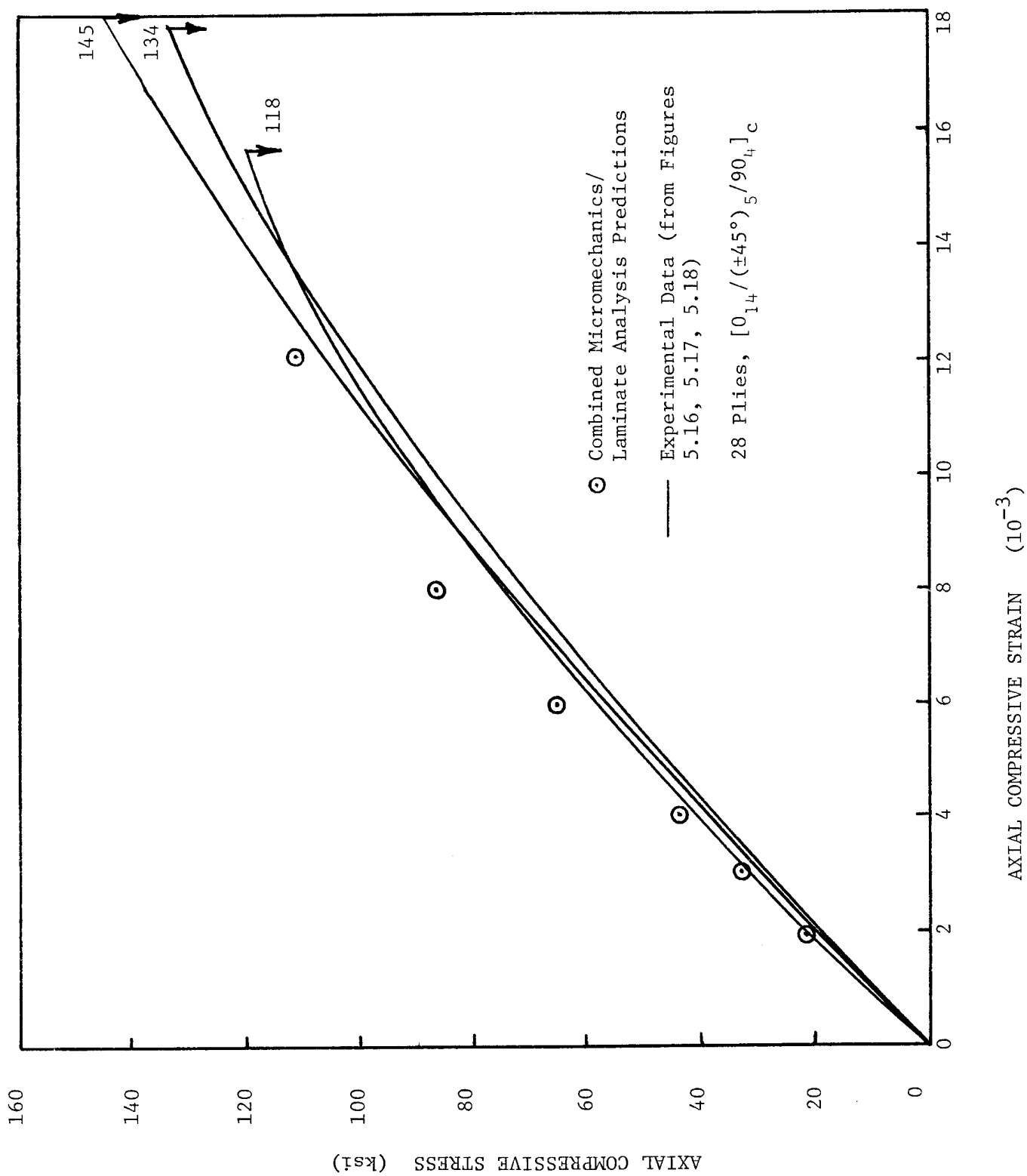
Figure 6.24 Comparison of 065°F, 1 percent moisture (-65FW) experimental data for three ply drop-off no. 1, thin section laminates with combined micromechanics/laminate analysis prediction.

AXIAL COMPRESSIVE STRAIN (10^{-3})

Figure 6.25 Comparison of -65°F, 1 percent moisture (-65FW) experimental data for two ply drop-off no. 2, thin section laminates with combined micromechanics/laminate analysis prediction.

TABLE 6.9.   PLY STRESS RATIOS CALCULATED FROM LAMINATE ANALYSIS FOR USE IN
MICROMECHANICS ANALYSIS FOR PLY DROP-OFF NO. 1 LAMINATE AT
RTD CONDITION, 28 PLY (THIN) SECTION

HYGROTHERMAL LOADS (ΔT = -200°F, ΔM = 0%)

STRESSES (ksi)	0° PLIES	+45° PLIES	-45° PLIES	90° PLIES
$\bar{\sigma}_z$	-1.12	-6.21	-6.21	-11.29
$\bar{\sigma}_x$	4.20	4.50	4.50	4.80
$\bar{\tau}_{zx}$	0.0	-0.51	0.51	0.0

-1 KSI AXIAL COMPRESSIVE STRESS LOADING

STRESSES (ksi)	0° PLIES	+45° PLIES	-45° PLIES	90° PLIES
$\bar{\sigma}_z$	-1.657	-0.580	-0.580	0.497
$\bar{\sigma}_x$	0.06	-0.056	-0.056	-0.119
$\bar{\tau}_{zx}$	0.0	0.105	-0.105	0.0

TABLE 6.10.   PLY STRESS RATIOS CALCULATED FROM LAMINATE ANALYSIS FOR USE IN
MICROMECHANICS ANALYSIS FOR PLY DROP-OFF NO. 1 LAMINATE AT
RTD CONDITION, 30 PLY (THICK) SECTION

HYGROTHERMAL LOADS (ΔT = -200°F, ΔM = 0%)

STRESSES (ksi)	0° PLIES	+45° PLIES	-45° PLIES	90° PLIES
$\bar{\sigma}_z$	-0.88	-6.62	-6.62	-12.35
$\bar{\sigma}_x$	4.12	4.46	4.46	4.80
$\bar{\tau}_{zx}$	0.0	-0.57	0.57	0.0

-1 KSI AXIAL COMPRESSIVE STRESS LOADING

STRESSES (ksi)	0° PLIES	+45° PLIES	-45° PLIES	90° PLIES
$\bar{\sigma}_z$	-1.590	-0.556	-0.556	0.474
$\bar{\sigma}_x$	0.0075	-0.053	-0.053	-0.113
$\bar{\tau}_{zx}$	0.0	0.105	-0.105	0.0

Figure 6.26 Comparison of room temperature, dry (RTD) experimental data for three ply drop-off no. 1, thin section laminates with combined micromechanics/laminate analysis prediction.

Figure 6.27 Comparison of room temperature, dry (RTD) experimental data for three ply drop-off no. 1, thick section laminates with combined micromechanics/laminate analysis prediction.

TABLE 6.11.   PLY STRESS RATIOS CALCULATED FROM LAMINATE ANALYSIS FOR USE IN
             MICROMECHANICS ANALYSIS FOR PLY DROP-OFF NO. 2 LAMINATE AT
             RTD CONDITION, 26 PLY (THIN) SECTION

HYGROTHERMAL LOADS ($\Delta T = -200°F$, $\Delta M = 0\%$)

STRESSES (ksi)	0° PLIES	+45° PLIES	-45° PLIES	90° PLIES
$\bar{\sigma}_z$	-0.92	-7.09	-7.09	-13.26
$\bar{\sigma}_x$	4.05	4.42	4.42	4.78
$\bar{\tau}_{zx}$	0.0	-0.61	0.61	0.0

-1 KSI AXIAL COMPRESSIVE STRESS LOADING

STRESSES (ksi)	0° PLIES	+45° PLIES	-45° PLIES	90° PLIES
$\bar{\sigma}_z$	-1.448	-0.558	-0.558	0.331
$\bar{\sigma}_x$	0.0	-0.052	-0.052	-0.104
$\bar{\tau}_{zx}$	0.0	0.091	-0.091	0.0

TABLE 6.12.   PLY STRESS RATIOS CALCULATED FROM LAMINATE ANALYSIS FOR USE IN
             MICROMECHANICS ANALYSIS FOR PLY DROP-OFF NO. 2 LAMINATE AT
             RTD CONDITION, 30 PLY (THICK) SECTION

HYGROTHERMAL LOADS ($\Delta T = -200°F$, $\Delta M = 0\%$)

STRESSES (ksi)	0° PLIES	+45° PLIES	-45° PLIES	90° PLIES
$\bar{\sigma}_z$	-0.88	-6.62	-6.62	-12.35
$\bar{\sigma}_x$	4.12	4.46	4.46	4.80
$\bar{\tau}_{zx}$	0.0	-0.57	0.57	0.0

-1 KSI AXIAL COMPRESSIVE STRESS LOADING

STRESSES (ksi)	0° PLIES	+45° PLIES	-45° PLIES	90° PLIES
$\bar{\sigma}_z$	-1.590	-0.556	-0.556	0.474
$\bar{\sigma}_x$	0.0075	-0.053	-0.053	-0.113
$\bar{\tau}_{zx}$	0.0	0.105	-0.105	0.0

Figure 6.28 Comparison of room temperature, dry (RTD) experimental data for three ply drop-off no. 2, thin section laminates with combined micromechanics/laminate analysis prediction.

6.63
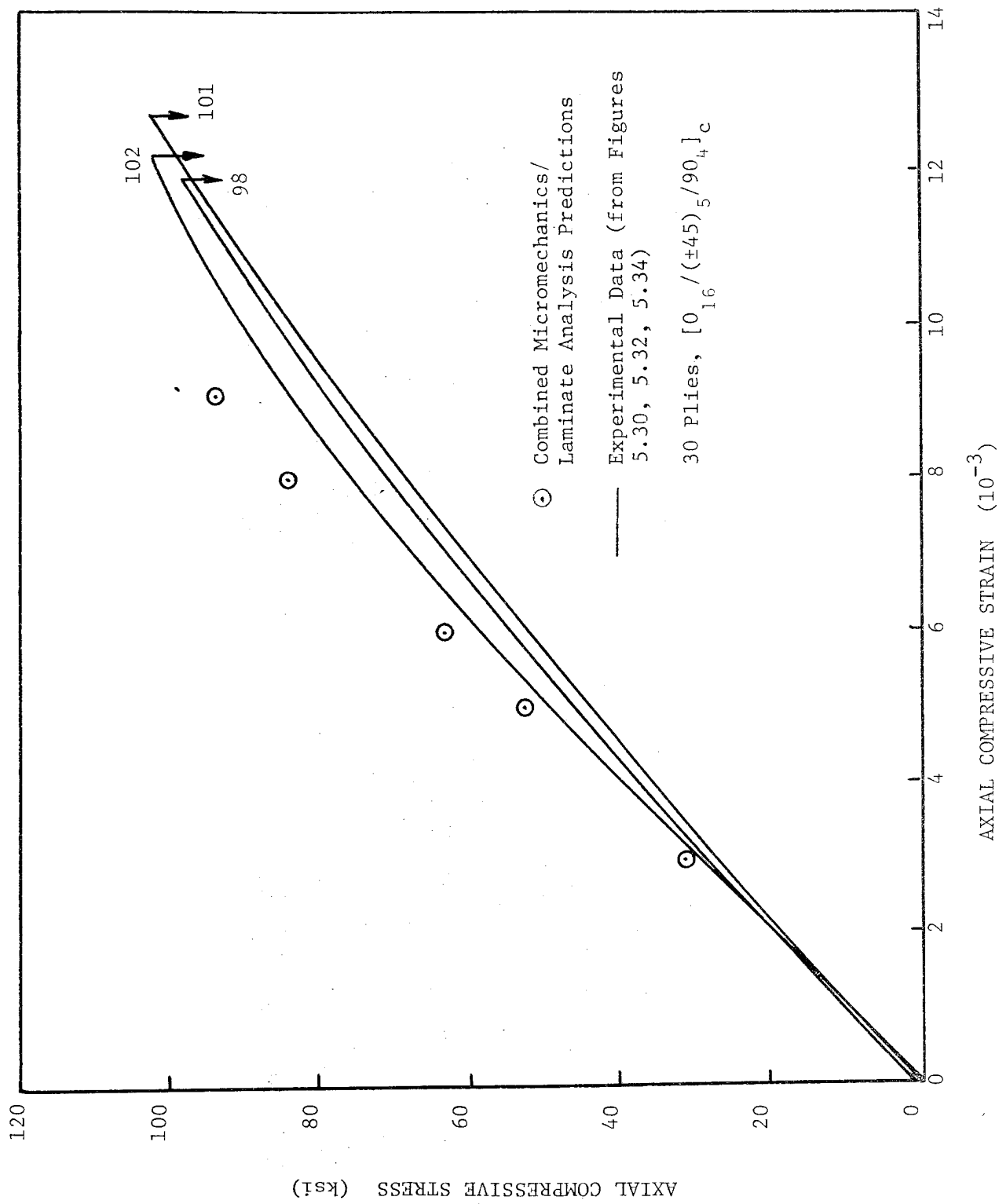
Figure 6.29 Comparison of room temperature, dry (RTD) experimental data for three ply drop-off no. 2, thick section laminates with combined micromechanics/laminate analysis prediction.

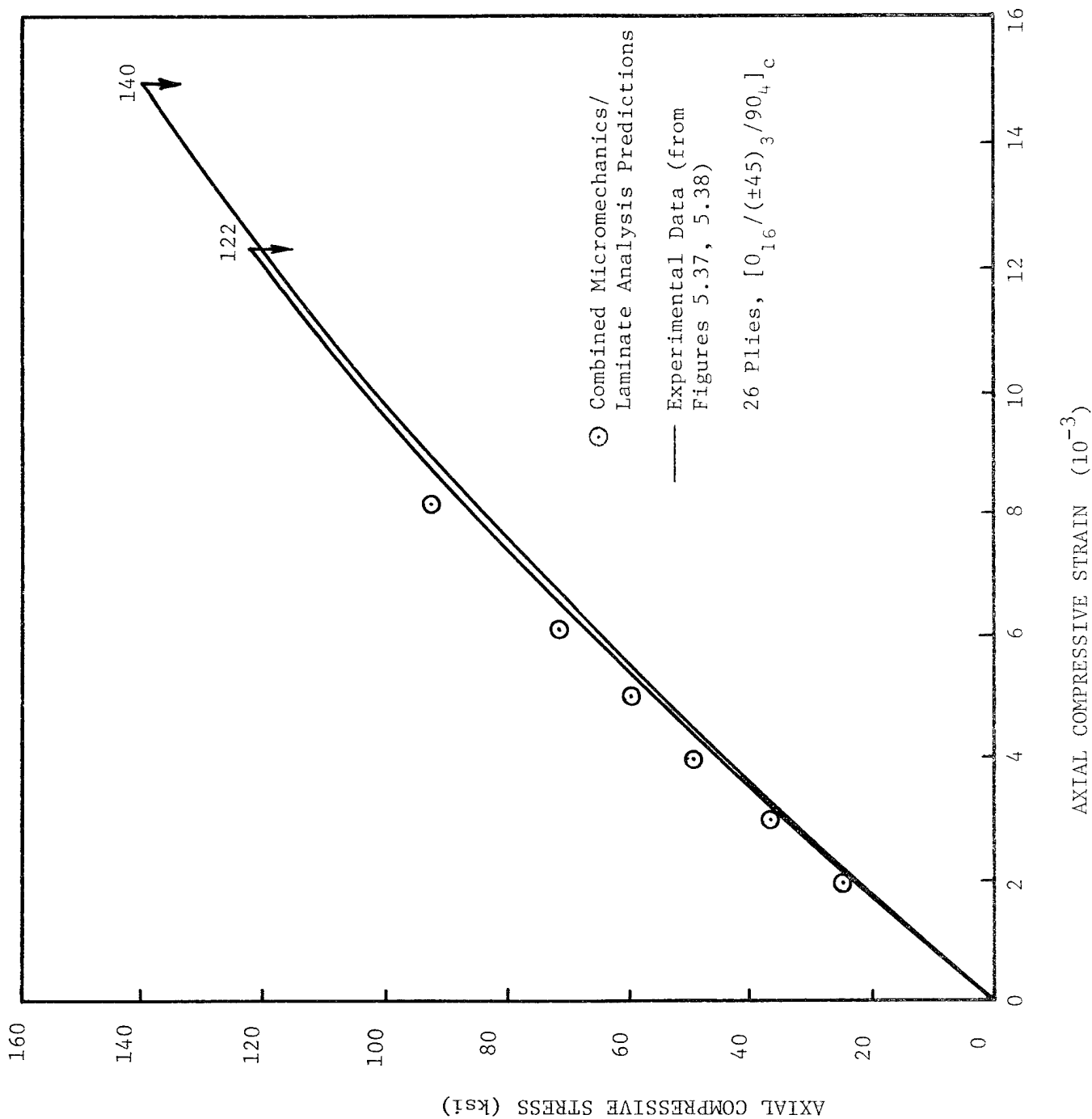TABLE 6.13. PLY STRESS RATIOS CALCULATED FROM LAMINATE ANALYSIS FOR USE IN
MICROMECHANICS ANALYSIS FOR PLY DROP-OFF NO. 1 LAMINATE AT
RTW CONDITION, 28 PLY (THIN) SECTION

HYGROTHERMAL LOADS ($\Delta T = -200°F$, $\Delta M = 1\%$)

STRESSES (ksi)	0° PLIES	+45° PLIES	-45° PLIES	90° PLIES
$\bar{\sigma}_z$	-0.78	-4.35	-4.35	-7.91
$\bar{\sigma}_x$	2.94	3.15	3.15	3.36
$\bar{\tau}_{zx}$	0.0	-0.35	0.35	0.0

-1 KSI AXIAL COMPRESSIVE STRESS LOADING

STRESSES (ksi)	0° PLIES	+45° PLIES	-45° PLIES	90° PLIES
$\bar{\sigma}_z$	-1.664	-0.584	-0.584	0.503
$\bar{\sigma}_x$	0.007	-0.055	-0.055	-0.118
$\bar{\tau}_{zx}$	0.0	0.105	-0.105	0.0

TABLE 6.14. PLY STRESS RATIOS CALCULATED FROM LAMINATE ANALYSIS FOR USE IN
MICROMECHANICS ANALYSIS FOR PLY DROP-OFF NO. 2 LAMINATE AT
RTW CONDITION, 26 PLY (THIN) SECTION

HYGROTHERMAL LOADS ($\Delta T = -200°F$, $\Delta M = 1\%$)

STRESSES (ksi)	0° PLIES	+45° PLIES	-45° PLIES	90° PLIES
$\bar{\sigma}_z$	-0.64	-4.94	-4.97	-9.29
$\bar{\sigma}_x$	2.83	3.09	3.09	3.34
$\bar{\tau}_{zx}$	0.0	-0.42	0.42	0.0

-1 KSI AXIAL COMPRESSIVE STRESS LOADING

STRESSES (ksi)	0° PLIES	+45° PLIES	-45° PLIES	90° PLIES
$\bar{\sigma}_z$	-1.448	-0.558	-0.558	0.331
$\bar{\sigma}_x$	0.0	-0.052	-0.052	-0.104
$\bar{\tau}_{zx}$	0.0	0.084	-0.084	0.0
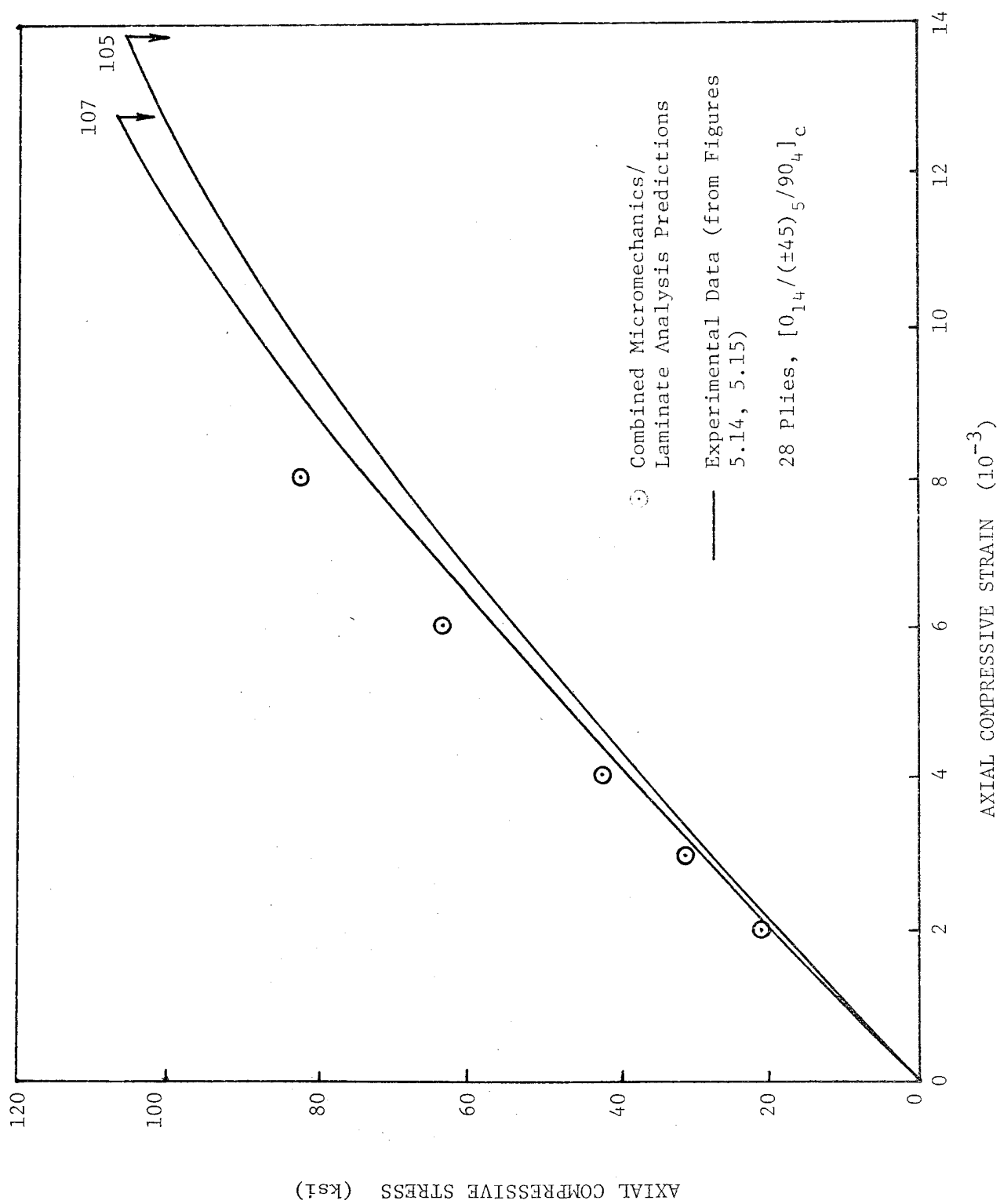
Figure 6.30 Comparison of room temperature, wet (RTW) experimental data for two ply drop-off no. 1, thin section laminates with combined micromechanics/laminate analysis prediction.

6.66
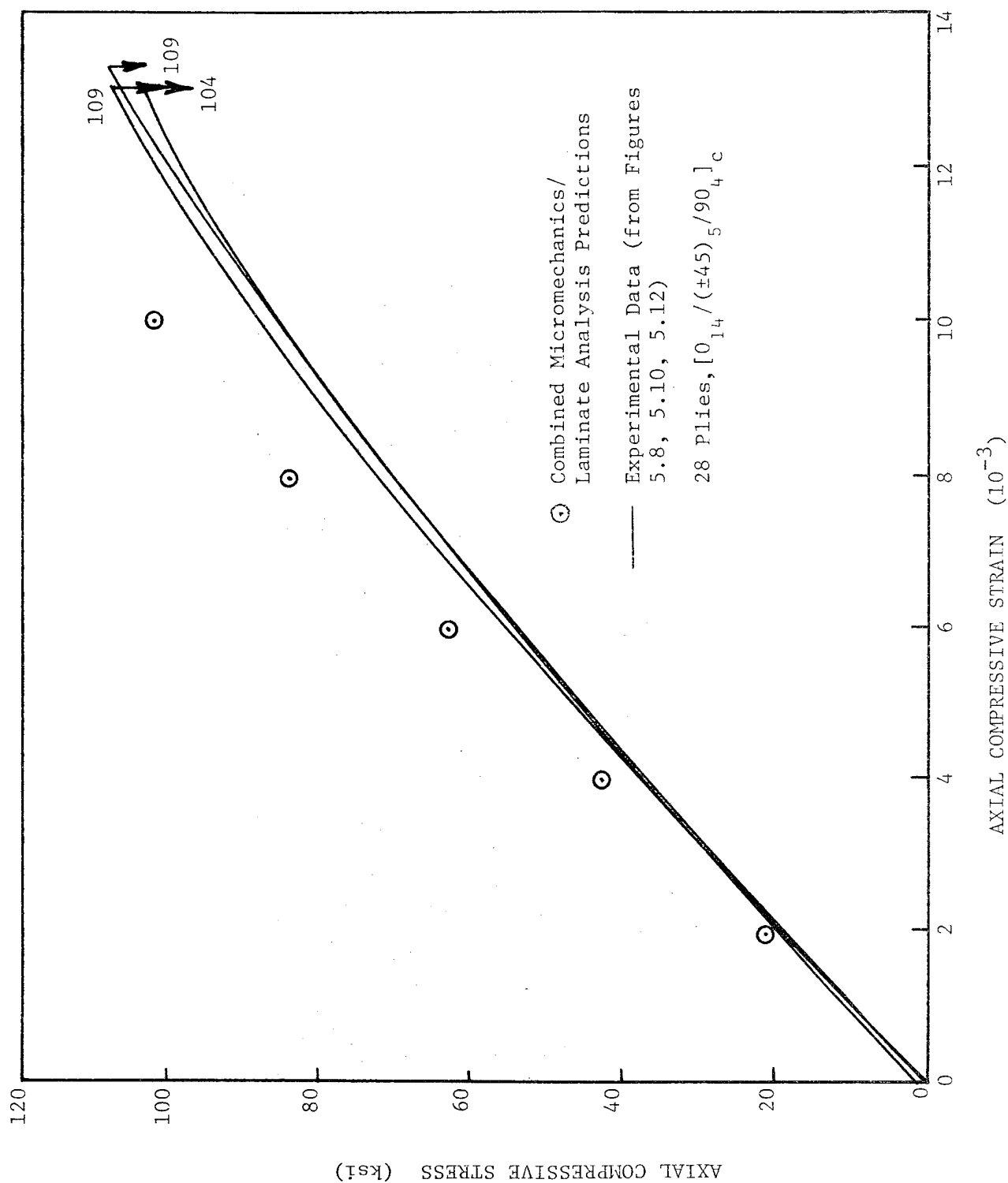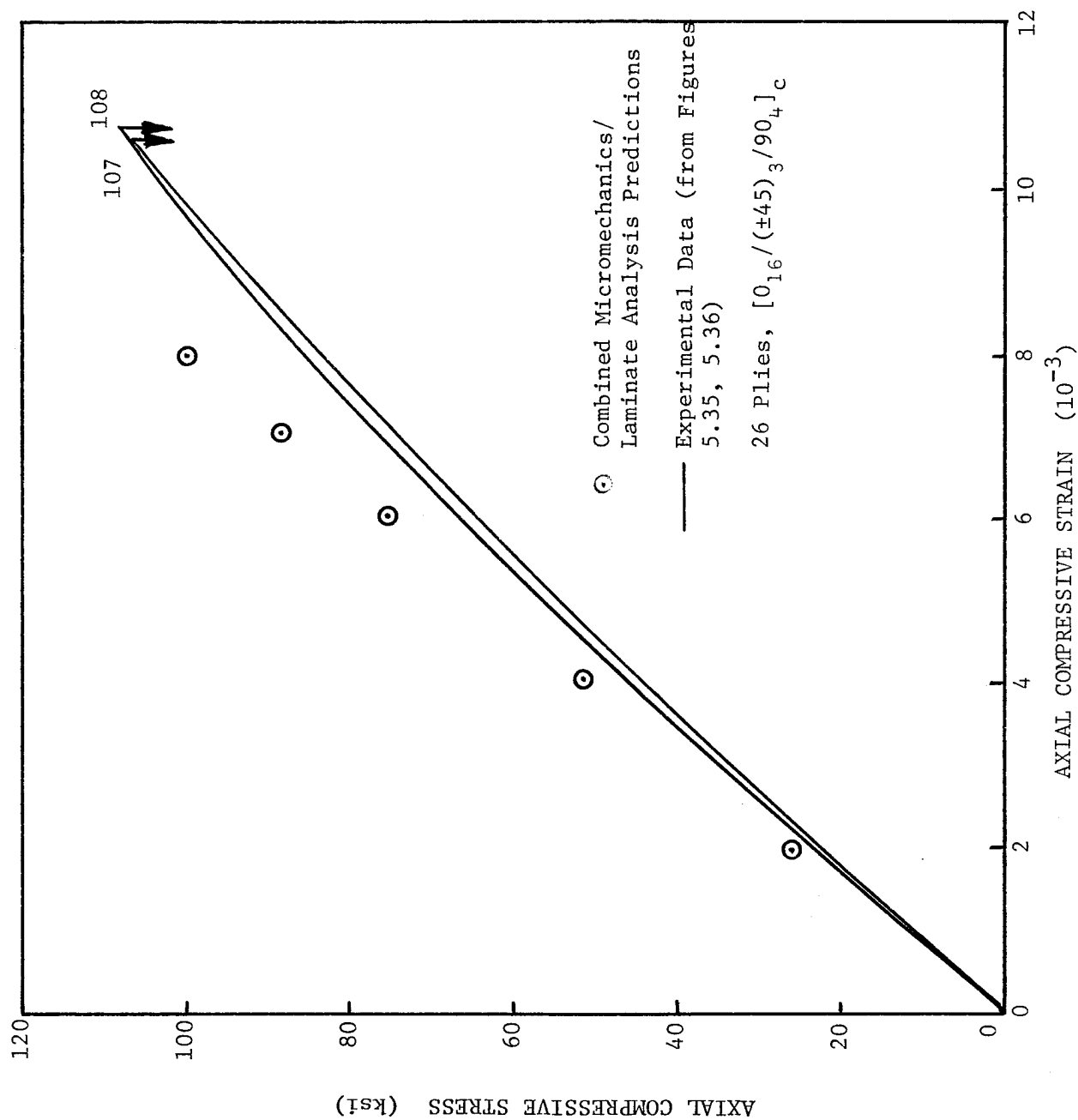
Figure 6.31 Comparison of room temperature, wet (RTW) experimental data for two ply drop-off no. 2, thin section laminates with combined micromechanics/laminate analysis prediction.
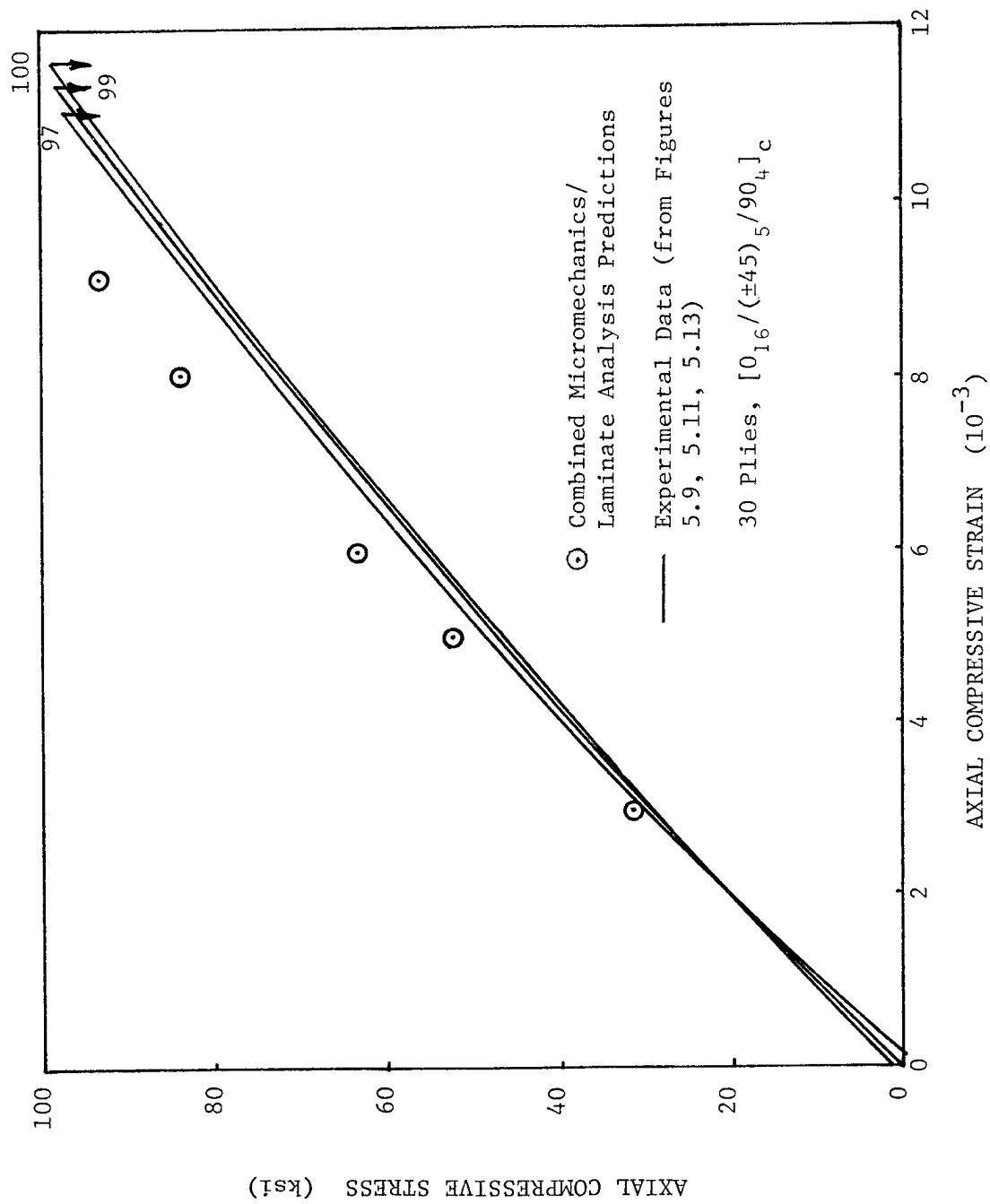
TABLE 6.15. PLY STRESS RATIOS CALCULATED FROM LAMINATE ANALYSIS FOR USE IN MICROMECHANICS ANALYSIS FOR PLY DROP-OFF NO. 1 LAMINATE AT 218°FW CONDITION, 28 PLY (THIN) SECTION

HYGROTHERMAL LOADS ($\Delta T = -75°F$, $\Delta M = 1\%$)

STRESSES (ksi)	0° PLIES	+45° PLIES	-45° PLIES	90° PLIES
$\bar{\sigma}_z$	-0.07	-0.45	-0.45	-0.83
$\bar{\sigma}_x$	0.30	0.32	0.32	0.34
$\bar{\tau}_{zx}$	0.0	-0.02	0.02	0.0

-1 KSI AXIAL COMPRESSIVE STRESS LOADING

STRESSES (ksi)	0° PLIES	+45° PLIES	-45° PLIES	90° PLIES
$\bar{\sigma}_z$	-1.699	-0.573	-0.573	0.552
$\bar{\sigma}_x$	0.007	-0.042	-0.042	-0.097
$\bar{\tau}_{zx}$	0.0	0.069	-0.069	0.0

TABLE 6.16. PLY STRESS RATIOS CALCULATED FROM LAMINATE ANALYSIS FOR USE IN MICROMECHANICS ANALYSIS FOR PLY DROP-OFF NO. 2 LAMINATE AT 218°FW CONDITION, 26 PLY (THIN) SECTION

HYGROTHERMAL LOADS ($\Delta T = -75°F$, $\Delta M = 1\%$)

STRESSES (ksi)	0° PLIES	+45° PLIES	-45° PLIES	90° PLIES
$\bar{\sigma}_z$	-0.06	-0.52	-0.52	-0.97
$\bar{\sigma}_x$	0.29	0.31	0.31	0.34
$\bar{\tau}_{zx}$	0.0	-0.03	0.03	0.0

-1 KSI AXIAL COMPRESSIVE STRESS LOADING

STRESSES (ksi)	0° PLIES	+45° PLIES	-45° PLIES	90° PLIES
$\bar{\sigma}_z$	-1.467	-0.552	-0.552	0.357
$\bar{\sigma}_x$	0.0	-0.045	-0.045	-0.084
$\bar{\tau}_{zx}$	0.0	0.058	-0.058	0.0
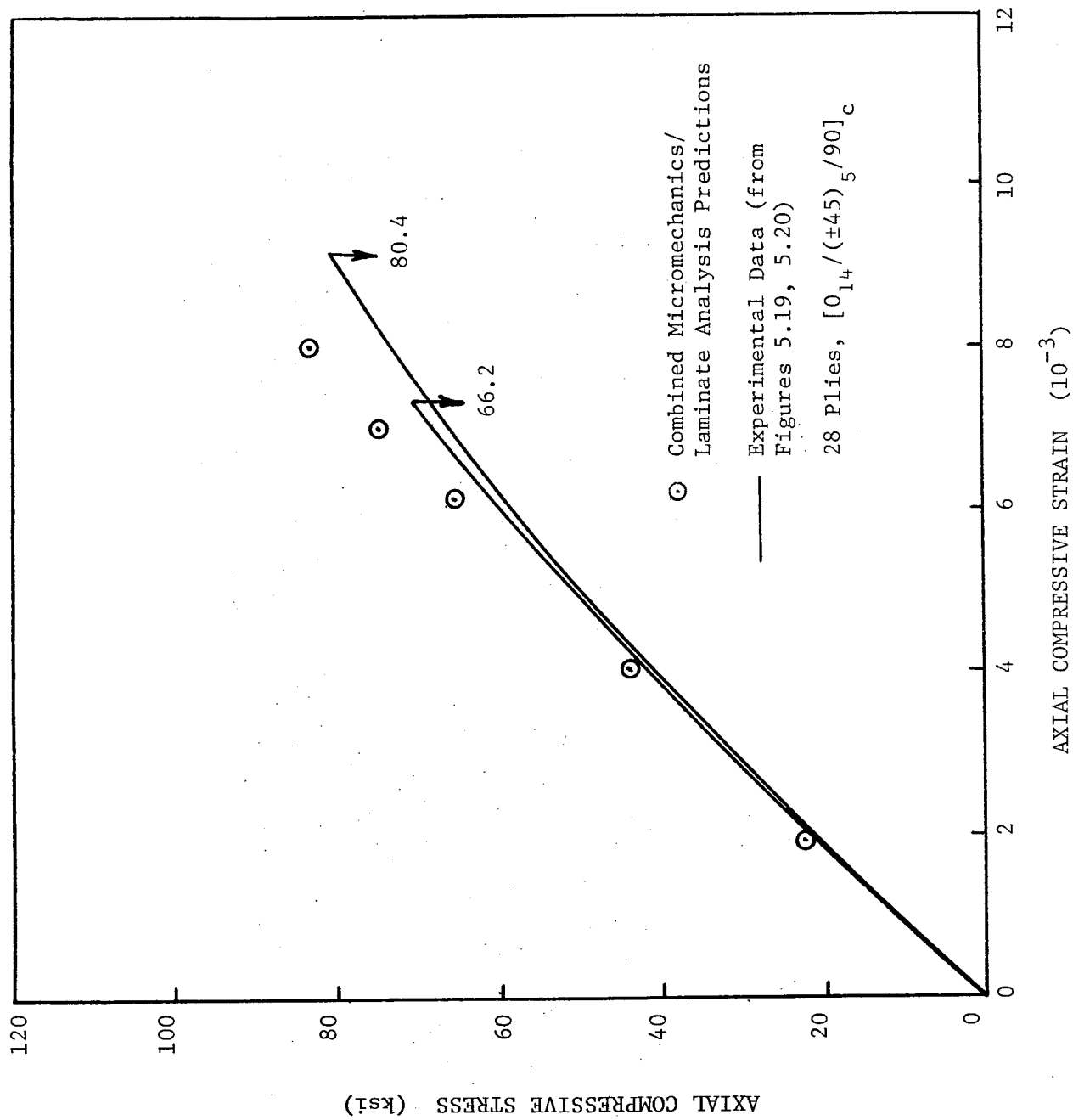
Figure 6.32 Comparison of 218°F, 1 percent moisture (218FW) experimental data for two ply drop-off no. 1, thin section laminates with combined micromechanics/laminate analysis prediction.
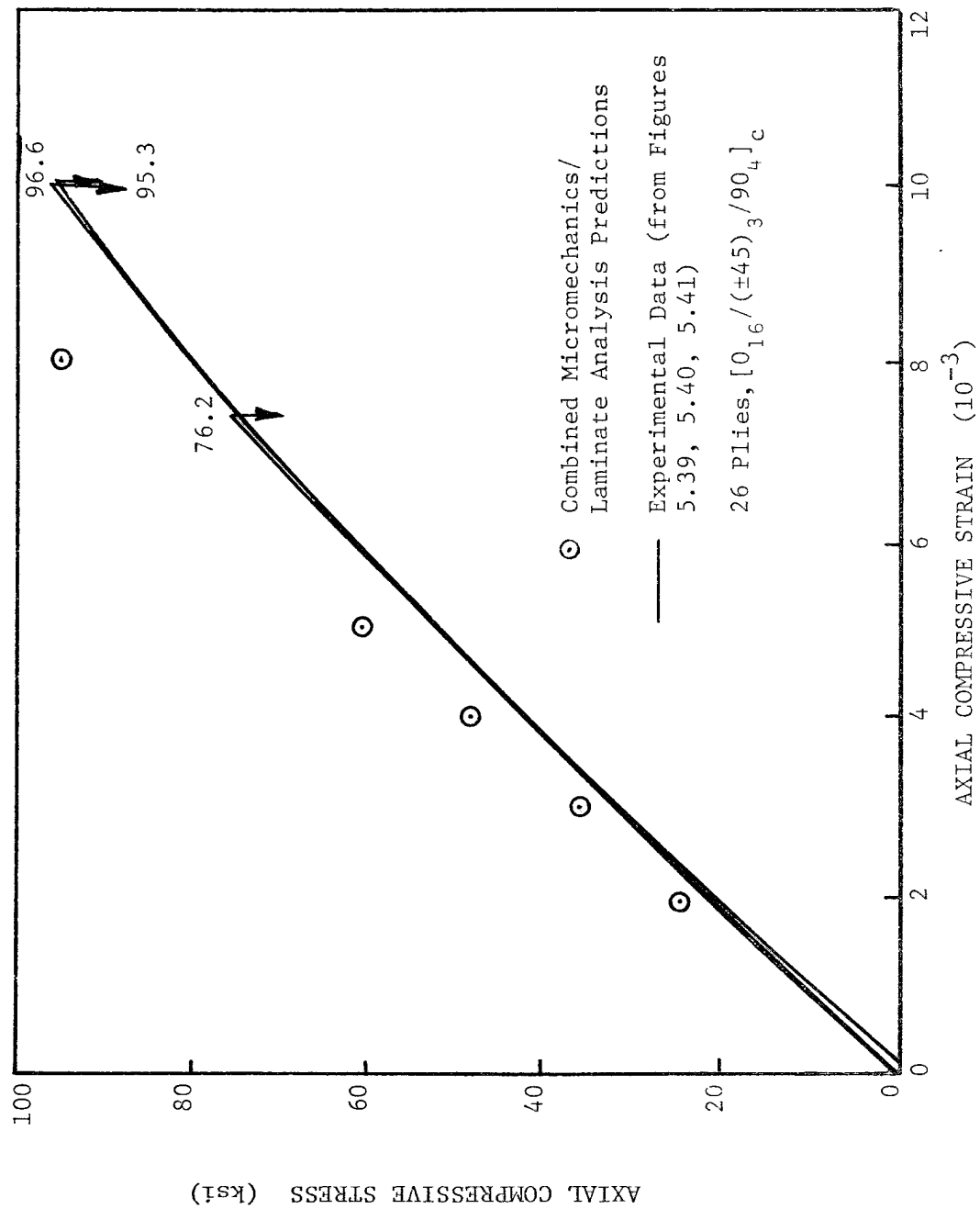
Figure 6.33 Comparison of 218°F, 1 percent moisture (218FW) experimental data for three ply drop-off no. 2, thin section laminates with combined micromechanics/laminate analysis prediction.

## 6.4. Analysis of Ply Drop-off Effects

It was anticipated that the scanning electron microscopy (SEM) work, discussed in Section 6.2, would readily reveal the presence of the ply drop-offs, and their influence on the fracture modes observed. This was not the case, however. Thus, it was necessary to rely on optical methods of determining the geometry of the ply drop-offs. A Polaroid MP-4 or 35mm single lens reflex camera was found to produce the best results, better than an optical microscope.

In the following subsections, the ply drop-off geometries will be defined, the analysis method described, and some preliminary results presented.

6.4.1 Ply Drop-off Geometries

The two ply drop-off geometries considered in the present study are perhaps most clearly defined by the schematic diagrams of Figures 3.1 and 3.2. The purpose of the present three-dimensional analysis is to accurately model the local geometry in the region of each type of ply drop-off. Figure 6.34 is an approximately 40X magnification view of the 0° ply drop-offs in a Ply Drop-off No. 1 laminate, shown schematically in Figure 3.1. Figure 6.34 includes the lower free surface (tool surface, as defined in Figure 3.1). Thus, the orientation of any ply shown can be identified by counting plies from this lower surface.

The abrupt discontinuities created by the two 0° ply drop-offs are obvious in Figure 6.34. Also, it will be noted that the adjacent 0° plies on the inner side of the drop-off ply are disturbed very little, as might be expected. Likewise, the adjacent 90° ply on the outer side is grossly deformed locally. The individual fibers have moved into the gap at the discontinuity, filling this space, somewhat at the expense of 90° ply material directly to the left of the 0° ply drop-off site. The thinning of this 90° ply is particularly obvious in the region of the lower ply drop-off. The local disturbance in geometry tends to disappear within about 10 ply thicknesses (i.e., about 0.050") from the ply drop-off, however.

Figure 6.34. Photomicrograph of Longitudinal Cross Section of Ply Drop-Off No. 1 Laminate (40X)

6.72

Had the middle ply of the three-ply set of 0° plies been selected as the drop-off ply, the geometry would have been somewhat different. Then, there would not have been ply material mobile enough to fill the discontinuity at the end of the drop-off ply. Undoubtedly, a resin pocket would have then formed, perhaps causing an even more severe stress concentration.

It will be noted in Figure 6.34 that the two 0° ply drop-offs are not exactly lined up. They are only staggered by about five ply thicknesses (i.e., about 0.025"), however, which is considered to represent a quite accurate layup procedure, remembering that 12 plies were layed up between the two discontinuous plies. The finite element analysis to be applied will establish the degree of mutual influence between these widely separated discontinuities. It is anticipated that the predicted stress fields will not interact significantly.

Figure 6.35 shows a Ply Drop-off No. 2 laminate cross section. Again, the lower surface (the tool surface, as defined in Figure 3.2) is shown in the photograph, so plies can be identified by counting up from the bottom, using Figure 3.2 as a reference. The two inner (+45° ply) drop-offs, being staggered one-half inch to the left of the outer drop-offs (see Figure 3.2), are well out of the field of view of Figure 6.35.

The -45° ply drop-offs are seen to have deformed considerably, resulting in a long tapered region at the end of the discontinuous plies. Unlike the 0° ply drop-offs shown in Figure 6.34, the fibers in the -45° ply do have sufficient mobility to fill the space created. It is also significant that the adjacent (continuous) +45° ply toward the center of the laminate does not have this same mobility, being uncut, and hence does not deform locally to help fill the space. Likewise, the three adjacent 0° plies on the outer side of the drop-off ply, having even less mobility, also do not move locally.

There is a gradual geometry change in the 10-20 ply thickness (0.050" - 0.100") region around the drop-off, however, including the 0° plies. This local disturbance of the axial alignment of the 0" plies undoubtedly has a significant influence on the local laminate response to the axial compressive loading, since the scanning electron microscopy (SEM) work of Section 6.2
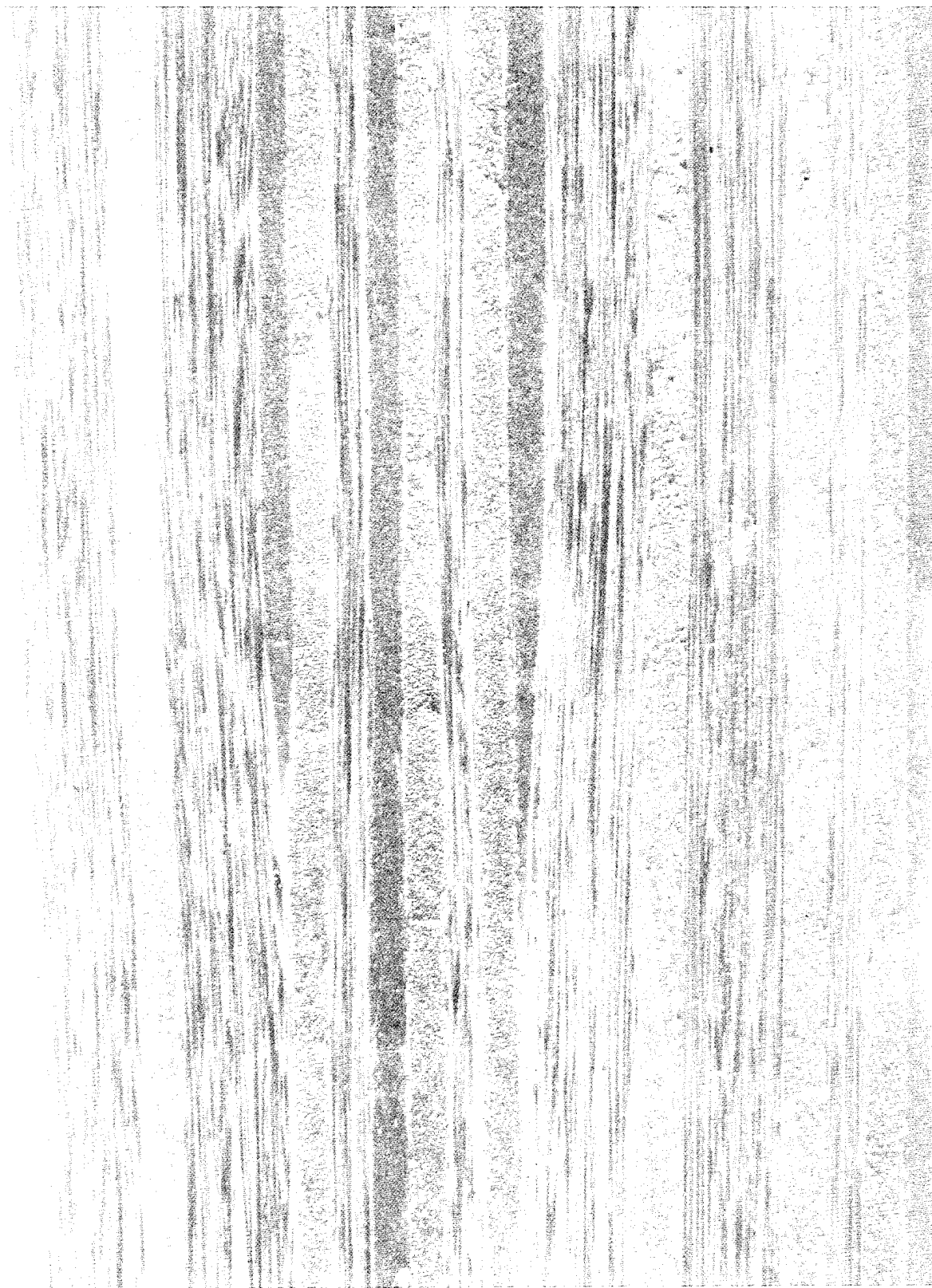
Figure 6.35. Photomicrograph of Longitudinal Cross Section of Ply Drop-Off No. 2 Laminate (40X)

clearly identified local buckling to be a dominate failure mode. On the other hand, if an axial tensile loading were to be applied, this 45° ply drop-off would probably have much less effect.

The cross section photomicrograph samples shown in Figures 6.34 and 6.35, along with others, are being used to establish the geometry of the finite element model required in the analysis described in the next subsection.

6.4.2 Three-Dimensional Finite Element Analysis

The rigorous analysis of the influence of ply drop-offs requires an approach which includes anisotropic (orthotropic or transversely isotropic), inelastic material behavior. While a number of both 2-D and 3-D finite element analyses of elastic response exist, anisotropic, inelastic analyses have not been available [4]. Thus, during the past three or more years, the Composite Materials Research Group at the University of Wyoming has been developing such an analysis and related computer program. While being sponsored in part by In-House funding, and in part by the Army Research Office [15], it was the type of problems represented by the present ply drop-off geometry which motivated the work. This work has just been completed [4]. Thus, there was not adequate time to include actual ply drop-off analysis results in the present report. However, the analysis method will be briefly described here; detailed results will be included in the Final Report of the third-year study [16].

The unique features of this analysis include a full three-dimensional finite element analysis approach, orthotropic materials, elastoplastic stress-strain response, both temperature- and moisture-dependent material properties, an octahedral shear yield criterion, use of a modified form of the Prandtl-Reuss flow rule, and completely general mechanical loadings combined with arbitrary thermal and moisture exposure histories.

The finite element solution procedure also incorporates many recent developments. Three-dimensional isoparametric elements are used, in conjunction with a reduced integration technique. A frontal solution technique is then used to solve the resulting stiffness equations.

These various features will be briefly discussed in the following subsections. More complete details are given in Reference [4].

6.4.2.1 Assumptions

Implicit in the development of any plasticity model are assumptions associated with the behavior of the material. Several of these assumptions were employed in the present work; a discussion of their implications follows.

6.4.2.1.1 Yield Criterion

The basic limitation of all present yield criteria is the lack of sufficient experimental data to support the mathematical model by which the yield surface is described. Among the most frequently used yield criteria are those attributed to Tresca [17] and von Mises [18]. The more popular von Mises criterion [18] has been extended to describe anisotropic materials [19].

Several investigations have been concerned with defining a strength criterion specifically for composite materials. A criterion of this type is used as a failure surface or condition in stress space. When the stress state, expressed as some function of the stress components, lies on this surface, it satisfies the failure condition. That is, the material is assumed to have failed. These surfaces could also be used to define yielding, if the parameters describing such surfaces were expressed in terms of material yield stresses instead of material ultimate strengths.

One criterion of this type is the Tsai-Hill criterion [20]. In fact, this strength criterion is based on Hill's yield criterion [19].

Another strength criterion was presented by Tsai and Wu [8]. Several features of this strength criterion are:
  1) It is a scalar equation and is invariant, i.e., interactions between the stress components are independent material properties.

6.76

2) Since the strength components are expressed as tensor polynomials,
their transformation relations and the associated invariants are
well established.

3) Material axes can be rotated.

Although it seems physically attractive, some components in the tensor poly-
nomial require difficult and expensive biaxial testing for their determination.
Narayanaswami and Adelman [10] proposed a modified criterion, based on the
Tsai-Wu theory, in which terms requiring biaxial testing were assumed zero.
This criterion could also be modified and used as a yield criterion.

6.4.2.1.2 Hardening Rule

The stress-strain response after initial yielding differs among various
materials, and it also differs among various plasticity theories. This
post yielding response, called hardening, is described by specifying a sub-
sequent yield surface, often termed the loading surface or the hardening rule.
The choice of a hardening rule will depend on its ability to represent the
hardening behavior of the material under consideration, and upon the ease
with which it can be applied. These requirements, together with the necessity
of maintaining mathematical consistency with the yield function described in
the previous section, constitute the criterion for the selection of a harden-
ing rule.

Hill [19] proposed the isotropic hardening rule, which assumed that
during plastic flow the loading surface expanded uniformly about the origin
in stress space, maintaining the same shape, center and orientation as the
yield surface. Since fibrous composites are strongly anisotropic, the
directions of anisotropy remain effectively unchanged during deformation.
Thus, the isotropic work hardening rule is suitable for these materials.

The hardening behavior postulated in the theory of kinematic hardening is
due to Prager [21], and assumes that during plastic deformation the loading
surface translates in stress space, maintaining the size, shape, and orienta-
tion of the yield surface. The primary aim of this theory is to provide a
means of accounting for the Bauschinger effect.

A model of combined kinematic and isotropic hardening, in which the subsequent loading surfaces expand and translate, has been presented by Hodge [22]. However, since there are no published experimental data that show that this model fits the behavior of composites, its complexity does not justify its use.

6.4.2.1.3 Flow Rule

Plastic strain increments are related to their corresponding stress increments by means of a flow rule. A general approach for determining a flow rule is the use of the concept of a plastic potential. The assumption is made that there exists a scalar function of stress $f(\sigma_{ij})$, from which the components of plastic strain increment are proportional to $\frac{\partial f}{\partial \sigma_{ij}}$. This assumption leads to an incremental or associated linear flow theory of plasticity, in which the increment of plastic strain is in the direction of outward normal to the surface represented by $f(\sigma_{ij})$ in stress space, at the current value of stress. A strain rate vector deviating from the outward normal to the yield surface in a direction independent of the stress rate vector constitutes the nonassociated linear flow theories of plasticity. The nonassociated flow theories are particularly suitable for work-softening materials [23].

An associated flow rule that is generally used to describe elastic-plastic behavior is the Prandtl-Reuss relation, which is a generalization of the Levy-Mises equations. The Prandtl-Reuss assumption is that the plastic strain increments, $d\varepsilon_{ij}^p$, are proportional to the corresponding stress deviator, σ_{ij}', where the instantaneous non-negative value of the constant of proportionality is dependent on the work hardening. The concept of an effective stress and effective plastic strain [24] is in itself an assumption that is usually introduced to reduce the complexity of a multi-axial situation to one that can be related to uniaxial behavior. Thus, the proportionality parameter can be the ratio of the effective stress to the effective plastic strain increment.

6.4.2.2 Formulation

The stiffness concept that leads to the finite element analysis is presented in relation to the solution of elastoplastic problems in three-dimensional space. A transversely isotropic unidirectional composite lamina will be assumed. If the three principal axes of anisotropy are taken to be; 1 in the direction of the fibers, 2 transversely in the plane, and 3 normal to the plane of the lamina, the 2-3 plane will be the plane of transverse isotropy. As discussed earlier, the directions of anisotropy will not change during deformation. A quadratic form in the six components of stress, similar to Hill's yield condition [19], can then be chosen in the form

$$2f(\sigma_{ij}) = F(\sigma_2 - \sigma_3)^2 + G(\sigma_3 - \sigma_1)^2 + H(\sigma_1 - \sigma_2)^2$$

$$+ 2L\ \tau_{23}^2 + 2M\ \tau_{31}^2 + 2N\ \tau_{12}^2 = 1 \qquad (6.11)$$

where F, G, H, L, M, and N are parameters characteristic of the current state of anisotropy.

In the present study, the parameters of anisotropy are allowed to vary with changes in temperature and/or moisture content.

The form of Eq. (6.11) is valid only when the principal axes of anisotropy are taken to be the axes of reference; otherwise the stress components must be transformed. The functional dependence of the parameters of anisotropy on temperature and moisture follows directly when the yield stresses are expressed as functions of temperature and moisture content.

The obvious association, implied by the term "work-hardening," between the work used to produce plastic flow and the hardening created, suggests the hypothesis that the degree of hardening is a function only of the total plastic work, and is otherwise independent of the strain path. In order for plastic work to be performed, the state of stress must be on the yield surface, i.e., the stress state must also satisfy the condition given by Eq. (6.11). To enforce this constraint, the Lagrange multiplier $d\lambda$ is used [25].

6.79

Relating the six parameters of anisotropy to the strain history is an extremely complicated problem. The problem can be simplified, however, by the assumption that the yield stresses must increase in proportion with strain hardening. This assumption is justified by the fact that the directions of anisotropy in fibrous composites remain effectively the same during deformation. By analogy with the von Mises criterion for isotropic materials, Hill [19] suggested that if there is a functional relation between the equivalent stress $\bar{\sigma}$ and the work W, there must be one between $\bar{\sigma}$ and the effective (or equivalent) strain, $d\bar{\varepsilon}$. This is the analogue of the equivalent stress-equivalent strain curve for isotropic materials, the area under which is equal to the work per unit volume. If an effective stress-effective plastic strain curve is then constructed, the slope of such a curve at any point will be

$$H' = \frac{d\bar{\sigma}}{d\bar{\varepsilon}^P} \tag{6.12}$$

Continuing in this manner [4] yields the desired form for the stress-strain relation

$$\{d\sigma\} = [C^P]\{d\varepsilon\} \tag{6.13}$$

where

$$[C^P] = \begin{bmatrix} C_{11} - \dfrac{A_1^2}{B} & C_{12} - \dfrac{A_1 A_2}{B} & C_{13} - \dfrac{A_1 A_3}{B} & -\dfrac{A_1 A_4}{B} & -\dfrac{A_1 A_5}{B} & -\dfrac{A_1 A_6}{B} \\[2mm] & C_{22} - \dfrac{A_2^2}{B} & C_{23} - \dfrac{A_2 A_3}{B} & -\dfrac{A_2 A_4}{B} & -\dfrac{A_2 A_5}{B} & -\dfrac{A_2 A_6}{B} \\[2mm] & & C_{33} - \dfrac{A_3^2}{B} & -\dfrac{A_3 A_4}{B} & -\dfrac{A_3 A_5}{B} & -\dfrac{A_3 A_6}{B} \\[2mm] & \text{Symmetric} & & C_{44} - \dfrac{A_4^2}{B} & -\dfrac{A_4 A_5}{B} & -\dfrac{A_4 A_6}{B} \\[2mm] & & & & C_{55} - \dfrac{A_5^2}{B} & -\dfrac{A_5 A_6}{B} \\[2mm] & & & & & C_{66} - \dfrac{A_6^2}{B} \end{bmatrix} \tag{6.14}$$

is the plastic stiffness matrix, and

$$B = \frac{4}{9} \bar{\sigma}^2 H' + A_1 \sigma_1^* + A_2 \sigma_2^* + A_3 \sigma_3^*$$

$$+ 2A_4 \tau_{23}^* + 2A_5 \tau_{31}^* + 2A_6 \tau_{12}^*$$

(6.15)

where A_i (i = 1, ..., 6) are elements of {A}, and

$$\sigma_1^* = [H(\sigma_1 - \sigma_2) + G(\sigma_1 - \sigma_3)]/(F + G + H)$$

$$\sigma_2^* = [F(\sigma_2 - \sigma_3) + H(\sigma_2 - \sigma_1)]/(F + G + H)$$

(6.16)

$$\sigma_3^* = [G(\sigma_3 - \sigma_1) + F(\sigma_3 - \sigma_2)]/(F + G + H)$$

$$\tau_{23}^* = L\tau_{23}/(F + G + H)$$

For an orthotropic material, i.e., a material with three planes of symmetry,

$$\{A\} \equiv \left\{ \begin{array}{c} C_{11}\sigma_1^* + C_{12}\sigma_2^* + C_{13}\sigma_3^* \\[6pt] C_{12}\sigma_1^* + C_{22}\sigma_2^* + C_{23}\sigma_3^* \\[6pt] C_{13}\sigma_1^* + C_{23}\sigma_2^* + C_{33}\sigma_3^* \\[6pt] 2C_{44}\tau_{23}^* \\[6pt] 2C_{55}\tau_{31}^* \\[6pt] 2C_{66}\tau_{12}^* \end{array} \right\}$$

(6.17)

6.81

6.4.2.3 Material Model

To apply the method of analysis developed in the previous section to fibrous composites, the material properties in the 1,2, and 3 directions are needed. If the material is transversely isotropic, the properties in the 2 and 3 directions are the same. For mathematical consistency with the formulation, a relation between the effective stress and effective strain is required. Also, the tangent modulus H' of the effective stress-effective strain curve is needed. Furthermore, the dependence of the material properties on temperature and moisture content is required if hygrothermal loadings are to be handled, and the actual material response under varying conditions of environment is to be considered. Both the elastic and the plastic response of a material change with temperature, and for polymeric materials, with moisture also. Therefore, the entire effective stress-effective strain curve of the material for each state of the environment must be available.

Richard and Blacklock [13,26] have developed a three-parameter model which was found to fit stress-strain curves for composite materials very accurately [5]. This model is of the form

$$\sigma = E\varepsilon/[1 + |E\varepsilon/\sigma_o|^n]^{1/n} \qquad (6.18)$$

where σ_o and n are two independent parameters, and E is the initial slope of the stress-strain curve. Since the shape of an effective stress-effective strain curve is similar to a tensile stress-strain curve, a similar equation for the effective stress-effective strain can be written as

$$\bar{\sigma} = \bar{E}\,\bar{\varepsilon}/[1 + |\bar{E}\,\bar{\varepsilon}/\bar{\sigma}_o|^n]^{1/n} \qquad (6.19)$$

where $\bar{\sigma}$ is the effective stress and $\bar{\varepsilon}$ is the effective strain, as defined previously. The two independent parameters $\bar{\sigma}_o$ and n, together with the third parameter $\bar{E}$, which is the initial slope of the curve, are selected to best fit the experimental data.

By fitting Eq. (6.19) to the effective stress-effective strain curves for different temperatures and moisture contents, a functional relationship

6.82

of the parameters $\bar{E}$, $\bar{\sigma}_o$, and n to temperature and moisture can be established. In a similar manner, functional relationships can also be found for all other material properties.

6.4.2.4 Finite Element Formulation

Prior to the widespread application of digital computers, the inelastic behavior of solids was one of the most intractable problems in solid mechanics. The combination of large digital computers and the finite element method has made possible the solution of most of these hitherto intractable problems. However, in most of the previous literature on the subject, simple constant stress elements have been used. This was largely motivated by the difficulty of performing an exact integration in an element containing both elastic and plastic regimes. With numerical integration techniques already introduced into the formulation of complex elements [27] in the analysis, such difficulties disappear. Among the different numerical integration techniques, the Gause method [28] is most widely used.

A comparison of various complex elements in three-dimensional analyses by Clough [29] has shown that isoparametric, numerically integrated brick elements are more efficient in elastoplastic analyses than simple elements. This type of element, viz, the isoparametric element, was used in the present work.

The data required to incorporate any element into a static analysis can be conveniently organized into four characteristic matrices. These matrices define the elastic or plastic behavior, the spatial assembly into the structure, and the required output information for each element. The four matrices are:

1) The element stiffness matrix, $[C^e]$ or $[C^P]$.
2) The element initial stress-free $\{F\}_{mo}$ or $\{d\}_{mo}$ vector.
3) The element assembly matrix.
4) The element output matrix.

The element initial stress-free vector depends on whether a stress field or a displacement field is assumed for the element.

6.83

For any type of element, a force-deformation relationship is needed, which leads to the first two characteristic matrices, i.e., the element stiffness matrix and the initial stress-free vector. The form of this relation is

$$\{F\}_m = [C]_m \{d\}_m - \{F\}_{mo} \qquad (6.20)$$

where

$\{F\}_m$ = independent generalized forces for element m; a second subscript zero denotes initial values.

$[C]_m$ = element stiffness matrix (non-singular)

$\{d_m\}$ = independent generalized deformations for element m.

The third characteristic matrix is the element assembly matrix. To assemble the structural stiffness matrix in the assumed displacement method, which is used in this work, the independent deformation variables $\{d\}_m$ for each element have to be transformed into equivalent nodal displacements $\{\Delta\}_m$ in the global system, using the transformation (assembly) matrix $[a]_m$, i.e.,

$$\{d\}_m = [a]_m \{\Delta\}_m \qquad (6.21)$$

Depending on whether the assumed displacement method or the assumed stress method is used, the fourth characteristic matrix relates the independent variables to the required output information, i.e., stresses in the former case, and displacements in the latter.

6.4.2.5 Computer Program

While the principles of three-dimensional elastic stress analysis by the finite element method have been obvious from the early days of the development of the method [30], their practical implementation leads to some immediate obstacles. As the number of elements increases, so does the number of degrees of freedom, increasing the size of the stiffness matrix, which requires larger computer in-core storage. In early approaches to three-dimensional analyses, the simple tetrahedral element was the obvious choice.

Various families of isoparametric elements were introduced by Zienkiewicz, et al., in 1967 [31]. These elements are more efficient than tetrahedrons, and were utilized in the present analysis, thus allowing a greater accuracy to be achieved for a given number of degrees of freedom and given computation time.

In the present work, a computer program has been developed making use of many of the more recent developments in both areas of finite element analysis and computer programming. The following is a description of the main features of this program "NCLAP" (Nonlinear Composite Laminate Analysis Program).

A modular approach has been adopted for NCLAP, with the various main finite element operations being performed by separate subroutines. The basic finite element steps are performed by primary subroutines, which rely on auxiliary subroutines to carry out secondary operations. The construction falls into three phases.

Phase 1. Data are input and checked for possible preparation errors, an important feature when considering the amount of data input required for three-dimensional problems.

Phase 2. Stiffness and stress matrices and the applied load vector are generated. The nature of laminated composite problems requires elements with large aspect ratios, i.e., the ratio between minimum and maximum characteristic dimensions of an element in the mesh. This is because the thickness of a lamina is typically very small compared to its surface area. Large aspect ratios lead to an ill-conditioned stiffness matrix, i.e., the diagonal terms become very small compared to the off-diagonal terms, a situation that can lead to large solution errors. However, by using reduced integration techniques [32], the problem can be overcome.

Phase 3. A "frontal" solution technique [33,34] is used for the solution of the stiffness equations. The advantages of using this method rather than the well-known banded matrix method are:

1) In solving the stiffness equations using a banded matrix, the order in which the nodes are numbered is very important since it influences the bandwidth. Using the frontal solution technique, however, does not require any ordering of nodal numbers. Hence, if a mesh is to be modified at a later time, no renumbering is needed. This saves considerable time and effort in data preparation.

2) For higher order elements, less core storage is needed. Several examples which justify this statement can be found in Reference [35].

3) Since variables are eliminated in this method as soon as conceivably possible, operations on zero coefficients are minimized and the total number of arithmetic operations is less than with other methods. Thus, less storage and computer time is used.

4) Because any new equation occupies the first available space in the front, there is no need for a bodily shifting of the in-core equations as in many other large capacity equation solvers.

In any incremental analysis, the use of smaller load increments implies a larger number of increments to achieve the same total applied load. Hence, more time is spent in reconstructing stiffness equations. A main feature of the computer program NCLAP is that it allows for the use of small load increments without increasing the computing time significantly. The stiffness matrix is reconstructed only for those elements that become plastic, or when hygrothermal loading is considered.

6.4.3 Numerical Results

Because the three-dimensional finite element analysis to be used to analyze the local region around the ply drop-offs has just recently been completed [4], there was not adequate time to include detailed results in the present publication. Such results will be presented in subsequent reports. However, the sample problems included in Reference [4] make it clear that this analysis will be a valuable tool in predicting the influence of ply drop-offs also.

6.4.4 Summary of Ply Drop-off Analysis

Polishing and photography techniques required to identify the exact local geometries of the ply drop-off regions have been developed, as demonstrated by Figures 6.34 and 6.35. The three-dimensional finite element analysis required is now fully operational, as indicated by the example problems included in Reference [4].

The distinct geometries in the ply drop-off regions can clearly be expected to show a predicted difference in the response under load. Further, it is expected that the analysis will permit the study of stacking sequence on local stress distributions. That is, it will be used to quantify such factors as how close ply drop-offs can be spaced without causing detrimental stress interactions. This will be a complex function of the orientation of the ply being dropped off, the orientations of adjacent plies, and the type of loading. Only simple uniaxial compressive loadings were studied in the present program. The analysis is equally capable of analyzing complex, mutli-axial loadings, combined with arbitrary temperature and moisture gradients, if desired.

Thus, it is envisioned that the finite element analysis will be used as a detailed screening tool, to identify promising configurations for actual fabrication and test.

SECTION 7

CONCLUSIONS AND RECOMMENDATIONS

7.1 GENERAL

This section presents the program conclusions (7.2) and recommendations (7.3) that resulted from the experimental effort at Northrop and the analytical effort at the University of Wyoming.

7.2 CONCLUSIONS

7.2.1 Experimental Data - Northrop

Static ultimate compressive strength properties at $-65°$FW, RTD, RTW, and $218°$FW for both PDO #1 and PDO #2 were as good or better than those of the plain laminates. Modulus of elasticity values dropped slightly for PDO #1 but either stayed the same or increased slightly for PDO #2 as compared with those of the plain laminate. Except for the 218 FW condition the Poisson's Ratio values dropped significantly for both PDO #1 and PDO #2 when compared with plain laminate properties. At $218°$FW the PDO #1 values of Poisson's Ratio increased substantially while PDO #2 remained about the same as those of the plain laminate. At $-65°$FW proportional limit values for both PDO #1 and #2 increased substantially while at RTD conditions, there was a significant drop compared to plain laminate values. At RTW, the PDO #1 proportional limit value dropped significantly while the PDO #2 value increased significantly compared to plain laminate values. At $218°$FW the PDO #1 and #2 values remained about the same as those of the plain laminate.

Fatigue endurance limit stress levels of PDO #1 are significantly reduced at $-65°$FW, RTD, RTW and $218°$FW conditions compared to plain laminate values. A comparative F-N curve plot at RTD conditions in Figure 7.1 shows this. PDO #1 residual strength shows a significant drop at $-65°$FW and $218°$FW conditions but a significant increase at RTD and RTW conditions compared to plain laminate properties.
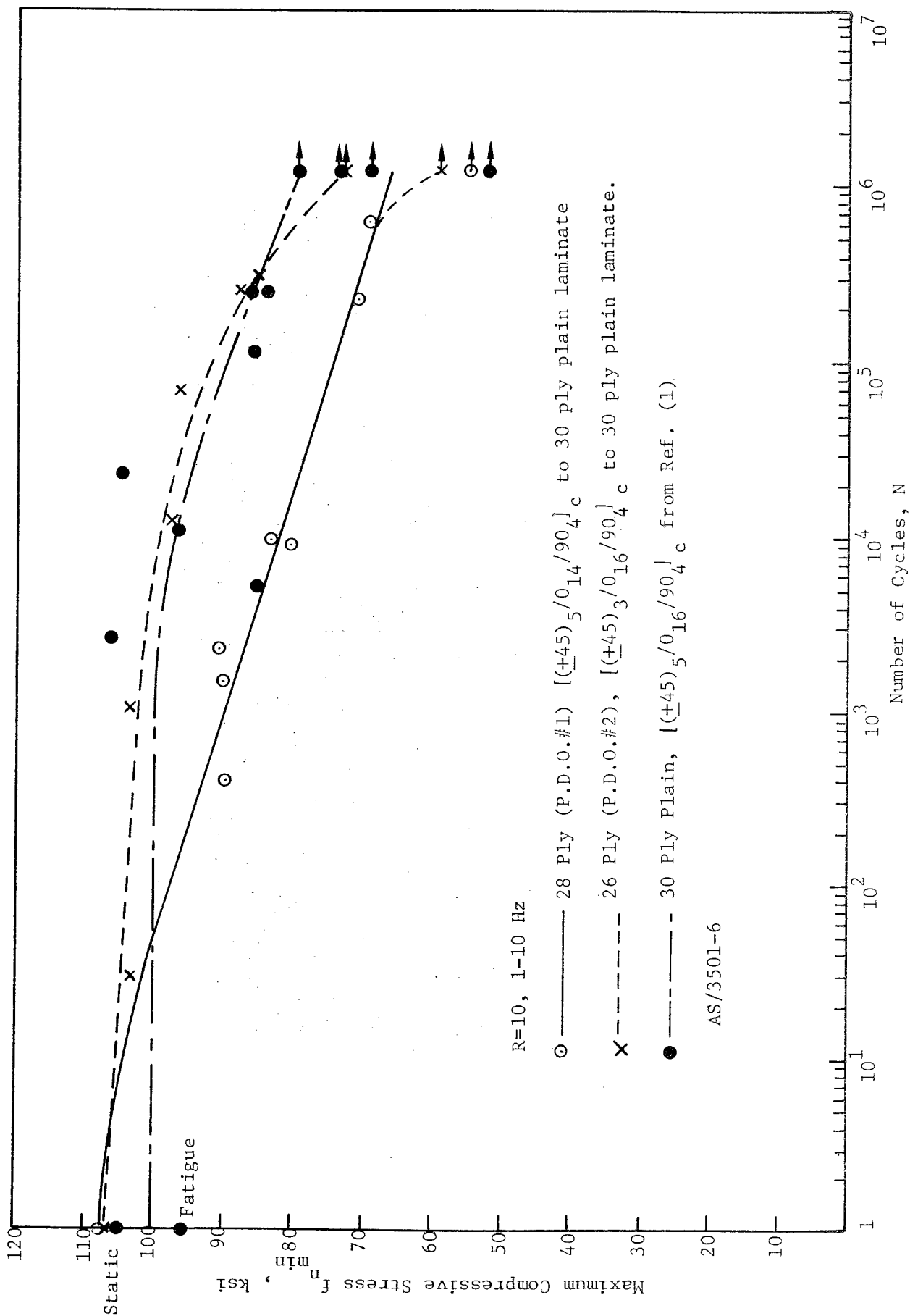
Figure 7.1 Constant Cycle Fatigue Behavior of Graphite/Epoxy Composites RTD (With and Without Ply Drop-offs)

The PDO #2 fatigue endurance limit stress levels show significant
increases at -65°FW and RTW conditions, but show small decreases at RTD
and 218°F conditions compared to plain laminate properties. At RTD and RTW
conditions the residual strength shows substantial increases, whereas,
at -65°FW a slight increase is shown and at 218°FW a slight decrease is
recorded.

Static ultimate compressive strength and modulus of elasticity at all
environments used appear to change only slightly or increase substantially
(strength only) for PDO #1 and #2 compared to plain laminate properties.
However changes in proportional limit values and Poisson's ratio are sub-
stantial in some cases for these ply drop-offs as compared with plain
laminate properties.

Significant reduction in fatigue endurance limit occurs in all environ-
ments studies for PDO #1 whereas the PDO #2 values remained the same or
increased in these environments compared to plain laminate results.
Residual strength for PDO #1 dropped significantly at -65°FW and 218°FW while
it showed substantial increases at RTD and RTW conditions. For PDO #2
residual strength showed substantial increases for -65°FW, RTD, and RTW
conditions, but had a slight drop at 218°FW compared with plain laminate
properties.

7.2.2 Analytical Data-University of Wyoming

Major advances were made during this second-year effort in the development
of methods of analysis. With the exception of the combination of the longitudi-
nal shear loading and crack propagation capabilities into one computer program,
and the addition of a crack propagation capability to the three-dimensional
finite element analysis, the analytical tools required to analyze the
effects of defects are now set. This is in significant contrast to the status
at the beginning of the first-year study [1], when only the basic micromechanics
analysis was available [5]. Thus, during the third-year study [16], emphasis
will shift to utilizing these new analysis capabilities both to study in greater
detail the existing experimental data, and to evaluate the influences of
porosity.

The theory/experiment correlations presented in this report clearly demonstrate the ability of these large scale numerical analyses to simulate actual experimental conditions. The ability to predict the gross stress-strain response of a laminate of arbitrary lay up orientation, and then predict the local state of stress down to the level of individual fibers, has been demonstrated. The next step is then obvious; the use of these same analyses to design improved composite laminates for whatever loading and environmental conditions are to be encountered.

Specific conclusions of the present study include the further verification that scanning electron microscopy (SEM) is an extremely valuable tool in identifying local failure modes, not otherwise observable. The SEM study showed fiber microbuckling to be a dominate failure initiation mode. The micromechanics analysis correlates with this observation, predicting high interface stresses and fiber-matrix debonding under corresponding conditions, this debonding leading to loss of lateral support for the individual fibers, and hence fiber microbuckling.

The abrupt geometry change associated with the 0° ply drop-off geometry (Ply Drop-off No. 1), and the associated disturbance of the axial alignment of the adjacent 0° plies, which in turn adversely influences the resistance to local buckling, is assumed to account for the experimental trends observed.

The Ply Drop-off No. 2 configuration (with ±45° ply drop-offs), was found to result in a less abrupt discontinuity in local geometry. Offsetting this, however, is the fact that the percentage of 0° plies is higher when ±45° plies are removed. It is the 0° plies in which the failure initiating fiber microbuckling occurs. As a result, there appear to be few clear trends in the experimental data.

There was a distinct difference in the -65°F and room temperature failure modes under all conditions. The -65°F specimens failed in a much more brittle manner. This was exhibited on the microlevel by much more extensive ply delamination in the fracture region. In contrast, the 218°F specimens exhibited almost no local delamination, more fiber microbuckling (due to the reduced matrix strength and modulus at the elevated temperature), and a more ductile failure mode.

In general, the experimentally observed influences of ply drop-offs are difficult to interpret at present. It is hoped that further analysis during the third-year effort will help explain the experimental results obtained.

7.3 RECOMMENDATIONS

7.3.1 Experimental Effort - Northrop

Additional static and fatigue testing in statistically significant quantities should be performed to verify the degraded properties of ply drop-offs.

7.3.2 Analytical Effort - University of Wyoming

The longitudinal shear loading capability and the crack propagation capability should be combined into one micromechanics computer program. In addition, a crack propagation capability should be added to the three-dimensional finite element laminate analysis. These improved analysis tools could then be used to further analyze the existing experimental data, in an attempt to more fully explain the trends observed.

Subsequently, these analysis tools should be reduced to a form readily useable by the designer. They can then be used to define candidate laminated composite configurations for specific design applications.

SECTION 8

REFERENCES

1. G.C. Grimes and D.F. Adams, "Investigation of Compression Fatigue Properties of Advanced Composites," Report NOR 79-17, Northrop Corporation, Hawthorne, California, October 1979.

2. C.R. Saff, "Compression Fatigue Life Prediction Methodology for Composite Structures - Literature Survey," Report No. NADC-78203-60, Naval Air Development Center, Warminster, Pennsylvania, June 1980.

3. D.A. Crane and D.F. Adams, "Finite Element Micromechanical Analysis of a Unidirectional Composite Including Longitudinal Shear Loading," Report UWME-DR-001-104-1, University of Wyoming, Department of Mechanical Engineering, Laramie, Wyoming, December 1980.

4. M.M. Monib and D.F. Adams, "Three-Dimensional Elastoplastic Finite Element Analysis of Laminated Composites," Report UWME-DR-001-103-1, University of Wyoming, Department of Mechanical Engineering, Laramie, Wyoming, November 1980.

5. A.K. Miller and D.F. Adams, "Micromechanical Aspects of the Environmental Behavior of Composite Materials," Department Report UWME-DR-701-111-1, Mechanical Engineering Department, University of Wyoming, Laramie, Wyoming, January 1977.

6. O.C. Zienkiewicz, The Finite Element Method, McGraw-Hill Book Co., New York, New York, 1977.

7. T.R. Branca, "Creep of a Unidirectional Metal Matrix Composite Subjected to Axial and Normal Lateral Laods," TAM Report 341, Theoretical and Applied Mechanics Department, University of Illinois, Urbana, Illinois, June 1971.

8. S.W. Tsai and E.M. Wu, "A General Theory of Strength for Anisotropic Materials," Journal of Composite Materials, Vol. 5, January 1971, pp. 58-80.

9. R.M. Jones, Mechanics of Composite Materials, Scripta Book Co., Washington, D.C., 1975.

10. R. Narayanswami and H.M. Adelman, "Evaluation of the Tensor Polynomial and Hoffman Strength Theories for Composite Materials," Journal of Composite Materials, Vol. 11, October 1977, pp. 366-377.

11. Unpublished Solid Rod Torsion Experimental Data, Composite Materials Research Group, Department of Mechanical Engineering, University of Wyoming, Laramie, Wyoming, 1980.

12. D.F. Adams and R.L. Thomas, "The Solid Rod Torsion Test for the Determination of Unidirectional Composite Shear Properties," Textile Research Journal, Vol. 39, No. 4, April 1969, pp. 339-345.

13. R.M. Richard and J.M. Blacklock, "Finite Element Analysis of Inelastic Structures," AIAA Journal, Vol. 7, No. 3, March 1969, pp. 432-438.

14. R.D. Kriz, W.W. Stinchcomb and D.R. Tenney, "Effects of Moisture, Residual Curing Stresses and Mechanical Load on the Damage Development in Quasi-Isotropic Laminates," Report No. 16, NASA-Virginia Tech. Composites Program, February 1980.

15. "Laminate Analyses, Micromechanical Creep Response, and Fatigue Behavior of Polymer Matrix Composite Materials," Army Research Office Grant No. DAAG 29-79-C-0189, Composite Materials Research Group, University of Wyoming, September 1979-September 1982.

16. "Effects of Materials and Processes Defects on the Compression Static and Fatigue Properties of Advanced Composites," Naval Air Systems Command Contract N00019-80-C-0484, Composite Materials Research Group, University of Wyoming, August 1980-January 1982.

17. H. Tresca, Comptes Rendus Acad. Sci., Vol. 59, Paris, France, 1864, pp. 754-799.

18. R. von Mises, Gottinger Nachrichten, math.-phys. Klasse, Mathematisch-Physikalische, Nachrichten, 1913, pp. 582-592.

19. R. Hill, The Mathematical Theory of Plasticity, Oxford University Press, London, England, 1950.

20. S.W. Tsai, "Strength Theories of Filamentary Structures," Fundamental Aspects of Fiber Reinforced Plastic Composites, Wiley Interscience, New York, New York, 1968, pp. 3-11.

21. W. Prager, "A New Method of Analyzing Stress and Strain in Work-Hardening Solids," J. Appl. Mech., Vol. 23, December 1956, pp. 493-496.

22. P.G. Hodge, Jr., "A General Theory of Piecewise Linear Plasticity," J. of Appl. Mech. and Phy. of Solids, Vol. 5, 1957, pp. 242-260.

23. H. Armen, "Assumptions, Models and Computational Methods for Plasticity," Comp. & Struct., Vol. 10, August 1979, pp. 161-174.

24. G.N. White, Jr., and D.C. Drucker, "Effective Stress and Effective Strain in Relation to Stress Theories of Plasticity," J. Appl. Phys., Vol. 21, October 1950, pp. 1013-1021.

25. M.J. Forray, _Variational Calculus in Science and Engineering_, McGraw-Hill Book Co., New York, New York, 1968.

26. R.M. Richard, and B.J. Abbott, "Versatile Elastic-Plastic Stress-Strain Formula," _Proc. ASCE_, Vol. 101 (EM4), 1975, pp. 511-515.

27. O.C. Zienkiewicz, _The Finite Element Method in Engineering Science_, McGraw-Hill Book Co., London, 1971.

28. R.D. Cook, _Concepts and Applications of Finite Element Analysis_, John Wiley and Sons, Inc., New York, New York, 1974.

29. R.W. Clough, "Comparison of Three Dimensional Finite Elements," Proc. of the Symposium on Application of Finite Element Methods in Civil Engineering, Vanderbilt University, Nashville, Tennessee, 1969, pp. 1-26.

30. J.H. Argyris, "Matrix Analysis of Three Dimensional Media - Small and Large Displacements," _J. AIAA_, Vol. 3, January 1965, pp. 45-51.

31. O.C. Zienkiewicz, _The Finite Element Method_, McGraw-Hill Book Co., London, England, 1967.

32. O.C. Zienkiewicz, R.T. Taylor, and J.M. Too, "Reduced Integration Technique in General Analysis of Plates and Shells," _Int. J. Num. Meth. Engng._, Vol. 3, April 1971, pp. 275-290.

33. B.M. Irons, "A Frontal Solution Technique for Finite Element Analysis," _Int. J. Num. Meth. Engng._, Vol. 2, January 1970, pp. 5-32.

34. A. Alizadeh and G.T. Will, "A Substructured Frontal Solver and its Application to Localized Material Nonlinearity," _Comp. & Struc._, Vol. 10, September 1979, pp. 225-231.

35. D.K.Y. Kan, "A Simple Front Solution Technique for Finite Element Method," Report CNME-CR-51, Dept. of Civil Engineering, University College of Swansea, Swansea, U.K., 1971.

APPENDIX A

SPECIFICATIONS

Definitions for these Instruction Sheets

QC   - Quality Control

ID/CF   - Impact Damage/Compression Fatigue: specifications applicable
to these research programs.

MMS   - McDonnell-Douglas Aircraft (MCAIR) Material Specification

PS   - Process Standard

IT-58   - Northrop Materials Test Specification

W   - weight

V   - volume

μ - 10^{-6}, micro

NAI   - Northrop Material Specification

mil   - 0.001 inch

MMM-A-132 - Military specification on structural adhesives

T-Peel   - A cleavage-fracture peel test described in MMM-A-132

QC INSTRUCTION SHEET ID/CF NO. 1

TITLE: PREPREG REQUIREMENTS FOR HERCULES AS/3501-6 GRAPHITE/EPOXY AND
NARMCO 8517 GLASS/EPOXY PREPREGS

1. Incoming graphite/epoxy prepreg shall conform to the requirements as set
forth in MMS-549. In case of conflict between this document and MMS-549,
the requirements of this document shall take precedence. Acceptance test-
ing shall be performed at Northrop to verify these requirements and in
accordance with NCATR P.S. 21332. In case of conflict, this document
will take precedence.

TABLE 1. AS/3501-6 ACCEPTANCE REQUIREMENTS

| PROPERTY | ACCEPTANCE REQUIREMENTS* | | TEST METHOD |
	TYPE I	TYPE II	
Nongraphite content (%W)	42 ± 3	35 ±3	P.S. 21332
Flow (%)	12 to 30	15 to 30	P.S. 21332
Volatile content, 250F (%W)	1.5 maximum	1.5 maximum	P.S. 21332
0° flexural strength, ksi	220 min avg	220 min avg	IT-58 Para. 3.14
Laminate fiber volume (%V)	62 ±3	62 ±3	IT-58 Para. 3.14
Laminate void content (%V)	1 maximum	1 maximum	IT-58 Para. 3.14
Laminate specific gravity	1.59 to 1.63	1.59 to 1.63	IT-58 Para. 3.15
Transverse tension (μ-in/in)	5,000 min avg 4,000 min individual	5,000 min avg 4,000 min individual	IT-58** IT-58**

Laminates to be cured per instructions in Process Instruction Sheet 1.

Material that has been stored more than six months at 0F, or has been exposed
to room temperature for more than 40 hours, must be retested prior to use.

*Based on a minimum of three determinations.
**Clip-on extensometer may be used for strain measurements.

II.   Incoming glass/epoxy prepreg shall conform to the requirements as set forth in Table 2, and NAI 1372, Type I, Grade A, Style 1581. In case of conflict between this document and NAI 1372, the requirements of this document shall take precedence. Acceptance testing shall be performed at Northrop to verify these requirements.

TABLE 2. 8517 GLASS/EPOXY ACCEPTANCE REQUIREMENTS

PROPERTY	ACCEPTANCE REQUIREMENTS	TEST METHOD IT-58 (paragraph)
Prepreg		
Resin content (%W)	35.0 ±3.0	3.11
Volatile content (%W)	2 max	3.11
Laminate		
Flexural strength, ksi	100 min	3.4
Interlaminar shear strength, ksi	3 min	3.6
Laminate ply thickness, mils/ply	10.0 ±1.0	---
Laminate resin content (%W)	34.0 ±2.0	3.14

Laminates to be cured for 90 minutes at 350F and 50 psi per Process Instruction Sheet No. 1.

Material that has been stored for more than six months at 0F, or has been exposed to room temperature for more than 100 hours, must be retested prior to use.

Fiberglass cloth used in this prepreg material should have a Silane finish (epoxy compatible) on it prior to impregnating and B-staging by the material vendor.

Prepared by   _Glenn C. Grime_, _N.M.Bhatia_

Approved by   _Ralph M.Verette_

QC INSTRUCTION SHEET ID/CF NO. 2

TITLE: ADHESIVE REQUIREMENTS FOR AF-143 and FM-123-2 (OR AF-126-2) FILM
ADHESIVES

I. Incoming receiving and monthly acceptance testing and inspection of
adhesives will be performed in accordance with this document.

II. Incoming AF-143 adhesive properties shall conform to the requirements as
set forth in Table 2 and NAI 1370, Type 1-2A. In case of conflict between
this document and NAI 1370, the requirements of this document shall take
precedence. Acceptance testing shall be performed at Northrop to verify
these requirements.

TABLE 2. AF-143 ADHESIVE PHYSICAL AND MECHANICAL PROPERTIES REQUIREMENTS

NUMBER OF SPECIMENS	PROPERTY	ACCEPTANCE REQUIREMENTS	TEST METHOD (paragraph)
3	Flow, percent	120 to 240	4.4.3 NAI 1370
4	RT tensile shear	3,300 psi	4.4.6 NAI 1370
4	250F tensile shear	2,800 psi	4.4.6 NAI 1370

Cure Cycle

Specimens shall be cured at a pressure of 50 ±5 psi, the curing temperature
shall be 350 ±10F for 60 to 70 minutes. The heatup rate from RT to 225F
shall be 3F/min to 6F/min.

III. Incoming FM-123-2 or AF-126-2 adhesive properties shall conform to the
requirements set forth in Table 2 and NAI 1286, Type 1-2C. In case of
conflict between this document and NAI 1286, the requirements of this
document shall take precedence. Acceptance testing shall be performed
at Northrop to verify these requirements

TABLE 3.   FM-123-2 AND AF-126-2, TYPE 1-2C ADHESIVE PHYSICAL AND MECHANICAL
           PROPERTIES REQUIREMENTS

NUMBER OF SPECIMENS	PROPERTY	ACCEPTANCE REQUIREMENTS	TEST METHOD (paragraph)
3	Flow, percent average	200 ±20	4.4.3, NAI 1286
4	RT tensile shear, min avg	4,500 psi	MMM-A-132
4	180F tensile shear, min avg	2,500 psi	MMM-A-132
6	RT T-peel, min avg	12 in-lbs/in	4.5.5.10 MMM-A-132

Cure Cycle

Specimen shall be cured at a pressure of 35 ±5 psi, the curing temperature
shall be between 250F and 275F for 90 to 100 minutes. The heatup rate from
RT to 225F shall be 3F/min to 6F/min.

Prepared by _Glenn C. Grimes_, NMDhatia

Approved by _Ralph M Verette_

W. S. Cumberge

QC INSTRUCTION SHEET ID/CF NO. 3

TITLE: DESTRUCTIVE INSPECTION FOR SOLID LAMINATE ASSEMBLIES

I.   Selection of Specimens

1.   Destructive test specimens shall be cut and tested from each assembly
     per appropriate drawing number (see Process Instruction Sheet ID/CF NO.1) or
     Fabrication Work Order in the minimum numbers and types listed below:

     a.   3 physical property specimens
     b.   3 transverse compression specimens
     c.   2 longitudinal compression specimens
     d.   2 transverse tension specimens

2.   The properties of the test specimens shall meet the requirements as set
     forth in Table A-1.

3.   The test specimens shall conform to the dimensions of the appropriate
     drawing or specification. Dimensions of the longitudinal and transverse
     compression specimens shall be in accordance with Figure A-1.

TABLE A-1 PHYSICAL AND MECHANICAL PROPERTY REQUIREMENTS

PROPERTY	ACCEPTABLE REQUIREMENTS	TEST METHODS
Fiber volume	59 $\pm$4 percent	IT-58, para. 3.14
Void Content	$\leq$ 1 percent	IT-58, para. 3.14
Specific gravity	1.56 to 1.62	IT-58, para. 3.15
Transverse compression: a) $[90]_{nc}$	30 ksi	See Figure A-1
b) $\pm$45/0/90	50 ksi	See Figure A-1
Longitudinal compression strength minimum, individual: a) $[0]_{NC}$	120 ksi	See Figure A-1
b) $\pm$45/0/90	94 ksi	See Figure A-1
Transverse Tension: $\pm$45/0/90	30 ksi	ASTM D-3039 & Fig. 7.

Prepared by _Glenn C. Grimer_

Approved by _EM Verette_

UNLESS OTHERWISE SPECIFIED, 0.XX DIMENSION SHALL
    BE ± 0.30 INCH
    0.XXX DIMENSION SHALL
    BE ± 0.010 INCH

1. TOP AND BOTTOM SURFACES SHALL BE FLAT AND
   PARALLEL TO 0.005 INCH.

2. SPECIMEN THICKNESS SHALL NOT VARY MORE THAN
   0.005 INCH FROM NOMINAL.

3. SPECIMEN LONGITUDINAL EDGES SHALL BE PARALLEL
   TO = 0.003 INCH.

4. FOR LONGITUDINAL TEST SPECIMENS, 0° FIBERS
   PARALLEL TO 3.000 INCH SIDES.

5. FOR TRANSVERSE TEST SPECIMENS/0° FIBERS PERPEN-
   DICULAR TO 3.000 INCH SIDES.

STRAIN GAGES, IF SPECIFIED
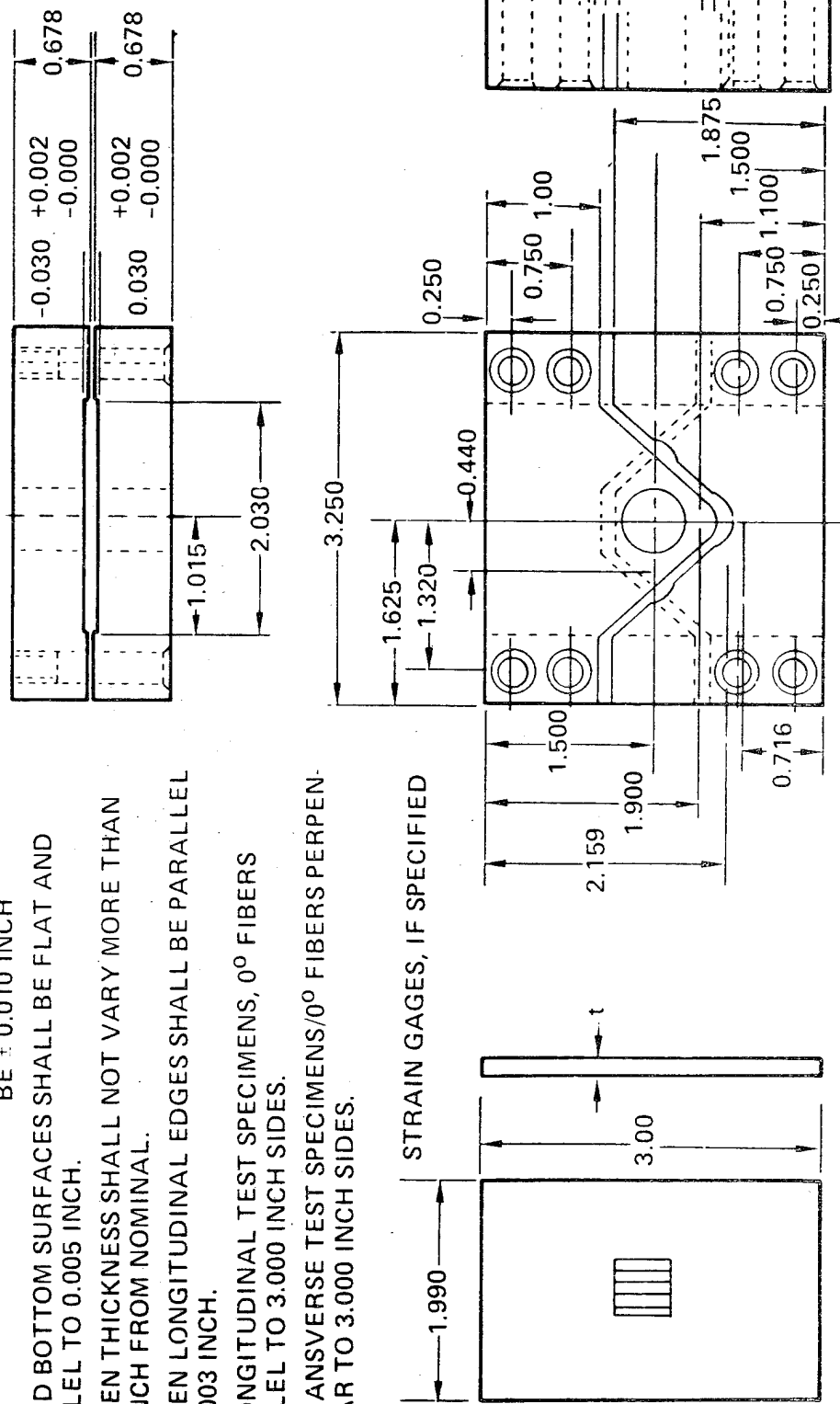
Figure A.1   Static Test Specimen and Fixture

A.8

QC INSTRUCTION SHEET ID/CF NO. 4

TITLE: NONDESTRUCTIVE EVALUATION OF SOLID LAMINATE ASSEMBLIES AND SPECIMENS

Ultrasonic nondestructive inspection will be used to provide a record of defects found, not to reject parts on a go, no go basis. Major defects will be called to the attention of the Program Office for disposition. However, the defect records will be used as a research tool to pinpoint anomalies in data and determine what size and kind of defects are critical. The real physical nature and size of defects will be determined only when such information is important to the research program.

I. Nondestructive Evaluation (NDE) Solid Laminate Assemblies

NDE will be accomplished on the full-size laminated assemblies after cure and before cutting specimens. Ultrasonic nondestructive inspection will be utilized with a full-scale recording of the inspection required. Indexing shall be 0.030 inch to 0.040 inch.

1. Defect Standard Panel

A defect standard panel will be furnished that contains built-in defects from one-eighth-inch diameter (or square) to one-inch diameter (or square). Defects will be located in the middle of the laminate thickness. This defect panel will be furnished to the inspection facility or subcontractor performing the NDT so he can properly adjust his instruments just before inspection of each bonded assembly. In case an appropriate defect standard is not available, 3/8-inch diameter lead tape will be used on the back side of the panel for setting up the instrumentation.

2. Defect Map Record

The defect map record, properly identified with location points will be kept on file for future reference. Defects found on each laminated assembly can be located on the actual specimens at any time by using the Mylar master cutting diagram overlay.

II. Specimen Inspection

Each solid laminate specimen (prior to test) will be inspected for dimensional conformance to the appropriate drawing or specification. A permanent record of the inspection will be made and filed. Specimens that do not meet the requirements will be dispositioned by the Program Office.

Visual inspection of the specimen for defects or external damage will be made. Nicks, scratches, indentations, surface voids*, excessive roughness**, or delaminations and splintering shall be recorded and called to the attention of the Program Office. Any other major damage or defects observed will be called to the attention of the Program Office.

---

*Approximate size: one ply thickness diameter (0.005 inch), report if total number exceeds six.

**Roughness in excess of 10 percent of the total specimen surface area should be reported.

Prepared by *Glenn C Grimes, NMBhatia*

Approved by *Ralph M Verette*

W. H. Sheldon

PROCESS INSTRUCTION SHEET ID/CF No. 1

TITLE: SOLID LAMINATE ASSEMBLIES

I. Process Specification P.S. 14240 (MCAIR)

P.S. 14240 specification applies. However, in case of conflict with this document (PIS - ID/CF-1), the latter takes precedence.

II. Layup of Graphite Prepreg

1. Cut, layup, and debulk books of material as necessary.

2. Over a clean caul plate covered with nonporous Armalon, layup the graphite prepreg books precut to the size, stacking order, and number of plies, as specified in the appropriate drawing or specification. Use cork, coreprene, or silicone rubber dams around circumference.

3. A ply of porous Armalon shall be placed over the graphite prepreg followed by plies of 120 glass bleeder cloth. A ratio of one ply of 120 glass cloth to four plies of graphite shall be used.

4. One ply of nonporous Armalon shall be placed on top of the last ply of 120 glass bleeder cloth.

5. Wrap the assembly with a minimum of three layers of Osnaburg cloth.

6. Vacuum bag the entire assembly.

III. Cure Cycle

1. Apply full vacuum (24-inch to 28-inch Hg) to the bagged assembly and apply 85 $\pm$5 psig autoclave pressure.

2. Heat to 240 $\pm$10F at a heatup rate of 3F/min to 6F/min, hold at 240F for 60 to 70 minutes.

3. Increase autoclave pressure to 100 psig and vent vacuum bag, heat to 350F at a rate of 1F/min to 6F/min.

4. Hold at 350F for two hours (120 $\pm$10 minutes).

5. Cool the assembly to 150F or less under pressure.

6. Release the pressure and then remove assembly from autoclave.

7. Postcure the assembly at 350F for a minimum of 8 hours in an air-circulating oven.

PROCESS INSTRUCTION SHEET ID/CF NO. 1

IV. Nondestructive Inspection

1. The assembly shall be submitted to the inspection facility (in-house or subcontract service) for nondestructive inspection.

2. The assembly shall meet the NDT requirements as set forth in QC Instruction Sheet ID/CF No. 4.

3. If the requirements of QC Instruction Sheet No. 4 are not met, the Program Office shall be notified and a disposition made.

V. Destructive Inspection

1. Trim the assembly to final dimensions and cut QC specimens as specified in appropriate drawings or specifications.

2. From the drawing designated area of the assembly, destructive test specimens will be fabricated as described in QC Instruction Sheet ID/CF No. 3.

3. Test specimens fabricated per paragraph 4.2 shall meet the minimum requirements set forth in Q.C. Instruction Sheet ID/CF No. 3.

4. If the minimum requirements of QC Instruction Sheet ID/CF No. 3 are not met, the Program Office shall be notified and a disposition made.

5. Two full-size test specimens cut from the fabricated panels as specified in the appropriate drawing or specification shall be tested for baseline QC verification per QC Instruction Sheet ID/CF No. 3.

6. If the full-size test specimens from paragraph 5.5 meet the minimum requirements as set forth by QC Instruction Sheet ID/CF No. 3, the balance of the test specimens shall be released for machining and testing.

7. If the minimums of QC Instruction Sheet ID/CF No. 3 are not met, the Program Office shall be notified and a disposition made.

VI. Fabrication of 8517 Fiberglass Tabs

1. Over a clean caul plate covered with nonporous Armalon, layup the required size laminate of 8517 fiberglass cloth pregreg, as specifided. One peel ply shall be placed on top of the last ply of fiberglass prepreg.

2. One ply of nonporous Armalon shall be placed on top of the peel ply.

3. Wrap the assembly with at least two-ply Osnaburg cloth.

4. Vacuum bag the entire assembly.

5.   Cure the assembly for 90, -0 +10 minutes at 350 ±10F using 35 ±5 psi autoclave pressure plus full vacuum (approximately 50 psi total).

6.   Heatup rate to 350F is to be 3F/min to 6F/min.

7.   Fiberglass tabs shall be cut from the fiberglass laminate to the dimensions specified.

VII.   Secondary Bonding of 8517 Fiberglass Tabs

1.   The fiberglass tabs shall be bonded to the assembly using AF-143, FM-123, or AF-126, as specified in appropriate drawings and specifications.

2.   The bonding cycle for AF-143 shall be 350 ±10F for 60 to 70 minutes using 50 ±5 psi per NAI 1370. Heatup rate from RT to 225F shall be 3F/min to 6F/min. The bonding cycle for FM-123 or AF-126 shall be between 250F and 275F for 90 to 100 minutes using 35 ±5 psi. Heatup rate from RT to 225F shall be 3F/min to 6F/min.

VIII. Machining of Test Specimens

1.   Test specimens shall be sectioned from the assembly as specified in the appropriate drawings and specifications.

Prepared by _Glenn C. Grimes_, NMBhatia

Approved by _Ralph M. Verette_

J. S. Underwood

APPENDIX B

AS/3501-6 GRAPHITE/EPOXY PREPREG QUALITY ASSURANCE
LOT DATA REPORT – HERCULES INC.

August 2, 1979

Customer: Northrop

Purchase Order No: 111-952814

Materials: Graphite Fiber/Epoxy Material, 3501-6/AS1, 12" prepreg tape.

Specification: MMS 549 Amend 4, Type I

Quantity: 53.00 lbs.

Lot No: 1261   Manufactured July 12, 1979

Spool No: 7A

Resin Lot No: 064K & 064L   Manufactured by Hercules Inc.

I.   Fiber Properties   136-1   Manufactured by Hercules Inc.

Tensile Str., ksi	466
Tensile Mod., msi	33.9
Wt./Unit Length, lb/in X 10^{-6}	45.09
Density, lb/in^3	0.0648

II. Prepreg Physical Properties

	Spec Req	
Spool No.		1
Resin Flow, %	10-25	17.5
Volatiles, %	1.5 max	0.96
Tack	Conforms	Conforms

III. Laminate Mechanical Properties

	Spec Req	Panel No.	Avg. Individual
48" Data		Spool 1	
0° Tensile Str., RT, ksi*	200	8842	253/271,222,265
0° Tensile Mod., RT, msi*	18.0	8842	20.7/20.5,20.8,20.8
0° Elongation, RT, $\mu in/in$ X 10^3	Record	8842	12.4/13.5,10.6,13.0
Short Beam Shear, RT, ksi	15.0	8843	20.1/20.4,20.0,20.0
Short Beam Shear, $250^o F$, ksi	9.0	8843	13.3/13.4,13.5,13.0
Short Beam Shear, $250^o F$, ksi (24 hr water boil)	7.5	8843	9.8/9.6,9.8,10.0

*Normalized to 0.0416 Panel Thickness
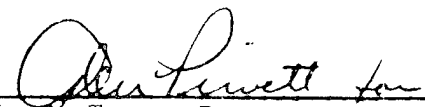
IV. Panel Physical Properties
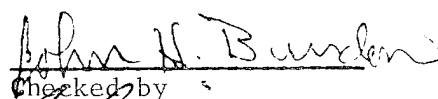
	Spec Req	
Spool No./Panel No.		1/8842
Ply Thickness, inches	0.0052 ± 0.0003	0.0053

V.   Individual Spool Physical Properties

	Average/Individual	Average/Individual
Spec Rec	42 ± 3	145-155
Spool No.	Resin Content, %	Fiber Areal Wt. gm/m^2
7A	43.3/43.4,43.2,43.3	147/146,148,148

L. D. Trump, Representative
QUALITY ASSURANCE DEPARTMENT

Checked by

G. Grimes, NORTHROP

LDT:me/wl

B.2

FINAL INSPECTION REPORT
BW-6000/946 (8-75)

LOT NO.	SPOOL NO.	PRODUCT Magnamite®
1261	7A	3501-6/AS1

FEET FROM START	DEFECT LENGTH	DEFECT TYPE/REMARKS
88'	3'	tow alignment
393'	15"	resin starved
411'	3'	tow alignment
980'	end of spool	

NET FOOTAGE: 972' 9"

INSPECTED BY (SIGNATURE AND STAMP) David Harris

DATE 2 AUG 79
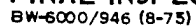
B.3

APPENDIX C

LAMINATE FABRICATION WORK ORDERS

Q. C.

Laminate,

LAMINATE FABRICATION WORK ORDER
PANEL FABRICATION

LAMINATE NO.   ACL __4177__

PREPREG: Resin __3501-6__
Fiber __AS1__
Manufacturer __HERCULES__
Manufacturing Date __7-12-79__
Batch No. _____
Lot No. __1261__
Spool No. __7A__
Material Form __12" TAPE__

LAMINATE: Size __6" X 8"__
No. Plies __16__
Ply Orientation __0°__

LAY UP: Bleeder Type __120 glass__   Plies Bleeder __3:1 (6 ply)__
Peel Ply: Yes/(No) Type _____;   1 side/2 sides.
Type Bag: Rubber/(Nylon)
Pressure Plate: Material __NONE__ ;   Thickness __Lam. Thick. -.083__

CURE: Full vac. + 85 PSI
HEAT To 240°F - Hold 60 Min.
Rise to 100 PSi. - VENT BAg.
HEAT To 350°F - Hold 2 hr.

COMMENTS: Cool To 150°F under pressure
PosT Cure 8 hr @ 350°F

FABRICATOR: __Faucher__

Sales Order __30286__
WPA _____
Date __8-7-79__
Program __Fab/Quality Assurance__ __Program Specimens__
Responsible Engr. __Grimes__

Control Tag Reading _____

0° Dimension __8"__

AVERAGE —	LAMINATE PHYSICALS
% Resin Cont.	28.52200
Sp. gr.	1.62325
% Fiber Vol.	64.45728
% Voids	-0-
Date	8-24-79
Analysis By	Faucher
Approved By	

Date Completed: __8-20-79__

ADHESIVE: _____ BATCH: _____ LOT: _____

RECORDED TEMP OF ROOM: _____°F   RECORDED RELATIVE HUMIDITY: _____

Assembly-A

LAMINATE FABRICATION WORK ORDER
PANEL FABRICATION

LAMINATE NO.   ACL   *4210*   Sales Order *30286*

WPA _____

PREPREG: Resin *3501-6*   Date *9-5-79*

Fiber *AS-1*   Program *Fab/Q.A. Prog. Specms.*

Manufacturer *HERCULES*   Responsible Engr. *Grimes*

Manufacturing Date _____

Batch No. _____

Lot No. *1261*

Spool No. *7-A*   Control Tag Reading _____

Material Form *12" TAPE*

LAMINATE: Size *30" X 60"*   0° Dimension *30"*

No. Plies *30*

Ply Orientation (*±45/0/90/0₂/90/0₂/±45/0/±45/0/±45/0₂/90/0₂/90/0/±45*)

LAY UP: Bleeder Type *120 GLASS*   Plies Bleeder *12 Ply*

Peel Ply: Yes/No; Type _____; 1 side/2 sides.

Type Bag: Rubber/(Nylon)

Pressure Plate: Material *NONE* ;   Thickness ————

CURE: *Full Vac + 85 Psi.*
HEAT To 240°F - hold 60-70 Min.
Rise Pressure To 100 Psi. Vent
Bag. HEAT To 350°F Hold

COMMENTS: *120 Min.*
Cool to 150°F under pressure
Post Cure 8 hr. @ 350°F.

AVERAGE —	LAMINATE PHYSICALS
% Resin Cont _____ Sp. gr. _____ % Fiber Vol. _____ % Voids _____	
Date _____	
Analysis By _____	
Approved By _____	

FABRICATOR: *Fourcher*   Date Completed: _____

ADHESIVE:_____ BATCH:_____ LOT:_____

RECORDED TEMP OF ROOM: _____°F RECORDED RELATIVE HUMIDITY:_____

Assembly - B

LAMINATE FABRICATION WORK ORDER
PANEL FABRICATION

LAMINATE NO.   ACL   *4211*

Sales Order *30286*

WPA _____

PREPREG: Resin   *3501/6*

Date   *9-5-79*

Fiber   *AS-1*

Program _____

Manufacturer   *HERCules*

Responsible Engr. *Grimes*

Manufacturing Date _____

Batch No. _____

Lot No.   *1261*

Spool No.   *7A*

Control Tag Reading _____

Material Form   *12" TAPE*

LAMINATE: Size   *20" x 60"*

0° Dimension   *20"*

No. Plies   *30*

Ply Orientation *(±45/0/90/0₃/90/0₂/∓45/0/∓45/0/∓45/0₃/90/0₂/90/0/∓45)*

LAY UP: Bleeder Type   *120 GLASS*

Plies Bleeder   *12 ply*

Peel Ply: (Yes)/No; Type _____ ;   1 side/(2 sides.)

Type Bag: Rubber/(Nylon)

Pressure Plate: Material   *NONE*   ;   Thickness ————

CURE: *Full VAC + 85 PSI.*
HEAT TO 240°F - HolD 60-70
Min. Rise Pressure To 100 P.S I.
Vent bag.

COMMENTS: *HEAT TO 350°F - Hold 120 Min,*
Cool to 150°F under Pressure
Post Cure 8 hr. @ 350°F

AVERAGE —	LAMINATE PHYSICALS
% Resin Cont	_____
Sp. gr.	_____
% Fiber Vol.	_____
% Voids	_____
Date	_____
Analysis By	_____
Approved By	_____

FABRICATOR: *Fourcher*

Date Completed: *9-14-79*

ADHESIVE:_____ BATCH:_____ LOT: _____

RECORDED TEMP OF ROOM: _____ °F   RECORDED RELATIVE HUMIDITY:_____

LAMINATE FABRICATION WORK ORDER
PANEL FABRICATION

LAMINATE NO.   ACL _4216 #1_

Sales Order _30286_

WPA _____

PREPREG: Resin _8517_

Date _9-13-79_

Fiber _Glass_

Program _Fab. Quality Assuran_ _Prog: Specimins_

Manufacturer _NARMCO_

Responsible Engr. _Grimes_

Manufacturing Date _7-12-79_

Batch No. _9_

Lot No. _____

Spool No. _2_

Control Tag Reading _____

Material Form _38"_

LAMINATE: Size _48" X 38"_

O° Dimension _48"_

No. Plies _15_

Ply Orientation _0°_

LAY UP: Bleeder Type _NONE_

Plies Bleeder _NONE_

Peel Ply: (Yes) No; Type _1 side_ ;   1 side/2 sides.

Type Bag: Rubber (Nylon)

Pressure Plate: Material _NONE_ ;   Thickness _____

CURE: _Full vac + 35±5 p.s.i._ _Heat To 350°F - Hold_ _90 Min, Cool To 150°F_

AVERAGE —	LAMINATE PHYSICALS	
% Resin Cont		
Sp. gr.		
% Fiber Vol.		
% Voids		
Date		
Analysis By		
Approved By		

COMMENTS: _____

FABRICATOR: _Foucher_

Date Completed: _9-12-79_

ADHESIVE: _____ BATCH: _____ LOT: _____

RECORDED TEMP OF ROOM: _____ °F   RECORDED RELATIVE HUMIDITY: _____

APPENDIX D

CURE CYCLE TIME-TEMPERATURE RECORDS

LAMINATE ASSEMBLY A (ACL-4210) AUTOCLAVE CURE CYCLE BASED
ON PART THERMOCOUPLES' TEMPERATURE RECORDINGS VS. TIME
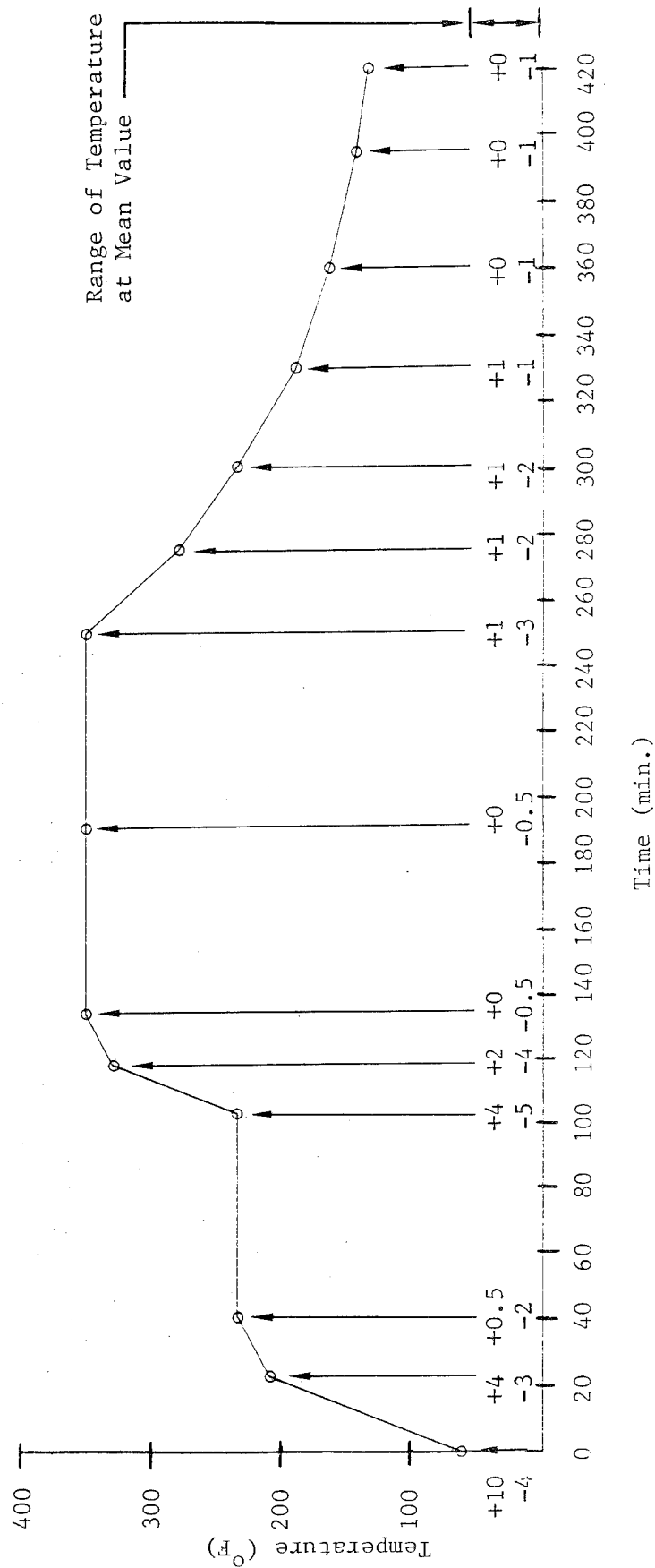
Figure D.1. Part Cure Cycle, Laminate Assembly A
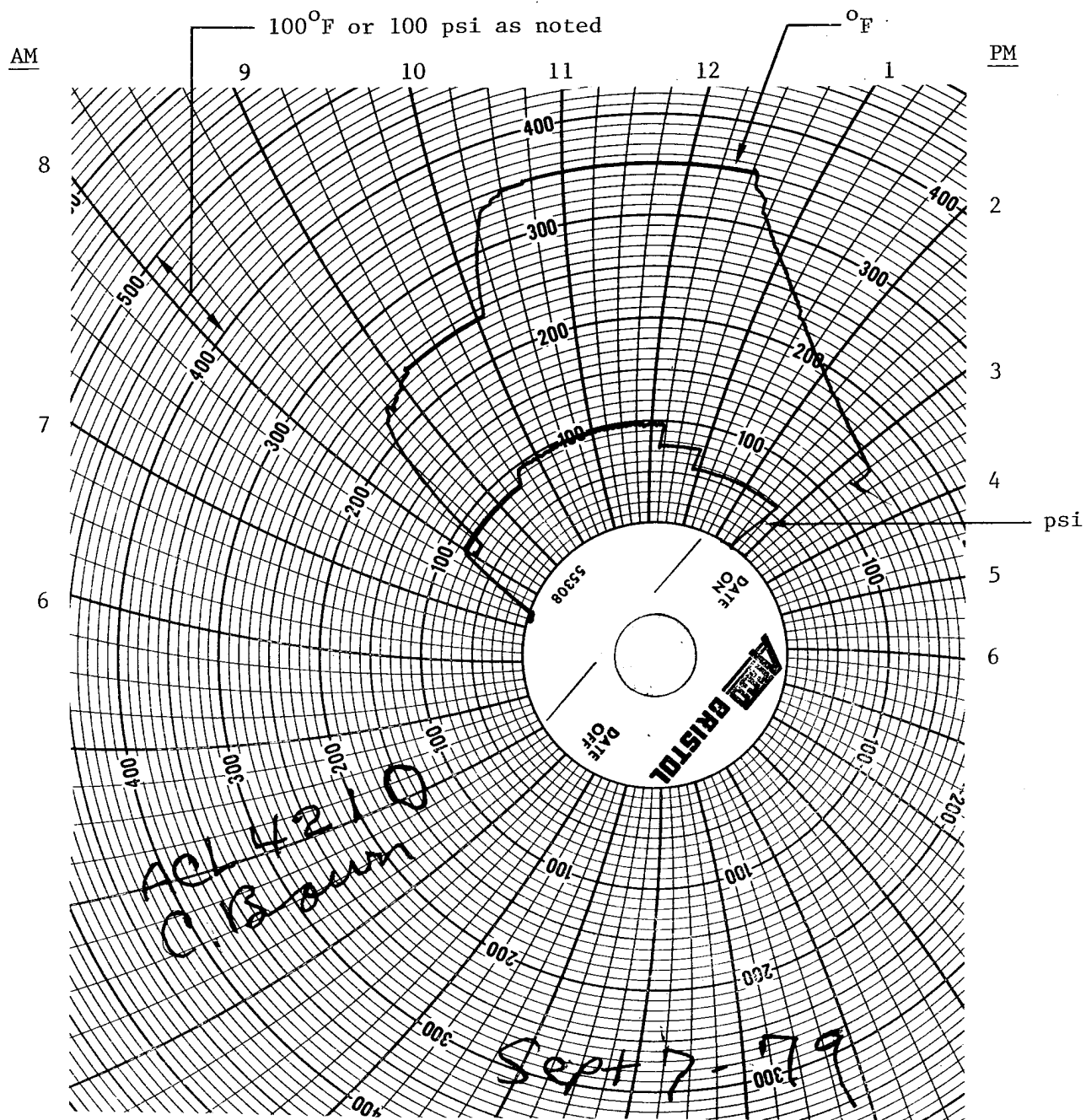
Figure D.2.   Autoclave Pressure and Air Temperature-Time Record,
Laminate Assembly A

APPENDIX E

COMPOSITE TENSILE TEST RESULTS

```
            *** COMPOSITE TENSILE TEST RESULTS ***

14-MAR-80           TEST FRAME I.D. 50.1              BY AM

     SPEC #: GRIMES 3-1          MATERIAL : ACL4210

        *** DATA FILENAME : RKI:B00013.DGT ***

        TEMP : RT              ENVIRONMENT : AIR

    SPEC WIDTH =  .997  IN        SPEC THICK. =  .178  IN

           STROKE XDER RANGE =  .5  IN
           LOAD XDER RANGE =  25  KIPS

        NOMINAL STROKE RATE =  8.33333E-04  IN/SEC
        MEASURED STROKE RATE =  8.30978E-04  IN/SEC

STRAIN GAGE I.D.    STRAIN XDER RANGES    SHUNT CAL STRAIN USED
-----------------------------------------------------------------
   A1L                .0194584              5.00000E-03
   B1L                .0191698              5.00000E-03
   A2T                .0191048              5.00000E-03
   B2T                .0191563              5.00000E-03

        *** STRAIN GAGE G.F. =  2.09  ***
   *** MANUFATURER'S MAX STRAIN LIMIT =  .04  ***

     FAILURE CRITERION USED :  20 % DROP IN LOAD

        *** ULTIMATE LOAD =  19.3942  KIPS ***

     *** ULTIMATE TENSILE STRENGTH =  109.284  KSI ***


*****************************************************************
            GAGE I.D.              STRAIN @ FAILURE
-----------------------------------------------------------------
         A1L                   .0102568
         B1L                   .0103388
         A2T                  -3.79856E-03
         B2T                  -3.53742E-03
-----------------------------------------------------------------


*****************************************************************
                    *** COMMENTS ***

FAILED IN CENTER





*****************************************************************
                                    14-MAR-80
```

E.2

14-MAR-80   TEST FRAME I.D. 50.1   BY AM

SPEC #: GRIMES 3-1   MATERIAL : ACL4210

************* SUMMARY OF LEAST SQUARE FITS *************

REF #	GAGE I.D.	MODULUS KSI	CORRELATION COEFF	STRESS FIT LIMITS KSI
1	A1L	10388.5	.999646	10
	B1L	10569.2	.99982	TO
	A2T	-28350.1	-.999706	40
	B2T	-31211.6	-.999549	

****

*** COMPOSITE TENSION TEST OF SPEC# GRIMES 3-1:ACL4210 ***
*** MAX LOAD = 19.3942 KIPS ***
*** TENSILE STRENGTH = 109.284 KSI ***
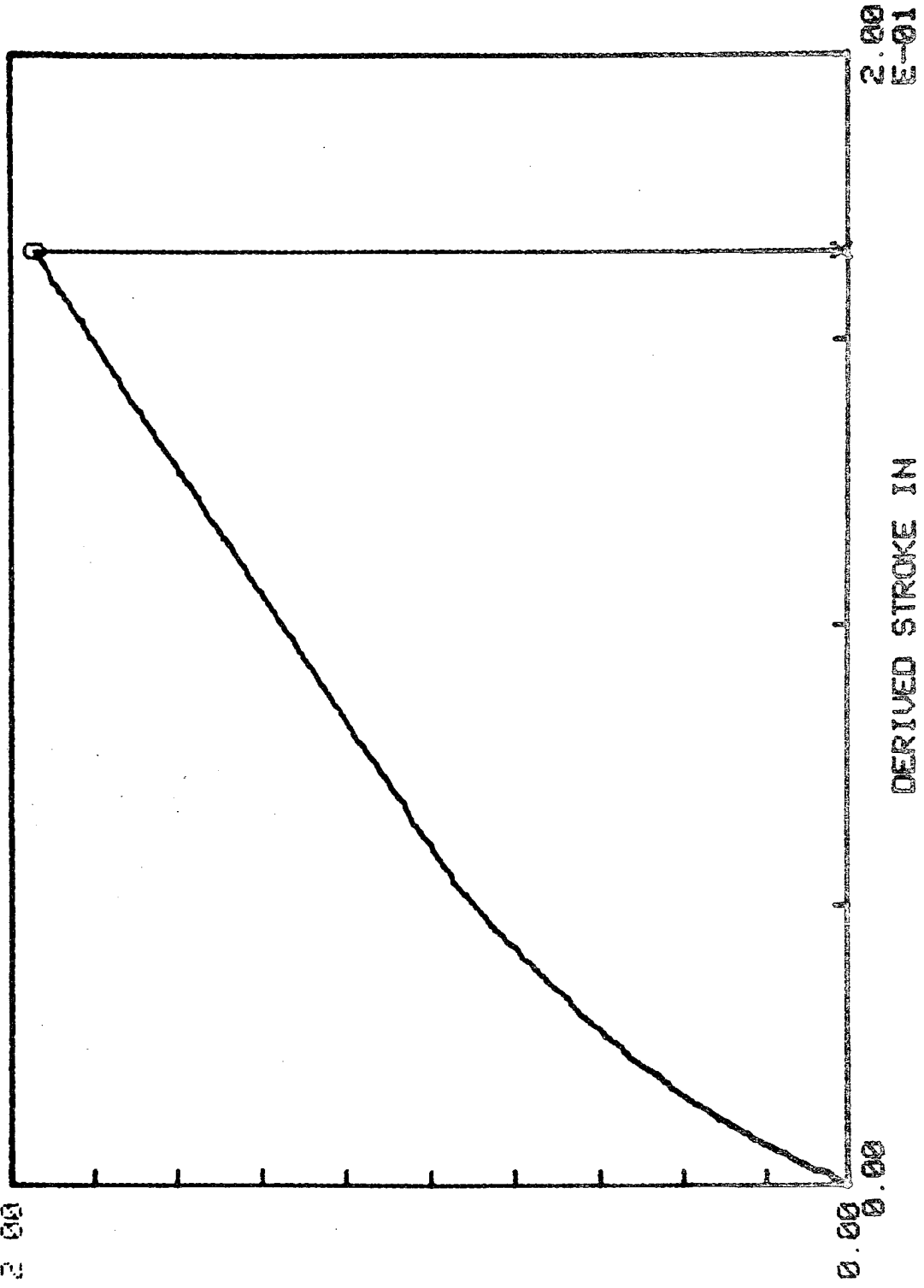
DERIVED STROKE IN

E.4

*** COMPOSITE TENSILE TEST OF SPEC# GRIMES 3-1:ACL4210 ***

REF #1 : A1L
REF #2 : B1L
REF #3 : A2T
REF #4 : B2T

FIT #1

MOD#1= 10388 KSI
MOD#2= 10569 KSI
MOD#3= -28351 KSI
MOD#4= -31212 KSI

E@F#1= .0102568
E@F#2= .0103388
E@F#3= -3.79856E-03
E@F#4= -3.53742E-03

STRAIN COMPONENTS

E.5

```
             *** COMPOSITE TENSILE TEST RESULTS ***

14-MAR-80           TEST FRAME I.D. 50.1              BY AM

    SPEC #: GRIMES 3-2            MATERIAL : ACL4210

       *** DATA FILENAME : RKI:B00014.DGT ***

          TEMP : RT              ENVIRONMENT : AIR

   SPEC WIDTH = 1.015  IN        SPEC THICK. = .18  IN

              STROKE XDER RANGE =  .5  IN
              LOAD XDER RANGE =  25  KIPS

         NOMINAL STROKE RATE = 8.33333E-04  IN/SEC
         MEASURED STROKE RATE = 8.15150E-04  IN/SEC

STRAIN GAGE I.D.      STRAIN XDER RANGES      SHUNT CAL STRAIN USED
--------------------------------------------------------------------
     A1L                 .0193818               5.00000E-03
     B1L                 .0191257               5.00000E-03
     A2T                 .0191093               5.00000E-03
     B2T                 .0191511               5.00000E-03

            *** STRAIN GAGE G.F. = 2.09  ***
      *** MANUFATURER'S MAX STRAIN LIMIT = .04  ***

   FAILURE CRITERION USED :  20 % DROP IN LOAD

      *** ULTIMATE LOAD = 21.446  KIPS ***

      *** ULTIMATE TENSILE STRENGTH = 117.384  KSI ***


**********************************************************************
          GAGE I.D.                 STRAIN @ FAILURE
--------------------------------------------------------------------
     A1L                       .0109455
     B1L                       .011324
     A2T                      -4.02350E-03
     B2T                      -3.88261E-03
--------------------------------------------------------------------


**********************************************************************
                      *** COMMENTS ***

FAILED IN GRIPS




**********************************************************************
                                     14-MAR-80
```

E.6

*** COMPOSITE TENSILE TEST RESULTS ***

14-MAR-80	TEST FRAME I.D. 50.1	BY AM

SPEC #: GRIMES 3-2   MATERIAL : ACL4210

************** SUMMARY OF LEAST SQUARE FITS **************

REF #	GAGE I.D.	MODULUS KSI	CORRELATION COEFF	STRESS FIT LIMITS KSI
1	A1L	10410.1	.999814	10
	B1L	10395.5	.999838	TO
	A2T	-29823	-.999725	40
	B2T	-30166.2	-.999697	

****

*** COMPOSITE TENSILE TEST OF SPEC# GRIMES 3-2:ACL4210 ***

REF #1 : A1L
REF #2 : B1L
REF #3 : A2T
REF #4 : B2T

FIT #1
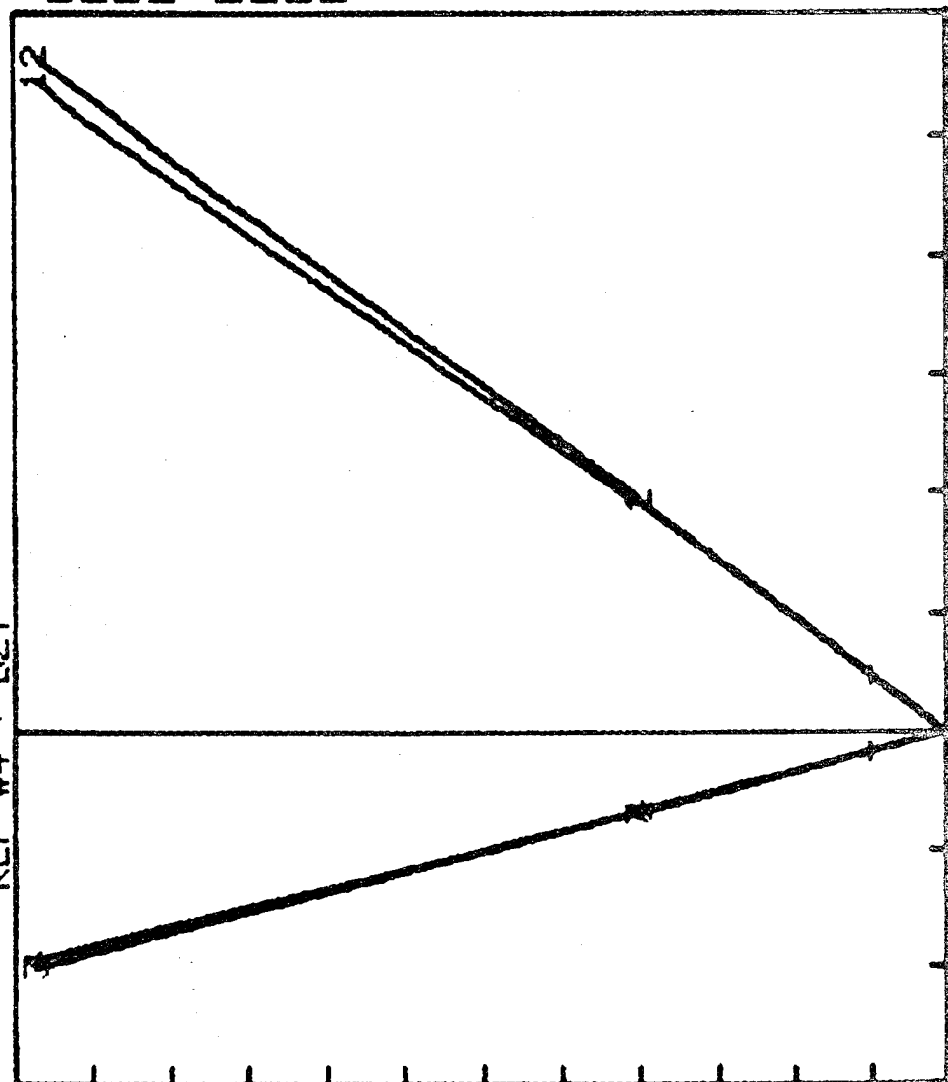
MOD#1= 10410 KSI
MOD#2= 10395 KSI
MOD#3= -29023 KSI
MOD#4= -30167 KSI

EOF#1= .0109455
EOF#2= .011324
EOF#3= -4.02350E-03
EOF#4= -3.88261E-03

STRAIN COMPONENTS

E.8

*** COMPOSITE TENSION TEST OF SPEC# GRIMES 3-2:ACL4210 ***
*** MAX LOAD = 21.446 KIPS ***
*** TENSILE STRENGTH = 117.384 KSI ***

DERIVED STROKE IN

TENSILE LOAD KIPS
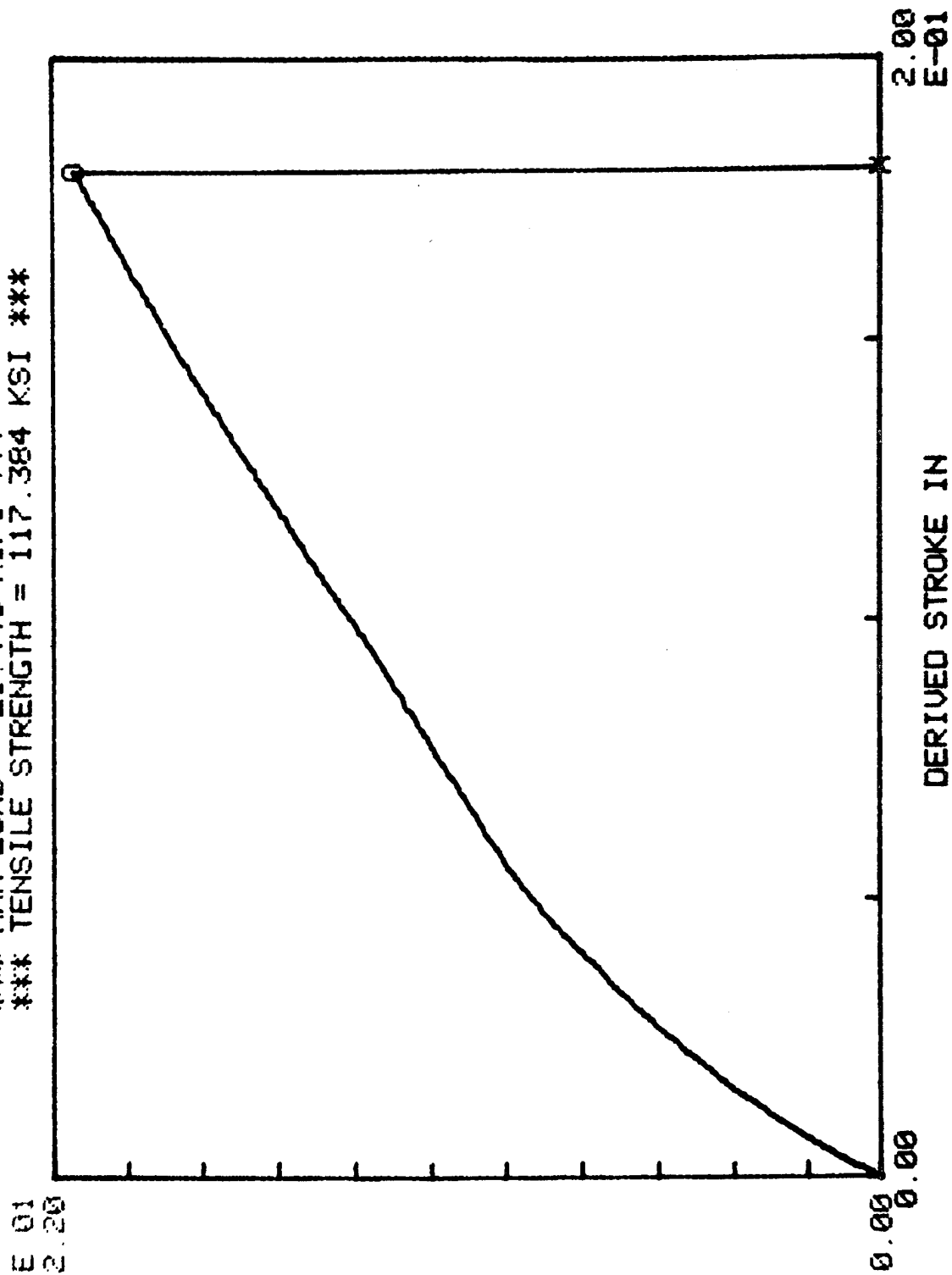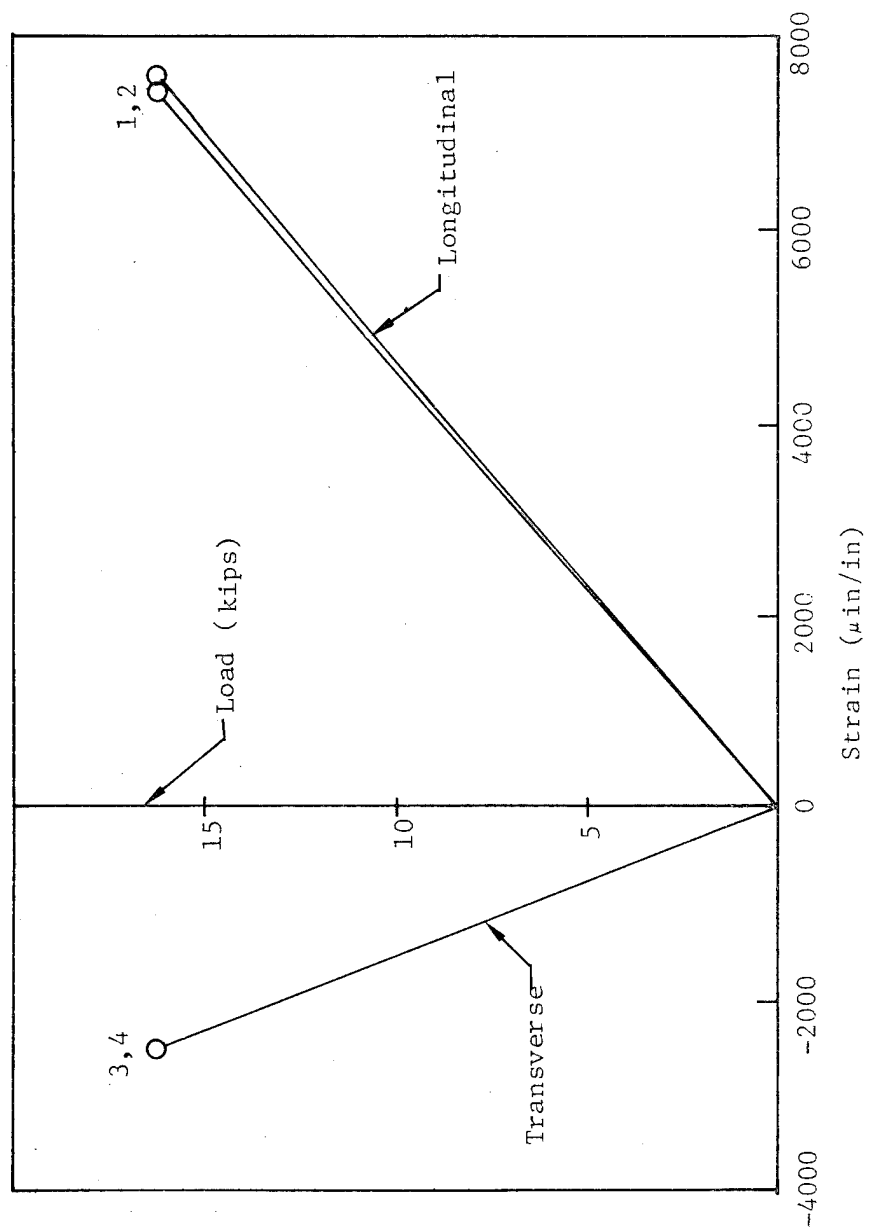
Tensile Specimen ACL 4210A-3-3 Load-Strain Curves, RTD
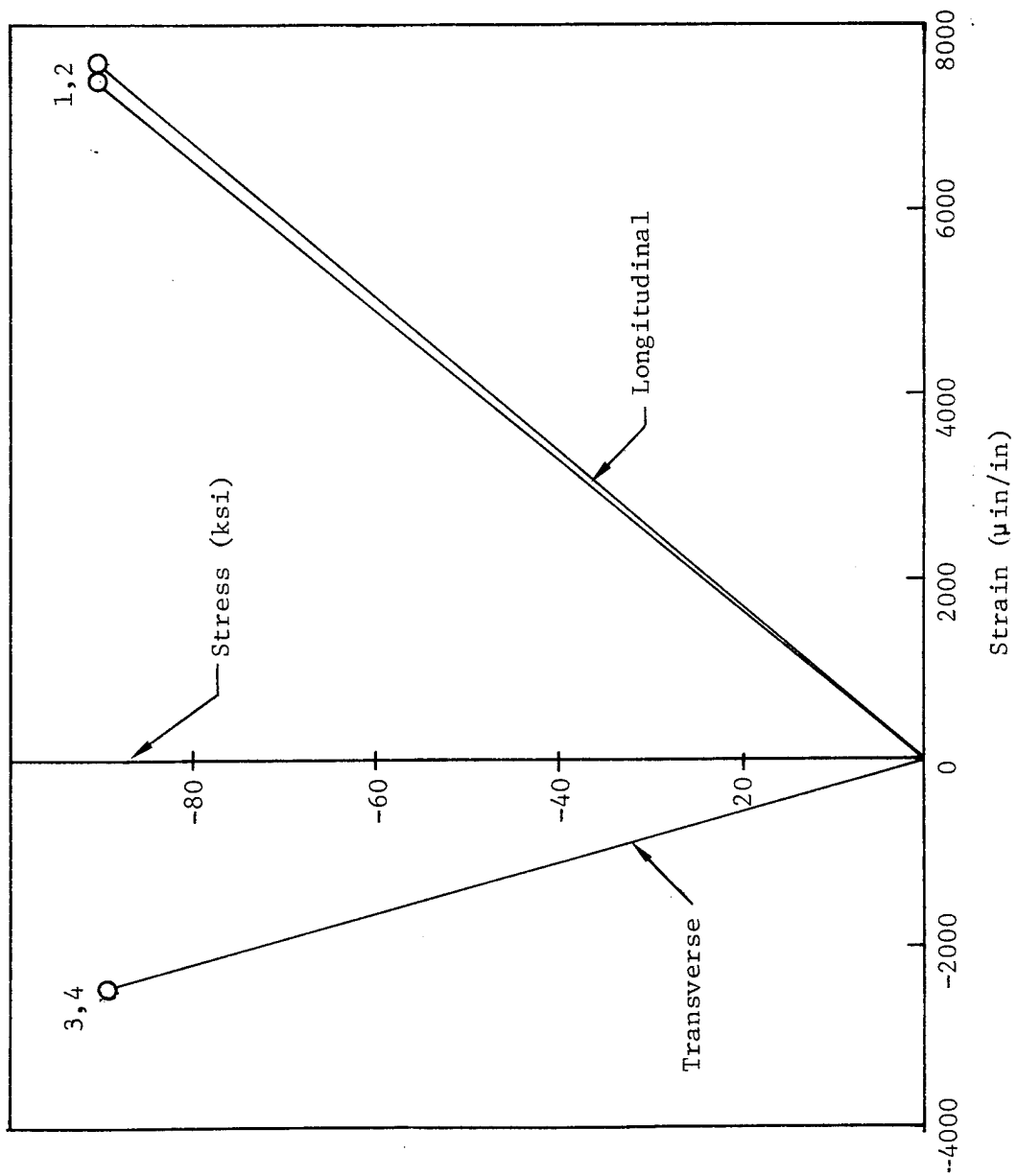
Tensile Specimen ACL 4210A-3-3 Stress-Strain Curves, RTD,

*** COMPOSITE TENSILE TEST RESULTS ***

14-MAR-80   TEST FRAME I.D. 50.1   BY AM

    SPEC #: GRIMES 6-1   MATERIAL : ACL4218

      *** DATA FILENAME : RKI:B00015.DGT ***

      TEMP : RT   ENVIRONMENT : AIR

   SPEC WIDTH = 1.008 IN   SPEC THICK. = .167 IN

            STROKE XDER RANGE = .5 IN
            LOAD XDER RANGE = 25 KIPS

        NOMINAL STROKE RATE = 8.33333E-04 IN/SEC
        MEASURED STROKE RATE = 8.25496E-04 IN/SEC

STRAIN GAGE I.D.   STRAIN XDER RANGES   SHUNT CAL STRAIN USED

    A1L   .0193623   5.00000E-03
    B1L   .0189996   5.00000E-03
    A2T   .0190472   5.00000E-03
    B2T   .0191897   5.00000E-03

        *** STRAIN GAGE G.F. = 2.09 ***
    *** MANUFATURER'S MAX STRAIN LIMIT = .04 ***

    FAILURE CRITERION USED : 20 % DROP IN LOAD

      *** ULTIMATE LOAD = 18.4985 KIPS ***

      *** ULTIMATE TENSILE STRENGTH = 109.843 KSI ***

****
        GAGE I.D.   STRAIN @ FAILURE

        A1L   -3.83083E-03
        B1L   .0107575
        A2T   .0110078
        B2T   -3.77795E-03

****
                    *** COMMENTS ***

FAILED IN TEST SECTION

****
                                        17-MAR-80

E.12

*** COMPOSITE TENSILE TEST RESULTS ***

14-MAR-88   TEST FRAME I.D. 50.1   BY AM

    SPEC #: GRIMES 6-1   MATERIAL : ACL4210

    ************* SUMMARY OF LEAST SQUARE FITS *************

REF #	GAGE I.D.	MODULUS KSI	CORRELATION COEFF	STRESS FIT LIMITS KSI
1	A1L	-20100.6	-.999742	63
	B1L	10290.6	.999935	TO
	A2T	10081.3	.999901	93
	B2T	-29036	-.99977	

    ****

*** COMPOSITE TENSILE TEST OF SPEC# GRIMES 6-1:ACL4210 ***

REF #1 : A1L
REF #2 : B1L
REF #3 : A2T
REF #4 : B2T

MOD#1= -28750 KSI
MOD#2= 10236 KSI
MOD#3= 10098 KSI
MOD#4= -28831 KSI

E0F#1= -3.83083E-03
E0F#2= .0107575
E0F#3= .0110078
E0F#4= -3.77795E-03

STRESS KSI

STRAIN COMPONENTS
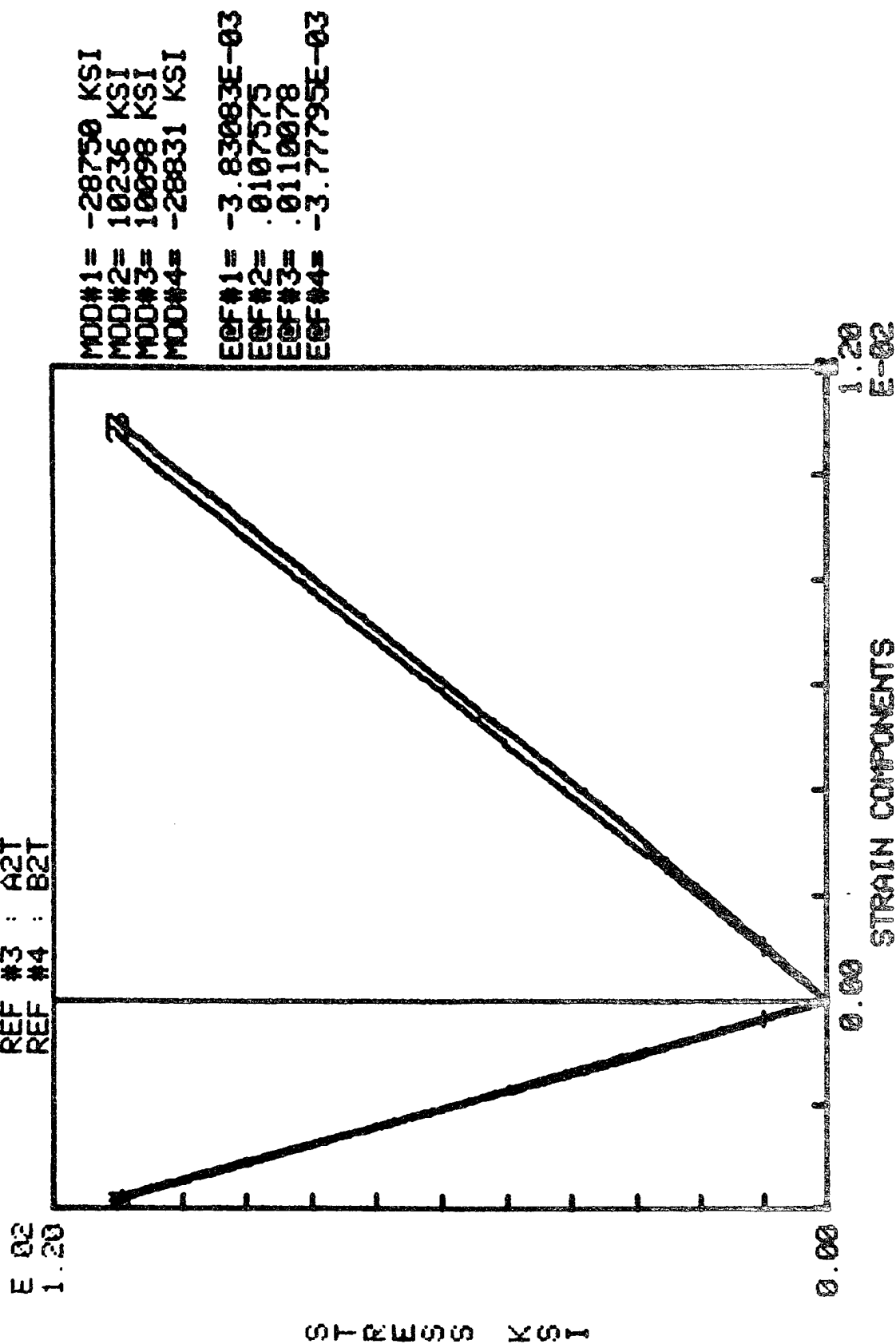
*** COMPOSITE TENSION TEST OF SPEC# GRIMES 6-1:ACL4210 ***
*** MAX LOAD = 18.4905 KIPS ***
*** TENSILE STRENGTH = 109.843 KSI ***

TENSILE LOAD KIPS

DERIVED STROKE IN
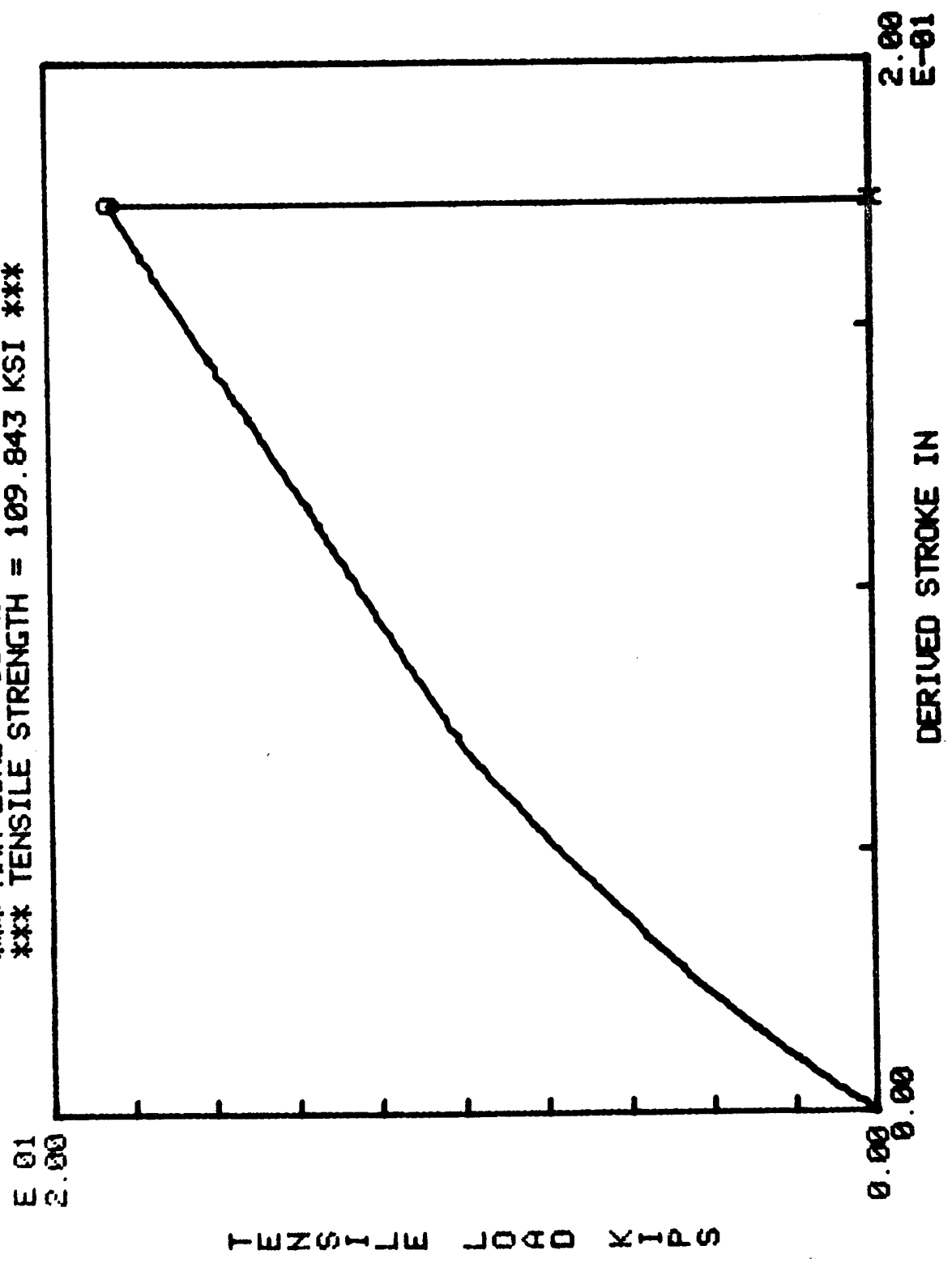
```
*** COMPOSITE TENSILE TEST RESULTS ***

18-MAR-80              TEST FRAME I.D. 50.1                    BY AM

       SPEC #: GRIMES 6-2              MATERIAL : ACL4210

           *** DATA FILENAME : RK1:B00020.DGT ***

           TEMP : RT                   ENVIRONMENT : AIR

       SPEC WIDTH =  1.009  IN      SPEC THICK. =  .167  IN

                STROKE XDER RANGE =  .5  IN
                LOAD XDER RANGE =  25  KIPS

           NOMINAL STROKE RATE =  8.33333E-04  IN/SEC
           MEASURED STROKE RATE =  8.23307E-04  IN/SEC

STRAIN GAGE I.D.      STRAIN XDER RANGES      SHUNT CAL STRAIN USED
----------------------------------------------------------------------
    A1L                  .0193363                  5.00000E-03
    B1L                  .0190676                  5.00000E-03
    A2T                  .01911                    5.00000E-03
    B2T                  .0191695                  5.00000E-03

               *** STRAIN GAGE G.F. =  2.09  ***
       *** MANUFATURER'S MAX STRAIN LIMIT =  .04  ***

       FAILURE CRITERION USED :  20 % DROP IN LOAD

           *** ULTIMATE LOAD =  18.466  KIPS ***

           *** ULTIMATE TENSILE STRENGTH =  109.589  KSI ***


*************************************************************************
           GAGE I.D.                   STRAIN @ FAILURE
-----------------------------------------------------------------------
       A1L                          .0108536
       B1L                          .0107122
       A2T                          -3.75292E-03
       B2T                          -3.78332E-03
-----------------------------------------------------------------------

*************************************************************************
                       *** COMMENTS ***

SPECIMEN FAILED IN THIN SECTION




*************************************************************************
                         18-MAR-80
```

E.16

*** COMPOSITE TENSILE TEST RESULTS ***

SPEC #: GRIMES 6-2   MATERIAL : ACL4210

************* SUMMARY OF LEAST SQUARE FITS *************

REF #	GAGE I.D.	MODULUS KSI	CORRELATION COEFF	STRESS FIT LIMITS KSI
1	A1L	9799.6	.999856	10
	B1L	10218.7	.999801	TO
	A2T	-28787.6	-.999689	40
	B2T	-28925.5	-.999759	

****

*** COMPOSITE TENSION TEST OF SPEC# GRIMES 6-2:ACL4210 ***
*** MAX LOAD = 18.466 KIPS ***
*** TENSILE STRENGTH = 109.589 KSI ***
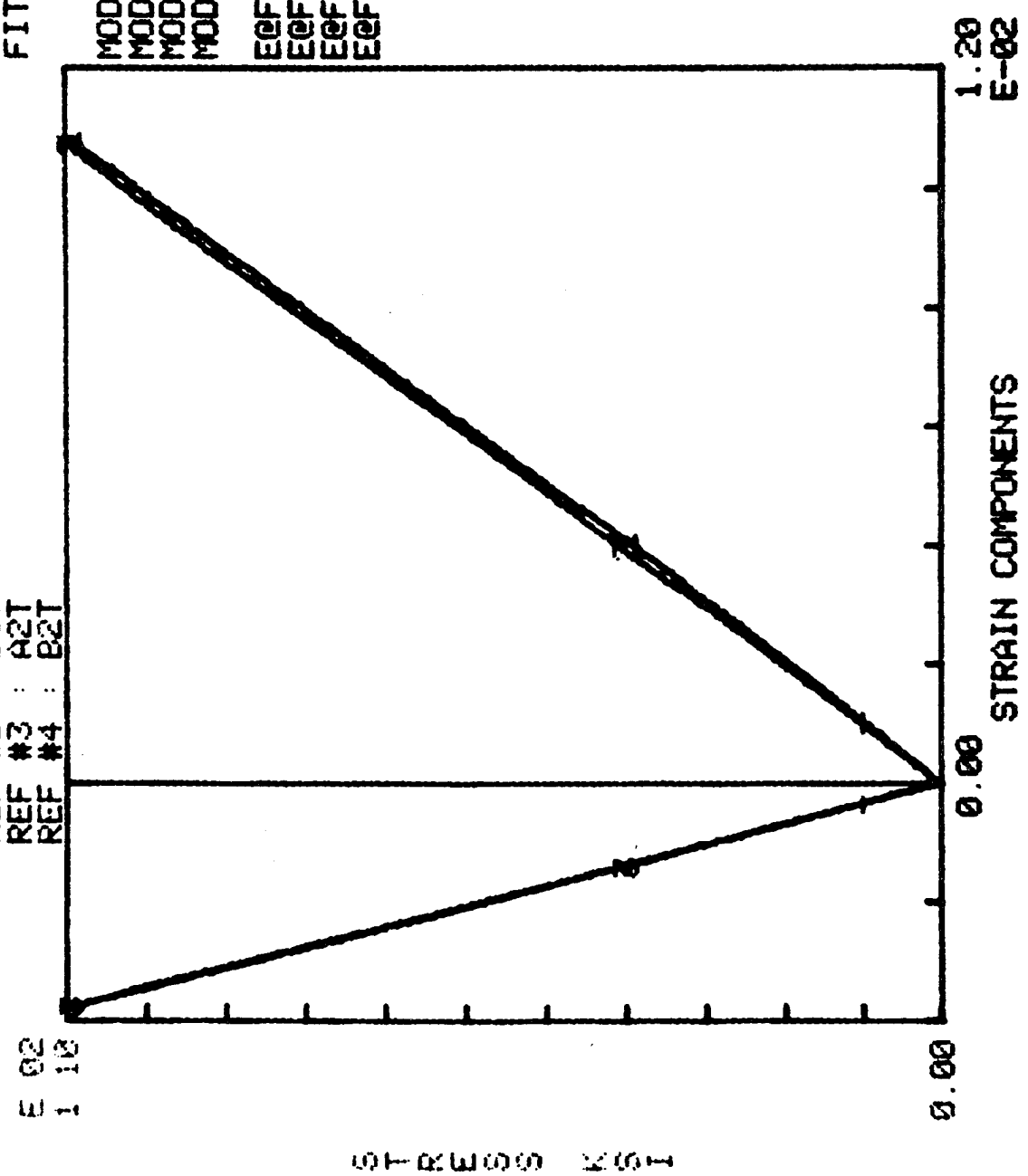
DERIVED STROKE IN

TENSION LOAD KIPS
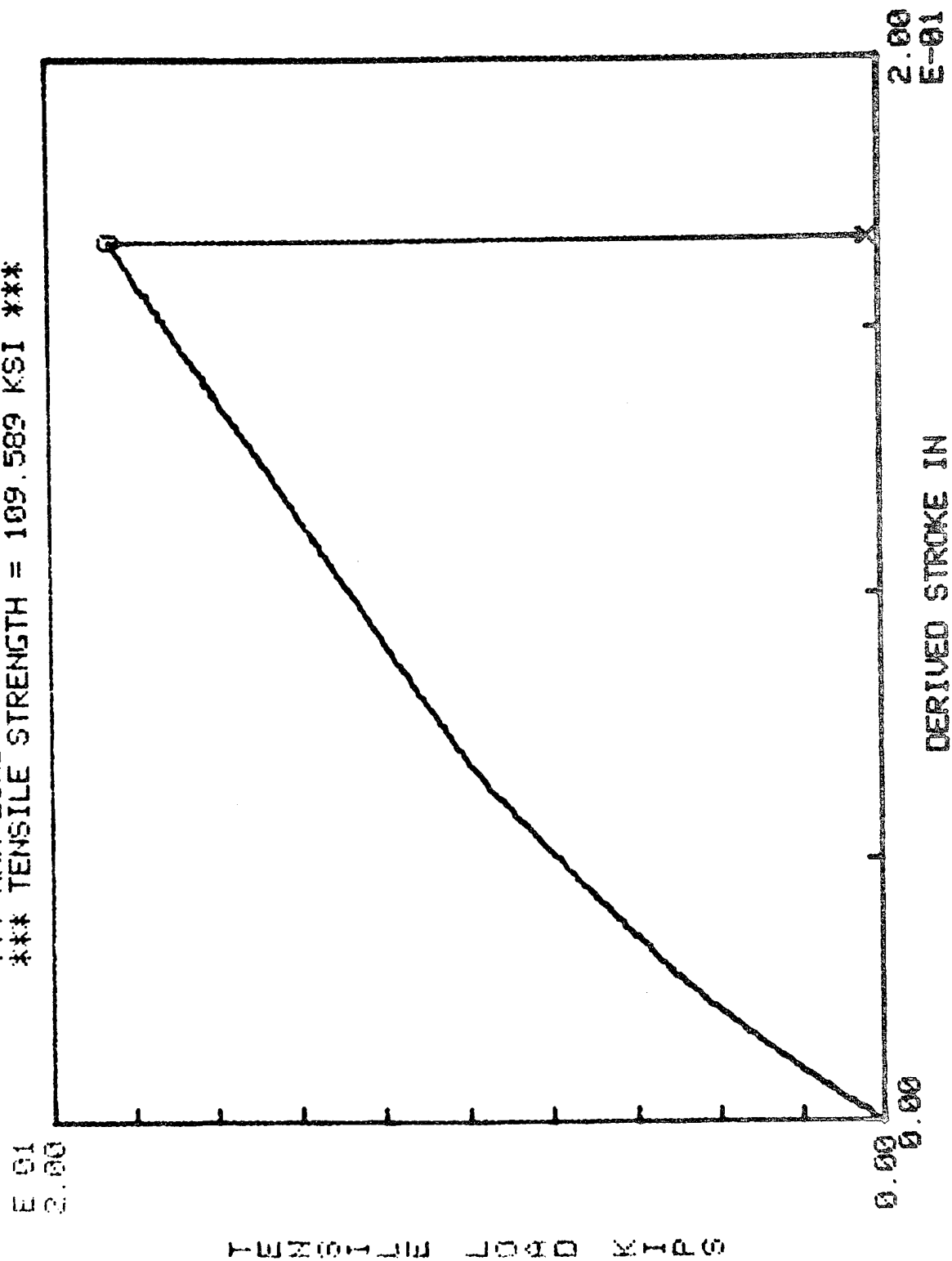
*** COMPOSITE TENSILE TEST OF SPEC# GRIMES 6-2:ACL4210 ***

REF #1 : A1L
REF #2 : B1L
REF #3 : A2T
REF #4 : B2T

FIT #1

MOD#1= 9799 KSI
MOD#2= 10218 KSI
MOD#3= -28788 KSI
MOD#4= -28926 KSI

E@F#1= .0108536
E@F#2= .0107122
E@F#3= -3.75292E-03
E@F#4= -3.78332E-03

STRAIN COMPONENTS

STRESS KSI

1.20
E-02

0.00

E.19

```
                    *** COMPOSITE TENSILE TEST RESULTS ***

18-MAR-80              TEST FRAME I.D. 50.1                    BY AM


        SPEC #: GRIMES 6-3              MATERIAL : ACL4210


            *** DATA FILENAME : RK1:B80016.DGT ***


            TEMP : RT                  ENVIRONMENT : AIR


        SPEC WIDTH =  1.012  IN        SPEC THICK. = .166  IN


                STROKE XDER RANGE = .5  IN
                LOAD XDER RANGE = 25  KIPS


            NOMINAL STROKE RATE = 8.33333E-04  IN/SEC
            MEASURED STROKE RATE = 8.21089E-04  IN/SEC


    STRAIN GAGE I.D.     STRAIN XDER RANGES      SHUNT CAL STRAIN USED
    -----------------------------------------------------------------

        A1L                 .0193397               5.00000E-03
        B1L                 .0190598               5.00000E-03
        A2T                 .019119                5.00000E-03
        B2T                 .0192085               5.00000E-03


            *** STRAIN GAGE G.F. =  2.09  ***
        *** MANUFATURER'S MAX STRAIN LIMIT = .04  ***


        FAILURE CRITERION USED :  20 % DROP IN LOAD


            *** ULTIMATE LOAD = 17.4402  KIPS ***


            *** ULTIMATE TENSILE STRENGTH =  103.815  KSI ***


    ***************************************************************
                GAGE I.D.                  STRAIN @ FAILURE
    -----------------------------------------------------------------

            A1L                        .0103548
            B1L                        .0100932
            A2T                       -3.63326E-03
            B2T                       -3.60336E-03
    -----------------------------------------------------------------


    ***************************************************************
                        *** COMMENTS ***

SPECIMEN FAILED IN GRIP








    ***************************************************************
                              18-MAR-80
```
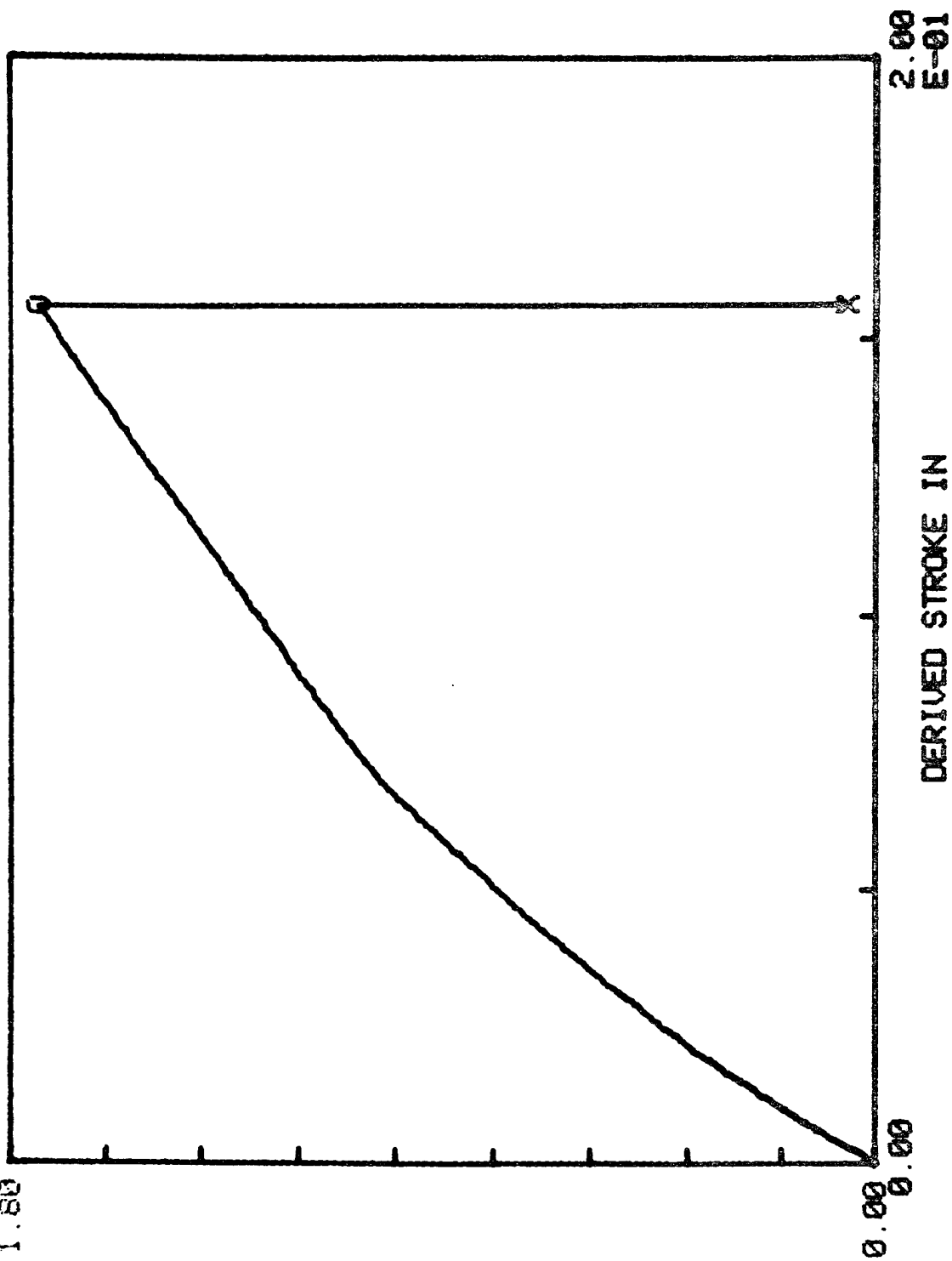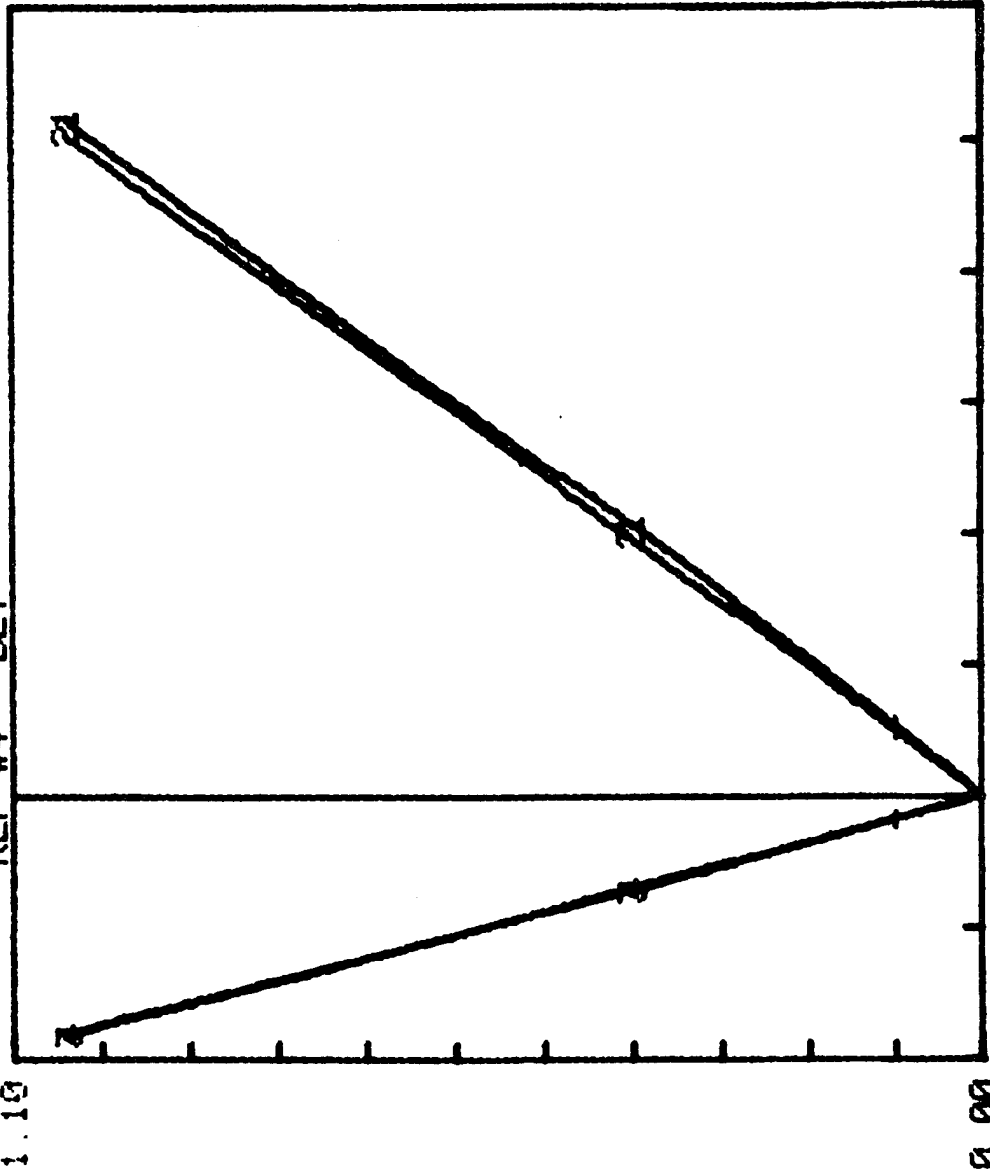
*** COMPOSITE TENSILE TEST RESULTS ***

18-MAR-80	TEST FRAME I.D. 50.1	BY AM

SPEC #: GRIMES 6-3   MATERIAL : ACL4210

************* SUMMARY OF LEAST SQUARE FITS **************

REF #	GAGE I.D.	MODULUS KSI	CORRELATION COEFF	STRESS FIT LIMITS KSI
1	A1L	9702.37	.999816	10
	B1L	10396	.999745	TO
	A2T	-27923.2	-.999624	40
	B2T	-29199.1	-.999661	

****

E.21

*** COMPOSITE TENSION TEST OF SPEC# GRIMES 6-3:ACL4210 ***
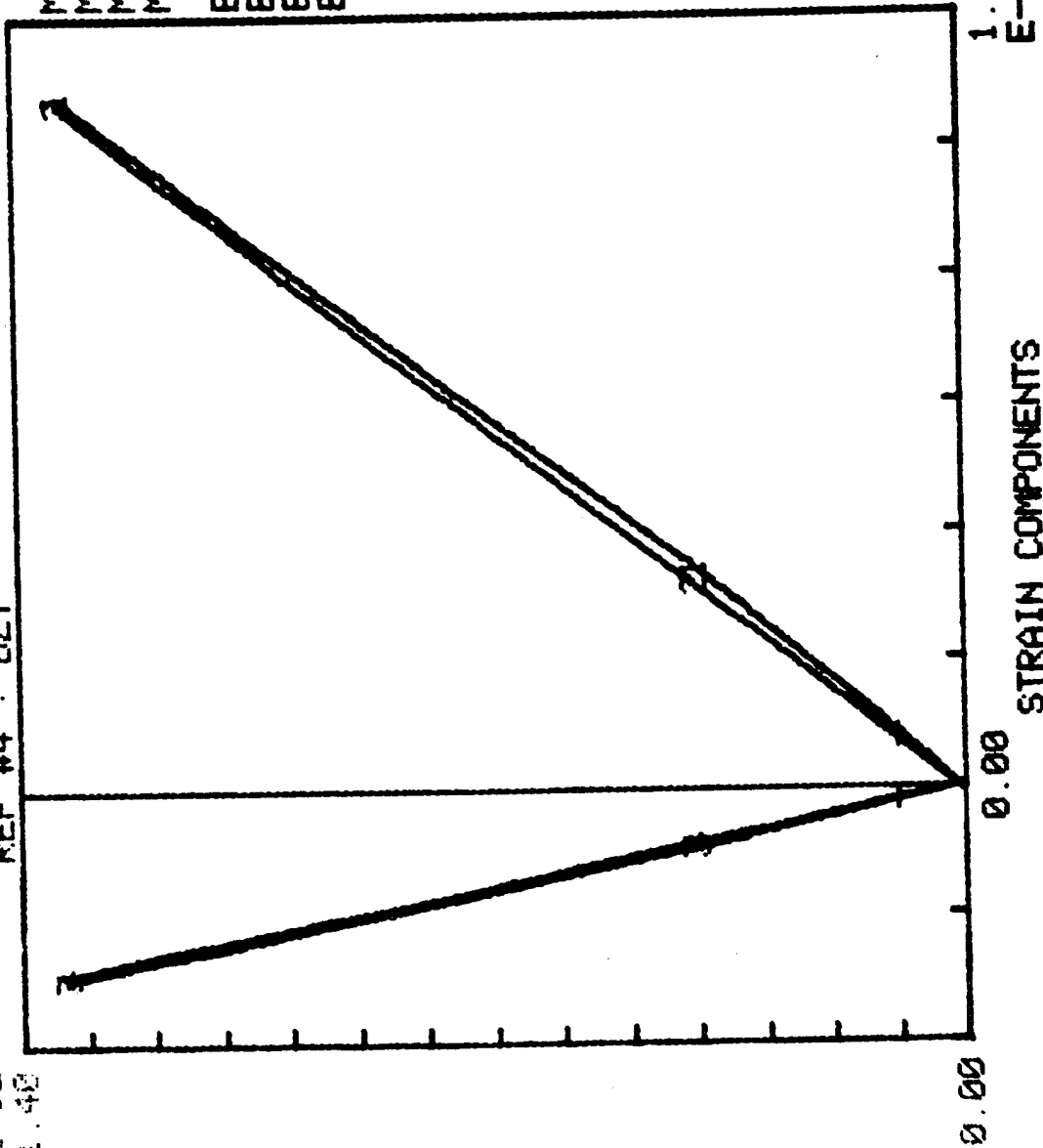*** MAX LOAD = 17.4402 KIPS ***
*** TENSILE STRENGTH = 103.815 KSI ***

E.22

*** COMPOSITE TENSILE TEST OF SPEC# GRIMES 6-3:ACL4210 ***

FIT #1

REF #1 : A1L
REF #2 : B1L
REF #3 : A2T
REF #4 : B2T

MOD#1= 9702 KSI
MOD#2= 10396 KSI
MOD#3= -27924 KSI
MOD#4= -29200 KSI

E@F#1= .0103548
E@F#2= .0100932
E@F#3= -3.63326E-03
E@F#4= -3.60336E-03

STRAIN COMPONENTS

STRESS KSI

```
            *** COMPOSITE TENSILE TEST RESULTS ***

18-MAR-88            TEST FRAME I.D. 50.1                    BY AM
```

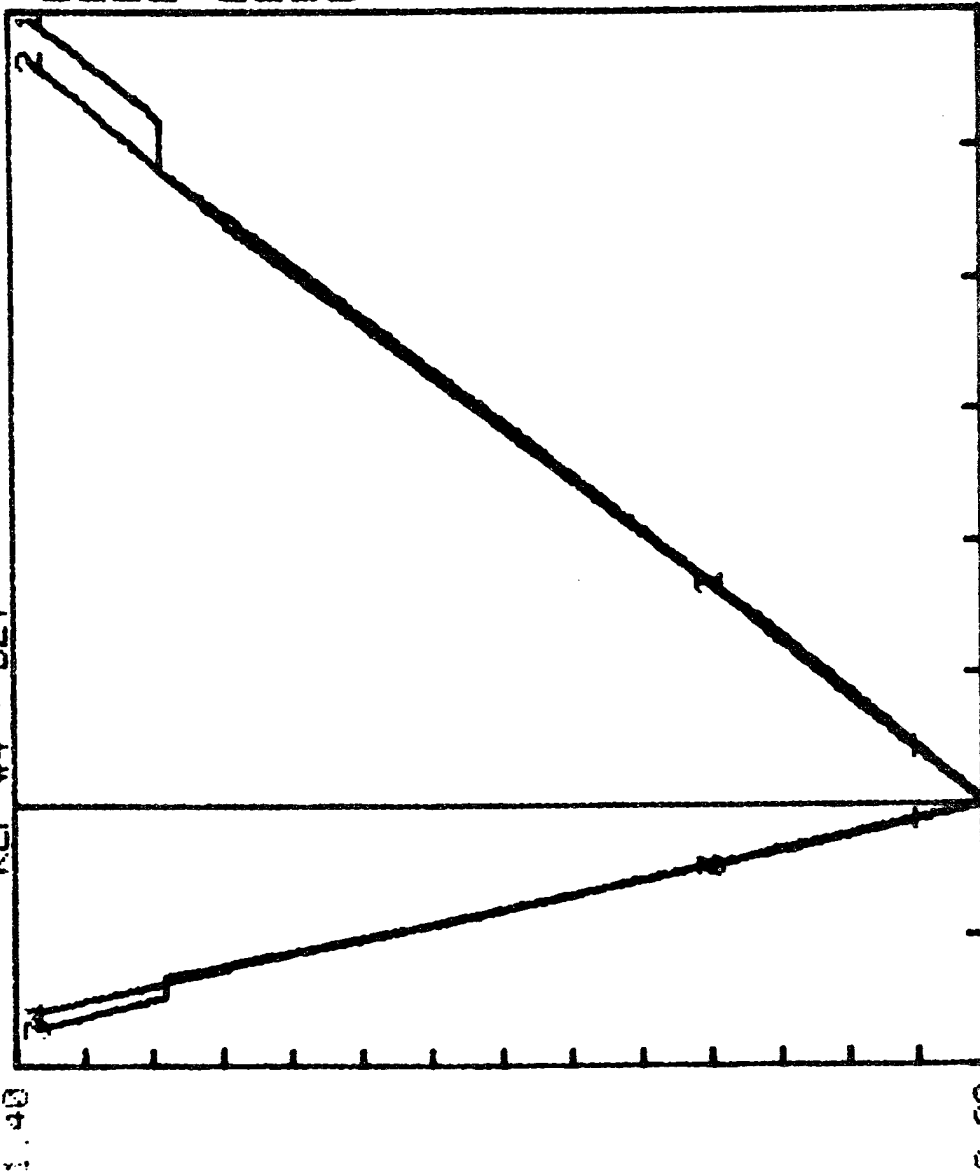   SPEC #: GRIMES 9-1   MATERIAL : ACL4210

            *** DATA FILENAME : RK1:B00017.DGT ***

            TEMP : RT   ENVIRONMENT : AIR

        SPEC WIDTH = 1.014 IN   SPEC THICK. = .149   IN

                STROKE XDER RANGE =   .5 IN
                LOAD XDER RANGE =   25 KIPS

            NOMINAL STROKE RATE = 8.33333E-04   IN/SEC
            MEASURED STROKE RATE = 8.33285E-04   IN/SEC

STRAIN GAGE I.D.   STRAIN XDER RANGES   SHUNT CAL STRAIN USED

    A1L   .0192678   5.00000E-03
    B1L   .0190022   5.00000E-03
    A2T   .0191302   5.00000E-03
    B2T   .0192018   5.00000E-03

            *** STRAIN GAGE G.F. = 2.09 ***
    *** MANUFATURER'S MAX STRAIN LIMIT = .04 ***

    FAILURE CRITERION USED : 20 % DROP IN LOAD

        *** ULTIMATE LOAD = 20.0904 KIPS ***

        *** ULTIMATE TENSILE STRENGTH = 132.973 KSI ***

****
            GAGE I.D.   STRAIN @ FAILURE

            A1L   .0108152
            B1L   .0106939
            A2T   -2.96251E-03
            B2T   -2.87042E-03

****
                    *** COMMENTS ***

SPECIMEN FAILED IN CENTER OF THIN SECTION

****
                    18-MAR-88
```

E.24

| 18-MAR-88 | TEST FRAME I.D. 50.1 | BY AM |

SPEC #: GRIMES 9-1          MATERIAL : ACL4210

************* SUMMARY OF LEAST SQUARE FITS **************

| REF | GAGE | MODULUS | CORRELATION | STRESS FIT |
| # | I.D. | KSI | COEFF | LIMITS KSI |
| 1 | A1L | 11642.9 | .999817 | 10 |
|   | B1L | 12447.3 | .999807 | TO |
|   | A2T | -42442.1 | -.999469 | 40 |
|   | B2T | -46188.6 | -.999337 | |

**********************************************************

*** COMPOSITE TENSION TEST OF SPEC# GRIMES 9-1:ACL4210 ***
*** MAX LOAD = 20.0904 KIPS ***
*** TENSILE STRENGTH = 132.973 KSI ***

DERIVED STROKE IN

TENSILE DISC DELTA XHALB

E.26

*** COMPOSITE TENSILE TEST OF SPEC# GRIMES 9-1:ACL4210 ***

REF #1 : A1L
REF #2 : B1L
REF #3 : A2T
REF #4 : B2T

FIT #1

MOD#1= 11642 KSI
MOD#2= 12447 KSI
MOD#3= -42443 KSI
MOD#4= -46189 KSI

EOF#1= .0108152
EOF#2= .0106939
EOF#3= -2.96251E-03
EOF#4= -2.87042E-03

STRESS KSI

STRAIN COMPONENTS

1.40 E 02

0.00

0.00    1.20 E-02

```
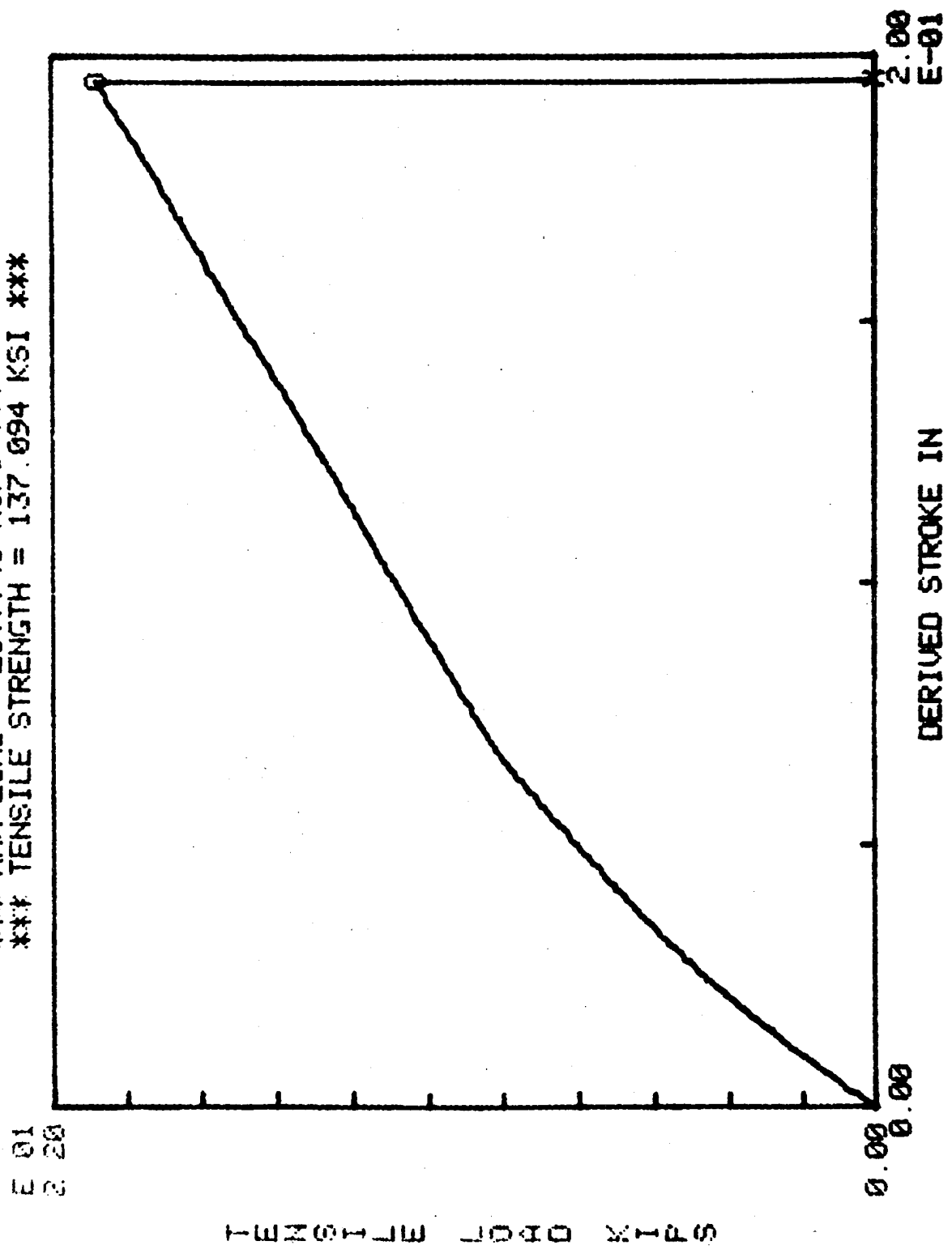*** COMPOSITE TENSILE TEST RESULTS ***
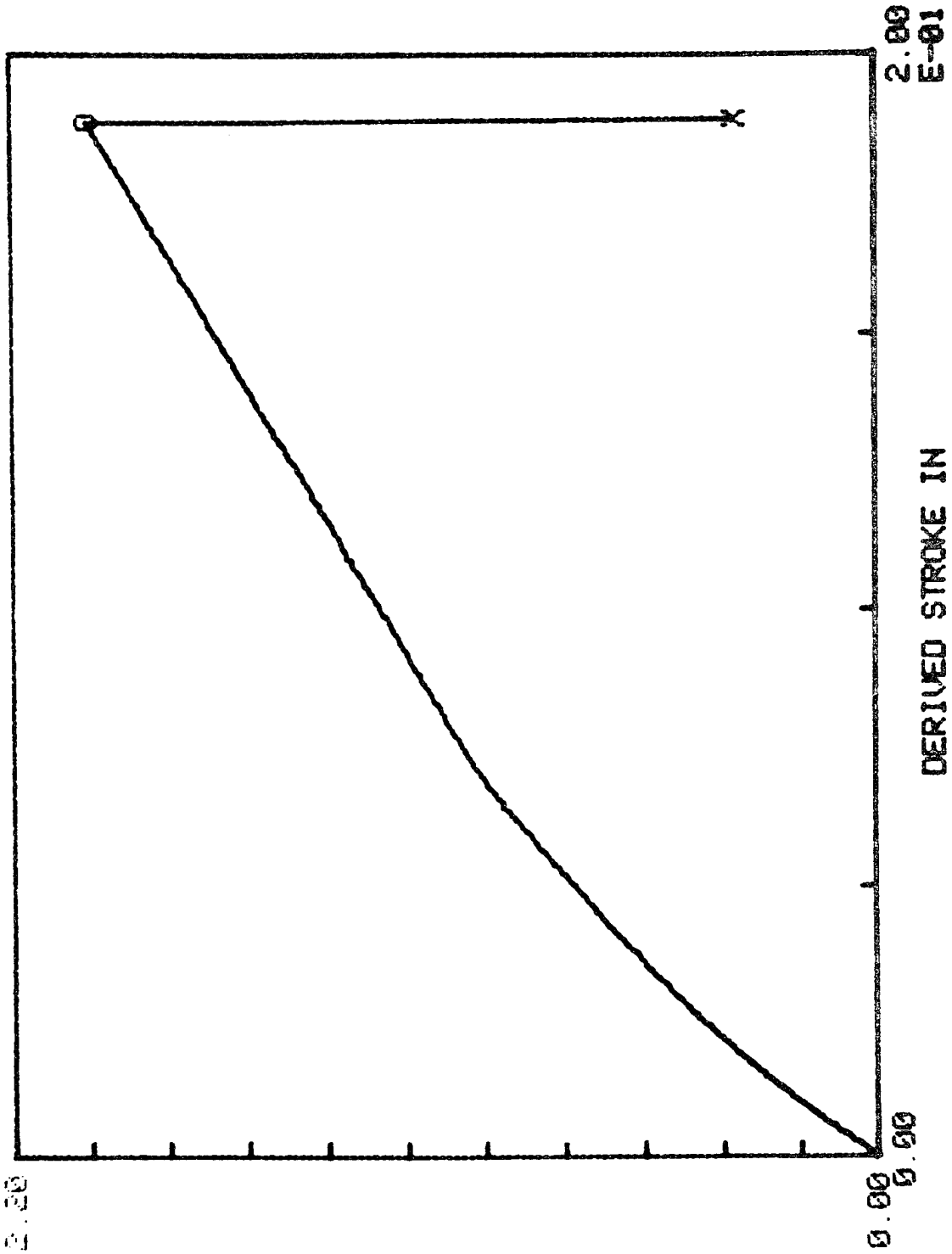
18-MAR-88            TEST FRAME I.D. 50.1                BY AM

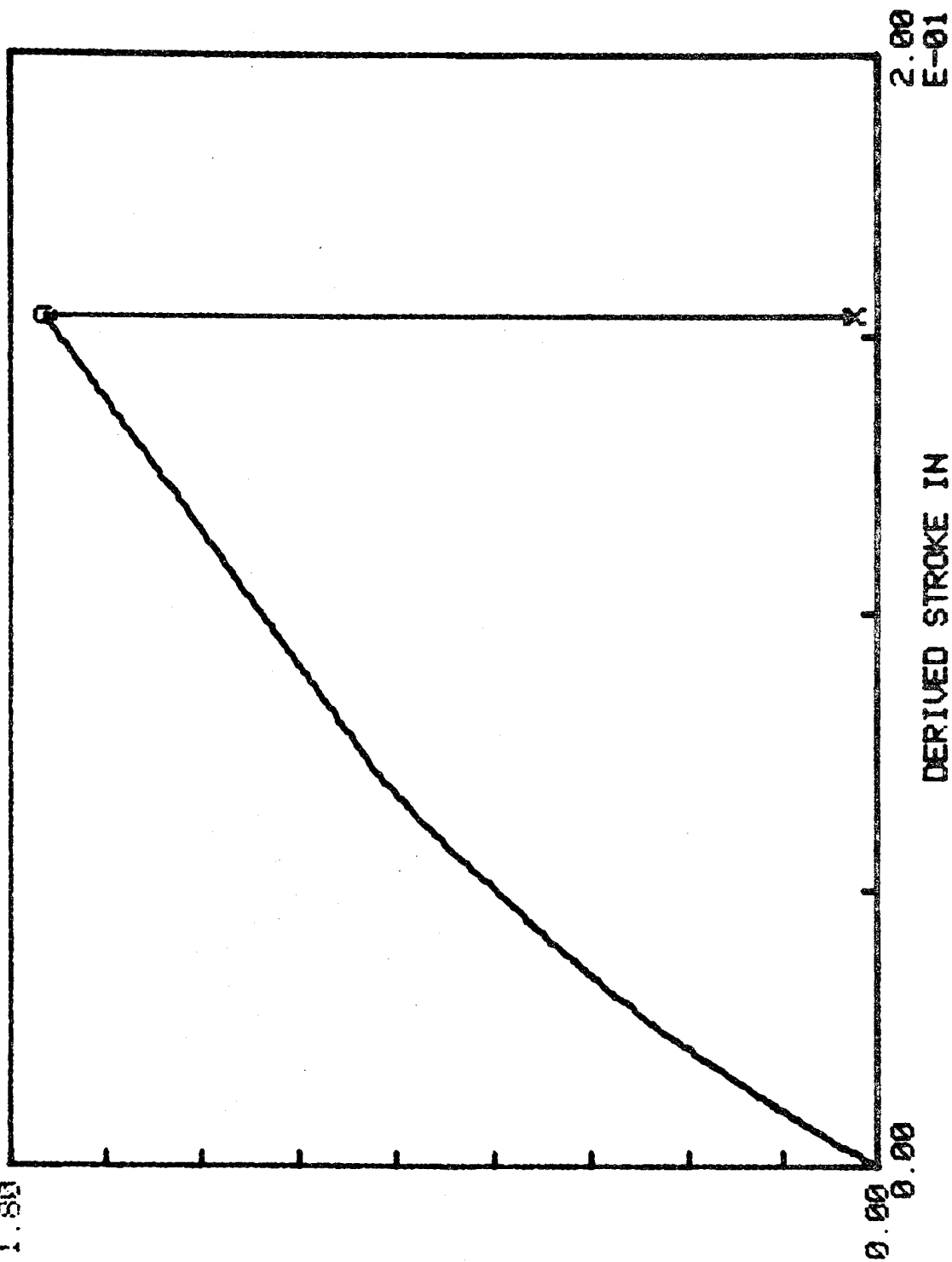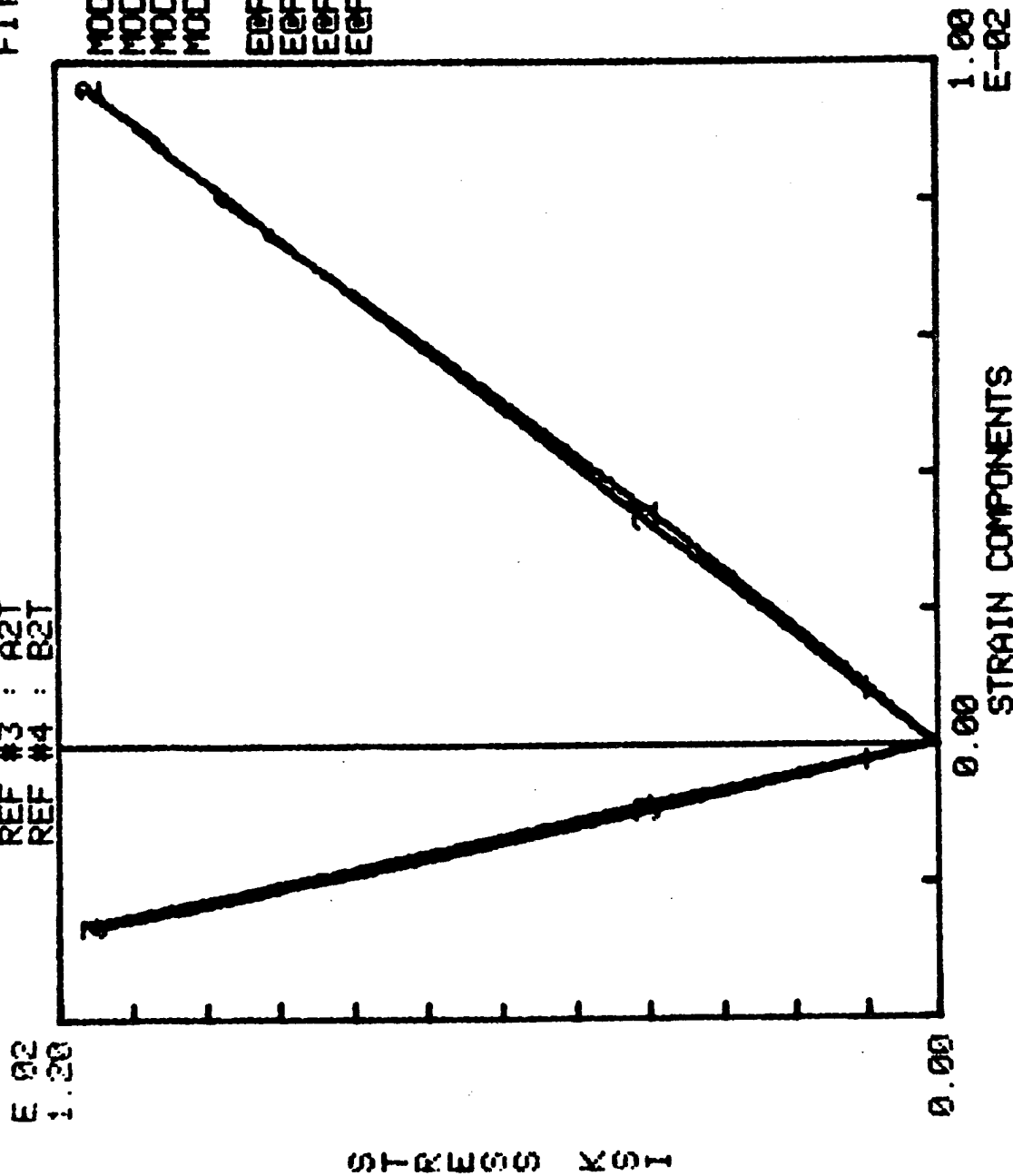        SPEC #: GRIMES 9-2              MATERIAL : ACL4210

          *** DATA FILENAME : RK1:B00021.DGT ***

          TEMP : RT                     ENVIRONMENT : AIR

        SPEC WIDTH = 1.017 IN          SPEC THICK. = .149 IN

                  STROKE XDER RANGE = .5 IN
                  LOAD XDER RANGE = 25 KIPS

          NOMINAL STROKE RATE = 8.33333E-04 IN/SEC
          MEASURED STROKE RATE = 8.32644E-04 IN/SEC

STRAIN GAGE I.D.    STRAIN XDER RANGES      SHUNT CAL STRAIN USED
--------------------------------------------------------------------
    A1L                .0193382            5.00000E-03
    B1L                .0190569            5.00000E-03
    A2T                .0191175            5.00000E-03
    B2T                .0192018            5.00000E-03

          *** STRAIN GAGE G.F. = 2.09 ***
     *** MANUFATURER'S MAX STRAIN LIMIT = .04 ***

    FAILURE CRITERION USED : 20 % DROP IN LOAD

        *** ULTIMATE LOAD = 20.7743 KIPS ***

        *** ULTIMATE TENSILE STRENGTH = 137.094 KSI ***


***********************************************************************
        GAGE I.D.                      STRAIN @ FAILURE
--------------------------------------------------------------------
        A1L                            .0118844
        B1L                            .0112833
        A2T                            -3.42751E-03
        B2T                            -3.16121E-03
--------------------------------------------------------------------


***********************************************************************
                    *** COMMENTS ***

SPECIMEN FAILED IN GRIP




***********************************************************************
                              18-MAR-88
```

18-MAR-88   TEST FRAME I.D. 50.1   BY AM

SPEC #: GRIMES 9-2   MATERIAL : ACL4210

************** SUMMARY OF LEAST SQUARE FITS **************

REF #	GAGE I.D.	MODULUS KSI	CORRELATION COEFF	STRESS FIT LIMITS KSI
1	A1L	11991	.999675	10
	B1L	11994.7	.999818	TO
	A2T	-44374	-.999475	40
	B2T	-44138.6	-.999326	

****

E.29

*** COMPOSITE TENSILE TEST OF SPEC# GRIMES 9-2:ACL4210 ***

REF #1 : A1L
REF #2 : B1L
REF #3 : A2T
REF #4 : B2T

FIT #1

MOD#1= 11990 KSI
MOD#2= 11994 KSI
MOD#3= -44374 KSI
MOD#4= -44139 KSI

EOF#1= .0118844
EOF#2= .0112833
EOF#3= -3.42751E-03
EOF#4= -3.16121E-03

STRAIN COMPONENTS

STRESS KSI

*** COMPOSITE TENSION TEST OF SPEC# GRIMES 9-2:ACL4210 ***
*** MAX LOAD = 20.7743 KIPS ***
*** TENSILE STRENGTH = 137.094 KSI ***

TENSILE LOAD KIPS

DERIVED STROKE IN

*** COMPOSITE TENSILE TEST RESULTS ***

18-MAR-80	TEST FRAME I.D. 50.1	BY AM

SPEC #: GRIMES 9-3   MATERIAL : ACL4210

*** DATA FILENAME : RK1:B00018.DGT ***

TEMP : RT   ENVIRONMENT : AIR

SPEC WIDTH = 1.011 IN   SPEC THICK. = .148 IN

STROKE XDER RANGE = .5 IN
LOAD XDER RANGE = 25 KIPS

NOMINAL STROKE RATE = 8.33333E-04 IN/SEC
MEASURED STROKE RATE = 8.21826E-04 IN/SEC

STRAIN GAGE I.D.	STRAIN XDER RANGES	SHUNT CAL STRAIN USED
A1L	.0193028	5.00000E-03
B1L	.019021	5.00000E-03
A2T	.0191164	5.00000E-03
B2T	.0191668	5.00000E-03

*** STRAIN GAGE G.F. = 2.09 ***
*** MANUFATURER'S MAX STRAIN LIMIT = .04 ***

FAILURE CRITERION USED : 20 % DROP IN LOAD

*** ULTIMATE LOAD = 17.2692 KIPS ***

*** ULTIMATE TENSILE STRENGTH = 115.414 KSI ***

****

GAGE I.D.	STRAIN @ FAILURE
A1L	9.59951E-03
B1L	9.61735E-03
A2T	-2.66153E-03
B2T	-2.59366E-03

****
*** COMMENTS ***

SPECIMEN FAILED IN GRIPS

****

18-MAR-80

*** COMPOSITE TENSILE TEST RESULTS ***

18-MAR-80   TEST FRAME I.D. 50.1   BY AM

    SPEC #: GRIMES 9-3   MATERIAL : ACL4210

    ************** SUMMARY OF LEAST SQUARE FITS **************

REF	GAGE	MODULUS	CORRELATION	STRESS FIT
#	I.D.	KSI	COEFF	LIMITS KSI
1	A1L	11560.4	.999827	10
	B1L	12039.1	.999831	TO
	A2T	-41036.2	-.999579	40
	B2T	-45101.4	-.999496	

****

E.33

*** COMPOSITE TENSION TEST OF SPEC# GRIMES 9-3:ACL4210 ***
*** MAX LOAD = 17.2692 KIPS ***
*** TENSILE STRENGTH = 115.414 KSI ***

TENSILE LOAD KIPS

DERIVED STROKE IN

E.34

*** COMPOSITE TENSILE TEST OF SPEC# GRIMES 9-3:ACL4210 ***

REF #1 : A1L
REF #2 : B1L
REF #3 : A2T
REF #4 : B2T

FIT #1

MOD#1= 11560 KSI
MOD#2= 12039 KSI
MOD#3= -41037 KSI
MOD#4= -45102 KSI

E0F#1= 9.59951E-03
E0F#2= 9.61735E-03
E0F#3= -2.66153E-03
E0F#4= -2.59366E-03

STRESS KSI

E 02
1.20

0.00

STRAIN COMPONENTS

0.00   1.00
              E-02

· E.35

APPENDIX F

NONDESTRUCTIVE INSPECTION EQUIPMENT

<u>TECHNIQUE DATA SHEET</u>

GENERAL INSPECTION LABORATORIES, INC.

   TEST PROCEDURE NO._____   PREPARED BY _W. Bulger_____

   REV. NO._____   DATE _5-12-7?_____

   SUPPLEMENT_____   PAGE_____OF_____

   METHOD_Reflector Plate_____

PART INFORMATION

   PART NO._____   MATERIAL_____

   PART NAME_____

   STAGE OF FABRICATION_____

   SURFACE FINISH_____

INSPECTION CRITERIA

   SPECIFICATION/ACCEPTANCE CRITERIA_____

   ACCEPTANCE CLASS_____

   METHOD_Reflector Plate_____   TECHNIQUE _Longitudinal_____

   SCAN (A,B,C,_C Scan_____   COUPLANT___Tapwater w/R5I Rust
                                                            Lik

EQUIPMENT/INSTRUMENTATION

   SYSTEM MFG/MODEL___Uresco-RB100_____   S/N___75-101_____

   ULTRASONIC UNIT MFG/MODEL_USIP-11_____   S/N___21197-3462_____

   RECORDER MFG/MODEL_NDT URA-1_____   S/N___71209-2_____

   DRY PAPER: _Yes_____

   SQUIRTER MFG/MODEL_____   COLUMN DIAMETER_____

   MANIPULATOR MFG/MODEL___Uresco-400_____

   SEARCH UNIT (TRANSDUCER) MATERIAL: TRANSMITTER (Tx)_Z_ RECEIVER(Rx)____

      Tx: Freq._5___MHz S/N_P684__ Size_1/2"∅_ Focus_3"_ EBD_.180

      Rx: FREE WATER PATH_____

      Rx: Freq:_____MHz S/N_____ Size_____Focus_____EBD____

          FREE WATER PATH_____

   ANGLE_Normal_____

   REFERENCE STANDARD S/N__ACL 3136_____   DEFECT SIZE_Various_____

REFERENCE SET-UP

   DGC_____Off_____   PULSE ENERGY__3_____RESOLUTION_3_____

   REJECT___Off_____   FREQUENCY__.5-2.5__DB_36-Ti to Comp. 12-Comp._

   TOTAL WATER PATH_____

   ALARM GATE INCLUDES_Reflected signal_____ ALARM LEVEL_50%_____

   SCAN RATE_6_____IPS SCAN INDEX_.030_____INCH

   RECORDING RATIO_____1:1_____

APPENDIX G

Photographs of Failed Specimens

Figure G.1 Test Series I Failed Specimens

ACL 4210 A
-1-6

ACL 4210A ACL 4210 A
-1-11   -2-21

ACL 4210 A
-2-22

T.S. I

T.S. III

ACL 4210 A
-4-5

ACL 4211 B
-10-36

ACL 4211 B
-11-38

T.S. IV

T.S. VII

Figure G.2   Test Series I, III, IV, and VII Failed Specimens

ACL 4210 A
-1-2

ACL 4210 A
-1-3

ACL 4210 A
-1-4

ACL 4210 A
-1-5

ACL 4210 A
-1-12

ACL 4210 A
-2-13

ACL 4210 A
-2-14

ACL 4210 A
-2-15

ACL 4210 A
-2-16

T. S. II

Figure G.3 Test Series II Failed Specimens

ACL
4210A
-2-20

ACL
4210A
-2-19

ACL
4210A
-2-18

ACL
4210A
-1-10

ACL
4210A
-1-9

TS III

ACL
4210A
-1-8

ACL
4210A
-1-7

Figure G.4   Test Series III Failed Specimens

Figure G.5 Test Series IV Failed Specimens

Figure G.6 Test Series V Failed Specimens

Figure G.7 Test Series VI Failed Specimens

ACL 4210A   ACL 4210A   ACL 4210A   ACL 4210A
   -4-2   -4-4   -4-6   -4-7

ACL 4210A   ACL 4210A   ACL 4210A   ACL 4210A
   -4-8   -4-9   -4-10   -4-11

T.S. VIII

Figure G.8   Test Series VIII Failed Specimens

G.9

Figure G.9   Test Series IX Failed Specimens

Figure G.10   Test Series X Failed Specimens

Figure G.11   Test Series X, XI, XV, and XVIII Failed Specimens

Figure G.12 Test Series XI Failed Specimens

Figure G.13   Test Series XII Failed Specimens

Figure G.14 Test Series XIII Failed Specimens

Figure G.15   Test Series XIV Failed Specimens

ACL 4210A   ACL 4210A   ACL 4210 A   ACL 4210A
-7-2   -7-4   -7-6   -7-7

ACL 4210 A   ACL 4210 A   ACL 4210 A   ACL 4210A
-7-8   -7-9   -7-10   -7-11

T.S. XVI

Figure G.16   Test Series XVI Failed Specimens

Figure G.17 Test Series XVII Failed Specimens

Figure G.18 Test Series XVIII Failed Specimens

Figure G.19   Test Series XIX Failed Specimens

APPENDIX H

DISTRIBUTION LIST

	No. of Copies
Naval Air Systems Command ATTN: Code AIR-5163D3 Washington, DC 20361	8
Office of Naval Research (Code 472) Washington, DC 20350	1
Office of Naval Research, Boston 495 Summer St. Boston, MA 02210 ATTN: Dr. L. H. Peebles	1
Naval Research Laboratory Codes 6306 and 6120 Washington, DC 20350	2
Naval Surface Weapons Center Code R-31 White Oak, Silver Spring, MD 20910	1
Naval Air Propulsion Test Center ATTN: J. Glatz Trenton, NJ 08628	1
Commander U.S. Naval Weapons Center China Lake, CA 92555	1
Naval Ship R&D Center ATTN: Mr. M. Krenzke, Code 727 Washington, DC	1
Naval Sea Systems Command Navy Dept. Codes 05R and 05D23 Washington, DC 20360	2

Commander
Naval Air Development Center
ATTN: Aero Materials Laboratory
      Aero Structures Division
      Radomes Section
Warminster, PA 18974
	3

DISTRIBUTION LIST (Cont'd)

	No. of Copies

Air Force Materials Laboratory
ATTN: Codes LC (1 copy)
           LN ("   ")
           LTF ("   ")
           LAE ("   ")
Wright-Patterson AFB, OH   45433
	4

Air Force Flight Dynamics Laboratory ATTN: Code FDTC Wright-Patterson AFB, OH 45433	1
U.S. Applied Technology Laboratory U.S. Army Development Laboratories (AVRADCOM) ATTN: DAVDL-ATL-ATS Fort Eustis, VA 23604	1
Director Plastics Technical Evaluation Center Picatinny Arsenal Dover, NJ 07801	1
Department of the Army Army Materials & Mechanics Research Center Watertown, MA 02172	1
NASA Langley Research Center Hampton, VA	1
NASA Headquarters Code RV-2 (Mr. N. Mayer) 600 Independence Ave., SW Washington, DC 20546	1
AVCO Corporation Applied Technology Division Lowell, MA 01851	1
Bell Aerospace Co. ATTN: Mr. F. M. Anthony Buffalo, NY 14240	1
The Boeing Company Aerospace Division P. O. Box 3707 Seattle, WA 98124	1
Boeing-Vertol Co. P. O. Box 16858 ATTN: Dept. 1951 Philadelphia, PA 19142	1

DISTRIBUTION LIST (Cont'd)

No. of Copies

Brunswick Corporation Technical Products Division 325 Brunswick Lane Marion, VA 24354	1
Celanese Research Company Box 1000 ATTN: Mr. R. J. Leal Summit, NJ 07901	1
Defense Ceramic Information Center Battelle Memorial Institute 505 King Ave Columbus, OH 43201	1
E. I. DuPont de Nemours & Co. Textile Fibers Dept Wilmington, DE 19898	1
Ewald Associates, Inc. 105 Skyline Drive Morristown, NJ 07960	1
Fiber Materials Inc. ATTN. Mr. J. Herrick Biddeford Industrial Park Biddeford, ME	1
General Dynamics Convair Aerospace Division ATTN: Tech Library P. O. Box 748 Ft. Worth, TX 76101	1
General Dynamics Convair Division ATTN: Mr. W. Scheck; Dept 572-10 P. O. Box 1128 San Diego, CA 92138	1
General Electric R&D Center ATTN: Mr. W. Hillig Box 8 Schnectady, NY 12301	1
General Electric Company Valley Forge Space Center Philadelphia, PA 19101	1

DISTRIBUTION LIST (Cont'd)

	No. of Copies
B. F. Goodrich Aerospace & Defense Products 500 South Main St Akron, OH 44318	1
Graftex Division EXXON Industries 2917 Highwoods Blvd Raleigh, NC 27604	1
Great Lakes Research Corporation P. O. Box 1031 Elizabethton, TN	1
Grumman Aerospace Corp ATTN: Mr. G. Lubin Bethpage, LI, NY 11714	1
Hercules Incorporated ATTN: Mr. E. G. Crossland Magua, UT 84044	1
HITCO 1600 W. 135th St Gardena, CA 90406	1
Illinois Institute of Technology Research Center ATTN: Dr. K. Hofer 10 West 35th St Chicago, IL 60616	1
Lockheed California Co. ATTN: Mr. J. H. Wooley Box 551 Burbank, CA 91520	1
Lockheed-Georgia, Co ATTN: Mr. L. E. Meade Marietta, GA 30063	1
Lockheed Missiles & Space Co. ATTN: Mr. H. H. Armstrong, Dept 62-60 Sunnyvale, CA 94088	1
Material Sciences Corporation 1777 Walton Road Blue Bell, PA 19422	1

DISTRIBUTION LIST (Cont'd)

	No. of Copies
McDonnell Douglas Corp McDonnell Aircraft Co. ATTN: Mr. J. Juergens P. O. Box 516 St. Louis, MO 63166	1
McDonnell-Douglas Corp Douglas Aircraft Co ATTN: Mr. R. J. Palmer 3855 Lakewood Blvd Long Beach, CA 90801	1
Monsanto Research Corp 1515 Nicholas Road Dayton, OH 45407	1
North American Aviation Columbus Division 4300 E. Fifth Ave Columbos, OH 43216	1
Northrop Corp One Northrop Avenue ATTN: Mr. G. Grimes, Mail Code 3852-82 Hawthorne, CA 90250	1
Philco-Ford Corp Aeronutronic Division Ford Road Newport Beach, CA 92663	1
Rockwell International Corp ATTN: Mr. C. R. Rousseau 12214 Lakewood Blvd Downey, CA 90241	1
Stanford Research Institute ATTN: Mr. M. Maximovich 333 Ravenswood Ave, Bldg 102B Marlo Park, CA 94025	1
TRW, Inc Systems Group One Space Park, Bldg. 01; Rm 2171 Redondo Beach, CA 90278	1
TRW, Inc 23555 Euclid Ave Cleveland, OH 44117	1

DISTRIBUTION LIST (Cont'd)

	No. of Copies
Union Carbide Corporation Chemicals & Plastics One River Road Bound Brook, NJ	1
Union Carbide Corporation Carbon Products Division P. O. Box 6116 Cleveland, OH 44101	1
United Aircraft Corporation United Aircraft Research Laboratories E. Hartford, CT 06108	1
United Aircraft Corporation Pratt & Whitney Aircraft Division East Hartford, CT 06108	1
United Aircraft Corporation Hamilton-Standard Division ATTN: Mr. T. Zajac Windsor Locks, CT	1
United Aircraft Corporation Sikorsky Aircraft Division ATTN: Mr. J. Ray Stratford, CT 06602	1
University of California Lawrence Livermore Laboratory ATTN: Mr. T. T. Chiao P. O. Box 808 Livermore, c A 94550	1
University of Maryland ATTN: Dr. W. J. Bailey College Park, MD 20742	1
University of Wyoming Mechanical Engineering Dept ATTN: Dr. D. F. Adams Laramee, WY 82071	1
Westinghouse R&D Center ATTN: Mr. Z. Sanjana 1310 Beulah Road Churchill Boro Pittsburgh, PA 15235	1

DISTRIBUTION LIST (Cont'd)

No. of Copies

Robert A. Signorelli   1
Mail Stop 106-1
NASA Lewis Research Center
Cleveland, Ohio 44135

Dr. Ingr. Dr. Schutz   1
Laboratorium for Betriebsfestigkeit
61 Darmstadt-Neu Kranichstien
Bartningstrasse 47, Germany

Dr. C. C. Chamis, Mat'ls & Struct. Div.   1
NASA Lewis Research Center
Cleveland, Ohio 44135

Joe Noyes   1
Compositek Engineering Corp.
6925-1 Aragon Circle
Buena Park, CA 90620

Dr. Satish Kulkarni   1
2864 Aptos Way
San Ramon, CA 94583

K. N. Lauraitis, Dept. 74-71/204/2   1
Lockheed California Company
Burbank, CA 91508

Dr. G. C. Sih, Packard Lab. #19   1
Lehigh University
Institute of Fracture & Solid Mechanics
Bethlehem, PA 18015

LTV Aerospace Corp.   1
Attn: O. E. Dhonau
P. O. Box 5003
Dallas, Texas 75222

Rockwell International   1
Attn: Dr. L. M. Lackman
L. A. International Airport
Los Angeles, CA 90009

Air Force Flight Dynamics Lab.   1
Attn: Dr. G. P. Sendeckji/FBE
Wright-Patterson AFB, Ohio 45433

DISTRIBUTION LIST (Cont'd)

	No. of Copies
Air Force Materials Lab Attn: Dr. J. M. Whitney/MBM Wright-Patterson AFB, Ohio 45433	1
Southwest Research Institute Attn: Dr. L. R. Calcote Box 28510 San Antonio, Texas 78284	1
Vought Corporation Advanced Technology Center, Inc. Attn: J. W. Renton P. O. Box 6144 Dallas, Texas 75222	1
Hughes Helicopter Attn: Chief Librarian Centinela & Teale Sts. Culver City, CA 90230	1
Bell Helicopter Attn: S. C. Aker Fort Worth, Texas 76101	1